Wireless Link Quality Modelling and Mobility Management Optimisation for Cellular Networks

van Minh Nguyen

Telecom ParisTech

École Doctorale Informatique, Télécommunications, et Électronique

Thèse de Doctorat en Télécommunications

Modélisation Stochastique de Liaisons Sans Fil et Gestion de la Mobilité dans les Réseaux Cellulaires

par

Van Minh Nguyen

Rapporteurs:

    Prof. Eitan Altman,   *Directeur de Recherche, INRIA-Univ d´Avignon*

    Prof. Gerhard Fettweis,   *Directeur de Vodafone Chair, TU Dresden*

Thèse soutenue le 20 juin 2011 devant le jury composé de:

Prof. Daniel Kofman,	*Directeur de LINCS, Telecom ParisTech*	Président
Prof. François Baccelli,	*Directeur de TREC, INRIA-ENS*	Directeur
Prof. Eitan Altman,	*Directeur de Recherche, INRIA-Univ d´Avignon*	Examinateur
Prof. Jean-Marie Gorce,	*Directeur de CITI Lab, INSA Lyon-INRIA*	Examinateur
Ing. Laurent Thomas,	*Directeur de Dépt. de Recherche, ALU Bell Labs*	Examinateur

19 Août 2011

Telecom ParisTech

École Doctorale Informatique, Télécommunications, et Électronique

A thesis submitted in partial fulfillment for the degree of

Doctor of Philosophy

Wireless Link Quality Modelling and Mobility Management for Cellular Networks

by

Van Minh Nguyen

Reviewers:

Prof. Eitan Altman,	*Research Director, INRIA-Univ of Avignon*
Prof. Gerhard Fettweis,	*Head of Vodafone Chair, TU Dresden*

Dissertation defense on June 20th 2011. Jury Committee:

Prof. Daniel Kofman,	*Director of LINCS, Telecom ParisTech*	President
Prof. François Baccelli,	*Director of TREC, INRIA-ENS*	Advisor
Prof. Eitan Altman,	*Research Director, INRIA-Univ of Avignon*	Examiner
Prof. Jean-Marie Gorce,	*Head of CITI Lab, INSA Lyon-INRIA*	Examiner
Ing. Laurent Thomas,	*Head of Research Dept, ALU Bell Labs*	Examiner

August 19, 2011

"All men by nature desire knowledge."

Aristotle (384 BC - 322 BC)

"Everything has its beauty but not everyone sees it."

Confucius (551 BC - 479 BC)

Abstract / Résumé

The quality of communication in a wireless network is primarily determined by the wireless link signal quality expressed in term of signal-to-interference-plus-noise ratio. The fact that better signal quality enhances the communication quality incites to look for states where each receiver connects to a transmitter providing it with the best signal quality. Using stochastic geometry and then extreme value theory, we obtain the distribution of the best signal quality, of the interference, and of the maximum signal strength in both bounded and unbounded path loss conditions. We then investigate temporal variations of wireless links, which are also essential to wireless networking, in terms of level crossings of a stationary process $X(t)$. We prove that the length of an excursion of $X(t)$ above a level $\gamma \to -\infty$ has an exponential distribution, and obtain results associated with the crossings of several levels. These results are then applied to mobility management in cellular networks. We focus on the handover measurement function, which differs from the handover decision-execution by identifying the best neighbouring cell to which a connection switching is to be decided and executed. This function has an important influence on the user's experience, though its operation has been questionable due to the complexity of combining control mechanisms. We firstly address this topic with an analytical approach for emerging macro cell and small cell networks, and then with a self-optimisation approach for neighbour cell lists used in today's cellular networks.

La qualité de communication dans un réseau sans fil est déterminée par la qualité du signal, et plus précisément par le rapport signal à interférence et bruit. Cela pousse chaque récepteur à se connecter à l'émetteur qui lui donne la meilleure qualité du signal. Nous utilisons la géométrie stochastique et la théorie des extrêmes pour obtenir la distribution de la meilleure qualité du signal, ainsi que celles de l'interférence et du maximum des puissances reçues. Nous mettons en évidence comment la singularité de la fonction d'affaiblissement modifie leurs comportements. Nous nous intéressons ensuite au comportement temporel des signaux radios en étudiant le franchissement de seuils par un processus stationnaire $X(t)$. Nous démontrons que l'intervalle de temps que $X(t)$ passe au-dessus d'un seuil $\gamma \to -\infty$ suit une distribution exponentielle, et obtenons également des résultats caractérisant des franchissements par $X(t)$ de plusieurs seuils adjacents. Ces résultats sont ensuite appliqués à la gestion de mobilité dans les réseaux cellulaires. Notre travail se concentre sur la fonction de 'handover measurement'. Nous identifions la meilleure cellule voisine lors d'un handover. Cette fonction joue un rôle central sur l'expérience perçue par l'utilisateur. Mais elle demande une coopération entre divers mécanismes de contrôle et reste une question difficile. Nous traitons ce problème en proposant des approches analytiques pour les réseaux émergents de types macro et pico cellulaires, ainsi qu'une approche d'auto-optimisation pour les listes de voisinage utilisées dans les réseaux cellulaires actuels.

Keywords: max sinr, interference, max signal, shot noise, extreme values, level crossing, self-optimisation, mobility management, handover measurement, neighbour cell list

Acknowledgements

Faithful to Aristotle's maxim, I have been following my innate desire for knowledge in pursuing this Doctor of Philosophy thesis. I take this moment of writing the PhD dissertation as a pause to look back at the past. I realise that the road of human emancipation from nature through knowledge enrichment and creation is a special journey, which is fully enjoyable, peaceful, but also truly challenging. I cannot imagine how hard it would have been without the precious help of advisors, colleagues, friends, and family.

Foremost, I would like to express my deep gratitude to my advisor Professor François Baccelli who has greatly inspired me with his genuine scientific attitudes, his special abilities of sharp cognition and thorough observation. I am sincerely grateful for his devoted advising and availability, even to correct each word of my manuscripts, despite of his strict time constraint. Especially, on my behalf and on that of other foreign students who would let me, I would like to give my sincere thanks and high respects for his willingness to provide us with all the help we needed in one thousand and one kinds of problems that a foreigner encounters, particularly with bureaucratic administrations.

Special thanks I would like to dedicate to Alcatel-Lucent Bell Labs France for granting me its best financial funding and efficient support for a great research condition, where I acquired a fruitful professional experience. For this, I would like to sincerely thank Mr Laurent Thomas who had trustfully received me within his department and directly supervised me. He has always given me his total confidence, supports, and in particular shared with me precious amicable advices.

I wish to sincerely thank Professor Daniel Kofman and Professor Jean-Marie Gorce for serving as members on the jury committee. I am highly grateful to Professor Eitan Altman and Professor Gerhard Fettweis for their time to review my thesis and for their invaluable suggestions. Especially, their appreciations are really a precious encouragement to my professional endeavour.

I would like to thank many people with whom I had great teamwork and fruitful collaborations. In particular, many thanks go to Holger Claussen, Head of Autonomous Networks and Systems Research Department at Bell Labs in Ireland, for his friendly and efficient collaboration. Thanks to him, we could quickly obtain a real network scenario and conduct evaluations of our algorithms. I also learnt from him valuable experiences in writing papers. Warm thanks I would like to send to Chung Shue (Calvin) Chen, Research Expert at Bell Labs-INRIA Joint Research Centre. I appreciate very much his strong efforts in conducting numerical computations of many tricky integrals. I shared a really enjoyable time with him during many long work discussions, midnight works, stressful time at each approaching deadline, and also during relaxing tennis games.

I was lucky to meet and collaborate with many good people from different organisations. I would like to express my appreciation and gratitude to them all. In particular, I would like to thank Dr Iraj Saniee, Head of Mathematics Research at Bell Labs in Murray Hill, for his enthusiasm and efforts to invite me to his department. It is a deep regret that we did not obtain necessary approval for my internship in his department. I appreciate the occasions in which I met and discussed with Dr Piyush Gupta, who is also from Bell Labs Mathematics Research. I would like to express my special thanks to Dr Gee Rittenhouse, Head of Bell Labs Research, for his support at the end of my time at Bell Labs. I wish to thank Prof Merouane Debbah, Head of Alcatel-Lucent Chair on Flexible Radio at Supélec, for interesting discussions at Supélec; Dominique Morice and his colleagues at Network Performance Optimization (NPO) team for providing valuable network data as well as many discussions; Jean-Michelle Pugeat and his colleagues at R&D team of Alcatel-Lucent in Vélizy for helpful meetings on products and algorithms. In particular, I appreciate very much and would like to send faithful thanks to

Contents

List of Figures

List of Tables

Abbreviations

Acronym	What (it) Stands For
2G, 3G, 4G	**2**nd, **3**rd, and **4**th **G**eneration
3GPP	**3**rd **G**eneration **P**artnership **P**roject
BS	**b**ase **s**tation
cdf	**c**umulative **d**istribution **f**unction
cf	**c**haracteristic **f**unction
CSID	**c**ell **s**ynchronization **i**dentifier
GSM	**G**lobal **S**ystem for **M**obile **C**ommunications
HO	**h**and**o**ver
iff	**if** and only i**f**
i.i.d	**i**ndependently and **i**dentically **d**istributed
IMT	**I**nternational **M**obile **T**elecommunications
LTE	**L**ong **T**erm **E**volution
MS	**m**obile **s**tation
NCL	**n**eighbour **c**ell **l**ist
NGMN	**N**ext **G**eneration **M**obile **N**etworks
OFDM	**O**rthogonal **F**requency **D**ivision **M**ultiplexing
OFDMA	**O**rthogonal **F**requency **D**ivision **M**ultiple **A**ccess
PCI	**p**hysical **c**ell **i**dentity
pdf	**p**robability **d**ensity **f**unction
p.p.	**p**oint **p**rocess
rv(s)	**r**andom **v**ariable(**s**)
SINR	**s**ignal-to-**i**nterference-plus-**n**oise **r**atio
SON	**S**elf-**O**rganizing **N**etwork
UE	**u**ser **e**quipment
WCDMA	**W**ideband **C**ode **D**ivision **M**ultiple **A**ccess
WiMAX	**W**orldwide **I**nteroperability for **M**icrowave **A**ccess
w.r.t.	**w**ith **r**espect **t**o

Notation

Convention	Meaning
$(a)_n$	$:= a(a+1)(a+2)\dots(a-n+1)$ for n an integer number with convention that $(a)_0 = 1$
$\log(x)$	natural logarithm of positive real number x
x_{dB}	positive quantity x expressed in decibel scale, $x_{\mathrm{dB}} = 10\log_{10} x$
$x \approx y$	x is approximately equal to y
$f \sim g$, as $x \to a$	means that $\lim_{x\to a}(f(x)/g(x)) = 1$,
$f = o(g)$, as $x \to a$	$\lim_{x\to a}(f(x)/g(x)) = 0$,
$f = O(g)$, as $x \to a$	$\limsup_{x\to a}\|f(x)/g(x)\| < \infty$, for real functions f, g, 'as $x \to a$' can be implicitly understood for $a = +\infty$.
$\xrightarrow{d}$, $\xrightarrow{p}$	convergence in distribution, convergence in probability
$\stackrel{\mathrm{def}}{=}$, $:=$	equal by definition
$\|\cdot\|$	absolute value / modulus of a number, Euclidian distance between two points, and Lebesgue measure of a set in an appropriate measurable space
$\mathrm{MDA}(H)$	the max domain of attraction of the extreme value dist. H
$\mathrm{D}(G_\alpha)$, $\mathrm{D}(\alpha)$	the domain of attraction of G_α, and of an α-stable dist.

Symbol	Meaning
A	constant given by $A_{\mathrm{dB}} = P_{\mathrm{tx,dB}} - L_{0,\mathrm{dB}} - N_{0,\mathrm{dB}}$
B, R_B	network area, and radius of disk-shaped network area B
${}_nF_m$	hypergeometric function
I_n, I_S, I	interference from n nodes, from set S, and total interference
j	the imaginary unit, $j^2 = -1$
$l(\cdot)$, L_0	path loss function, fixed-term path loss
M_n, M_S	maximum of n random variables, and of set S
N_0, N_{F}	thermal noise, and noise figure
P_i, Q_i	signal strength, and signal quality received from node i
p_i	$:= AX_i$, "virtual transmission power" of node i
P_{tx}	node's transmission power
R_{min}	bounding distance (coupling distance) of bounded path loss
S	set of considered objects, e.g., random variables, nodes,
$\mathbf{x}_i$, $\mathbf{y}$	location of node i, and location of receiver, e.g., mobile station
X_i	random variable, shadowing, fading, or combining shadowing-fading
Y_n, Y_S	$\stackrel{\mathrm{def}}{=} \max_{i=1}^{n} Q_i$, and $\stackrel{\mathrm{def}}{=} \max_{i\in S} Q_i$: maximum of signal quality
v	mobile user's speed

α	$:= 2/\beta$, parameter of α-stable distribution
β	path loss exponent
$\Gamma(\cdot), \Gamma(\cdot, \cdot)$	the Gamma, and the upper incomplete Gamma functions
λ	network density
Λ	standard Gumbel distribution
Φ	standard Gaussian distribution
$\widetilde{\Phi}$	marked Poisson point process
ρ	retaining probability of a thinning on a Poisson p.p.
ρ_n	acceleration factor of autonomous scanning
C_n	maximum achievable capacity received from n nodes
$\mathbb{C}$	the set of complex numbers
$\mathbb{L}$	the space of absolutely integrable functions
$\mathbb{N}$	the set of positive integers
$\mathbb{R}, \mathbb{R}_+, \mathbb{R}_+^*$	the real line, the positive real half-line $[0, +\infty)$,
	and the strictly positive real half-line $(0, +\infty)$
$\mathbb{R}^n$	n-dimensional Cartesian space
$\Re(x)$	real part of complex number x
$\mathbf{1}(\mathcal{A})$	the indicator function of $\mathcal{A}$: $\mathbf{1}(\mathcal{A}) = 1$ if $\mathcal{A}$ holds and $\mathbf{1}(\mathcal{A}) = 0$ otherwise.
$\mathcal{L}_f, \mathcal{L}_X$	Laplace transforms of function f, and of rv X
$\widehat{f}$	Fourier transform of function f
∂	partial derivative
$\square$	end of a proof
$\mathbf{E}X$	mathematical expectation of random variable X
$\mathrm{var}(X)$	variance of random variable X
$\mathbf{P}(\mathcal{A})$	probability of event $\mathcal{A}$
F_X, f_X	cdf and pdf of random variable X
$\overline{F}_X$	$:= 1 - F_X$, tail distribution of random variable X
ϕ_X	characteristic function of random variable X

To my family.

Chapter 1

Introduction

A wireless link between a transmitter and a receiver is subject to variations in frequency, time, and space. The received signal power is traditionally characterised by a superposition of three components called path loss, shadowing, and fading. The path loss describes the power attenuation due to the radio propagation in free space. It is commonly expressed by a deterministic function of the transmission distance. The shadowing describes variations of the signal power due to obstacles during the transmission. And the fading characterises rapid fluctuations which are generated by the relative motion of the receiver and by the multi-path reception of the original signal. The shadowing and fading are conventionally characterised by probabilistic laws [7, 8].

In a wireless network composed of communicating nodes, interference occurs when multiple nodes transmit simultaneously on a common frequency. The quality of communication is primarily determined by the signal quality expressed in term of the ratio of the received signal power over that of the interference caused by other nodes plus the thermal noise power, namely signal-to-interference-plus-noise ratio. This incites to look for states where each receiver connects to the transmitter from which it obtains the best signal quality. The best signal quality is thus a fundamental information to assess many quantities of interest as well as to the network design and optimisation.

> The ***first contribution*** of the thesis is the wireless link modelling with
> results centred on the distribution of the best signal quality.

On the way of establishing these results, we obtain a variety of interesting results and observations of wireless links [1], particularly on the interference and the maximum signal strength received from multiple nodes. The results are presented in Part II of the thesis. To better present our approach and results, let us consider a concrete setting. Assume that there are n transmitters from which a receiver receives signal powers $(P_1, P_2, \ldots, P_n)$. The interference power with respect to the signal of a transmitter i is $I_i = P_1 + \cdots + P_{i-1} + P_{i+1} + \cdots + P_n$. And the signal quality of transmitter i is $Q_i = P_i/(N_0 + I_i)$ where N_0 refers to the thermal noise power. The best signal quality between these n transmitters is given as $Y_n = \max(Q_1, \ldots, Q_n)$. Since the random variables $(Q_1, Q_2, \ldots, Q_n)$ depend one another due to the terms $(I_i, i = 1, \ldots, n)$, obtaining the distribution of Y_n is not so straightforward. By denoting $I = P_1 + \cdots + P_n$, it is clear that $I_i = I - P_i$, leading to $Q_i = P_i/(N_0 + I - P_i)$. With a simple observation, we can see

---

[1] *"Remember that happiness is a way of travel - not a destination."* ROY M. GOODMAN.

that $Y_n = M_n/(N_0 + I - M_n)$ where we denote by M_n the maximum signal strength received between the n transmitters, i.e. $M_n = \max(P_1, \ldots, P_n)$. This means that the transmitter which provides the maximum signal power will provide the best signal quality. More importantly, it suggests that we can derive the distribution of the best signal quality Y_n by means of the joint distribution of the maximum signal strength M_n and the total interference I. That is the guiding idea throughout our work.

To support our above idea, we firstly need information about the spatial distribution of nodes. In the literature, there have been two common approaches to obtain this information: either using a deterministic model, or using a stochastic model. A deterministic model requires complete information on the network structure or needs to be constrained to a regular topology such as grid or hexagonal structures. It results in expenses in obtaining precise information of the network, and difficulties in mathematical generalisations [9, 10]. Too idealised models based on regular structure are also inconvenient. The spatial distribution of nodes is therefore often treated as random according to some point process. Although a stochastic model is not able to describe the locations of nodes precisely, it can provide some degree in mathematical generalisation and is especially suitable for the system-level analysis. In particular, Poisson point processes offer computational convenience [11]; they have been intensively used to model the spatial distribution of nodes in a wireless network, see §6.2. And in this thesis, we will do so. Using this setting, our results are as follows.

- In **Chapter 7**, we obtain the exact formulations of the joint density of the maximum signal strength received from a disk-shaped network area B and the total interference, and the distribution of the best signal quality. Some highlighted observations are that under an unbounded typical path loss model, the maximum signal strength received from the whole network follows a Fréchet distribution, and the total interference is a skewed α-stable distribution, independently of the type of fading. And under favourable conditions, their joint density exists everywhere of the two-dimensional Euclidean plane, except at the origin if B is bounded. (This work was realised in collaboration with François Baccelli, and was published in the proceedings of WiOPT 2010 conference.)

- In **Chapter 8**, we show that the singularity of the path loss function decides the heavy-tailed behaviour of wireless links. In case of unbounded power-law path loss, the signal strength is regularly varying, leading to very heavy-tailed interference and maximum signal strength. This is explained by the dominant component created by the singularity of path loss function. This common dominant component in addition strengthens the dependence between the interference and the maximum signal strength. By contrast, in case of bounded path loss, the tail behaviour of the signal strength is mainly imposed by the type of fading. Especially, under lognormal shadowing, the signal strength lies on both the domains of attraction of a Gumbel distribution and a Gaussian distribution, leading to the asymptotic independence of the maximum signal strength and the interference when the number of observed nodes tends to infinity. This allows us to obtain an approximation of the distribution of the best signal quality which is analytically more tractable than its exact formulation. (This work was done with François Baccelli, Laurent Thomas, and Chung Shue Chen, and was published in the EURASIP JWCN 2010.)

Now, we are interested in temporal variations of wireless links. In the time domain, wireless signal often crosses a given threshold due to its variations over the time. From the point of view

of wireless networking, some mechanisms are needed to control the network operation when the signal quality of a link is too low or very high. For example, when the signal quality is too low, meaning that the signal quality stays below a low level, the communication becomes unreliable, requiring for a switching of the communication to another transmitter. Understanding properties associated with the crossings of wireless links has been an important topic. It is known under *level crossing* theory which has been investigated since the middle of the last century with first milestones credited by Rice [12, 13], and Kac and Slepian [14]. For a stationary normal process, they contributed fundamental results on the mean number of crossings of one level, and the asymptotic trajectory of excursions of above a very large level. The application of these results to mobile radio communications has received increasing attention, especially since the paper of Mandayam et al. [15] appearing in 1996, and republished in 1998 in [16]. However, the introduction of new control mechanisms in emerging cellular systems gives rise to the need of more theoretical investigation of this problem.

> The **second contribution** of the thesis is an investigation of some
> properties of level crossings of a stationary process.

Consider a normal stationary process; we investigate its excursions above a very small level, and its crossings of several adjacent levels.

- In **Chapter 9**, we show that the length of an *up*-excursion above a very *small* level has an exponential distribution of rate equal to the mean crossing rate of this level. This complements the well known result saying that the length of an up-excursion above a very large level has a Rayleigh distribution (see §5.3). We then obtain the mean number of crossings, and the distribution of the length of an up-excursion, above successive large levels. (This work was realised during the completion of the thesis dissertation, and is subject to a future publication.)

The above results should have diverse implications. Here, we are interested in their applications to mobility management in cellular networks. Let us briefly describe the cellular concept and the need for mobility management. Basically, to guarantee a level of quality of communications, it is necessary to keep the signal quality of wireless links above an acceptable level. That requires a low level of interference, meaning that only a few nodes are allowed to transmit simultaneously. This can be satisfied in a broadcasting situation where there is only one-way communication from a transmitter to a population of receivers, such as radio television systems, or a lecture note given by a professor to a large number of students in a big room. But the problem arises when many people need to talk. To see the problem, let us take an example of a brainstorming exercise between students guided by a professor. Each student is motivated to present his/her idea to the group, and the professor may give comments and animates the group activity. If the group has too many students, the chance for a student to present his/her idea becomes very low. The idea here is to divide the class into a number of groups, each group is assigned a professor and works in a separated room. This gives chance to each student to show his/her idea, of course at the cost of increasing the number of professors. This is also the logic behind the cellular network concept which uses a number of base stations spatially separated to provide communication services to a large region. The geographic area where the signal quality of a base station is better than that of any other base station and is better than a required level is called a (radio) cell. A mobile station in a cell is guaranteed communications with the base station of this cell. But the situation here is more complicated than the above example of brainstorming

exercise. A mobile user may move across cells during a communication (e.g. a phone call). One needs a mechanism to switch the call automatically from one cell to another seamlessly and transparently to the user. This is realised by a procedure called mobility management, or also *handover*. It consists in two subfunctions: (i) determining a base station with the best signal quality, and then (ii) switching the connection to the best base station, called handover target. The first function requires a measurement of the signal quality of neighbouring base stations and is called *handover measurement*, and the second function is called *handover decision-execution*. These two functions have a strong influence on the quality of service in terms of call drops and throughput degradation: the handover measurement decides the quality of the handover target and the quality of service during the measurement, while the handover decision-execution is responsible for reliable and efficient connection switching. The handover decision-execution has been intensively studied with a rich literature including handover parameter optimisation (optimising parameters used for controlling the handover procedure), handover optimal control (deciding whether or not to switch the connection), and handover execution protocol design (performing fast and reliable connection switchings). Meanwhile, the handover measurement has received less attention. Even nowadays one often implicitly means the handover decision-execution when talking about handover, while forgetting the handover measurement function. Most prior works on this topic were based on simulations and only investigated a certain specific aspect (see §4.3). There lacks a unified framework for this function.

> The **third contribution** of the thesis is the analysis and optimisation of
> handover measurement function of cellular networks.

Basically, the more cells are measured, the more chance to find a good handover target. That is so obvious as the situation where the more candidates we examine for a job position, the more chance we can find an appropriate employee. But the time spent for the measurement (or for interviews) matters. A longer measurement time introduces more overhead, and more importantly it can cause call dropping with the serving cell when its own signal deteriorates. Knowing when to perform a handover measurement, and how to perform it optimally is critical. We use the results developed in the previous chapters to investigate this handover measurement function.

- In **Chapter 10**, we develop a general analytical framework for the handover measurement with a characterisation of key probabilistic events under the interference-limited condition in a multicell system. The overall operation of handover measurement involving all control parameters is described by a state diagram, which allows for determining different quantities of interest of the handover measurement. An application of this framework to the current specification of LTE networks indicates the necessity for an improvement in the terminal's measurement capability of this cellular standard. (This work was realised with Chung Shue Chen and Laurent Thomas, and with the advising of François Baccelli; a part of this work will be presented in the ICC 2011 conference.)

- In **Chapter 11**, we propose an effective implementation of the standardised mobility management, namely autonomous cell scanning, for data dense small cell networks. This solution helps to cope with one of the most challenging issues of the small cell networking. The results suggest that in a typical setting, the mobile should perform autonomous scanning with 30 cells to achieve effective performance. (This work was done with François Baccelli, Laurent Thomas, and Chung Shue Chen, and was published in the EURASIP JWCN 2010.)

- In **Chapter 12**, we focus on a problematic element of the handover measurement in today's commercial cellular networks. That is the neighbour cell list. To describe this element, let us take again the above example of competition for job position. Instead of interviewing every candidate, we may firstly filter out only those who are eligible and of potential interest to our job, and then interview each of them for more details. This allows to save time, and it provides an equivalent result if the short list is appropriately selected. The neighbour cell list used in cellular networks is similar to this short list of job candidates. The mobile performs the handover measurement by measuring cells comprised in the list of pre-selected neighbouring cells of its serving cell. The performance of the handover measurement consequently depends closely on the configuration of neighbour cell list. The problem is that a good configuration of neighbour cell list is a real everyday concern, and generates expenses to the network operator. In this chapter, we propose a measurement-based self-optimisation of neighbour cell lists. Primary advantages of the proposed solution are that it frees out all mathematical abstractions [2] and operator's manual operations, while generating optimised neighbour cell lists without introducing network overheads. Simulation results with a real network deployment confirms its efficiency. (This work was done with Holger Claussen, and was published in the proceedings of PIMRC 2010.)

The above results are of diverse nature and their development requires different mathematical tools. Part I is reserved for background notions. Chapter 2 describes basic properties of wireless links, including a literature review of the field. Chapter 3 describes the cellular network concept, from its history, to a brief technical description, and its current evolution. These two chapters can be skipped for a reader who is already familiar with these elementary information. Chapter 4 describes in more details different aspects of mobility management, including its state-of-the-art. Reader is recommended to take at least a quick scan of §4.1 and §4.2 before going into Part III. Chapter 5 briefly describes three mathematical theories: §5.1 describes extreme value theory and is required for Chapter 8, §5.2 describes stochastic geometry and is required for Chapter 7, and §5.3 describes level crossing theory and is required for Chapter 9. Chapter 6 summarises assumptions which are used throughout the thesis; reading this chapter is thus highly recommended before going to any subsequent chapter, except Chapter 12. Part II is focused on wireless link modelling and level crossings, the results of this part are used for Part III. But those interested in mobility management optimisation without dealing with too many mathematical developments can start Part III considering that mathematical results used therein are already proved.

1.1 Bibliography

Articles

(A1) V. M. Nguyen and F. Baccelli. "A stochastic geometry model for the best signal quality in a wireless network". In *Proceedings of the 8th IEEE International Symposium on Modeling and Optimization in Mobile, Ad-Hoc and Wireless Networks (WiOpt 2010)*, pp. 465-471. Avignon, France, June 2010.

(A2) V. M. Nguyen, F. Baccelli, L. Thomas, and C. S. Chen. "Best signal quality in cellular networks: asymptotic properties and applications to mobility management in small cell networks". *EURASIP*

---

[2] *"As far as the laws of mathematics refer to reality, they are not certain; and as far as they are certain, they do not refer to reality."* Geometry and Experience, 1921, ALBERT EINSTEIN.

J. Wireless Commun. and Netw., special issue on Femtocell Networks, pp. 1-14, Mar. 2010. doi:10.1155/2010/690161.

(A3) V. M. Nguyen. "Extreme value modeling of the best signal quality and applications for small cell networks". Invited talk in the *Joint workshop of Bell Labs, Fraunhofer Heinrich Hertz Institute, and Deutsche Telekom Labs on The Future of Communications: Science, Technologies, and Services.* Berlin, June 2010.

(A4) V. M. Nguyen, C. S. Chen, and L. Thomas. "Handover measurement in mobile cellular networks: analysis and applications to LTE". To appear in *Proceedings of IEEE ICC 2011.* Kyoto, Japan, June 2011.

(A5) V. M. Nguyen and H. Claussen. "Efficient self-optimization of neighbour cell lists in macrocellular networks". In *Proceedings of IEEE 21st International Symposium on Personal Indoor and Mobile Radio Communications (PIMRC 2010)*, pp. 1921-1926. Istanbul, Turkey, Sept. 2010.

(A6) V. M. Nguyen and L. Thomas. "Efficient dynamic multi-step paging for cellular wireless networks". *Bell Labs Tech. J., special issue on Core and Wireless Networks*, 14(2), pp. 203-221. Aug. 2009. doi: 10.1002/bltj.20380.

(A7) V. M. Nguyen. "Some properties of level crossings of a stationary process and applications". In preparation.

(A8) V. M. Nguyen, C. S. Chen, and L. Thomas. "A generalized framework of handover measurement in mobile cellular networks". In preparation for *IEEE Trans. Netw.*

Patent Applications

(P1) V. M. Nguyen and H. Claussen. "Method for automatically configuring a neighbor cell list for a base station in a cellular wireless network". *European Patent Application* No. 08291260.1 (filed 31.12.2008), *International Patent Application* No. PCT/EP2009/009204 (filed 21.12.2009)

(P2) V. M. Nguyen and O. Marcé. "Adaptive time allocation to reduce impacts of scanning". *European Patent Application* No. 08291265.0 (filed 31.12.2008), *International Patent Application* No. PCT/EP2009/009205 (filed 21.12.2009)

(P3) V. M. Nguyen and Y. El Mghazli. "Method and equipment for dynamically updating neighboring cell lists in heterogenous networks". *European Patent Application* No. 09290135.4 (filed 25.02.2009)

(P4) V. M. Nguyen and Y. El Mghazli. "Method and apparatus for new cell discovery". *US Patent Application* No. 12/383,907(filed 30.03.2009), *International Patent Application* No. PCT/US2010/026496 (filed 08.03.2010)

(P5) V. M. Nguyen, L. Thomas, and O. Marcé. "Method and controller for paging a mobile set in a cellular network". *European Patent Application* No. 09305029.2 (filed 12.01.2009)

(P6) O. Marcé, A. Petit, and V. M. Nguyen. "Method for enhancing the handover of a mobile station and base station for carrying out the method". *European Patent Application* No. 09305189.4 (filed 02.03.2009), *International Patent Application* No. PCT/EP2010/052425 (filed 25.02.2010)

Standard Contributions

(S1) R3-092949, Alcatel-Lucent/V. M. Nguyen. "Identifying coverage islands". *3GPP LTE Standard Contribution.* TSG-RAN WG3#66, Nov. 2009.

(S2) R3-092950, Alcatel-Lucent/V. M. Nguyen. "UE measurements in coverage islands". *3GPP LTE Standard Contribution.* TSG-RAN WG3#66, Nov. 2009.

(S3) R3-092951, Alcatel-Lucent/V. M. Nguyen. "Handling of UE measurements and transfer of UE history for mobility robustness optimization". *3GPP LTE Standard Contribution.* TSG-RAN WG3#66, Nov. 2009.

Part I

Background and Assumption

Chapter 2

Basics of Wireless Link Modelling

A wireless communication network is composed of a set of nodes which communicate with one another over wireless links. A wireless link between a transmitter-receiver pair is constrained by impairments due to other transmissions and the environment. Wireless link modelling is essential to wireless networking. It consists in characterising macroscopic properties such as the received signal power, signal quality, and interference. This chapter is aimed at describing physical properties of wireless links such as path loss, fading, and interference.

2.1 Radio Propagation Modelling

The radio propagation is subject to variations in frequency, time, and space; understanding its characteristics is essential for the wireless network design. A radio channel is traditionally characterised by a superposition of three components with large-, medium-, and small-scale propagation effects [7, 8].

Path Loss. The large-scale effect is due to the spatial separation between the transmitter and the receiver. The transmitted signal power decays along with the propagation path, and the so-called *path loss* is defined as the ratio of the transmitted power at $\mathbf{x}$, $P_{\text{tx}}(\mathbf{x})$, over the received power at $\mathbf{y}$, $P_{\text{rx}}(\mathbf{y})$, and is given as follows, [8, 17]:

$$l(d) \overset{\text{def}}{=} P_{\text{tx}}(\mathbf{x})/P_{\text{rx}}(\mathbf{y}), \tag{2.1.1}$$

where $d = |\mathbf{y} - \mathbf{x}|$ which is the Euclidean distance between $\mathbf{y}$ and $\mathbf{x}$. Theoretically the path loss is completely described by Maxwell's equations. This however often results in complex mathematical equations which are not very practical to system engineering. Therefore, the path loss is practically characterised by prediction models.

Prediction models proposed so far can be roughly classified into three types: theoretical, site-specific, and empirical models [18]. Theoretical models are derived from an analytical formulation of the physical environment and are often constrained to simplification assumptions such as those used by Walfisch and Bertoni [19]. Site-specific models are based on simulations such as ray tracing technique, e.g., [20, 21], and are able to provide a high degree of precision. It

however requires complete information of the physical environment including the precise location of obstacles [22], and is thus not feasible for some complex environments. Empirical models are based on statistical analysis over a large number of experimental measures. They provide quite simple equations which are analytically and numerically tractable, and do not require precise information of the environment. A classic example of empirical models is that formulated by Hata [23] from the field measurements provided by Okumura et al. [24]. Some more sophisticated empirical models are proposed in COST-231 project [25] where both experimental measurements and analytical formulations are used to provide fine adjustments to path loss prediction models. Providing these advantages, empirical models are used by cellular technology standardisation bodies for network simulation and performance evaluation purposes [26, 27]. Since empirical models are only accurate for environments which have similar propagation conditions as those where the experimental measurements were made, one specific model is recommended for each deployment environment (e.g., urban, suburban, and rural), or for a range of cell sizes (e.g., macro cells, micro cells, and small cells). For example, COST 321-Hata model which is an extension of the Hata model was proposed for macro cells at 2 GHz, and COST 231-Walfish-Ikegami model extending the Walfish-Ikegami model [19] was proposed for micro and small cells.

Besides, it is necessary to note that the radio propagation has different characteristics between near-field and far-field. The far-field, or Fraunhofer region, of a transmitting antenna is defined as the region beyond the Fraunhofer distance d_F, which is related to the largest linear dimension of the transmitter antenna aperture, D, and the carrier frequency, f, as follows [8]:

$$d_\mathrm{F} = \frac{2}{c} \cdot f \cdot D^2, \tag{2.1.2}$$

where c is the speed of light in vacuum. In practice, the base station antenna dimension is less than 1 meter, and personal communication wireless networks are operating on frequency bands ranging from one to four GHz. This roughly results in d_F about less than 1 to few meters. It means that personal wireless communications are in far-field.

In the far-field, i.e., $d \gg d_\mathrm{F}$, the path loss defined in (2.1.1) is commonly expressed in decibel scale by empirical models as:

$$l_\mathrm{dB}(d) = L_{0,\mathrm{dB}} + 10\beta \log_{10}(d), \tag{2.1.3}$$

where β is the path loss exponent, which practically takes values between 2 and 4, and $L_{0,\mathrm{dB}}$ is the fixed-term path loss which depends on system parameters such as operating frequency band, heights of base station antenna and of mobile station antenna.

Shadowing. Unlike the large-scale effect which depends on the transmitter-receiver spatial separation and the propagation medium, the medium- and small-scale effects are due to the relative motion of the receiver, obstacles along with the propagation path, and multi-path reception of the signal which are all subject to a high degree of randomness. Medium- and small-scale are thus often characterised by statistical models.

The medium-scale variation of the signal power is essentially due to obstacles such as buildings, vehicles, and trees which may absorb, reflect, and diffract the arriving signal. This effect is so-called *shadowing* or *slow fading*. The variation of the signal power due to the shadowing is at a scale of multiple of seconds or minutes [22]. This random phenomenon has been so far described by some statistical laws such as log-normal [7, 8, 28], Gamma [29–31], Weibull and

Nakagami [32, 33] distributions. Between these, log-normal distribution has been supported by experimental measurements [34, 35] and by a physical basis [36]. It has been the most popular model of the shadowing and commonly accepted by cellular standardisation bodies [37].

It follows that the variation of the signal power due the shadowing in decibel scale is described by a normal distribution of mean $\mu_{S,dB} = 0$ and standard deviation $\sigma_{S,dB}$. The value of $\sigma_{S,dB}$ depends closely on the deployment environment; experimental measurements showed that it ranges from 4 to 13 dB [38–41] with a typical value of 10 dB for macro and micro cell deployments [26, 27]. This is related to a representation in linear scale by a log-normal distribution of parameters (μ_S, σ_S) which has the following probability density function

$$f_S(x) = \frac{1}{x\sqrt{2\pi}\sigma_S} \exp\left(-\frac{(\log x - \mu_S)^2}{2\sigma_S^2}\right) \mathbf{1}(x > 0), \tag{2.1.4}$$

where $\mathbf{1}(\cdot)$ is the indicator function, $\mu_S = 0$, and

$$\sigma_S = \frac{\log 10}{10}\sigma_{S,dB}. \tag{2.1.5}$$

Fading. The relative motion of the receiver (i.e., mobile station) and dynamics of surrounding structures in the propagation environment cause rapid fluctuations of the signal power over small travel distance or short period of time. The small-scale effect, so-called *fast fading* or simply *fading*, is used to describe this phenomenon.

The presence of reflecting and scattering objects in the propagation medium creates multiple versions of the transmitted signal which arrive at the receiver antenna at slightly different times and amplitudes. The relative motion of the receiver compared to the transmitter and that of surrounding objects also result in random frequency modulation of the multipath components due to the Doppler effect. The signal received at the mobile station antenna is composed of a large number of plane waves having randomly distributed amplitudes, phases, and frequencies. These multipath components combine at the receiver antenna and cause fluctuations of the resulting signal power.

Statistical modelling of the fading effect was proposed by Clarke [42]. Under the assumption that amplitudes and phases of multipath components are mutually independent and that there is no dominant summand (i.e., *non-line-of-sight* propagation channel, NLOS), by the central limit theorem the amplitude and phase of the received signal are distributed according to Gaussian distributions [37]. As a result, the envelope of the received signal which is given by the square root of the sum of two quadrature Gaussian components obeys a Rayleigh distribution, which has the following probability density function

$$f_R(x) = \frac{x}{\sigma^2} \exp\left(-\frac{x^2}{2\sigma^2}\right) \mathbf{1}(x \geq 0), \tag{2.1.6}$$

where $2\sigma^2$ is the average power of the received signal [8].

When there is a dominant multipath component such as *line-of-sight* (LOS) propagation path, random multipath components are superimposed on the quasi-stationary dominant signal. The envelope of the received signal is distributed according to a Rician distribution which has the
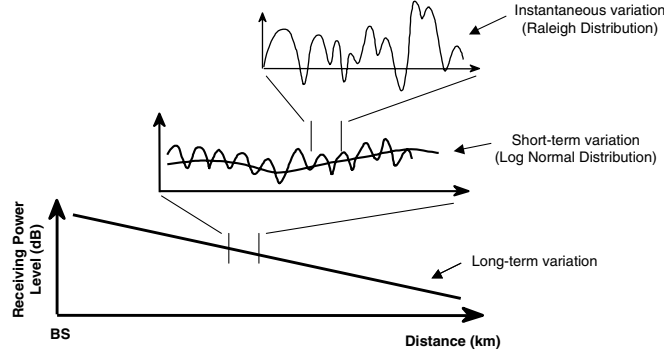
FIGURE 2.1: Propagation characteristics of wireless signal. Source: [1]

following density function [12]

$$f_R(x) = \frac{x}{\sigma^2} \exp\left(-\frac{x^2 + V^2}{2\sigma^2}\right) J_0\left(\frac{xV}{\sigma^2}\right) \mathbf{1}(x \geq 0), \tag{2.1.7}$$

where V denotes the peak amplitude of the dominant signal, and J_0 is the modified Bessel function of the first kind and zero-order, see [43, Chap. 9]. Rician distribution reduces to Rayleigh distribution when $V = 0$, i.e., NLOS.

Using the Rayleigh and Rician distributions in modelling of the fading is well supported by analytical formulation of the physical properties of the channel as described above. Though, it was not totally confirmed by all experimental measurements. The Nakagami distribution was proposed as a more general distribution which can be adjusted to fit a variety of empirical data [37].

The fluctuation of the received signal envelope due to the fading depends on the relative speed of the receiver antenna, but typically it is at order of some milliseconds in time or half of wavelength in space. This effect therefore has influence on the bit-level but not on the link budget, and it is compensated by techniques like *interleaving*, *diversity reception* [8, 44], and *frequency hopping* (in GSM [45]). In particular, this variation scale of the fading is much faster than the best interruption time of hard handover (see Chapter 4) of today's cellular technologies. For example, the Mobile WiMAX standard with the frame duration of 5 ms is subjected to a minimum handover interruption of 50 ms, WiMAX Forum [46]. Between advanced technologies which are under specification and are targeted to the IMT-Advanced family (see §3.1), LTE-Advanced targets to a handover interruption greater than 20 ms for the best case, 3GPP TS 36.133 [47], and IEEE 802.16m targets the best handover interruption delay of 30 ms for intra-frequency handover and 100ms for inter-frequency handover, IEEE 802.16m [48]. Therefore, analytical models of handover often consider that the fading is averaged out.

Received Signal Strength. To this end we have described three factors which characterise a radio propagation channel. These can be depicted in Figure 2.1 where long-term variation represents the large-scale path loss due to the spatial receiver-transmitter separation, short-term variation describes the shadowing, and instantaneous variation reflects the multi-path fading. By combining all these three components, the signal strength received by a receiver at **y** from a

transmitter i at $\mathbf{x}_i$ can be commonly described in linear scale as follows

$$P_i(\mathbf{y}) = \frac{AX_i}{l(|\mathbf{y} - \mathbf{x}_i|)}, \tag{2.1.8}$$

where A is a constant which is related to the transmission power $P_{\text{tx,dB}}$ and the fixed-term path loss $L_{0,\text{dB}}$ which are expressed in decibel scale as follows

$$10\log_{10} A = P_{\text{tx,dB}} - L_{0,\text{dB}}. \tag{2.1.9}$$

The random variables $(X_i, i = 1, 2, \ldots)$ refer to either the shadowing, or fading, or combining shadowing-fading effect. And the typical far-field model of l is given by (2.1.3) as

$$l(|\mathbf{y} - \mathbf{x}|) = |\mathbf{y} - \mathbf{x}|^\beta. \tag{2.1.10}$$

In the literature we can also find the following notation

$$p_i := AX_i, \tag{2.1.11}$$

which is sometime called *"virtual transmission power"* [49] for merits that this is independent of the transmitter-receiver spatial separation, and that the effects of shadowing and/or fading can be taken into account by considering random transmission powers. It follows that, the received signal strength given by (2.1.8) can be slightly generalised as follows

$$P_i(\mathbf{y}) = \frac{p_i}{l(|\mathbf{y} - \mathbf{x}_i|)}. \tag{2.1.12}$$

2.2 Interference and Noise

A communication network is normally composed of a large number of communicating nodes. Such a situation introduces interference which is generated when multiple nodes are transmitting on the same frequency. Theoretically, the interference may increase or decrease the power of the useful signal as a result of a superposition of multiple waves having the same frequency. However, in most of the cases it is a noisy source to the useful signal.

The interference also occurs when nodes transmit on adjacent frequency bands, and it is so-called *adjacent-channel interference* to distinguish with the *co-channel interference* or simply *interference* which is described above. The adjacent-channel interference is basically due to imperfection in the reception devices, and it can be minimised by keeping the frequency separation between channels as large as possible [50]. Practically, the adjacent-channel interference is almost negligible compared to the co-channel interference.

The interference power is thus the sum of the signal powers received from all transmitters which share the same frequency with the transmitter of interest, and excluding the signal power of the latter.

The thermal noise is due to the intrinsic thermal generation property of electronic devices and ambient temperature. It is usually modelled as Additive White Gaussian Noise (AWGN) and is characterised by average noise power N_0. The thermal generation of the reception device is

characterised by *noise figure*, N_F, [51] which is about 9 dB for the mobile handset [26, 27, 52]. The average thermal noise power is given by [8, Appd. B]:

$$N_0 = k_\text{B} T_0 \times W \times N_\text{F}, \tag{2.2.1}$$

where W is the equivalent bandwidth of the device, k_B is Boltzmann's constant given by 1.38×10^{-23} Joules/Kelvin, and T_0 is the ambient temperature which is typically taken as 290 Kelvins. In wireless network specifications, we find back this value of the factor $k_\text{B} T_0$ which is referred to as *thermal noise density* taken as -174 dBm/Hz [27, 52]. This allows to consider that the average thermal noise power is constant.

2.3   Signal Quality

Since the radio propagation is of broadcasting nature, the quality of the wireless communication channel in a wireless network composed of many nodes is strongly constrained by the interference and the background thermal noise of the receiver antenna. To take these impairments into account, the *signal-to-interference-plus-noise ratio* (SINR) is used as a basic metric for the description of the *signal quality*. As its name indicates, SINR is the ratio of the received signal power over that of the interference caused by other nodes plus the thermal noise power. In wireless networks, especially in cellular networks, the information about the SINR of the communication link between a mobile station and its serving base station is the basis of many important network control mechanisms such as *cell selection*, *handover decision making*, and *scheduling*.

Let Ω_k be the set of all nodes sharing a common frequency band k. The signal quality Q_i expressed in term of the SINR received at $\mathbf{y}$ from node $i \in \Omega_k$ is thus given by

$$Q_i(\mathbf{y}) = \frac{P_i(\mathbf{y})}{N_0 + \sum_{j \in \Omega_k, j \neq i} P_j(\mathbf{y})}, \quad \text{for } i \in \Omega_k. \tag{2.3.1}$$

For notational simplicity, consider

$$A := A/N_0. \tag{2.3.2}$$

Then

$$Q_i(\mathbf{y}) = \frac{P_i(\mathbf{y})}{1 + \sum_{j \neq i, j \in \Omega} P_j(\mathbf{y})}, \quad \text{for } i \in \Omega_k. \tag{2.3.3}$$

2.4   Literature Review

The literature on wireless link modelling has mainly focused on network interference modelling.

The modelling of the network interference plays an important role in numerous problems of network analysis and design such as capacity and outage analysis, modulation adaptation, and the design of interference mitigation techniques. It has been so far one of the biggest concerns of wireless networking with very rich prior arts. It can be summarised in some major approaches. By considering the interference as a sum of a large number of random signal strengths, the first approach uses the central limit theorem to model the interference by a Gaussian distribution. Viterbi [53], Habbab et al. [54], Cheng and Beaulieu [55], Beaulieu and Abu-Dayya [56] are some examples of this approach. The second approach including Jones and Skellern [57], Santucci et al.

[58], Cho and Hong [59], Tsai [60] consider lognormal shadowing and deterministic distances to interfering nodes. The interference as a sum of lognormal random variables is approximated by a lognormal distribution by using different approximation methods, see e.g. Fenton [61], Schwartz and Yeh [62], Beaulieu and Xie [63], Wu et al. [64]. The third approach proposed mathematical models for the impulsive interference including the Gaussian-mixture model such as in Trunk and George [65], Trunk [66], Ilow et al. [67], and the stable model such as in Shao and Nikias [68], Nikias and Shao [69], Ilow and Hatzinakos [70], Yang and Petropulu [71]. A recent major approach models the interference from the perspective of a shot noise and develops exact mathematical results for it. This includes Baccelli and Blaszczyszyn [49, 72], Haenggi and Ganti [73], Win et al. [9], Fontana [74], Salbaroli and Zanella [75], Inaltekin et al. [76].

Unlike the interference, according to our bibliography research there has been no work investing the mathematical modelling of the best signal quality in a wireless network despite its important implication in many applications and network design.

2.5 Summary

The macroscopic variation of the radio signal amplitude is described by three multiplicative components including path loss, shadowing, and fading. The path loss is commonly formulated as a decaying power-law of the spatial separation between the receiver and transmitter. The shadowing introduces medium-scale variations of the signal power and is often described by a lognormal distribution. The fading characterises the multipath reception of the transmitted signal, it causes fluctuations of the received signal power at a scale of order of some milliseconds.

The signal degradation due co-channel transmissions is described by the interference, while the variation due to intrinsic thermal noise at the electronic device is described as a Additive White Gaussian Noise of constant spectral density. Finally, the signal quality is expressed in term of the signal-to-interference-plus-noise ratio (SINR).

The literature on wireless link modelling has mainly focused on network interference. Whereas, there has been no investigation on the best signal quality.

Chapter 3

Cellular Networks

3.1 Historical Background

First deployments of wireless networks on the world dates back to the 1920s. These systems used one big base station operating on the whole allocated spectrum to provide the service coverage for a city-wide area. Due to the interference constraint, the network was only able to handle a small number of simultaneous calls over a wide geographic region. As a result, the wireless phone call was a really luxury service. In addition, the long distance between a user to the base station was also a constraint. It required high transmission power of the user's device, and resulted in quick drain of the device battery.

The cellular network architecture was invented and efficiently solved the above limitations. As we know, the distance-dependent pathloss is the dominant factor in the power attenuation of the transmitted signal, see Chapter 2. The interference can be reduced if two co-channel base stations are spatially separated enough. That is the logic behind cellular system concept invented in 1947 by Douglas H. Ring, an engineer of Bell Labs. In his memoranda [77], he suggested that the wireless network deployment should use a number of smaller base stations instead of only one big base station in order to provide a wide range mobile service. As such, each base station transmits with lower power and provides sufficient service coverage in a radio cell. To reduce the interference, the allocated frequency spectrum should be reused among cells but not in adjacent cells as it is illustrated in Figure 3.1.

The promise behind the cellular network design is thus the frequency reuse between spatially separated base stations. But on the other hand, as it splits the coverage area into radio cells, it requires a system to handover the call automatically without interruption when the user moves across cells during a conversation. Until the early 1970s, Amos E. Joel Jr, a Bell Labs engineer, invented a concept for automatic call handover in mobile cellular networks [78]. The cellular concept and automatic call handover, as well as some other technical developments invented during this time formed the mobile cellular system as we know today.

The First Generation (1G) of mobile cellular systems was successfully deployed mostly in the 1980s. The first commercial automated 1G cellular network was launched in Japan by Nippon Telegraph and Telephone (NTT) in 1979. After that, the next cellular network to be deployed was the Nordic Mobile Telephone (NMT) system in Denmark, Finland, Norway and Sweden in

(a) Pre-cellular deployment   (b) Cellular deployment
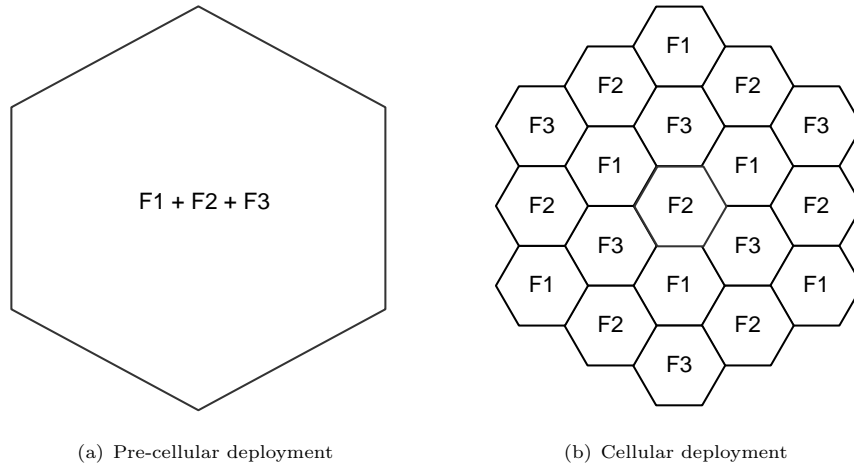
FIGURE 3.1: Cellular concept.

1981. In the United States, AT&T commercially launched its Advanced Mobile Phone System (AMPS) in 1983. Later, in the United Kingdom, the first mobile call was realised by Vodafone in January 1st 1985 [79]. In continental Europe, C-Netz was officially launched in Germany in 1985 while Radiocom2000 was deployed in France in 1986. All the 1G cellular networks used analog transmission for traffic channels while some of them such as Radiocom2000 used digital signaling transmission.

In the early 1990s, we observed the emergence of the Second Generation (2G). It differed from the 1G by using the digital transmission and by broader standardisation processes. There are four main standards of 2G on the world including European Global System for Mobile (GSM) communications and its derivatives, Digital AMPS (D-AMPS) in the United States which is a digital version of the 1G analog AMPS, Interim Standard 95 (IS-95) which was developed by Qualcomm and was later branded as cdmaOne, and Personal Digital Cellular (PDC) in Japan [80]. Between 2G standards, GSM was widely adopted almost over the world, its first deployment was in Finland in 1991 and has been so far the most successful 2G system. It is known that the open standardisation was responsible for its initial success. This has enabled GSM to be further enhanced and developed without becoming incompatible with existing products [81].

Although the 2G systems was more broadly standardised with the participation of more countries than 1G systems, there was a lack of a global consensus between standards. As a results, different standards use different technologies for physical layer, and operate on different spectrums. This led to the incompatibility problem between systems and the international roaming was not always possible in 2G. In term of services, the 2G systems provide essentially voice call with transmission throughput as low as tens of kilo bits per second. Other low data rate services were also supported such as Short Message Service (SMS).

The 2G standards then followed different paths to gradually evolve in order to support higher data rates such as email, Internet access, and multimedia messaging (MMS). The evolved 2G systems for higher data rates were collectively referred to 2.5G as a transitional generation to later 3G. Between these, GSM was evolved to General Packet Radio Services (GPRS), and then to Enhanced Data Rates for GSM Evolution (EDGE). By using Adaptive Modulation and Coding (AMC) and eight-phase shift keying (8PSK) coding scheme, EDGE is able to provide

maximum data rates theoretically as high as 384 Kbps. The cdmaOne was upgraded to 2.5G with CDMA2000 1xRTT which can also provide theoretically 384 Kbps data rate [80]. The Japanese Personal Digital Cellular (PDC) has also evolved to packet data network (PDC-P) to provide faster data connections. NTT DoCoMo developed a data service called *i-mode* which provides a good platform for wireless e-mail service.

The cellular systems continued to evolve to the Third Generation standards which provide better data services by using packet-switched mode co-existing with the circuit-switched mode of previous generations. The evolution to 3G was apparently more bustling with a worldwide regulation level. It was initiated with the standardisation work for the next-generation system by the European Telecommunications Standards Institute (ETSI) in the same year that GSM was commercially launched [81]. This new system is called the Universal Mobile Telecommunications System (UMTS). It composes of Universal Terrestrial Radio Access (UTRA) radio interface, and core network evolved from GSM/GPRS core Mobile Application Part (MAP). After the initiative of the ETSI, numerous 3G programs were also launched in the United States, Japan, and Korea to evolve their systems to 3G.

Taking into account the interoperability issue of 2G standards, the initial objective assigned to 3G standardisation process was to define only one truly global 3G standard. This goal was finally far from reality due to multiple technical, local regulation, and political reasons. There were many concurrent proposals for 3G system; and the International Telecommunication Union (ITU) indeed specified a set of requirements for a 3G family. This is called International Mobile Telecommunications-2000 (IMT-2000) in which the number 2000 refers to year 2000. The requirements are specified for the entire end-to-end functionality of a member of IMT-2000 family, i.e. including those for terminal, radio interface, radio access network, core network, and inter-networking aspects. It is given in ITU-T Recommendation Q.1701 [82]. Some highlighted requirements for IMT-2000 terrestrial mobile systems are summarised below:

- **Services**: support both circuit-switched and packet-switched modes for enhanced voice service and various packet services.
- **Data rate**: at least 144 Kbps everywhere to 2048 Mbps in indoor office radio environment.
- **Handover**: support intra-system handover with high user's speed.
- **Interoperability**: compatible and roaming among systems of IMT-2000 family using a single subscription.
- **Support and use** capabilities and services of existing 2G systems, and be open for further enhancements.

After the requirements were defined, there were as many as 15 proposals worldwide of which about ten were for terrestrial mobile systems and the other five were for satellite communication [81]. Proposals were evaluated by the ITU. The selected candidates were classified into first five categories given in Table 3.1. In 2007, the radio interface which is based on the IEEE 802.16e standard was added to IMT-2000 [83]. It is officially known under the name OFDMA TDD WMAN as part of ITU-R M.1457 Recommendation [84]. However, WiMAX was not branded as 3G but it has been intended and has evolved to become a 4G system.

Core networks (CN) also followed the same evaluation path as radio standards did. At the beginning, two (end-to-end) systems were adopted for IMT-2000 family, those are UMTS and CDMA2000 [85]. And after OFDMA TDD WMAN radio interface was added to IMT-2000,

TABLE 3.1: Terrestrial Radio Standards of IMT-2000 Family

Full Name	Common Names
Direct Spread (DS) CDMA	WCDMA (UTRA FDD)
Multi-Carrier (MC) CDMA	CDMA2000 1x and 3x CDMA2000 1x EV-DO CDMA2000 1xEV-DV
TDD CDMA (TD-SCDMA)	UTRA TDD 3.84 Mcps UTRA TDD 1.28 Mcps
Single-Carrier (SC) TDMA	UWC-136 (EDGE)
FDMA/TDMA (freq-time)	DECT
OFDMA TDD WMAN	WiMAX

TABLE 3.2: Terrestrial Mobile Systems of IMT-2000 Family

System	Radio	Core	Spec
UMTS	DS CDMA TDD CDMA SC TDMA	GSM evolved UMTS CN	3GPP
CDMA2000	MC CDMA	ANSI-41 evolved CN	3GPP2
WiMAX	OFDMA WMAN	WiMAX CN	WiMAX Forum

WiMAX became a third member of 3G system. Based on the requirements defined by the ITU, the 3rd Generation Partnership Project (3GPP) has taken over the standardisation for the UMTS system. The CDMA2000 system is an evolution of cdmaOne standard, and its standardisation has been developed by the 3rd Generation Partnership Project 2 (3GPP2). The WiMAX Forum has been developing the end-to-end WiMAX system, see Table 3.2.

The first commercial 3G system was launched by NTT DoCoMo in Japan in 2001. That was the WCDMA technology branded FOMA. The second network to be commercially launched was the 1xEV-DO technology by SK Telecom in South Korea in 2002.

All the IMT-2000 compliant system standards have been evolved to provide even higher performance, more services, and better spectrum efficiency. The radio access network of UMTS has been evolved to Evolved UTRAN (EUTRAN) which is branded as Long Term Evolution (LTE). In parallel, the UMTS core network has been evolved to System Architecture Evolution (SAE) at the beginning, and it was later changed to Evolved Packet Core (EPC). EUTRAN as the radio interface and EPC as the core network formed a new all-IP system called Evolved Packet System (EPS) of UMTS.

Standardisation bodies and service providers initially considered LTE and WiMAX as 4th Generation (4G) radio standards. But first releases of these two candidates (i.e. 3GPP LTE Release 8 and WiMAX based on IEEE 802.16e radio interface) did not fulfill the ITU 4G requirements. They are classified as pre-4G or 3.9G radio standards. Similar to the standardisation process for 3G, the ITU set up IMT-Advanced family as technical requirements and evaluation processes for 4G. Some highlighted requirements of IMT-Advanced specified in ITU-R Recommendation M.2134 [86] include:

- **All-IP** architecture and Provide ubiquitous access.
- **Higher spectral efficiencies**: peak 15 bit/s/Hz in the downlink, and 6.75 bit/s/Hz in the uplink.
- **High peak data rates**: peak downlink speed at 100 Mbps for high mobility communication and 1 Gbps for low mobility communication.
- **Scalable channel bandwidth**: between 5 and 20 MHz, optionally up to 40 MHz.
- **Lower latencies** to enable new delay-sensitive applications (interruption time of intra-frequency handover is 27.5 ms, and of inter-band handover is 60 ms).
- **High mobility support**: support high speed vehicular up to 350 km/h. Provide optimized system performance for low mobility environments. Provide global roaming capabilities.
- **Improved cell-edge performance** and support for larger cell sizes.
- **Low-cost and low-complexity** terminals for worldwide use.

By the ITU submission deadline on October 7th 2009, two candidates submitted to IMT-Advanced were 3GPP LTE-Advanced and IEEE WirelessMAN-Advanced which are both actually under development. LTE-Advanced is being standarised by 3GPP as a major improvement of LTE under Release 10. It is targeted to reach and surpass the IMT-Advanced requirements. Its key performance features include peak spectrum efficiency of 30 bit/s/Hz in downlink and 15 bit/s/Hz in uplink, peak data rates of 1 Gbps in downlink and 500 Mbps in uplink. WirelessMAN-Advanced is an evolution of Mobile WiMAX by the IEEE 602.18m standard for radio interface.

3.2 Technical Description

Like any communication network, the ultimate objective of the cellular network is to provide the end-user with reliable communication services. It is designed to have an abstract end-to-end architecture composed of a radio access network (RAN) and a core network as given in Figure 3.2. The core network provides all services to the end-users including connection to other networks, while the radio access network *relays* the communication channels between the end-user and the core network over the radio interface. RAN is implemented with the cellular concept that we have seen in §3.1. It is basically made up of base stations, and eventually other network elements depending on technology. The radio access network deals with all the characteristics of wireless communication while the core network is a wired-line network.
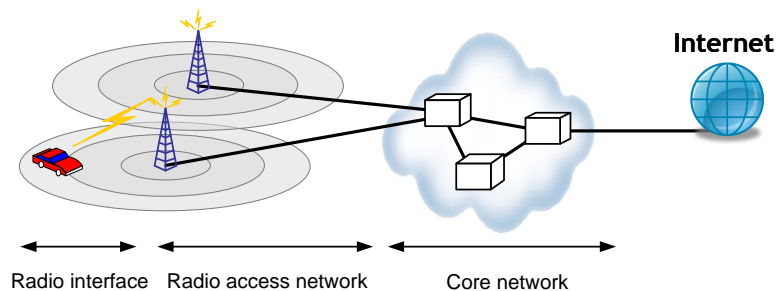
FIGURE 3.2: Cellular network

Within the scope of the thesis, we restrict our interest here is to basic technical aspects of the radio access network. In what follows, we begin with a description on how the radio resource is shared within the network, and how the cellular network is practically deployed, then we explain the protocol stack of the radio access network which ensures the reliable radio communication in coping with the dynamics of a mobile radio environment.

3.2.1   Radio resource sharing

The constraint that the interference occurs when a common radio resource is concurrently used by multiple transmitters leads to the need for radio resource sharing in cellular networks. It follows that each group having concurrent transmissions requires an appropriate sharing rule. We have therefore *frequency reuse* among cells, *duplexing* between downlink and uplink transmissions, and *multiple access* between mobile stations.

Frequency reuse.   The cellular network reallocates a spectrum bandwidth among cells in order to increase the network capacity. However, this introduces co-channel interference between cells. The frequency plannification is required to find a tradeoff of these two factors. It follows that, the entire allocated spectrum is split into N channels. The N channels are then allocated to each cluster of K contiguous cells such that no channel is allocated to more than one cell in one cluster. The entire allocated spectrum of N channels is reused over clusters of cells to cover the whole deployed area. This frequency planification is characterised by two parameters: reuse distance, and reuse factor. The *reuse distance* is the distance between two base stations which belong to two adjacent clusters and are allocated the same frequency channels. Using the homogeneous hexagonal topology of cellular deployment, the reuse distance is given as

$$D = R\sqrt{3K}$$

with R denoting cell radius [3]. The *reuse factor* is the rate at which the same frequency is reused in the network, and so equal to $1/K$ (some book defines as K).

Using small cluster size increases the frequency reuse factor, and hence increases the network capacity in term of number of simultaneous calls which can be handled by the network (i.e. Erlang traffic offer). However, this decreases D and so increases the co-channel interference, which results in poorer call quality. In GSM, the reuse factor is typically taken at 1/3, 1/4, 1/7, 1/9 and 1/12. In other radio standards which are able to better avoid co-channel interference such as CDMA and OFDMA (see later), the network can be deployed with a reuse factor equal to 1.

Duplexing.   The two-way communication between the mobile station and the base station also requires transmission coordination to avoid the interference. This is called *duplexing*. Two common duplexing techniques are *time-division duplex* (TDD) and *frequency-division duplex* (FDD). In TDD, the downlink and the uplink transmissions occur interlacedly in time and on the same frequency band. In FDD, both downlink and uplink transmissions use the whole time axis but they are allocated to separated frequency bands. Some system allows dynamic allocation of the resource between downlink and uplink (i.e. portion of transmission time in TDD, and portion of frequency band in FDD) to adapt to the asymmetric traffic between them.

Multiple access. Above we talked about the concepts used to avoid interference between cells, and between downlink and uplink transmissions. But note that the interference can also occur between mobile stations when they simultaneously communicate with the same base station. The transmission medium must be shared between mobile stations in such a way that there is no collision among transmission channels. This is done by using *multiple access* techniques. Multiple access techniques are hence fundamental of radio access technologies.

Two basic multiple access techniques are *Time-Division Multiple Access* (TDMA), and *Frequency-Division Multiple Access* (FDMA). In FDMA, the frequency bandwidth allocated to a cell is divided into a number of non-overlapping frequency carriers. Transmission channels between different mobile stations with the base station are assigned to different frequency carriers. In TDMA, each constant period of time is divided into a number of non-overlapping time slots. Mobile station-base station transmission channels are assigned to different time slots. For example, GSM standard uses FDMA × TDMA as multiple access. In this scheme, the total allocated spectrum is divided in frequency carriers of bandwidth 200 kHz. Then for each frequency carrier, each time period of 4.6152 milliseconds is divided into eight time slots of 0.5769 milliseconds. The minimum resource allocation in GSM is then 200 kHz times one slot [45].

A more advanced multiple access technique is *Code-Division Multiple Access* (CDMA). In this multiple access technique, the transmission channel between a mobile station and the base station is spread with a code. To briefly describe, the spreading code is composed of N_c pulses (also called *chip*s). For spreading purpose, the pulse duration of a chip T_c is smaller than that of a data bit T_b. The original data stream is then affected a XOR operation with the spreading code to produce a higher rate stream of chips. The ratio $T_b/T_c > 1$ is called spreadings factor. Roughly speaking, to transmit an original data stream of N_b bits, the system now needs to transmit a spread stream containing $N_c = N_b \times (T_b/T_c) > N_b$ chips. The orthogonality between transmission channels are ensured by the orthogonality between spreading codes. The same technique is also used to distinguish among cells such that each cell is assigned a spreading code which is orthogonal to the codes used for adjacent cells. Therefore, CDMA-based radio interface allow maximum frequency reuse factor equal to 1, i.e. each cell is allocated the total available spectrum. However, note that the transmission efficiency is not 100% due to the spreading effect which is determined by the spreading factor.

Another sophisticated multiple access scheme is *Orthogonal Frequency-Division Multiple Access* (OFDMA). It is a based on the Orthogonal Frequency-Division Multiplexing (OFDM). In OFDM, the total frequency band is divided into a number N narrow subcarriers with constant subcarrier frequency spacing. The serial stream of bits is mapped to N parallel sub-streams of lower data rate, i.e. equal to $1/N$ of the original bit rate. After that, a Discrete Fourier Transform (DFT) of size N will map the nth parallel sub-stream on nth subcarrier, for $n = 1, \ldots, N$. The DFT provides necessary condition so that the signals transmitted on subcarriers are *orthogonal*. In practical implementation, Fast Fourier Transform (FFT) and Inverse Fast Fourier Transform (IFFT) are used as algorithms for the computation of DFT and inverse DFT. In practice, N is a power of 2 and often takes large values, e.g. 512, 1024, or 2048, to increase the symbol time which better protects against channel delay spread. To implement OFDMA using OFDM, subcarriers are grouped into a number of subchannels, for example 48 channels in WiMAX [87, §8.4]. The transmission resource is represented as a grid of subchannels and time symbols. Then the multiple access is done by allocating resource units of this grid to users.
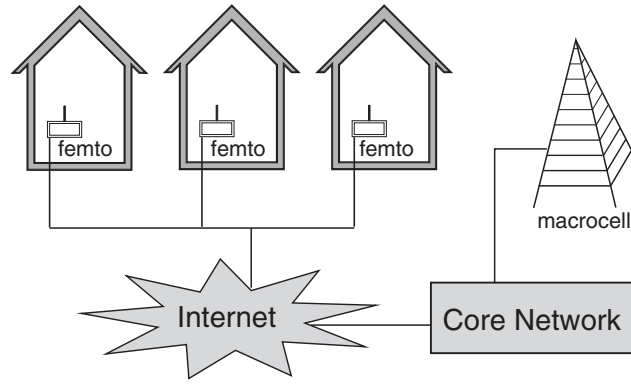
FIGURE 3.3: Typical deployment scenario of femtocell. Source [2, Fig 1.1]

3.2.2 Cellular deployment

In addition to the cluster size K, the cell size R is also a parameter which can be tuned to adjust the spectrum efficiency. If assume that with N frequency channels the network can handle M calls simultaneously per cluster. The network capacity is then proportional to $M/(K \times R^2)$ taken unit in number of calls per square kilometre. As a result, reducing the cell size R will increase the spatial reuse of the spectrum and increases the network capacity. However, this decreases the frequency reuse distance D leading to an increase in co-channel interference. And thus the network capacity in term of Shannon's capacity per square kilometre is reduced. Another important factor to be considered is the handover. The smaller cell size is, the more frequent mobile users move across cells, leading to short cell residence time and more handover executions. This requires fast handover protocol which is a big challenge to cellular technologies.

Therefore, there have been different network deployments using different cell sizes to the best adapt to the traffic demand. For regions with sparse population like rural areas, the traffic demand per square kilometre is low. Large cell sizes should be used in order to reduce the interference as well as to reduce the network infrastructure cost. Cellular networks with large cell size are called macro cell network (or macro-cellular network). With the same logic, there are micro cell networks and pico cell networks (also called small cell networks). Micro cell networks are often deployed in more dense traffic areas like suburban or urban areas, while pico cell networks are deployed in city centers or in commercial centres where there is high traffic demand. Terms "macro", "micro", and "pico" are employed to intuitively describe the order of cell sizes. The radius of macro cells is of order of kilometres, micro cell is of several hundred metres, while the radius of pico cells is about one hundred metres.

Indoor coverage is also a big concern of cellular deployment. Indoor environment is characterised by high power penetration due to buildings and walls. Using outdoor base stations to cover indoor is not efficient, and it drains the terminal's battery more quickly since the latter needs to transmits with high power to compensate the penetration loss. For this reason, the femtocell concept was first studied by Bell Labs in 1999 [2]. Femtocell, also known as "home base station", is a very small version of base station to be installed in house and in office. Femtocell access point can be installed by end-user and it is connected to the operator network via residential Internet link, e.g. DSL or optical fibre. Typical deployment of femtocell is given in Figure 3.3.
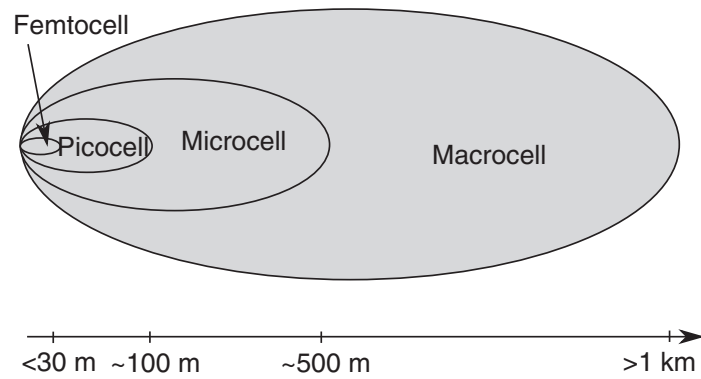
FIGURE 3.4: Cell size of different network deployments. Source [2, Fig 2.12]
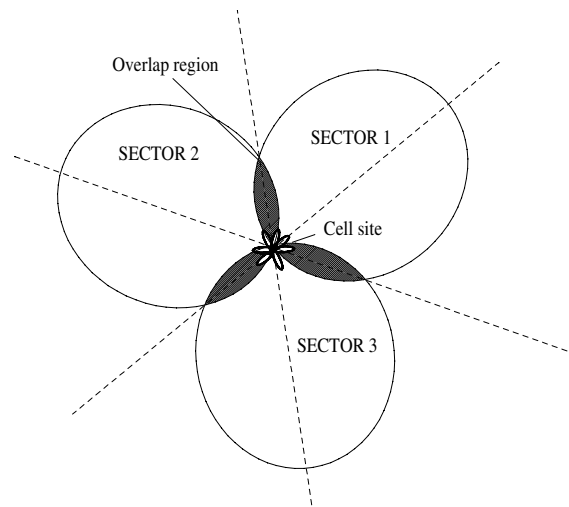
FIGURE 3.5: Cell sectorisation using three 120°-spread antennas. Source [3, Fig 1.10]

With coverage range of about ten metres, femtocell provides better indoor mobile services to the end-users. Cell sizes of different deployment scenarios are summarised in Figure 3.4.

Another cellular deployment is *distributed antenna systems* (DAS). Instead of using a big macro antenna with high transmission power, DAS uses a number of small antennas with low transmission power and spatially distributed in multi-floor or large buildings. Distributed antennas are connected to the same base station via coaxial cables or optical fibres, and they serve as extended relays of the base station in different places of the building. Therefore, the difference between DAS and a femtocell deployment is that a femtocell access point has all control functions of a normal base station, while a distributed antenna of DAS is just a relay of the base station's antenna. In DAS, no handover is required when a mobile moves among the coverage areas of antennas belonging to the same base station. Similar to femtocell, DAS can improve the indoor coverage. Besides, the signal quality near to the border of a macro cell is often very poor due to far propagation distance and other cell interference. This is referred to *cell edge* problem. This can be efficiency improved by using DAS.

The network capacity and spatial frequency reuse can be even improved by using cell sectorisation
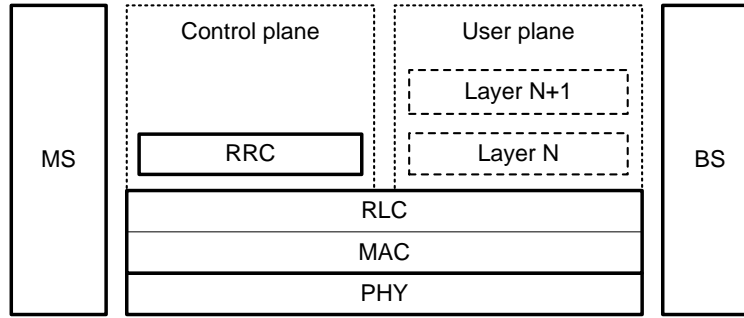
FIGURE 3.6: Protocol stack of radio access network

or using multi-antenna systems. In cell sectorisation, one cell is further divided into several sectors to increase the spatial reuse of spectrum. Cell sectorisation uses sectoral antennas with angle spread less than $360°$. The network capacity is increased with the number of sectors. The principle of cell sectorisation is thus similar to that of DAS except that sectorial antennas are installed on the base station's tower but not remote. Practical deployment often uses three $120°$-sectors, see Figure 3.5.

Adaptive Antenna Systems (AAS) are a dynamic and advanced version of cell sectorisation. In AAS, an antenna can dynamically reorient its main beam to focus on the user. This increases the spatial spectrum reuse and greatly enhance the communication quality. Another important multi-antenna system is multi-input multi-output (MIMO). It uses m transmitting antennas and n reception antennas to increase the capacity as well as to leverage the multi-path effect [22].

3.2.3 Protocol stack

It is obvious that the final objective of the network is to provide the end-user with communication services such as phone call, file up/down loading, web browsing. Whereas, due to the dynamics of the system which are reflected by a lot of random events such as the user's mobility, call arrival time, call duration, and amount of data down loaded, many control mechanisms are required to successfully support the user's services.

The data of user's services and of control mechanisms can be successfully relayed over the radio interface thanks to the fact that the base station and the mobile station agree on a common protocol for their mutual communication. Although each cellular standard has its own implementation of the communication protocol, they follow the same design philosophy which relies on a protocol stack as depicted in Figure 3.6. It is built up on layers according to the ISO (International Organization for Standardization) model. On top of this stack, the *user plane* is responsible for reliable communication of user's services, while the *control plane* is responsible for control mechanisms. These two planes are supported by the two layers at the bottom: physical (PHY) layer, and layer 2 which is divided into medium access control (MAC) and radio link control (RLC) sub-layers.

The physical layer is responsible for all the tasks which are related to the data transmission over the radio medium. The design for physical layer basically consists in defining how the radio resource is shared in the network, and how the data is physically transmitted (i.e. modulation

and coding). Duplexing techniques and Multiple access schemes described in §3.2.1 are in the scope of PHY layer.

The MAC sub-layer is responsible for coordinating access to physical medium. It handles data to be transmitted in queues, allocates available physical resource and schedules which data to be the next transmitted. Scheduling algorithms are implemented in MAC sub-layer. The MAC sub-layer also supports error correction with Hybrid Automatic Repeat Request (H-ARQ) mechanism which is a combination of Forward Error Correction (FEC) and Automatic Repeat Request (ARQ). In an ARQ scheme, the receiver uses an error-detecting code to check if the received packet contains error bits. It notifies the transmitter by ACK (if no error) and NACK (if error) messages. The transmitter will retransmit the packet if receiving a NACK. Practical implementation most often uses CRC (Cyclic Redundancy Check) for error detection, and uses Turbo code for error correction.

The RLC sub-layer is responsible for segmenting and concatenation of PDUs (Packet Data Units) received from its upper layer's. It uses ARQ mechanism to protect data transmission from errors.

As mentioned at the beginning of §3.2 that the core network provides all services to the end-user, the radio access network is completely opaque to the user plane, it just relays the user data between the mobile station and the core network. On the contrary, most of the control mechanisms are provided by the radio access network which is delegated by the base station from the viewpoint of the mobile station. The control plane contains Radio Resource Control (RRC) layer which corresponds to *networking* layer (layer 3) of the ISO referential protocol stack. This layer is responsible for efficient co-operation between multiple mobile stations and base stations to maximise the overall network performance. It includes all important control mechanisms and algorithms such as power control, cell association, and mobility management which aim at reducing the interference (between cells and between mobiles), minimising call drop due to user's mobility, and efficiently managing the mobile location (including location update and paging procedures [88]) for successful call delivery, etc.

Each standardisation body has its own implementation of the protocol stack, which results in different levels of network performance. However, by observation over generations of cellular networks, it can be seen that advances in physical layer, in particular multiple access technology with modulation and coding schemes, play a prominent role in the cellular technology evolution. In the next section, we provide a brief description of Long Term Evolution (LTE), which is one of the most recent and advanced cellular technologies with physical layer based on OFDMA technology.

3.3 Long Term Evolution (LTE) of UMTS

Long Term Evolution (LTE) is used under the Evolved UMTS Terrestrial Radio Access Network (EUTRAN) which is supported by an IP core network known as Evolved Packet Core (EPC). The entire architecture is named Evolved Packet System (EPS), previously called System Architecture Evolution (SAE). The standardisation process for LTE was started in 2004, its specification standards are summarised in Table 3.3. Currently, trial networks are being deployed by many major network operators all over the world.

TABLE 3.3: 3GPP Specification Standards for LTE

Specification	Contents
TS 36.300	Overall description
TS 36.1xy	Equipment requirements: UE, eNB, Repeater
TS 36.2xy	Physical layer
TS 36.3xy	Layers 2 and 3: MAC, RLC, and RRC
TS 36.4xy	System and architecture aspects
TS 36.5xy	Conformance testing

LTE was initially intended to be a 4G cellular radio access network. It provides an aggressive set of performance requirements while uses all-IP flatter architecture with MIMO and smart antennas as well as supports integrated femtocell deployment. It is designed to operate in wideband condition up to 20 MHz to provide high peak data throughput with 100 Mbps in downlink and 50 Mbps in uplink. LTE uses OFDMA technology for downlink to increase the spectrum efficiency and to facilitate complex system implementation, while uses SC-FDMA (Single Carrier Frequency-Division Multiple Access) for uplink to reduce the required terminal transmission power [89]. The network capacity is expected greater than 200 users per cell when operating on the common bandwidth of 5 MHz. The system is able to support a wide range of spectrum options from 1.25 MHz to 20 MHz in order to maximally leverage available spectrum gaps. Flat architecture with less network nodes provides reduced latencies, and supports full mobility up to 500 km/h without interruption to voice and real-time services.

Within the scope of the thesis, we aim at providing a comprehensive *brief* description of the system. For this purpose, we adopt a top-down approach by starting to talk about the system architecture and reference protocol models. We then describe control procedures while limiting our attention to those which are important to the thesis.

3.3.1   System Architecture

System architecture aspects are captured in 3GPP TS 36.300 [90] for EUTRAN, and in 3GPP TS 23.401 [91] and 3GPP TS 23.402 [92] for entire system architecture and functional splits. The architecture of the entire Evolved Packet System synthesised from these specification series is illustrated in Figure 3.7. It comprises Evolved UMTS Terrestrial Radio Access Networks (EUTRAN) and Evolved Packet Core (EPC). The main components of EPC include Mobility Management Entities (MME), Serving Gateways (S-GW) and Packet Data Network Gateways (PDN Gateway, also called P-GW).

The MME takes the main control function of EPC. It only operates in the control plane while is not involved in the user plane. Complete list of the functions provided by MME is specified in 3GPP TS 36.300 [90] and 3GPP TS 23.401 [91] series. Main functions of MME include:

- Mobility management: The MME is responsible for the mobility management of UEs for both active mode and idle mode. When a UE is first attached to the network, MME creates a record for this UE and sends the UE's location to the Home Subscriber Service (HSS) in the UE's home network via S6a interface. For UEs in active mode, the MME participates in control signalling of handover within EUTRAN and between EUTRAN and other 3GPP access networks (via S3 interface). For idle UEs, the MME keeps tracks of UE's Tracking
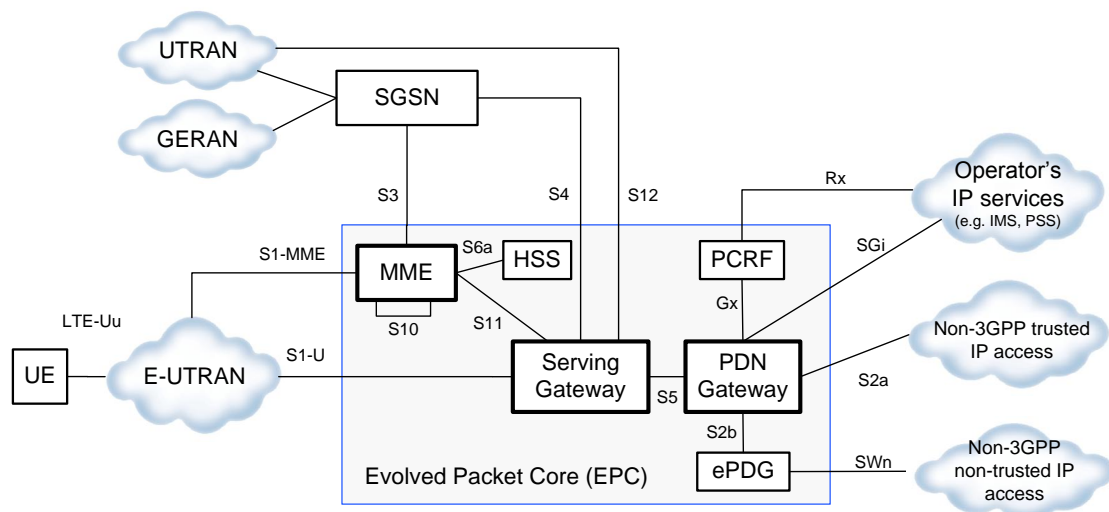
FIGURE 3.7: Evolved Packet System (EPS) architecture.

Area, and controls the Paging function when there is incoming data for idle UEs. MME also participates in the roaming function in interaction with home HSS.

- Managing bearer establishment: The MME retrieves UE's subscription profile from UE's home HHS to set up default bearer which gives the UE the IP connection. And during the UE activity, the MME is involved in the signalling control of setting up and releasing of dedicated bearer upon the request either from UE or from S-GW.

- Authentication, Authorisation, and Security: The MME initiates the authentication of a UE who registers to the network for the first time. MME compares the authentication response received from the UE with the information retrieved from the HHS in order to confirm/not confirm the authentication for the UE. The MME is also responsible for allocating each UE a temporary identity standing for the UE permanent identity.

The Serving Gateway (S-GW) mainly operates on the user plane and has very minor role in the control plane. It provides buffering, routing, and forwarding services of user data packets. There is no communication between S-GWs. At a given time, each UE is connected to only one S-GW through S1-U interface. The S-GW receives instructions from the MME through S11 interface and performs connection creation or deletion. When there is coming data for a UE in idle mode, the S-GW buffers the incoming data and notifies the MME so that the MME initiates a paging instruction to eNBs which belong to the last registered Tracking Area of the UE. During handover execution of a UE in active mode, the S-GW serves as an anchor point of data switching. S-GW connects to P-GW through S5 interface, and handles encryption of data packets as well as IP header compression. In case of inter-RAT handovers, the S-GW notifies the P-GW to change the data path to the target S-GW. S-GW also performs accounting function for inter-operator charging. More functions of S-GW are described in 3GPP TS 23.401 [91], and in 3GPP TS 23.402 [92] (for functions supporting connection with non-3GPP access networks).

Packet Data Network Gateway connects EPC to the operator's packet data network through SGi interface. It also acts as the edge router between EPC and other IP access networks. It allocates IP address to UE and performs traffic gating and filtering functions as required by the service. The P-GW sets up bearer upon request from S-GW or from Policy and Charging
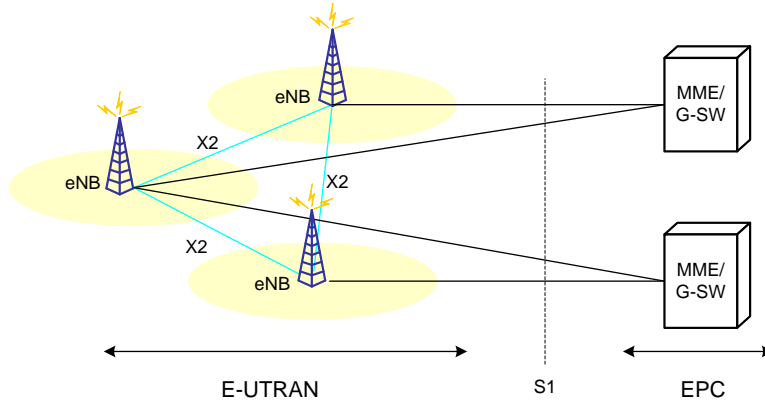
FIGURE 3.8: Evolved Universal Terrestrial Radio Access Network (EUTRAN) architecture
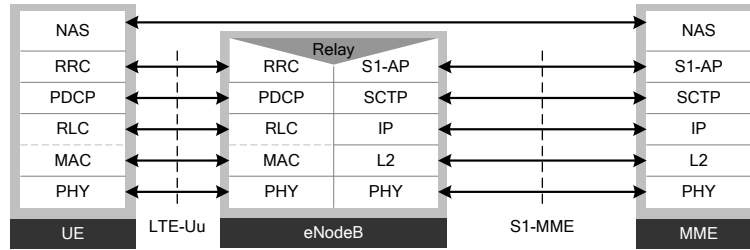
FIGURE 3.9: UE-MME Control Plane

Resource Function (PCRF). It will need to retrieve policy control information from PCRF to set up bearer when the request is from S-GW. Similar to S-GW, P-GW performs accounting function for inter-operator charging.

The EUTRAN solely comprises Evolved Nodes B (eNB) which connects to the EPC core network through S1 interface, and connect between them through X2 interface to form a mesh network, see Figure 3.8. EUTRAN uses a flat architecture in which eNB is the only network entity which provides mobile services to UE through LTE-UE interface. In particular, the function of UTRAN RNC (Radio Network Controller) in 3G 3GPP access networks are merged in to eNB. All the functions of radio access network are handled by eNB.

3.3.2 Protocol Architecture

We briefly describe the protocol architecture involving the radio interface. The control plane protocol stack is given in Fig 5.1.1.3-1 of 3GPP TS 23.401 [91], and it is shown in Figure 3.9. The Non-Access Stratum (NAS) protocol on the top of the control plane transports control signalling of MME to UEs. It is not visible to the eNodeB. The Radio Resource Control (RRC) provides the main controlling functions at the radio access interface (LTE-Uu). In addition, the Packet Data Convergence Protocol (PDCP) provides IP header compression (UP), encryption, and integrity protection (only for control plane) functions. The function of lower layers PHY, MAC, and RLC is as described in the reference model given in §3.2.3.
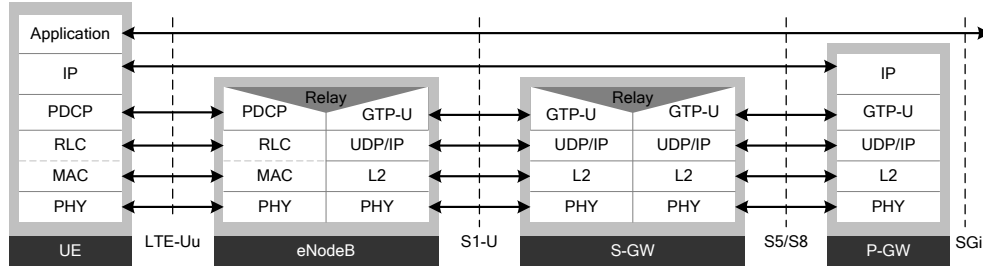
FIGURE 3.10: User Plane.

The user plane is shown in Figure 3.10 taken from Fig 5.1.2.1-1 in 3GPP TS 23.401 [91]. It reuses the same transport level of the control plane for the radio interface. The similarity between the user plane and control plane highlights the fact that the whole system is designed as a flat all-IP architecture (see, Holma and Toskala [89]). The user plane provides the user services through an IP tunnel established between UE and P-GW. Intermediate tunnels are established between relay nodes in the core network using a 3GPP-specific tunnelling protocol called the GPRS Tunnelling Protocol (GTP).

3.3.3 Downlink Physical Layer

Evolved system design provides high quality seamless mobility in LTE. Beside of flat network architecture, using only *hard* handover allows to reduce the system complexity. In LTE, the information used for handover decision is mainly provided by the UE in question. The UE follows physical layer procedures to measure necessary information which will be used by the eNodeB for handover decision making. While a more extensive description of the mobility management is provided in Chapter 4, in the sequel we describe physical layer procedures which support the mobility management function in LTE.

Frame Structure. The most basic element of any advanced development of a cellular technology is the physical layer. The OFDMA/SC-FDMA physical layer provides transmission resources available in time-frequency dimensions. This time-frequency resource is presented as a grid illustrated in Figure 3.11. In the time domain, both downlink and uplink transmissions use radio frames of 10 ms duration. Each radio frame consists of 10 subframes of 1 ms, and each subframe is divided into 2 slots of 0.5 ms. The 20 slots in a frame is numbered from 0 to 19. Further, each slot of 0.5 ms comprises seven or six OFDM symbols depending on whether normal cyclic prefix or extended cyclic prefix is configured in the cell. Longer prefix is desired to combat longer fading which can occur in large cell size or in multicell broadcast service [50]. In the frequency domain, one subcarrier has bandwidth of 15 kHz. Subcarriers are grouped in units of 12 subcarriers. The resource unit correponding to one unit of 12 subcarriers lasting for one slot is called Resource Block (RB). And one subcarrier lasting for one OFDM symbol is termed one Resource Element (RE) which is the smallest resource unit.

For Frequency Division Duplexing (FDD), the frame structure shown in Figure 3.11 is used for both downlink transmission and uplink transmission which are separated in paired radio spectrum, see Figure 3.12. This is termed frame structure of Type 1. In half-duplex FDD
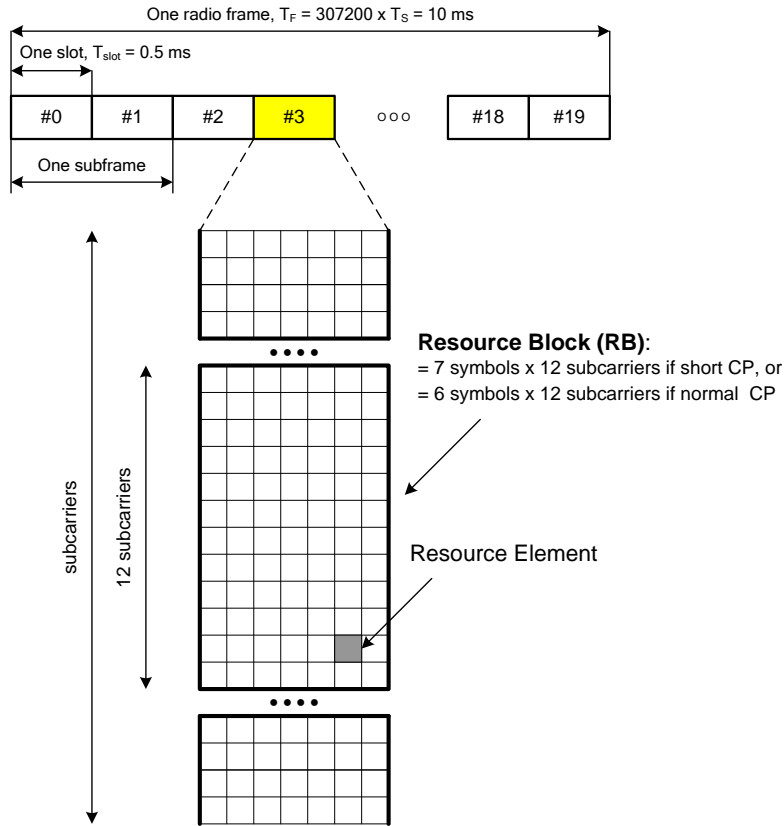
FIGURE 3.11: LTE Resource Grid
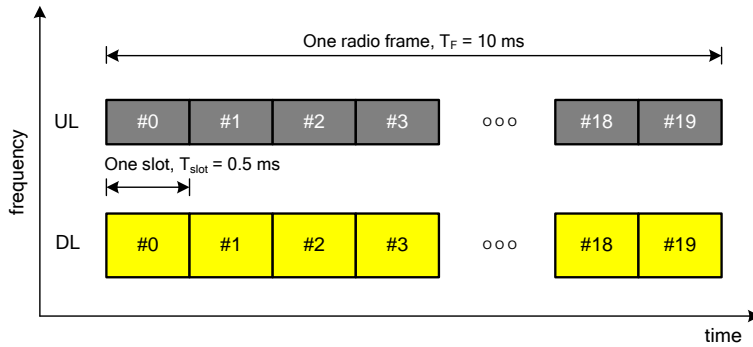
FIGURE 3.12: LTE FDD Frame Structure (Type 1)

operation, the UE is not allowed to transmit and receive at the same time while there are no such restrictions in full-duplex FDD.

For Time Division Duplexing (TDD) mode, the basic frame structure and Resource Grid remain the same, but one frame of 10 ms is organised as composing of two half-frames of 5 ms, see Figure 3.13. This allows for two downlink-uplink switching periods of 5 ms and 10 ms. This is classified as Type 2 frame structure. Only a subset of subframes is available for downlink transmission, the remaining subframes are used for uplink transmission and for special subframes. The special subframe allows for switching between downlink and uplink transmissions, and it is composed of three fields: DwPTS reserved for downlink transmission, UpPTS reserved for
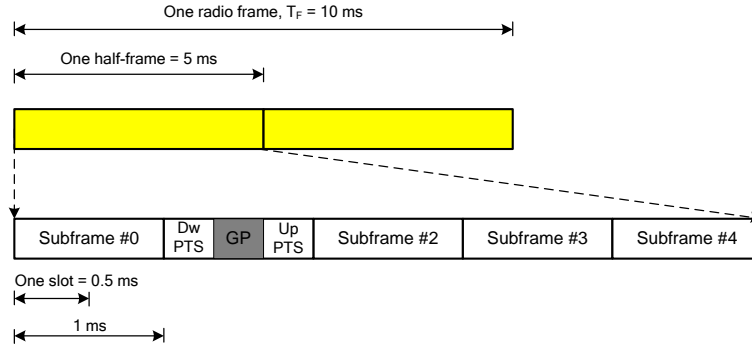
FIGURE 3.13: LTE TDD Frame Structure (Type 2). Source: Fig 4.2-1, 3GPP TS 36.211 [4]

uplink transmission, and central Guard Period (GP) which allows for the Time Advance function. Configurations available for the allocation of subframes between downlink and uplink are provided in Table 4.2-2 in 3GPP TS 36.211 [4].

Cell Search. The first step that a UE must carry out to access to the network is the *cell search*. This consists in undertaking a series of synchronisations to correctly align in time and in frequency with the cell frame structure. This allows the UE to read necessary system information parameters transmitted in the downlink, also to transmit in the uplink.

The synchronisation procedure includes three major steps. The first is symbol timing acquisition by which the UE determines the starting point of a symbol in frame structure. The second is frequency synchronisation by which the UE aligns it local oscillator with the frequency carrier structure. And third is sampling clock synchronisation.

The UE performs this three-stage synchronisation procedure either for *initial cell attachment* or for *new cell identification*. The initial cell attachment (initial synchronisation) is performed when the UE tries to access to the network (network attachment) or when it is powered on. Thereby, the UE detects a suitable cell and decodes system information required for authentication, authorisation, and registration. System information parameters are sent on physical broadcast channel (PBCH). The new cell identification is performed when the UE is already connected to a cell and in the process of detecting a neighbour cell (e.g. for handover purpose). In this case, the UE does not need to decode the basic system information, but it reads cell specific parameters and measures cell signal quality on the cell *Reference signals*.

Two physical signals are specially designed for the synchronisation in both scenarios. Those are the Primary Synchronization Signal (PSS), and the Secondary Synchronization Signal (SSS). The detection of these two signals allows for time and frequency synchronisation, as well as enables the UE to acquire the physical layer identity of the cell and the duplexing mode used in the cell. The cell search procedure with information acquisition at each synchronisation stage is summarised in Figure 3.14.

These two synchronisation signals are transmitted periodically at twice per 10 ms radio frame. The generation of sequences used for these synchronisation signals as well as their mapping to physical resource structure are described in §6.11 of [4]. The PSS is located in the last OFDM symbol of the 1st and 11th slots of each radio frame when FDD is used, and it is located in the 3rd symbol of the 3rd and 13th slots when TDD is used. Thus, acquisition of PSS allows UE first
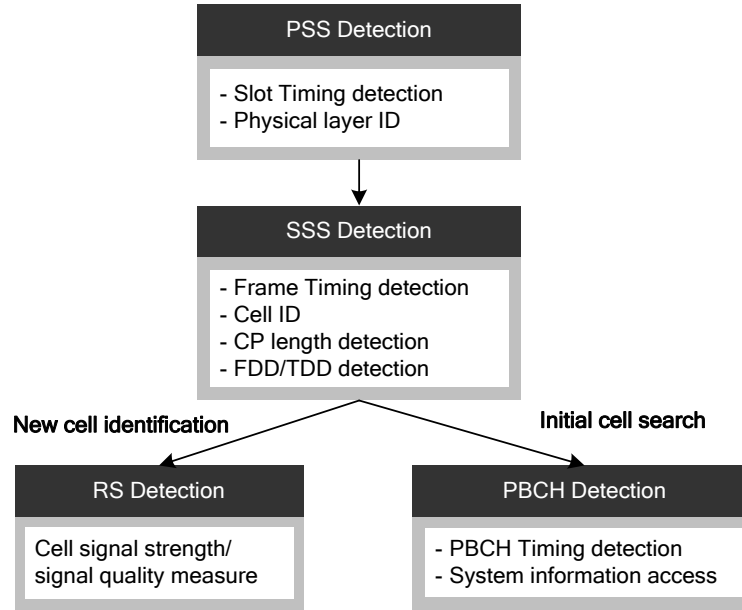
FIGURE 3.14: Cell search procedure. Source: inspired from Fig 7.1, Sesia et al. [5]

to determine the slot timing boundary. Whereas, the SSS is located in the symbol immediately preceding the PSS in FDD mode, and is located three symbols earlier in TDD mode. Thus, at the end of SSS detection, the UE is able to deduce the frame timing, the Cyclic Prefix length, and determine the duplexing mode used by the cell as well as MIMO antenna configuration. For the frequency synchonisation, the PSS and SSS are mapped to the central six Resource Blocks. This enables the UE to obtain the frequency synchronisation without any a priori knowledge of the allocated bandwidth.

In LTE, each cell is assigned two identifiers. The first is Cell Global Identifier (CGI) by which the cell is uniquely identified in the whole network. The second is Physical Cell Identifier (PCI) which is reused in the network. There are 504 PCIs in LTE which are grouped into 168 groups of three identifiers. Three PSS sequences are used to indicate the cell identity within the group, and 168 SSS sequences are used to indicate the identity of the group. Thus, at the end of SSS detection, the UE is able to determine the PCI of the cell.

Reference Signal. Once the UE identifies a cell issue from the cell search procedure, it begins to perform measurements as well as channel estimation for that cell. The downlink physical layer of LTE is designed to provide necessary physical signals for this purpose. Precisely, a number of Reference Signals are inserted in the transmitted signal of downlink from which the UE performs measurements and channel estimation of the cell (Reference signals are also available on uplink for eNodeB). In the LTE downlink, the physical OFDM which provides available resource under a two-dimensional time-frequency grid facilitates the multiplexing of Reference signals. It follows that, Reference Signals are mapped to specific Resource Elements of each slot.

There are five types of downlink reference signals specified in 3GPP TS 36.211 [4]:
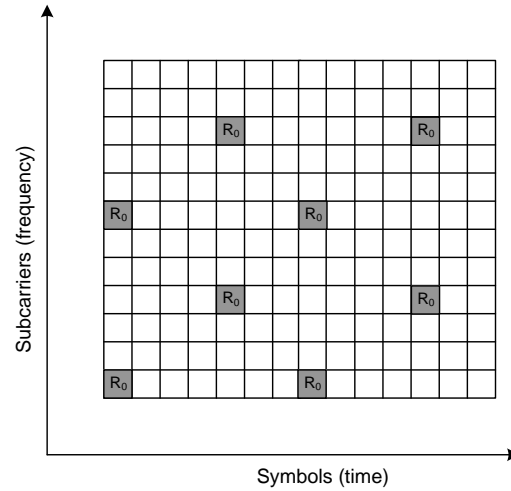
FIGURE 3.15: Mapping of cell-specific Reference Signals in case of normal CP length for one antenna port. Source: Figure 6.10.1.2-2, 3GPP TS 36.211 [4]

- Cell-specific reference signals: This is available to all UEs in the cell, and is also called Common Reference Signals (CRS). Its typical usage is for cell signal quality estimation in the handover measurement.
- UE-specific reference signals: This is only embedded to sent to specific UEs. A typical usage of the UE-specific RSs is to enable beamforming of the data transmissions [5].
- Positioning reference signals,
- MBSFN (Multimedia Broadcast multicast service Single Frequency Network) reference signals,
- CSI (Channel-State Information) reference signals.

We restrict our attention here to Cell-specific RSs. LTE maps Reference Signals in each slot (of 0.5 ms) to enable the estimation of the signal quality of neighbouring cell with low latency. More specifically, to support full mobility to high user's speeds, the mapping of cell-specific RSs to resource grid in case of normal CP length for one antenna port is shown in Figure 3.15. In the frequency domain, one RS is present every six subcarriers on a symbol which includes reference signals. On the next symbol which includes reference signals, the latter is mapped so that within each Resource Block there is one reference symbol every three subcarriers. Interpolation techniques are used for subcarriers which do not transport reference signals.

3.3.4 Radio Resource Control

The Radio Resource Control (RRC) layer is responsible for most of important functions related to the radio resource usage in the network, see §3.2.3. It involves System information broadcasting, Security activation, RRC connection control, Dedicated Radio Bearer control, and Mobility management. The RRC protocol is specified in 3GPP TS 36.331 [93] series.

The RRC connection control covers all aspects related to the (re-)establishment, modification, and release of RRC connection, including related aspects such as radio link failure detection.

As so, it is involved in the mobility management procedure which needs to establish new RRC connection in the target cell while releasing current RRC connections in the serving cell.

RRC Connection Establishment and Release. The RRC connection establishment must be carried out before the UE can obtain services with the network (through EPS bearers). The UE can only proceed the RRC connection establishment with a cell that it has identified through cell search procedure. The purpose of RRC connection establishment is to establish signalling connections which transport control information between the network and UE, and then to establish Dedicated Radio Bearers (DRBs) for the UE. In more details:

- The first stage of RRC connection establishment occurs at the radio interface within EU-TRAN. This establishes the Signalling Radio Bearer 1 (SRB1) between the eNodeB and the UE to transport RRC messages. Once SRB1 is established, the EUTRAN may eventually configure the UE to perform measurement reporting (see later).
- After that, S1 connection will be established between EUTRAN and EPC which allows EUTRAN to receive UE's context information from the EPC for security activation purpose. Note that the UE participates in the connection establishment procedure by sending required security information as well as response on the uplink.
- After the security activation procedure, EUTRAN initiates the establishment of Signalling Radio Bearer 2 (SRB2) which transports Non-Access Stratum (NAS) control messages between MME and UE on Dedicated Control Channels (DCCH). And then Data Radio Bearers (DRBs) are established.

When the UE terminates services and does not need dedicated data channels, or when there needs to switch the UE to another frequency or another cell, the RRC Connection release procedure is performed to release current control channels (SRB1, SRB2) and DRBs of the UE.

RRC state. For efficient RRC control, LTE defines two RRC states depending on the UE's activity: RRC_CONNECTED (also called *active* state) when there is active RRC connection for the UE, and RRC_IDLE (also called *idle* state) when the UE does not have RRC connection. In idle state, the UE performs cell selection and reselection for the Tracking Area update purpose, and it listens to paging messages which are sent by the network when there is incoming traffic to the UE. In the active state, the UE may perform handover procedure to select the best suitable serving cell. For the handover purpose, a number of functions are required. Those include neighbour cell measurement and measurement reporting performed by UE, and include on the other hand the configuration of reporting triggering conditions and handover decision performed by the network including the serving eNodeB.

Radio Link Failure. RRC connection may fail when the signal quality of the radio link is not sustainable due to radio impairments. A radio link failure incurs quality degradation or service loss. Since one of the main responsibility of Mobility management (precisely, handover) is to switch the UE to a new cell before a radio link failure occurs in the serving cell, it is important to know how a radio link failure occurs for the study and optimisation of handover in LTE.

A radio link failure occurs as described in Figure 3.16. LTE implements procedures enabling the detection, and recovery of a radio link failure. For the detection, the UE monitors the quality
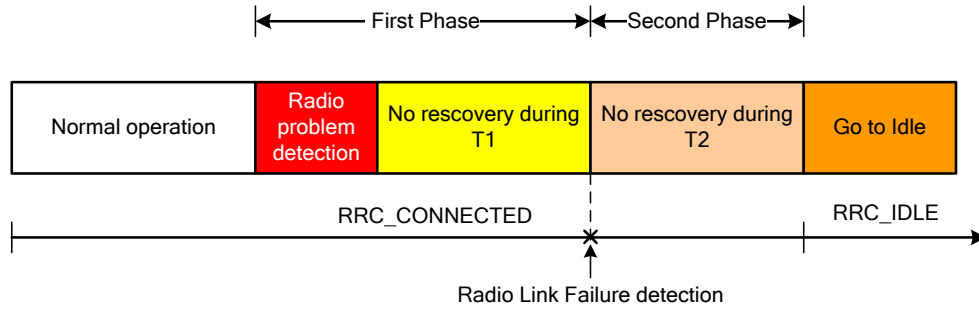
FIGURE 3.16: Radio Link Failure. Source: Figure 10.1.6-1, 3GPP TS 36.300 [6]

of its RRC connections. It is specified in [47, §7.6] that when the downlink radio link quality estimated over the last 200 ms period becomes worse than a threshold Qout, Layer 1 of the UE shall send an *out-of-sync* indication to higher layers. Upon receiving N310 consecutive "out-of-sync" indications from lower layers while neither timers T300, T301, T304, nor T311 is running (here we do not go into details of these indicators), the UE initiates timer T310. If upon either T310 expiry, or MAC random access problem, or RLC maximum number of retransmissions reached there has been no successful radio link recovery, then a radio link failure is considered to be detected, see 3GPP TS 36.331 [94].

Once a radio link failure is detected, a number of attempts are made to recover the radio link before T2 expiry. The second phase recovery (i.e. in the 2nd phase in Figure 3.16) consists in link re-establishment procedure with explicit signalling between the UE and eNodeB, (see Table 10.1.6-1 in 3GPP TS 36.331 [94]).

3.3.5 Handover

The handover procedure is used to switch UE from the serving cell to a target cell in UE's RRC_CONNECTED state. LTE only uses hard handover which allows the UE connecting to only one cell at a given time. There are handover within EUTRAN, and between EUTRAN and another radio access technology (RAT). Intra-EUTRAN handover has intra-frequency handover and inter-frequency handover. The intra-frequency handover corresponds to the case where the target cell and the serving cell operate on the same frequency, otherwise it is inter-frequency handover.

The EUTRAN decides to which cell a UE should hand over to. It provides UE with frequency list or cell list on which the UE should measure the radio signal quality. It also specifies how the UE performs measurements as well as reporting rules. We sequentially describe these functions in the sequel.

Measurement. The measurement is specified in §5.5 of 3GPP TS 36.331 [94] series. It can be summarised as illustrated in Figure 3.17. In this framework, the EUTRAN provides the measurement configuration applicable for a UE in RRC_CONNECTED state by means of dedicated signalling message `RRCConnectionReconfiguration`. The measurement configuration is thus specific to each UE, and the UE fully relies on this configuration to perform measurements.
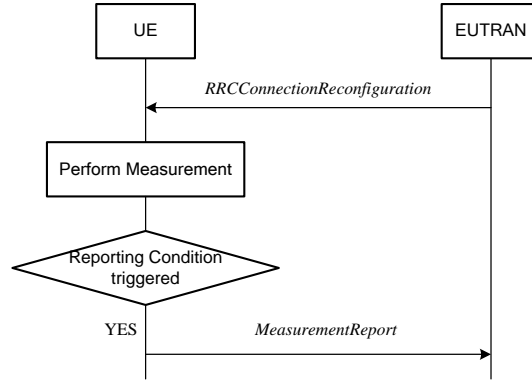
FIGURE 3.17: Measurement in LTE

The measurement configuration includes a list of Measurement Identities, given in `measIdList` parameter, of which each measurement identity links one *Measurement Object* to one *Reporting Configuration*. A measurement object can be a single EUTRA carrier frequency, or an explicit cell. A Reporting Configuration consists of a Reporting Criterion and a Reporting Format. The reporting criterion decides when the UE must send a measurement report, it can be periodic or event triggered. The reporting format indicates the quantities that the UE includes in the measurement report and associated information. The EUTRAN may specify measurement gaps in the measurement configuration to allow UE measuring cells of other frequency of other RAT.

The UE measures the signal quality of a cell on cell's Common Reference Signals (CRS). The UE first needs to perform the cell search procedure corresponding to the new cell identification scenario described before. Thanks to the specially designed procedures for Cell Search and Reference Signals, EUTRAN may only specify frequencies from which UE can identify cells and measure without need of more precise cell information.

From time to time, the EUTRAN may update the measurement configuration by sending parameters such as `measIdToRemoveList`, or `measIdToAddModList` to remove or add measure identities. The UE shall modify the current measurement configuration upon reception of this information.

The measurement configuration may have impacts on the mobility robustness. For instance, a lack of some measurement object may cause handover failure due to no suitable target cell found. It also needs to take into account the load balancing issue such that highly loaded cells should be removed from the `measIdList` or should be included in the *black list*. However, as the LTE network is assumed to operate with high frequency reuses, e.g., reuse 1, and UEs are assumed to be able to measure all intra-frequency cells, the optimisation of `measIdList` should be less critical than that for other cellular networks like GSM, WiMAX.

Seven trigger events are specified in 3GPP TS 36.331 [94] and are summarised in Table 3.4. Five events A1 to A5 are used for intra-EUTRA measurement, and two events B1 and B2 are used for inter-RAT measurement.

Layer 3 filtering model is applied for time averaging of measurements, it is defined by the following formula:

$$R_n = (1-a)R_{n-1} + a\,m_n,$$

TABLE 3.4: Trigger Events for Measurement Reporting in LTE

Event	Description
Event A1	Serving becomes better than threshold
Event A2	Serving becomes worse than threshold
Event A3	Neighbour becomes *offset* better than serving
Event A4	Neighbour becomes better than threshold
Event A5	Serving becomes worse than threshold1 and neighbour becomes better than threshold2
Event B1	Inter-RAT neighbour becomes better than threshold
Event B2	Serving becomes worse than threshold1 and inter-RAT neighbour becomes better than threshold2

where R_n is the resulting filtered measurement in the current *measurement moment n*, R_{n-1} is the previous filtered measurement, m_n is the current measurement provided by the physical layer, and $a = 2^{-\frac{k}{4}}$ where k is the *filter coefficient* taking integer values specified by the network, $k = 0$ as default value. The UE must apply this time averaging filter before evaluating reporting criteria.

Automatic Neighbour Relation (ANR). As we described above, the UE can obtain the Physical Cell Identifier (PCI) and measure all the cells of the same frequency by using the Cell Search procedure. In the measurement report sent to the eNodeB, measurement results are associated with PCIs. Since there are only 504 PCIs used in the network, there are many cells using the same PCI. The eNodeB has to map each reported PCI to a Cell Global Identifier (CGI) in order to identify the exact cell. To facilitate the task, eNodeB is configured with an Automatic Neighbour Relation table which provides a mapping of local PCIs to unique CGIs. The network configuration needs to avoid any PCI conflict such that two cells having the same PCI must be separated far enough. LTE standard defines self-optimisation algorithms to avoid PCI conflict in ANR tables (see 3GPP TR 36.902 [95]).

Handover Signalling Sequence. For Intra-EUTRAN handover, the serving and target eNodeB are both in the same EUTRAN. The HO procedure does not involve the EPC, i.e. preparation messages are directly exchanged between the eNodeBs. Figure 3.18 depicts the signalling sequence of basic handover scenario where the source and target eNodeB belong to the same MME/S-GW. From the measurement result reported by the UE, the source eNodeB takes a handover decision and requests the target eNodeB. Upon the handover acknowledgement from the target eNodeB, the source eNodeB notifies the UE for handover action by forwarding the `RRCConnectionReconfiguration` message which was prepared by the target eNodeB. This RRC configuration message includes the `mobilityControlInformation` providing information required for handover. The UE will then detach from the source eNodeB and perform random access procedure with the target eNodeB, meanwhile the source eNodeB buffers UE's data and forwards it to the target eNodeB. Upon successful random access, the UE sends a `RRCConnectionReconfigurationComplete` to confirm the successful handover. Once the data connection is successfully established via the target eNodeB, the source eNodeB releases resources used for UE upon reception of the notification from the target eNodeB.
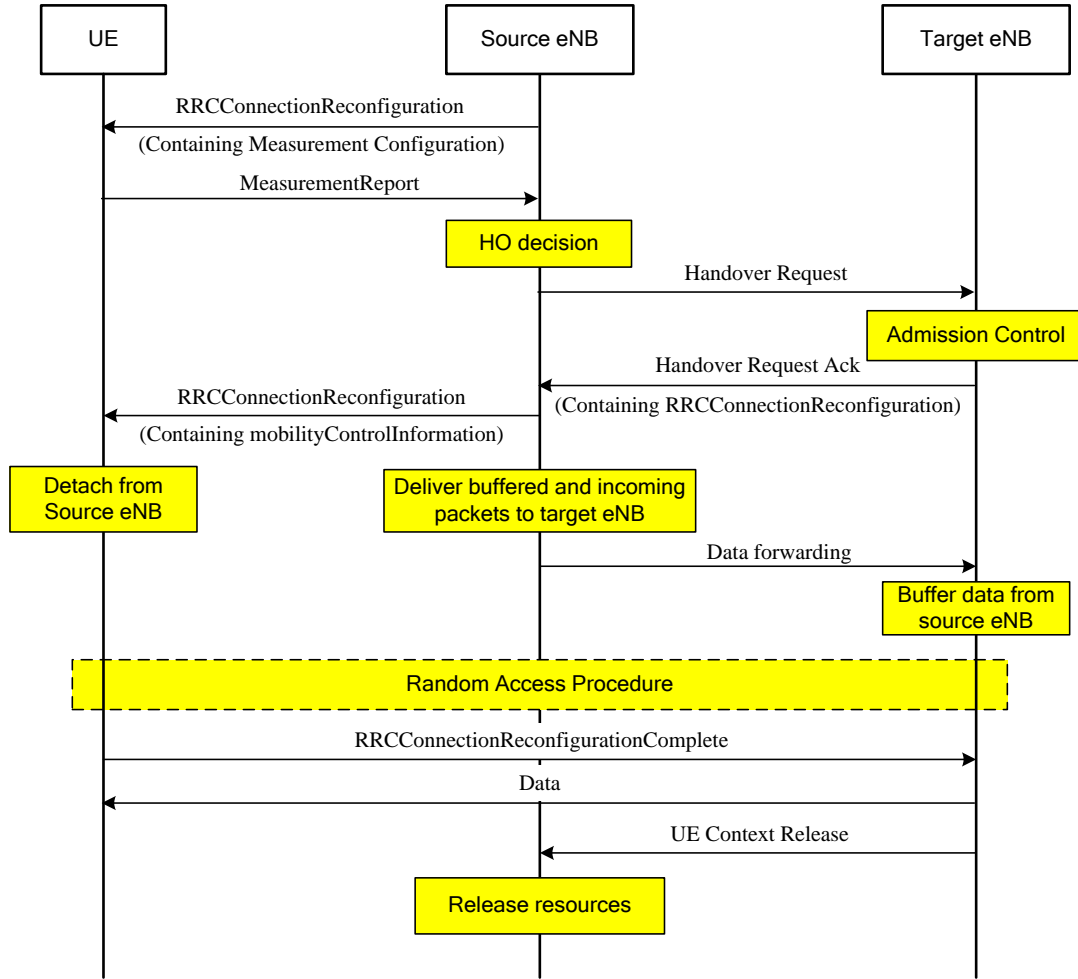
FIGURE 3.18: Intra-MME/SGW Handover

3.3.6 Evolution to LTE-Advanced

Upon the ITU's call for Radio Interface Technologies candidate for IMT-Advanced family, 3GPP took a decision by which LTE-Advanced will be an evolution of LTE, and its requirements will meet or event exceed IMT-Advanced requirements [96]. Requirements for LTE-Advanced was officially gathered in the technical report 3GPP TR 36.913 [97] titled "Requirements for Further Advancements for Evolved Universal Terrestrial Radio Access (E-UTRA) (LTE-Advanced)". These requirements are susceptible to further extensions, some of them currently obtain common agreements.

- Peak data rates of 1 Gbps for downlink and 500 Mbps for uplink.
- Peak spectral efficiency up to 30 bps/Hz for downlink and 15 bps/Hz for uplink with maximum MIMO configuration of 8×8 in DL and 4×4 in UL.
- The latency in control-plane is less than 10 ms for an active UE to get synchronised, and less than 50 ms for an idle UE to enter active mode.
- In an urban scenario with 500-metre inter-site distance and pedestrian users, the average spectral efficiency in DL must be 2.4 bps/Hz/cell, 2.6 bps/Hz/cell, and 3.7 bps/Hz/cell

with MIMO configurations 2×2, 4×2, and 4×4 respectively. And in the UL, it must be 1.2 bps/Hz/cell, and 2.0 bps/Hz/cell with SIMO 1×2, and MIMO 2×2 respectively.

- The mobility and coverage requirements are identical to LTE (i.e. Release 8) with additional requirements for indoor deployments.

- High spectrum flexibility and spectrum aggregation with transmission bandwidths up to 100 MHz in DL and UL.

- Backward compatibility and interworking with LTE and with other 3GPP legacy systems.

To fulfill these requirements, the 3GPP RAN1 working group working on the physical layer is currently evaluating techniques to enhance the LTE performance. Some important techniques are

- *Wider Bandwidth and Spectrum Aggregation.* One of the key enablers for high peak data rates is the use of wider bandwidth. LTE-Advanced uses transmission bandwidths up to 100 MHz. This large bandwidth mostly corresponds to noncontiguous spectrum deployments, and LTE-Advanced needs to support spectrum aggregation and flexible spectrum usage.

- *Coordinated Multiple Point Transmission and Reception* (CoMP). This technique consists in coordinating the transmission and reception between one UE and several eNodeBs. It is one of the most promising techniques helping to enhance data rates. Three potential impacts on specification include: measurement and feedback from UE, preprocessing schemes, and Reference Signal design [96].

- *Relaying* functionality to improve coverage, cell edge, and reduce deployment cost.

- *Extended MIMO transmission.* It consists in increasing the number of downlink transmission antennas to eight, and the number of uplink antennas to four to increase data rates.

3.4 Summary

The cellular concept is a deployment method of wireless networks. It uses a number of small base stations with low transmission power to provide mobile services to the deployment area. It greatly increases the network capacity thanks to the spatial reuse of the spectrum, and provides scalable network deployment and capacity enhancement thanks to a simple modification of cell sizes.

The cellular concept is used for radio access network deployment which must be supported by a (wired) core network to build up an entire end-to-end system.

The cellular concept introduces special technical challenges, especially mobility management, and efficient control of radio resource for optimal network performance. Advances in solving these technical challenges have driven mobile cellular communication evolution through generations. The first generation was deployed during late 1970s to the 1980s and is characterised by analog transmission. The second generation with digital transmission deployed since the early 1990s has successfully brought mobile services to the main stream market with a fast growth rate. It is though limited in interoperability between different 2G standards. The third generation started in 1999 has gradually evolved from existing 2G systems and provides more data

services. Its standardisation process received a worldwide coordination taken by the International Telecommunications Union, and is categorised as IMT-2000 family. The fourth generation known under ITU's IMT-Advanced family is currently being standardised. It is characterised by advanced physical layer using OFDMA and variants, smart antenna technologies, and flat all-IP architecture. It is set with promising performance capabilities for high data rate, high spectrum efficiency, high mobility support, and low latency.

Long Term Evolution is the brand name of the 3GPP's evolved 3G standards. It is technically the Evolved UMTS Terrestrial Radio Access Network (EUTRAN). This is supported by an all-IP core network termed Evolved Packet Core (EPC), and the entire system is called Evolved Packet System (EPC). Advanced technologies used for physical layer and the specially designed flat network architecture facilitate network control and enable aggressive network performance. LTE supports full mobility with high user speed while avoiding complicated handover configuration by using hard handover, and 504 Physical Cell Identifiers for the cell identification and measurement in the radio interface.

Chapter 4

Mobility Management in Cellular Networks

The cellular concept has been a very successful wireless networking architecture which benefits to the network capacity by the frequency reuse. However, in cellular network, it is inevitable that the user moves across multiple cells during an active call. A mechanism is therefore needed to switch the user's connection from one cell to another in a transparent way to the user. This so-called *mobility management* mechanism is realised thanks to a procedure called *handover* or *handoff*. Handover is an indispensable and critical function of any mobile cellular system [98]; its performance is extremely important in maintaining the desired quality of service (QoS) [50]. The mobility support together with the network capacity are two key performance requirements when describing a cellular generation.

In principle, a handover procedure involves two functions which are *handover measurement* and *handover decision-execution*. The first function is responsible for determining a best candidate cell to which the mobile will be transferred. This consists in measuring some parameters which are used as criteria for assessing candidate cells. The second function decides and realises the connection switching from the source cell to the selected target cell. This execution phase coordinates the multi-part handshake between the mobile, the source cell, and the target cell. While the execution phase needs to minimise the service degradation due to the connection switching, the measurement phase is required to identify the best candidate cell. The performance of the handover procedure hence depends on that of the measurement and the execution phases.

The criteria for assessing candidate cells could be based on several parameters such as those related to the radio condition, user move direction, and the cell load. These parameters could be measured by the mobile station or by base stations. For example, the mobile station can measure the radio link quality of neighbouring cells, then the best candidate cell could be the one with the best received radio signal quality. Or alternatively, by considering the reciprocity of the radio condition between downlink and uplink transmissions, base stations can be instructed to measure the radio signal quality received from a mobile, and then the base station which received the best radio signal quality from the mobile could be elected as the best handover candidate. As a result, there could be two handover measurement paradigms which are *mobile-assisted measurements* and *network-assisted measurements*. The former has the mobile measure parameters of neighbouring cells through the downlink, while the later requires base stations to monitor the

uplink signal quality received from the mobile. Since the mobile-assisted measurement helps, among others, to reduce the network control load generated by the mobility management by sharing the task between a large number of mobiles, it has been so far preferred by all of today's cellular standards.

The handover execution phase can be carried out by two modes: *make-before-break* and *break-before-make*. The make-before-break handover, also called *soft handover*, corresponds to the connection switching mechanism in which the mobile is connected simultaneously to several cells, and the current connection with the source cell is released *after* a new connection is established in the target cell. By contrast, the break-before-make handover, also called *hard handover*, refers to the mechanism in which no simultaneous connection is required. The current connection with the source cell is released *before* a new connection is established in the target cell.

There are some varieties of soft handover. For example, the soft handover used in 3GPP 3G networks allows the mobile to connect simultaneously to *two* cells which are the source and the target cells. In Mobile WiMAX, there are Macro-Diversity Handover (MDHO) and Fast Base Station Switching (FBSS) [87]. In these modes, the mobile and the serving base station maintain a set of base stations called *diversity set*. Both the mobile and serving base station can notify the counterpart for an update of diversity set. The mobile will add a new neighbouring cell to the diversity set if the signal quality of this cell is higher than a threshold. By the same principle, a cell will be removed from the diversity set if its signal quality is lower than a threshold. When operating in MDHO, the mobile station communicates simultaneously with all the base stations of the diversity set for both downlink and uplink control and data traffics. When operating in FBSS mode, an *anchor base station* is elected among the diversity set and the mobile only communicates with this anchor base station. So, this anchor base station serves as the serving base station of the mobile. The transition from an anchor base station to another is performed by the mobile without invocation of explicit handover signaling message. Both MDHO and FBSS have been standardised by IEEE 802.16 specification group, but they have never been implemented since the WiMAX Forum only recommended the hard handover scheme for Mobile WiMAX networks [99].

Soft handover benefits from diversity by combining the signals received from many cells. However, it requires simultaneous connection with multiple cells. In practice, mobile devices are equipped with one reception antenna for hardware cost and power consumption reasons, and therefore the soft handover is only possible when cells operate on a common frequency band. Besides, the macro-diversity in soft handover needs transmission synchronisation and coordination between base stations which complicate the control protocol and thus require a lot of engineering efforts. For these reasons, soft handover is not available in all cellular technologies, and particularly it is not used by LTE and LTE-Advanced. By contrast, hard handover does not require simultaneous connection with multiple cells, it can operate in all technologies regardless of whether cells are operating on the same frequency band or not. Hard handover is mandatory by all of today's cellular standards.

In addition, there have been more and more wireless technologies coexisting, network convergence is required to allow mobile users moving from one technology to another without loss of connection. A handover between different technologies is referred to as *vertical* or *inter-system* handover, for example handover between GSM and UMTS. This distinguishes from the horizontal handover (or handover for short) within one technology.

The handover execution mechanisms explained above can be controlled by the mobile station or by the serving base station. Consequently, there are so-called *mobile-controlled handover* and *network-controlled handover*. Between these, the network-controlled handover has been more preferred, particularly, for hard handover since the serving base station can communicate with all the involved parts including the mobile station, the target base station, and the core network, and thus allows to reduce the interruption time during the hard handover execution. Though, notice that in principle one could combine one handover measurement paradigm with one handover execution mechanism to result in one handover mode. For example, the mobile can perform both the neighbour measurement and the connection switching coordination; or the mobile performs the neighbour measurement and reports the result to the base station, and then the base station coordinates the connection transfer to the target cell. This later is referred to as *mobile-assisted network-controlled handover*. As explained above, mobile-assisted network-controlled handover consists in mobile-assisted measurement and network-controlled handover, it is the most widely used in today's cellular technologies [3, 5, 45, 87, 98, 100, 101]. From the perspective of this handover mode, in the subsequent sections we will describe in more details the mobile-assisted measurement as well as techniques employed today to enhance its performance.

4.1 Mobile-Assisted Handover Measurement

In the mobile-assisted handover, the mobile measures the radio condition and reads specific control parameters of neighbouring cells, such as cell signal quality, signal strength [102, 103], and Cell Individual Offset which provides the mobility management policy applied to that cell. This measurement procedure is referred to as *neighbour (cell) measurement* by the 3GPP terminology, or also *(neighbour cell) scanning* by the WiMAX terminology. The mobile proceeds the neighbour cell measurement with two phases: *cell identification* (or synchronisation) and *cell radio condition measurement*. To avoid any ambiguity due to terminologies, in the following *(cell) scanning* will be used to refer to the whole process which includes both the cell identification and cell radio condition measurement.

Since base stations can be asynchronous and can operate on different frequency bands, the mobile first needs to have frequency and time synchronisation with each neighbouring cell in order to read cell specific information as well as to measure cell radio condition. This consists in adjusting the mobile frequency reception window to the cell frequency band, and according the mobile time clock with the frame timing of the cell [104]. This synchronisation is very important since it is required for the mobility management purpose as well as for the network entry when the device is just powered on and gets access to the network. For this reason, cellular standards define synchronisation channels which have simple structure, use robust coding, and are periodically broadcasted in every cell in order to accelerate the synchronisation, for example SCH (Synchronisation CHannel) of GSM, 3G, and LTE networks.

Besides, due to the broadcasting nature of wireless communication, the signal received by the mobile is a superimposition of multiple signals from different cells. There needs a technique by which the mobile is able to separate this combining signal to synchronise with and measure each neighbouring cell. Cellular technologies realise this by associating each cell with a *cell synchronisation identity* (CSID) which helps to identify the cell in the radio interface. For instance, a GSM base station is attributed a Base Station Identity Code (BSIC) which when combined with a frequency carrier identifies one cell in a geographic area [45]. 3G networks can

use 512 scrambling codes [104], OFDMA-physical layer WiMAX network uses 114 pseudo-noise (PN) sequences [87, §8.4], while LTE uses in total 504 physical cell identities (PCI) for the cell identification (c.f. §3.3 in Chapter 3).

After the cell identification, the mobile reads specific information and measures the radio condition of that cell from downlink pilot channel, for instance BCCH (Broadcast Control CHannel) in GSM and CPICH (Common Pilot CHannel) in WCDMA networks. The mobile just needs to follow standardized procedure of the underlying technology to read cell specific information. By contrast, the estimation of the cell radio condition is much less straightforward since the radio signal is subject to variations due to impairments especially the fading effects. A basic requirement is that the target cell would provide the mobile with the best radio condition after the handover. But in fact it may happen that a cell currently provides good radio signal will become bad after some short time. Therefore, to increase the accuracy in prediction of the future radio condition, the mobile has to take several measurements of each cell and sometimes may apply some averaging technique such as the Layer-3 (L3) filtering of 3GPP LTE, 3GPP TS 36.331 [101, §5.5]:

$$R_n = (1 - 2^{-\frac{k}{4}})R_{n-1} + 2^{-\frac{k}{4}}m_n, \tag{4.1.1}$$

where R_n is the resulting filtered measurement in the current *measurement instant n*, R_{n-1} is the previous filtered measurement, m_n is the current measurement provided by the physical layer, and k is the *filter coefficient* taking an integer value which is specified by the network. Obviously, the *measurement cycle* which is the time spacing between two consecutive measurements m_{n-1} and m_n also has impacts on the prediction accuracy.

The time required for cell identification and measurement depends on the technology used for physical layer as well as the radio resource control (RRC) protocols of the underlying cellular technology. In GSM which employs TDMA (Time Division Multiple Access) for the physical layer, the mobile can measure a neighbouring cell belonging to the neighbour cell list during *idle slots* which occur every 26 TDMA frames (a GSM TDMA frame is composed of eight consecutive time-slots and lasts for 4.6152 ms), see Lagrange et al. [45, §8.6]. Unlike GSM, wideband systems such as 3G and 4G networks can allow adjacent cells operating on the same frequency band (i.e., high frequency reuse). And thus there are notions *intra-frequency cell* and *inter-frequency cell* which are used to refer to cells operating on a common frequency band with the serving cell, and on another frequency band, respectively. The mobile may not need to conduct the frequency synchronisation with an intra-frequency cell. As a result, scanning an intra-frequency cell is often faster than an inter-frequency cell. For instance, in WCDMA FDD the mobile is required to be able to identify an intra-frequency cell within 800 ms if that cell belongs to the mobile's monitored set, and within 30 seconds if not, see 3GPP TS 25.133 [105, §8.1.2.2]. Once cells are identified, the mobile is required to be able to measure eight identified intra-frequency cells within 200 ms, or six identified inter-frequency cells within 480 ms, see 3GPP TS 25.133 [105, §8] and [106]. 3GPP specifies similar requirements for the intra-frequency cell scanning in both LTE FDD and LTE TDD. When the signal quality of the synchronisation channel is good enough and some other conditions specified in 3GPP TS 36.133 [47, §9] are met, the mobile is required to identify a new intra-frequency cell within 800 ms, and after that it can measure eight identified intra-frequency cells within 200 ms. For the inter-frequency cell scanning, the mandatory performance is that the mobile is able to measure an inter-frequency cell within 480 ms. If the mobile is monitoring N_{freq} EUTRA carriers, the measurement period is hence $480 \times N_{\text{freq}}$ ms, see 3GPP TS 36.133 [47, §8] and [89].

(a) Scanning without measurement gap   (b) Scanning with measurement gaps
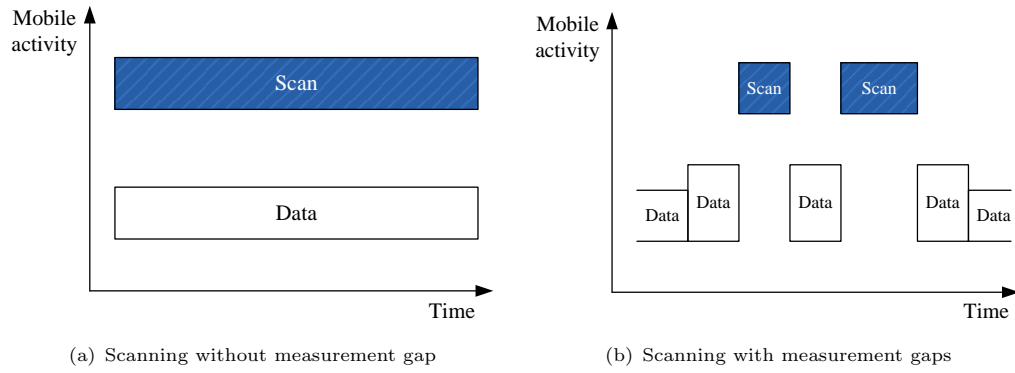
FIGURE 4.1: Neighbour cell scanning *Without* and *With* measurement gaps

It is often necessary to scan many cells in order to find a good target cell, and in that case the mobile will have to spend more time for the neighbour cell scanning. In parallel, the mobile also needs to conduct the data transmission with the serving cell for the on-going service. In the case that neighbouring cells to be scanned are operating on the same frequency band with the serving cell, the mobile can receive downlink channel of these intra-frequency cells and of the serving cell simultaneously. Thereby, the mobile may be able to scan neighbouring cells in parallel with having data transmission with the serving cell, see Figure 4.1(a). This simultaneous scanning-transmission mechanism is used in WCDMA and LTE networks for the intra-frequency cell scanning, and it is referred to as *scanning without measurement gap*.

However, when neighbouring cells to be scanned are on different frequency bands, the above simultaneous scanning-transmission is not possible, and some control mechanism is required to harmonise the on-going service and the neighbour cell scanning. The mobile will scan neighbouring cells during a certain *scanning interval* while the data transmission with the serving cell is temporarily suspended. After that, it resumes the data transmission with the serving cell during a certain *listening interval*, and so forth. In other words, the mobile activity switches between scanning and transmission which occur alternatively during scanning intervals interleaved with listening intervals, see Figure 4.1(b). The network instructs the mobile station on the scheduling of measurement gaps as well as the position of these gaps. For example, this information is sent in MOB_SCN-RSP (Scanning Response) message in WiMAX networks. This scanning mechanism was first defined by 3GPP for 3G networks and it is referred to as *compressed mode* [104, 106, 107]. The name "compressed mode" comes from the fact that a WCDMA network takes the information which would be normally sent and compresses the time it takes to send it. This mode continues to be used for the inter-frequency and inter-system handover measurement in LTE and is referred to as *scanning with measurement gaps* [6, 101]. Measurement gaps introduces capacity degradation. In addition, sending a larger volume of data during a compressed duration of time leads to increased transmission power, and so increases the interference and degrades neighbouring cells coverage.

As we have seen above, the neighbour cell scanning generates overheads such as control load, terminal power consumption, and especially capacity and coverage degradation when the compressed mode is required. As a result, algorithms which decide when to perform scanning are important to guarantee reliable handovers while maintaining low scanning overheads [106]. In GSM networks, TDMA is used for the multiple access; transmission and reception between a

mobile and its serving base station is performed in a time-slotted manner. By nature, the mobile can measure neighbouring cells between time-slots which are scheduled for the call emission or reception without need of explicit compressed mode. Therefore, in GSM networks the mobile performs the neighbour cell measurement all the time during an active call. In WCDMA and LTE networks, the mobile also continuously measures intra-frequency neighbouring cells when in connected-mode, i.e., when having active connections. For the inter-frequency and inter-system handover measurement and especially for the neighbour cell scanning in WiMAX networks, the mobile only performs a scanning when the specified conditions are met. A common condition is that the mobile starts scanning when the signal quality of the serving cell is worse than a minimum threshold, and it stops scanning when the signal quality of the serving cell is higher than a suitable threshold.

The network-controlled handover needs the mobile to report the measurement result. This also generates overheads due to reporting messages. Hence, the mobile only reports the measurement result when specified reporting criteria are fulfilled. Specific reporting events are specified in 3GPP TS 25.331 [108, §14] for 3GPP 3G networks, in 3GPP TS 36.331 [101, §5] for LTE (see Table 3.4 in Chapter 3), and in IEEE 802.16 [87], WiMAX Forum [109] for WiMAX networks. These reporting triggers can be summarised in three conditions:

(a) A suitable target cell is found. This is commonly expressed by the condition that the signal quality of a neighbout cell is better than a threshold, or offset better than that of the serving cell. In this case, the serving base station may initiate a handover to switch the mobile's connection to that cell.

(b) The signal quality of the serving cell is too bad. This is expressed by the signal quality of the serving cell worse than a minimum requirement. The mobile needs to report the measurement result so that the serving base station should initiate a handover to switch the mobile's connection to a better cell.

(c) The signal quality of the serving cell appears good enough again. This corresponds to the serving cell's signal quality better than a threshold. The mobile can stop the current neighbour cell scanning to reduce overheads.

4.2   Neighbour Cell List

The neighbour cell scanning should help to identify a suitable target cell as quickly as possible, at least before the signal quality of the serving cell becomes unsustainable. As we have seen in §4.1, the mobile needs to synchronise with a neighbouring cell before being able to measure that cell. The cell synchronisation may take quite long time and introduce significant latency in the handover measurement. Meanwhile, measuring cell radio condition may even take longer time especially when an averaging of several measured epochs is required to average out the fast fading effect. Nevertheless, the cell synchronisation can be considerably shortened if the mobile is provided information which describes the cell synchronisation and pilot channels such as frequency band, frame timing, and cell identity. In addition, it should be more easier to find a good handover target from a small number of good candidates than from all the possible cells. In light of that, cellular standards use a *neighbour cell list* (NCL) to assist mobiles in neighbour cell scanning. This list contains the information about the synchronisation and pilot channels of a number of cells which are preselected as "good" neighbours of the serving cell. Each

cell broadcasts its neighbour cell list periodically to all mobiles connected to itself, for example on the BCCH message in GSM and 3GPP networks, or on the MOB_NBR-ADV (Neighbour Advertisement) message in WiMAX. Mobiles only need to scan cells belonging to this list during a handover measurement.

Since the neighbour cell list serves as a list of recommended candidates, it has direct influence on the mobility management performance. It must contain a sufficiently large number of potential neighbouring cells to ensure that any mobile in the serving cell can find at least one handover target when its own signal deteriorates. But when the mobile's measurement capability is limited, a long list can result in delays in finding a suitable handover target. These delays may cause call drops when the user is moving at high speed or just staying during a short period in the serving cell. Therefore, proper determination of both the size and the content of the neighbour cell list is very important.

Many cellular standards specify a maximum allowable size of the neighbour cell list. In the GSM network, the TDMA $\times$ FDMA physical layer requires the mobile long time to complete a measurement of a number of neighbouring cells. For instance, the synchronisation with a neighbouring cell takes up to 500 ms under favorable conditions. The neighbour cell list is limited to 32 cells. In WCDMA networks, a neighbour cell list is defined for each cell, and is referred to as *neighbour set*. It is composed of up to 32 intra-frequency cells, 32 inter-frequency cells, and 32 cells from other Radio Access Technologies (e.g. GSM) [105]. However, when the union of the different neighbour sets contains more than 32 cells, some of the neighbours will not be measured. In WiMAX networks, although no maximum size is specified for the neighbour cell list, the mobile is assumed to measure at maximum first $N_{\text{MS\_max\_neighbours}}$ neighbouring cells of the neighbour cell list, see §6.3.21.1 in IEEE 802.16 [87]. And this parameter is set to 32 cells by WiMAX Forum [99].

Nevertheless, the accuracy of neighbour cell list computation remains a big day-to-day operators' concern, and it becomes a requirement of the Next Generation Mobile Networks (NGMN) alliance [110]. When in active mode in the GSM network, the mobile monitors cells comprised in the neighbour cell list periodically such that it takes a filtered measurement of each cell at about every 5 seconds (this averaging duration is configurable by the network operator). Using these periodic measurements the mobile determines a short list of the best six neighbouring cells which provides refined candidates for a handover target. Since the mobile station needs five seconds to read the broadcast channel of all these six neighbouring cells [45, p.273], it may happen that the mobile loses the connection before a suitable handover target is identified, especially when the user is moving relatively fast compared to the radio field variation like in tunnels exits or at big building sharp corners. In WCDMA networks, since the mobile is not assumed to monitor more than 32 cells, it may happen that the mobile detects some strong intra-frequency cells but can not add these cells in its active set due to the lack of space (active set is composed of neighbouring cells which the mobile can select for the soft handover). As a result, the mobile will continue to transmit a high power level when it already enters into this cell's coverage area. This generates high interference to other users which may degrade the quality and the network capacity. A proper configuration of the neighbour cell list is therefore very critical in order to avoid this situation [98]. Moreover, in the context of multi-standard cellular networks which combine legacy cellular access technologies such as LTE, WiMAX, and WiFi into a universal user service, seamless mobility needs to rely on the neighbour cell list concept for the cell scanning over all technologies, for example Media Independent Handover Services specified by IEEE 802.21 [111], and Access Network Discovery and Selection Function (ANDSF) specified by 3GPP TS 24.312

[112]. Hence, the definition of good inter-system neighbour cell lists is essential for reliable inter-system handover performance. A missing of important neighbouring cells is a common reason of handover failure. But if the neighbour lists are too long then the measurement time increases, and some important neighbours may be removed from the intra-system neighbour list [107].

The LTE technology intends to tackle this major operator concern. The current standard specifies the concept of automatic neighbour relation (ANR) table, c.f. §3.3 in Chapter 3. The ANR today is limited to the automatic configuration of the eNodeB internal data to translate a Physical Cell Identity reported by the mobile into a unique Cell Global Identity (CGI). The LTE ANR does not address the above neighbour cell list definition for the cell scanning purpose. It follows that the LTE mobile is assumed to measure autonomously the 504 existing PCIs for intra-frequency handover. However, as we have seen in §4.1 that the mobile is assumed to be able to measure eight identified intra-frequency cells during 200 ms, it will need a built-in algorithm to choose the PCIs to scan in each frame. The LTE assumption for inter-frequency and inter-system handovers is to rely on the classical pre-computed neighbour cell list.

4.3   Literature Review

4.3.1   Handover Optimisation

It is clear that handover is an important topic, it has received a lot of investigations since the early time of mobile cellular networking. The prior art on the handover analysis and algorithm design can be classified into handover control policy design, handover parameters optimisation, and automatic optimisation.

Optimal control.   This problem consists in designing optimal control policy which answers the question: under which conditions a handover needs to be performed so that the overall system performance is maximised? A Dynamic Program approach for this problem was firstly proposed by Rezaiifar, Makowski, and Kumar [113], which has been then supported and extended by many studies. Different papers investigating this approach are known for the following common points. A system composing of one mobile station moving between two base stations and discrete time model are considered. The interference and fast fading are usually ignored, while the shadow fading admits Gudmundson's autocorrelation function [41]. Considering a deterministic trajectory such as a strength line connecting the two base stations, analytical model is developed to predict the future signal powers received on the next moment $k + 1$. Handover control is designed as a decision rule that decides at each time moment whether or not to execute a handover in order to minimize a defined cost function.

Precisely, the above common setting with lognormal fading is considered in Rezaiifar et al. [113]. Basing on short range and short term assumption stating that the signal strength received and moment $k + 1$ only depends on the signal strength received at the last moment k and on the mobile position at moment $k + 1$, Rezaiifar et al. [113] proved that the signal strength received at the next moment $k + 1$ is conditional Gaussian given signal strength at k and the mobile location at $k + 1$ (c.f. §IV, equations (20) and (27) in [113]). The optimization objective was to find an optimal control policy which trades off between the signaling cost, if handover, and the service degradation, if not to handover. The call quality degradation cost is assumed proportional

to the difference of two received signal strengths. The call duration is modeled by a hang-up probability which is assumed Geometry distribution. The objective function is a discounted dynamic programming problem.

The key element of the solution finding is the value function of the formulated discounted dynamic programming. The structure of the value function was provided by equation (52) of [113]. This structure led to the conclusion that the optimal policy is a hysteresis-type handover control algorithm. It means that a handover should be performed when the signal strength of a neighbouring cell is better than that of the serving cell by a targeted margin. Note that it was called *threshold-type* handover in [113], but in fact the variable τ as used therein is a hysteresis margin.

The proposed handover control solution was then assessed by two metrics: average number of handovers and average call quality. This paper developed a first complete analytical solution based on dynamic programming. It though can be pointed out some limitations which are related to assumptions on short term, short range, and in particular the assumption on the complete knowledge of the user's move trajectory. These assumptions may limit the agreement of the work with a realistic scenario. For these reasons, one can use [113] for a benchmarking purpose.

It was realised that the hysteresis-based handover control has a drawback of creating unnecessary handovers in zones where both the serving cell and neighbouring cells have good signal quality. As a sequel, a combining absolute threshold and hysteresis-threshold handover policy was proposed by Zhang and Holtzman [114]. A handover is triggered only if the signal quality of the serving cell is below an absolute threshold and if the signal quality of neighbouring cell is better than that of the serving cell by a hysteresis margin. Simulation result therein confirmed the effectiveness of this combining handover policy. This result motivated Veeravalli and Kelly [115] in using the absolute threshold control policy for their handover optimisation framework. Instead of finding an optimal absolute threshold, they argued that the absolute threshold Δ should be selected as the required signal level for a satisfactory service, for instance Δ is set to the minimum tolerable level below which the service interrupt occurs. It was therefore assumed known. The optimisation problem was then to decide at each discrete-time moment k whether a handover needs to be performed or not in order to trade off two factors: the average number of handovers and the average number of service failures (i.e., call drops) during a given trajectory. They studied this optimisation problem under a setting with discrete time, lognormal shadow fading admitting Gudmundson's autocorrelation function, no interference, one mobile with two base stations, and deterministic call duration (i.e., hangup probability as introduced in [113] was not taken into account). The only stochastic factor of this model is the fading. The optimal handover control was formulated as a Bayes problem:

$$\phi^*(c) = \arg\min_{\phi}(c\mathbf{E}\{N_{\text{ho}}^{\phi}\} + \mathbf{E}\{N_{\text{serv. fail}}^{\phi}\}) \qquad (4.3.1)$$

where $\mathbf{E}\{N_{\text{ho}}^{\phi}\}$ is the average number of handovers, and $\mathbf{E}\{N_{\text{serv. fail}}^{\phi}\}$ is the average number of service failures of the handover policy ϕ. Here, a service failure is defined as the signal strength received from the serving cell falling below the required threshold Δ, and c is a tradeoff parameter. The latter is considered as the relative cost between handover signalling cost if handover and service degradation if not to handover.

An exact solution was first derived using the Dynamic programming. The optimal policy was established by using recursive method as given by equations (8) and (9) of [115]. Their consideration is that DP solution is impractical since it is complex, nonstationary, requires knowledge

on the mobile trajectory, and the globally optimal solution at a particular location depends on the future trajectory. To cope with this, they restricted the handover decision to only two local points instead of the entire the trajectory: the present time k, and the next time $k+1$, leading to a locally optimal decision which has the following structure:

$$\mathbf{P}(X_{k+1}^{(\overline{B}_k)} < \Delta \,|\, I_k) + c \underset{\text{ho}}{\overset{\text{not ho}}{\gtrless}} \mathbf{P}(X_{k+1}^{(B_k)} < \Delta \,|\, I_k), \tag{4.3.2}$$

where I_k is the information available at moment k; B_k and $\overline{B}_k$ are respectively the serving BS and the neighbouring BS at moment k.

A key point for solving (4.3.2) is that the authors assumed that under the lognormal shadow fading the conditional distribution of X_{k+1} given X_k is Gaussian. In fact, this was proved by Rezaiifar et al. [113], given in Proposition IV.1 therein, under the following form:

$$(X_{k+1}^{(i)} \,|\, X_k^{(i)}, S_k, S_{k+1}) \sim \mathcal{N}(\cdot, \cdot), \tag{4.3.3}$$

where S_k and S_{k+1} are the mobile locations at moments k and $k+1$. By the above assumption, Veeravalli and Kelly just needed to find the means and variances of the conditional Gaussian distributions. These are given by equations (11) and (12) of [115]. A conclusion from their equation (11) is that the conditional means require the knowledge of the distances from the mobile to the two base stations at moments k and $k+1$. Since this information is practically considered unavailable, they used an estimate for the conditional means, denoted $\hat{X}_{k+1}^{(i)}$. Thereby, the decision structure (4.3.2) is now given by the following policy:

$$\Phi\left(\frac{\Delta - \hat{X}_{k+1}^{\overline{B}_k}}{\sigma\sqrt{1-a^2}}\right) + c \underset{\text{ho}}{\overset{\text{not ho}}{\gtrless}} \Phi\left(\frac{\Delta - \hat{X}_{k+1}^{B_k}}{\sigma\sqrt{1-a^2}}\right),$$

where $\Phi(\cdot)$ is the normal Gaussian distribution function. In their numerical evaluation, the conditional means $\hat{X}_{k+1}^{(i)}$ is assumed equal to the current signal strength, i.e., $\hat{X}_{k+1}^{(i)} = X_k^{(i)}$.

As a summary, this paper considered absolute threshold handover, the optimal handover was designed to find a tradeoff between the number of handover and the number of call drops. The studied model assumed deterministic call duration, signal strength-based decision (no interference), and used a prediction of the near future signal strength. A a locally optimal solution was obtained for two local time samples (current time and the next time).

Motivated by the conjecture of Veeravalli and Kelly [115] that the locally optimal algorithm can easily be made to adapt to changes in system parameters, say S, Prakash and Veeravalli [116] extended their previous work to hysteresis-threshold approximation using locally optimal solution. The hysteresis-threshold handover control was defined therein as:

$$U_k = \begin{cases} 1\,(\text{handover}) & \text{if } \{\hat{X}_{k+1}^{\overline{B}_k} > t_1\} \,\& \{\hat{X}_{k+1}^{B_k} < t_2\} \,\& \{\hat{X}_{k+1}^{\overline{B}_k} > \hat{X}_{k+1}^{B_k} + h\} \\ 0\,(\text{no handover}) & \text{otherwise} \end{cases}. \tag{4.3.4}$$

The objective is to find an approximation of thresholds t_1, t_2, and hysteresis margin h as a function of the required signal level Δ which was used in the locally optimal (LO) algorithm by Veeravalli and Kelly [115]. For this purpose, the handover region determined by the LO algorithm as given in Fig. 2(b) of [115] is approximated by the region determined by three lines corresponding to three thresholds t_1, t_2, and h. The optimized parameters were finally obtained

with equations (19)-(21) of [116] as follows:

$$
\begin{aligned}
t_1 &= \Delta - \sigma'/\Phi(c), \\
t_2 &= \Delta + \sigma'/\Phi(c), \\
h &= -\sigma'/\Phi(1/2 + c),
\end{aligned}
$$

where $\sigma' = \hat{\sigma}\sqrt{1 - (\hat{a}^S)^2}$, where $(\hat{a}^S)^2$ is an estimation of the autocorrelation factor of the shadow fading from system parameter set S. No validation of the proposed solution was discussed.

Akar and Mitra [117] supported and extended the Bayes formulation and locally optimal solution structure proposed by Veeravalli and Kelly [115]. They incorporated a signal averaging filter into the discrete-time model. In addition, assuming a system with one mobile moving on the straight line connecting two base stations, the authors introduced the handover delay issue. The latter was formulated simply as the distance between the mobile location and the halfway point between the two BSs.

Itoh et al. [118] proposed a combining absolute distance and relative signal strength control policy which is a variant of the combining absolute and relative signal signal strength policy studied by Zhang and Holtzman [114]. Authors showed that this policy performs well in a lognormal fading condition when the distance estimator can be modelled as a wide-sense stationary additive white Gaussian noise.

Unlike the above studies, Lee et al. [119] approached the problem from the protocol design perspective. They proposed a semi-soft handover scheme. This relies on the principle of hard handover such that it interrupts *data* connections from the source cell before switch them to the target cell. On the other hand, it relies on the principle of the soft handover to establish parallel *control* connections with both the source and target cells during the handover execution. Authors believed that this hybrid handover scheme is able to overcome drawbacks of hard and soft handover schemes by reducing handover latency and outage probability in hard handover, while reducing the interference and resource consumption in soft handover.

Handover parameter optimisation. This problem deals with optimal parameter setting for a given handover policy and scheme. First approach for this problem is related to the analytical *cell-assignment* model. Basically, this approach considers a system composing of two cells i and j. The assignment of the mobile to one of the two cells is characterised by a point on the plane $\mathbb{R}^2$ whose x-axis represents cell i, and y-axis represents cell j. It segments the $\mathbb{R}^2$ plane into three regions I, J, and H such that $X[k] \triangleq (X_i[k], X_j[k]) \in I$ if the mobile is assigned to cell i, $X[k] \in J$ if the mobile is assigned to cell j, and $X[k] \in H$ if the difference of two received signal strengths is less than a hysteresis threshold. Using this assignment, a handover is considered as a jump of a point $X[k]$ from one region to the other one between I and J, and thereby handover probability and related metrics were formulated.

This approach was first proposed by Vijayan and Holtzman [120, 121] using continuous-time model, later Zhang and Holtzman [114] and Leu and Mark [122] supported this approach with a discrete-time model. All of these works were based on the level crossing analysis of the relative signal strength in order to to derive relevant properties. Zhang and Holtzman [114], Vijayan and Holtzman [120, 121] used asymptotic regime in which level crossing events form a Poisson process, while Leu and Mark [122] avoided this asymptotic assumption.

Automatic optimisation approach has also received practical attention, especially, from operators. It uses incremental tuning and control loops with field measurements to automatically optimise handover parameters. For handover in WCDMA networks, Vanghi and Chevallier [123] used field measurements of a commercial network, and showed some analysis results on the impact of handover measurement control parameters, such as parameters defining measurement reporting events and measurement coefficient factor. Also for WCDMA, Werner et al. [124] proposed an automatic optimisation of handover parameters using Fuzzy Controlling. They aimed at optimising the *cell individual offset* parameter taking into account the downlink cell load, soft handover overhead, the data throughput as well as the speed of the dominant user type in the cell.

Schröder et al. [125] expressed the motivation for automatic tuning of handover parameters for LTE. Authors provided some thoughts about a trial-and-error optimisation loop which automatically optimises handover parameters such that only one parameter is considered in each step. The optimisation is done by measuring the system performance and then increase or decrease a parameter p by a step value δ, or keep p unchanged. They realised simulation to show the impact of the hysteresis margin on the handover performance in LTE. Simulation results showed that the number of incoming HOs and number of HO attempts decrease as the handover hysteresis margin increases. By contrast, the call drop ratio increases with the hysteresis margin.

4.3.2 Handover Measurement

The handover measurement in WiMAX networks (either with IEEE 802.16e or with IEEE 802.16m radio interface) is performed by the mobile station through a *Scanning* procedure. IEEE 802.16 standards specify that the mobile station may perform an *Association* procedure with each scanned neighbouring base station. This association procedure serves as a pre-registration of the mobile station to the neighbouring base station, leading to faster handover execution. This however increases the scanning time, leading to scanning overheads due to measurement gaps in WiMAX. This requires appropriate scanning timing as well as scanning strategy which decides whether or not to perform association during the scanning. Within this context, Rouil and Golmie [126] proposed an adaptive scanning algorithm which allocates scanning intervals between multiple mobil stations in order to maximise data throughput while satisfying the required quality of service. Ulvan and Bestak [127] taken an analysis of different possible options combining scanning and association. They then proposed to use the option so-called *single base station scanning scheme*. In this scheme, the mobile station performs association procedure only with the neighbouring base station which provides the best signal quality, which is potentially the target base station.

For 3GPP technologies, Hiltunen et al. [128] provided a comparison between periodic and event-triggered intra-frequency handover measurement reporting in WCDMA by using simulations. They observed that periodic measurement reporting performs better than event-triggered mode, but at the expense of increased signalling cost for reporting messages. Kim and Kim [129] investigated simulations to see the impact of Hysteresis, Time-To-Trigger, and user's speed according to 3GPP Layer-3 filter measurement model to the handover measurement performance. Racz et al. [130] also used simulations to analyse the impact of intra-frequency handover protocol on the user perceived performance in term of TCP throughput in LTE. They observed that moving the handover control function to eNodeB does not impact the service quality.

Anas et al. [131] aimed at evaluating the handover performance in LTE taking into account standardised handover measurement parameters such as measurement bandwidth, Time-To-Trigger, handover margin, as well as user's speed. Anas et al. [132] investigated the effect of Layer-3 filtering on the handover measurement in LTE when linear filtering or dB filtering is used. The filter is said in linear scale (in dB scale, resp.) if the averaging formula affects on linear unit (on dB unit, resp.). Their conclusion from simulations was that both filtering scales provide similar performance.

Kurjenniemi and Henttonen [133] investigated the impact of the measurement bandwidth on the inter-frequency measurements of Reference Signal Received Power (RSRP) in LTE. In Chapter 3, we have seen that the Reference Signals are allocated to the six central physical resource blocks so that the synchronisation and cell measurement do not depend on the variable system bandwidth. In this study, Kurjenniemi and Henttonen concluded from simulations that larger bandwidth for Reference Signals does not improve the measurement accuracy significantly.

It can be seen that almost studies in the literature investigated the handover measurement issue with simulations. Each study provided insights into the impact of a specific parameter to the system performance. There has been not work which could provide an analytical understanding of the unified effect of parameters on the handover measurement performance.

4.3.3 Neighbour Cell List Self-Optimisation

The general concept of dynamic neighbour cell list planning due to Olofsson et al. [134], Magnusson and Olofsson [135] is one of the first attempts in the area of neighbour cell list self-optimisation. In this concept, a neighbouring cell is dynamically added to the neighbour cell list if the percentage of handovers from the serving cell to this neighbouring cell is above a predefined threshold. Now and then, some test frequencies are added to the neighbour frequency list to allow mobiles measuring cells which are not currently in the current NCL. This aims at discovering potential good neighbouring cells.

Following the motivation introduced in [134, 135], Guerzoni et al. [136] proposed an automatic optimisation algorithm. This algorithm mainly consists in identifying and ranking missing neighbours. Neighbouring cells are identified analytically, and then ranked based on the base station coordinates and the antenna direction. In parallel, the cells currently in the NCL are assessed using key indicators such as handover success rate and received signal quality. A cell currently comprised in the neighbour cell list is considered as "bad" if the handover success rate from the serving cell to that cell is below a certain threshold, or if its average received signal quality is worse than a predefined level. After that, good cells from the pool of missing cells are added to the neighbour cell list while bad cells in the current NCL are removed.

Realizing that the method proposed in [136] may produce a very large pool of potential missing neighbouring cells, and that the statistical confidence on the parameters used for ranking cells may not be optimal, Soldani and Ore [137] proposed an enhanced procedure for UTRA FDD networks. Basically, CDMA-based physical layer of 3G networks allows for high frequency reuses. As a result, a mobile station (i.e. 3G UE) often detects an important number of intra-frequency cells which are currently not comprised in the neighbour cell list. 3GPP 3G standards specify that a UE reports those detected cells under a *Detected Set report* to its serving Node B. Soldani and Ore exploited these reported Detected Sets to identify missing neighbouring cells. Then,

thresholds are used as a coach filter to limit the pool list. The objective here is to efficiently identify and filter missing cells, but not to compute an optimal neighbour cell list.

Further work by Parodi et al. [138] focused on automatically creating a neighbour cell list for newly deployed cells. Slightly similar to Soldani and Ore [137], neighbouring base stations located in a given range from the new base station are filtered out as potential neighbours. Then, using pathloss prediction models and antenna pattern, each cell in the pool is checked for overlap with the new cell. A number of the best neighbouring cells are finally selected for the neighbour cell list. In addition, a signalling implementation for LTE networks is proposed to allow a newly installed cell to detect its neighbours.

Three self-configuration methods for WiMAX networks are proposed in Li and Jantti [139] and are very similar to those discussed in [138].

The concept proposed by Amirijoo et al. [140, 141] used statistics collected from the network to optimise the neighbour relation table and to detect physical cell identifier (PCI) conflict in LTE.

The above studies contributed valuable concepts for the self-optimisation of neighbour cell lists. They showed that it is conceptually feasible to self-configure and to self-optimise neighbour cell lists for enhanced mobility management and reduced network operation expense. All these studies however still present a common drawback in the realisation of the proposed concepts. As we know, the main motivation behind the self-optimisation algorithm design is to maximise the mobility management performance and operation efficiency by using live network measurements. Meanwhile, the proposed concepts was mostly realised with static configuration parameters and thresholds, as well as with cell coverage prediction models. This limits the performance and the ability to adapt to dynamic changes in the radio environment. It can be also observed that there has been no analytical investigation which provides insights into the impacts of neighbour cell lists on the quality of mobility management.

4.4   Summary

Handover is an important feature of mobile cellular networking. Its function is split into handover execution and handover measurement functions. The handover execution is responsible for coordinating the connection switching while the handover measurement helps to find a suitable handover target cell. The handover with mobile station performing measurements and base station executing the connection switching is the most preferable scheme. It is called mobile-assisted network-controlled handover.

The handover measurement, also called scanning, has an important influence on the mobility management performance. It not only decides the quality of the target cell, but also impacts the radio resource usage and the quality of service. The neighbour cell list is used to assist mobile stations in the handover measurement. Proper configuration of the neighbour cell list as well as optimal design of parameters controlling handover measurement are of primary importance to the handover optimisation.

The handover control problem has received a lot of attention since the beginning of mobile cellular networking. It consists in designing rules which decide when to perform a handover. The handover measurement issue has been only investigated with simulations, and there is a lack of analytical understanding of this function. The self-optimisation of the neighbour cell list

has been studied in the literature with interesting concepts. However, they were not successfully realised as seen from the self-optimisation perspective.

Chapter 5

Mathematical Background

5.1 Modelling of Extreme Events

One of the main purposes of this thesis is to model essential stochastic characteristics of wireless links in large random networks, especially the best signal quality which is a maximum of random variables. Furthermore, as it will be shown later, the best signal quality can be represented as a function of the maximum signal strengths and of the interference, which are in turn maxima and sums of signal strengths behaving as random variables. For this reason, we shall describe some basic mathematical results firstly on the fluctuation of sums and maxima of independently and identically distributed (i.i.d.) random variables, and then on their joint behaviour.

5.1.1 Heavy-Tailed Distribution and Regular Variation

For a non-degenerate distribution function F with support on $\mathbb{R}$, the function defined as $\overline{F}(x) = 1 - F(x)$ is called the tail of the distribution function F, or *tail distribution* for short. It is clear that $\overline{F}$ is a non-increasing function, and $\overline{F}(x) \to 0$ as $x \to \infty$. The speed of the convergence $\overline{F} \to 0$ is a very important information when studying extreme events generated by this distribution. Roughly speaking, the "heavier" $\overline{F}$ is, the more probable it is that X takes large values.

In this subsection, we go through some basic notions about heavy-tails and regular variation of distribution functions. We begin with the following definition of heavy-tailed distributions.

Definition 5.1.1 (Heavy-tailed distribution). *A distribution function F is said to be* heavy-tailed *if*

$$\int_{\mathbb{R}} e^{\varepsilon x} F(\mathrm{d}x) = \infty, \quad \textit{for all } \varepsilon > 0. \tag{5.1.1}$$

This definition is equivalent to the statement that F is heavy-tailed if and only if

$$\lim_{x \to \infty} e^{\varepsilon x} \overline{F}(x) = \infty, \quad \text{for all } \varepsilon > 0,$$

see e.g. Theorem 2.6 in Foss et al. [142]. So, a distribution is heavy-tailed if its tail decays more slowly than any exponential $e^{-\varepsilon x}$ with $\varepsilon > 0$.

Some examples of heavy-tailed distributions include Pareto distributions, Cauchy distributions, and lognormal distributions. The class of the heavy-tailed distributions is a 'large' family in the sense that these distributions can have different tail behaviours in a neighbourhood near to their right endpoint. In order to have more insights into the tail behaviour of distribution functions, the *regular variation* property is introduced and it is specified in the following.

Definition 5.1.2 (Regular variation)**.** *For a positive, Lebesgue measurable function h on $(0, \infty)$,*

(a) *h is called* regularly varying *at ∞ of index $\alpha \in \mathbb{R}$ if*

$$\lim_{x \to \infty} \frac{h(tx)}{h(x)} = t^\alpha, \qquad t > 0.$$

(b) *h is called* slowly varying *at ∞ if it is regularly varying with index 0, i.e.*

$$\lim_{x \to \infty} \frac{h(tx)}{h(x)} = 1, \qquad t > 0.$$

(c) *h is called* rapidly varying *at ∞ if it is regularly varying with index $-\infty$, i.e.*

$$\lim_{x \to \infty} \frac{h(tx)}{h(x)} = \begin{cases} 0 & if \quad t > 1, \\ \infty & if \quad 0 < t < 1. \end{cases}$$

We denote by $\mathcal{R}_\alpha$ the class of the regularly varying functions, and denote by $\mathcal{R}_0$, $\mathcal{R}_{-\infty}$ the class of the slowly varying functions, the class of the rapidly varying functions, respectively.

From above definitions, it is easy to observe that if h is a regularly varying function at infinity with index α, then it can be represented as $h(x) = x^\alpha L(x)$ for some slowly varying function L.

The class of regularly varying functions plays an important role in the characterisation of domains of attraction of extreme events. In particular, we will use the following important representation theorem for regularly varying functions. It is given in [143], Theorem A3.3 and Theorem A3.12:

Theorem 5.1.3. *If $h \in \mathcal{R}_\alpha$ for some $\alpha \in \mathbb{R}$, then*

$$h(x) = c(x) \exp\left(\int_z^x \frac{\delta(u)}{u} du \right), \qquad x \geq z, \tag{5.1.2}$$

for some $z > 0$ where c and δ are measurable functions, $c(x) \to c_0 \in (0, \infty)$, $\delta(x) \to \alpha$ as $x \to \infty$. The reverse implication also hold.

Note that the class $\mathcal{R}_\alpha$ defined above includes $\alpha = -\infty$. In this case we have $\delta(x) \to -\infty$ as $x \to \infty$, and the representation (5.1.2) can be rewritten as

$$h(x) = c(x) \exp\left(-\int_z^x \frac{du}{a(u)} \right), \qquad x \geq z, \tag{5.1.3}$$

where a has a density a' satisfying $a'(x) \to 0$ as $x \to \infty$ [143, p. 571].

By Theorem 5.1.3, we can immediately observe that if $h \in \mathcal{R}_\alpha$ for some $\alpha \neq 0$. Then $h(x) \to \infty$ if $\alpha > 0$, and $h(x) \to 0$ if $\alpha < 0$, as $x \to \infty$, see Corollary A3.4 in [143]. Therefore, if a distribution function F is regularly varying with index α, then we can only have $\alpha \leq 0$. This

remark is important and throughout this section we will be only interested in the class $\mathcal{R}_{-\alpha}$ for $\alpha \geq 0$. In this case, we have a connection between the regularity and heavy-tailed beaviour. It is shown in [143, §1.4] that if a function h is regularly varying with non-positive index $-\alpha \leq 0$, i.e. $h \in \mathcal{R}_{-\alpha}$, then h is heavy-tailed.

For a non-negative random variable X with distribution function F such that $F(x) < 1$ for all $x \geq 0$, if $\overline{F} \in \mathcal{R}_{-\alpha}$ for some $\alpha > 0$, then moments of order δ are finite if $\delta < \alpha$ and infinite if $\delta > \alpha$, [143, Prop. A3.8]. As a sequel, regularly varying distribution functions are referred to as "very heavy-tailed" distributions. On the contrary, if $\overline{F} \in \mathcal{R}_{-\infty}$ then all moments of F are finite. In order words, $\mathcal{R}_{-\infty}$ contains 'moderately' heavy-tailed and light-tailed distributions.

5.1.2 Limit Laws of Sums

The characterisation of limit laws of sums of random variables is fundamental to statistical theory with rich research contributions and a wide range of applications. Given a sequence of i.i.d. random variables X_1, X_2, ..., let

$$S_n = X_1 + \cdots + X_n, \quad n \in \mathbb{N}.$$

The central limit theory is concerned with the question *what are possible limit laws of the sums S_n when appropriately centered and normalised.* This question is linked to the notation of *stable* distributions. A distribution function F is said *stable* if for i.i.d. random variables X, X_1, and X_2 with common distribution F we have the following identity in law:

$$c_1 X_1 + c_2 X_2 \overset{\mathrm{d}}{=} bX + a$$

for all non-negative constants c_1, c_2, and appropriate real numbers $b > 0$ and a. A random variable with a stable distribution function is also called stable. An example of stable distribution is the Gaussian distributions.

A key element of the answer is that the class of the possible limit laws of normalised and centered sums coincides with the class of the stable distributions, see e.g. Theorem 2.2.2 in [143]. For this reason the class of the stable distributions takes a central position in probability theory and mathematical statistics. The most common way to charaterise stable distributions is to describe their characteristic functions.

Theorem 5.1.4. *A stable distribution has for characteristic function*

$$\phi_\alpha(t) = \mathbf{E}\{\exp(jXt)\} = \exp(j\gamma t - c|t|^\alpha(1 - j\delta\,\mathrm{sign}(t)z(t,\alpha))), \quad t \in \mathbb{R}, \tag{5.1.4}$$

where γ is a real constant, $c > 0$, $\alpha \in (0,2]$, $\delta \in [-1,1]$, and

$$z(t,\alpha) = \begin{cases} \tan\left(\frac{\pi\alpha}{2}\right) & \text{if } \alpha \neq 1 \\ -\frac{2}{\pi}\log(|t|) & \text{if } \alpha = 1 \end{cases}.$$

The most important parameter of this representation is α. It determines basic properties of this class of distributions such as tail behaviour, limiting behaviour of sums. It is called *characteristic exponent*, and the corresponding distribution is called *α-stable*. Especially, when $\alpha = 2$ we obtain Gaussian distributions.

So, the limiting distribution of the sum of i.i.d. random variables when it exists can only be an α-stable distribution. This leads to the following definition taken from Definition 2.2.7 in Embrechts et al. [143].

Definition 5.1.5 (Domain of Attraction of the Sum). *The random variable X (the df F) is said to belong to the domain of attraction of an α-stable distribution G_α if there exists constants $a_n > 0$, $b_n \in \mathbb{R}$ such that*

$$a_n^{-1}(S_n - b_n) \xrightarrow{d} G_\alpha, \quad \text{as } n \to \infty. \tag{5.1.5}$$

We write $X \in D(G_\alpha)$ ($F \in D(G_\alpha)$). If we are interested only in the fact that X (or F) is attracted by some α-stable law whose concrete form is not of interest, we simply write $X \in D(\alpha)$ ($F \in D(\alpha)$).

The question is which α-stable law defines the domain of attraction of a given distribution function F. This is characterised by the following result, given by Theorem 2.2.8 in [143]:

Theorem 5.1.6 (Characterisation of Domain of Attraction). *Let F be some distribution function.*

(a) $F \in D(2)$ if and only if $\int_{|y| \leq x} y^2 F(\mathrm{d}y)$ is slowly varying.

(b) $F \in D(\alpha)$ for some $\alpha < 2$ if and only if

$$F(-x) = \frac{c_1 + o(1)}{x^\alpha} L(x), \qquad \overline{F}(x) = \frac{c_2 + o(1)}{x^\alpha} L(x), \quad \text{as } x \to \infty,$$

where L is slowly varying and c_1, c_2 are nonnegative constants such that $c_1 + c_2 > 0$.

We can see that

$$\int_{|y| \leq x} y^2 F(\mathrm{d}y) \to \mathbf{E}X^2, \quad \text{as } x \to \infty.$$

Hence, if $\mathbf{E}X^2 < \infty$ then $\int_{|y| \leq x} y^2 F(\mathrm{d}y)$ is slowly varying at infinity, and so F belongs to the domain of attraction of normal distribution. A complete characterisation of this is given by Corollary 2.2.9 in [143]:

Corollary 5.1.7 (Domain of Attraction of a normal distribution). *A random variable X is in the domain of attraction of a normal law if and only if one of the following conditions holds:*

(a) $\mathbf{E}X^2 < \infty$.

(b) $\mathbf{E}X^2 = \infty$, and $\mathbf{P}(|X| > x) = o\left(x^{-2} \int_{|y| \leq x} y^2 F(\mathrm{d}y)\right)$ as $x \to \infty$.

Given that a distribution function belongs to the domain of attraction of an α-stable law, an important question is to determine normalising and centering parameters a_n and b_n in (5.1.5) appropriately. The answer is given by the central limit theorem, taken from Proposition 2.2.13, Proposition 2.2.14, and Theorem 2.2.15 in [143].

Proposition 5.1.8 (Normalising constant). *The normalising constant a_n in (5.1.5) can be chosen as the unique solution of the equation*

$$\mathbf{P}(|X| > a_n) + a_n^{-2} \int_{-a_n}^{a_n} y^2 F(\mathrm{d}y) = n^{-1}, \quad n \geq 1. \tag{5.1.6}$$

In particular, if $\sigma^2 = \text{var}(X) < \infty$ and $\mathbf{E}X = 0$ then

$$a_n \sim n^{1/2}\sigma, \quad n \to \infty.$$

If $\alpha < 2$ we can alternatively choose a_n such that

$$a_n = \inf\{y : \mathbf{P}(|X| > y) < n^{-1}\}, \quad n \geq 1.$$

Proposition 5.1.9 (Centering constant). *The centering constant b_n in (5.1.5) can be chosen as*

$$b_n = n \int_{-a_n}^{a_n} yF(\mathrm{d}y), \tag{5.1.7}$$

where a_n is given in Proposition 5.1.8. In particular, we can take $b_n = n\widetilde{b}$ where

$$\widetilde{b} = \begin{cases} \mu & \text{if } \alpha \in (1, 2], \\ 0 & \text{if } \alpha \in (0, 1), \\ 0 & \text{if } \alpha = 1 \text{ and } F \text{ is sysmetric.} \end{cases} \tag{5.1.8}$$

With the above ingredients, we now have the central limit theorem (CLT):

Theorem 5.1.10 (General CLT). *Suppose that $F \in D(\alpha)$ for some $\alpha \in (0, 2]$.*

(a) If $\mathbf{E}X^2 < \infty$ then

$$(\sigma n^{1/2})^{-1}(S_n - n\mu) \xrightarrow{d} \Phi$$

for the standard normal distribution Φ with zero mean and unit variance.

(b) If $\mathbf{E}X^2 = \infty$ and $\alpha = 2$, or if $\alpha < 2$ then

$$(n^{1/\alpha}L(n))^{-1}(S_n - b_n) \xrightarrow{d} G_\alpha$$

for an α-stable distribution G_α, an appropriate slowly varying functions L, and centering constant b_n as in (5.1.7). In particular, we can take $b_n = n\widetilde{b}$ with $\widetilde{b}$ given in (5.1.8).

5.1.3 Limit Laws of Maxima

For some sequence of i.i.d. random variables $X_1, X_2, \ldots$, with common distribution F, let

$$M_n = \max(X_1, \ldots, X_n), \quad n \in \mathbb{N}. \tag{5.1.9}$$

Immediately we can write down the distribution of M_n without any difficulty:

$$\mathbf{P}(M_n \leq x) = \mathbf{P}(X_1 \leq x, \ldots, X_n \leq x) = F^n(x), \quad n \in \mathbb{N}. \tag{5.1.10}$$

Denote by x_F the right endpoint of F, i.e.,

$$x_F = \sup\{x \in \mathbb{R} : F(x) < 1\}. \tag{5.1.11}$$

Then we see that $F^n(x)$ is decreasing in n for all $x < x_F$, especially

$$\mathbf{P}(M_n \le x) = F^n(x) \to 0, \quad \text{as } n \to \infty,$$

while for $x \ge x_F$

$$\mathbf{P}(M_n \le x) = F^n(x) = 1.$$

This shows that M_n will concentrate on the right endpoint of F as $n \to \infty$. This in fact does not provide useful information. In the preceding section, we have seen that, when appropriately centered and normalised, a sum of i.i.d. random variables admits an α-stable distribution as limiting distribution. Here we have a similar question for maxima: whether we can obtain more insight into maxima by appropriately centering and normalising them. This question is one of the main topics of the extreme value theory which was addressed in the first time in Fréchet 1927 [144]. Therein, Fréchet showed that the limiting distribution of maximum of i.i.d. random variables when existing can have one of two known forms, called *Fréchet* distribution and *Weibull* distribution. Later, Fisher and Tippett 1928 [145] completed the work of Fréchet in determining the third limiting distribution which is *double exponential* distribution. This has received great attention in probability theory and mathematical statistics research with early works due to Gumbel 1934 [146], von Mises 1936 [147], and Gnedenko 1943 [148]. Results have been developed for different settings including extremes of i.i.d. observations, extremes of stationary sequences and processes, see c.f. [149], and multivariate extremes [150, 151]. Textbooks of Leadbetter et al. [149] and of Resnick [150] are of the best references for fundamental technical aspects, while the textbook of Embrechts et al. [143] provides a very intuitive description of the theory, and in particular shows its recent applications in finance and insurance.

Given the volume of the literature on the extreme value theory, we restrict our attention here to results which are pertinent to our later developments. More precisely, in this subsection we shall deal with results related to limiting laws of maxima of a sequence of i.i.d. random variables, and present in the next subsection results on the asymptotic joint distribution of the maximum and the sum.

Fundamentally, Fisher and Tippett [145] proved that under appropriate normalisation, if the normalised maximum tends in distribution to a non-degenerate distribution H, this latter must have one of the three known forms, which are commonly called extreme value distributions. It is stated in the following, taken from Theorem 3.2.3 in [143].

Theorem 5.1.11 (Fisher-Tippett Theorem)**.** *If there exists normalizing constants $c_n > 0$, $d_n \in \mathbb{R}$ and some non-degenerate distribution function H such that*

$$c_n^{-1}(M_n - d_n) \xrightarrow{d} H, \quad \text{as } n \to \infty. \tag{5.1.12}$$

Then H belongs to the type of one of the following three distribution functions:

$$\begin{aligned}
\text{Fréchet:} \quad \Upsilon_\theta(x) &= \begin{cases} 0, & x \le 0 \\ \exp(-x^{-\theta}), & x > 0 \end{cases}, \quad \theta > 0. \\[2mm]
\text{Weibull:} \quad \Psi_\theta(x) &= \begin{cases} \exp(-(-x)^\theta), & x \le 0 \\ 1, & x > 0 \end{cases}, \quad \theta > 0. \\[2mm]
\text{Gumbel:} \quad \Lambda(x) &= \exp(-e^{-x}), \quad x \in \mathbb{R}.
\end{aligned}$$

Definition 5.1.12. *We say that the distribution F (random variable X) belongs to the maximum domain of attraction of the extreme value distribution H if (5.1.12) holds for some constants $c_n > 0$ and $d_n \in \mathbb{R}$. We write $F \in \mathrm{MDA}(H)$ ($X \in \mathrm{MDA}(H)$).*

The limiting distribution of the maximum of i.i.d. random variables when it exists can only have one of the above three types of extreme value distributions. A first question is how to determine the maximum domain of attraction of a given distribution function. In other words, how to characterise the three maximum domains of attractions. This question was at first treated by Gnedenko [148]. Then Haan [152] improved the characterisation for the maximum domain of attraction of the Gumbel distribution so that it could be easier for applications. Before going to the characterisation of the maximum domains of attraction, we are interested in the following two results.

Definition 5.1.13. *Two distribution functions F and G are called tail-equivalent if they have the same right endpoint, i.e. $x_F = x_G$, and*

$$\lim_{x \uparrow x_F} \overline{F}(x)/\overline{G}(x) = c \tag{5.1.13}$$

for some constant $0 < c < \infty$.

Theorem 5.1.14 (Thm 2.1, Resnick [153])**.** *For two tail-equivalent distribution functions F and G such that (5.1.13) holds for some constant $0 < c < \infty$, if F belongs to the maximum domain of attraction of the extreme value distribution H with constants $c_n > 0$ and $d_n \in \mathbb{R}$, i.e.,*

$$F^n(c_n x + d_n) \to H(x), \quad \text{as } n \to \infty,$$

then

$$G^n(c_n x + d_n) \to H^{\frac{1}{c}}(x), \quad \text{as } n \to \infty. \tag{5.1.14}$$

It can be easily shown that for $c > 0$ [153, p.140]:

$$
\begin{aligned}
\Upsilon_\theta^c(x) &= \Upsilon_\theta\left(c^{-\frac{1}{\theta}}x\right), \\
\Psi_\theta^c(x) &= \Psi_\theta\left(c^{\frac{1}{\theta}}x\right), \\
\Lambda^c(x) &= \Lambda(x - \log c).
\end{aligned}
\tag{5.1.15}
$$

It means that a power with positive coefficient of an extreme value distribution will result in the an extreme value distribution of the same type. Thus, two tail-equivalent distributions belong the same maximum domain of attraction. The reverse is given in the following.

Theorem 5.1.15 (Thm 2.3, Resnick [153])**.** *Let F and G be distribution functions, and let H be an extreme value distribution. Suppose $F \in \mathrm{MDA}(H)$ and that $F^n(c_n x + d_n) \to H(x)$ as $n \to \infty$ for constants $c_n > 0$ and $d_n \in \mathbb{R}$. Then $G^n(c_n x + d_n) \to \widetilde{H}(x)$ as $n \to \infty$ with $\widetilde{H}$ non-degenerate if and only if for some $a > 0$, $b \in \mathbb{R}$:*

$$\widetilde{H}(x) = H(ax + b), \tag{5.1.16}$$

F and G are tail-equivalent,

and if

(i) $H(x) = \Upsilon_\theta(x)$, then $b = 0$ and $\lim_{x \to \infty} \overline{F}(x)/\overline{G}(x) = a^\theta$;

(ii) $H(x) = \Psi_\theta(x)$, then $b = 0$ and $\lim_{x \uparrow x_F} \overline{F}(x)/\overline{G}(x) = a^{-\theta}$;

(iii) $H(x) = \Lambda(x)$, then $a = 0$ and $\lim_{x \uparrow x_F} \overline{F}(x)/\overline{G}(x) = e^b$.

By the above two theorems, we only need to determine the maximum domain of attraction of some 'well-known' distribution functions. And then, in order to determine the maximum domain of attraction of a given distribution function, we just determine its tail-equivalent distribution whose attraction domain is already known.

We shall describe in the following the main properties of the three maximum domains of attraction. Although not all of the following results will be used in our later developments, they are described here for seek of completeness and also for the great interest of the results. The following definition will be used in the subsequent results.

Definition 5.1.16 (Generalised inverse of a monotone function, Defn 3.3.4 [143]). *Suppose that h is a non-decreasing function on $\mathbb{R}$. The generalised inverse of h is defined as*

$$h^\leftarrow(t) = \inf\{x \in \mathbb{R} : h(x) \geq t\},$$

with the convention that $\inf\{\varnothing\} = +\infty$.

For a distribution function F, its generalised inverse function of is called *quantile function*. We begin with a characterisation of the maximum domain of attraction of Fréchet distributions which was given by Theorem 4 in Gnedenko [148] and was restated in Theorem 3.3.7 in Embrechts et al. [143].

Theorem 5.1.17 (Characterisation of MDA(Υ_θ)). *The distribution function F belongs to the maximum domain of attraction of Υ_θ, $\theta > 0$, if and only if $\overline{F}(x) = x^{-\theta}L(x)$ for some slowly varying function L. If $F \in$ MDA(Υ_θ), then*

$$c_n^{-1} M_n \xrightarrow{d} \Upsilon_\theta, \tag{5.1.17}$$

where the constant c_n can be chosen as $c_n = (1/\overline{F})^\leftarrow(n)$.

It follows that $F \in$ MDA(Υ_θ) iff $F \in \mathcal{R}_{-\theta}$ with $-\theta < 0$ which is the class of regularly varying functions. And thus the maximum domain of attraction of the Fréchet distribution contains "very heavy-tailed distributions" in the sense that $\mathbf{E}\{(X^+)^\delta\} = \infty$ for $\delta > \theta$ where $X^+ = \max\{0, X\}$, see §5.1.1. Some examples include Pareto-like distributions, which are very heavy-tail such as Pareto, Cauchy, and α-stable distributions with $\alpha < 2$.

Now we characterise the maximum domain of attraction of Weibull distribution Ψ_θ. It can be shown that [143, §3.2]:
$$\Psi_\theta(-x^{-1}) = \Upsilon_\theta(x), \quad x > 0.$$

Therefore the maximum domain of attraction of Ψ_θ can be obtained from that of Υ_θ. The following result was given by Theorem 5 in Gnedenko [148], and was summarised in Theorem 3.3.12 in Embrechts et al. [143].

Theorem 5.1.18 (Characterisation of MDA(Ψ_θ))**.** *The distribution function F belongs to the maximum domain of attraction of Ψ_θ, $\theta > 0$, if and only if $x_F < \infty$ and $\overline{F}(x_F - x^{-1}) = x^{-\theta}L(x)$ for some slowly varying function L. If $F \in \text{MDA}(\Psi_\theta)$, then*

$$c_n^{-1}(M_n - x_F) \xrightarrow{d} \Psi_\theta, \tag{5.1.18}$$

where the constant c_n can be chosen as $c_n = x_F - F^{\leftarrow}(1 - n^{-1})$.

Thus, MDA(Ψ_θ) contains distribution functions with bounded support (to the right), and having very heavy-tailed behaviours.

Finally, we characterise the maximum domain of attraction of the Gumbel distribution Λ. Characterising MDA(Λ) requires more efforts than those for the above two domains of attraction. It was firstly addressed by Gnedenko [148], but he remarked that the characterisation of MDA(Λ) should not be regarded as completed and easy enough for applications. De Han [152] addressed this question and developed a complete characterisation which was later improved by Balkema and De Haan [154]. The following two main charaterisations were summarised in [150] and in [143, p.142-143] using vocabulary of the regular variation.

Theorem 5.1.19 (Characterisation I of MDA(Λ), Thm 3.3.26 [143])**.** *The distribution function F with $x_F \leq \infty$ belongs to the maximum domain of attraction of Λ if and only if there exists some $z < x_F$ such that:*

$$\overline{F}(x) = c(x)\exp\left(-\int_z^x \frac{g(t)}{a(t)}dt\right), \qquad for\ z < x < x_F, \tag{5.1.19}$$

where c and g are measurable functions satisfying $c(x) \to c > 0$, $g(x) \to 1$ as $x \uparrow x_F$, and $a(x)$ is a positive, absolutely continuous functions with density $a'(t)$ having $\lim_{x \uparrow x_F} a'(x) = 0$. For F with representation (5.1.19) we can choose normalising constants as

$$d_n = F^{\leftarrow}(1 - n^{-1}) \quad and \quad c_n = a(d_n). \tag{5.1.20}$$

A possible choice for the function a is

$$a(x) = \int_x^{x_F} \frac{\overline{F}(t)}{\overline{F}(x)}dt, \quad x < x_F. \tag{5.1.21}$$

It follows that the maximum domain of attraction of the Gumbel distribution contains distribution functions which can have right-bounded or right-unbounded support, i.e. both cases $x_F < \infty$ and $x_F = \infty$ are possible. This differs from MDA(Ψ_θ) which contains only distribution functions with right-bounded support. Further, it is observed that the representation (5.1.19) is not unique [143, p.143] as we can have some tradeoff between functions c and g. An alternative representation can be obtained as follows [150]:

$$\overline{F}(x) = c(x)\exp\left(-\int_z^x \frac{1}{a(t)}dt\right), \qquad for\ z < x < x_F, \tag{5.1.22}$$

for functions c and a satisfying conditions as in Theorem 5.1.19. As a sequel of (5.1.3), $\overline{F} \in \mathcal{R}_{-\infty}$, i.e. $\overline{F}$ is rapidly varying at x_F. In other words, MDA(Λ) contains distribution functions belonging to $\mathcal{R}_{-\infty}$. This differs MDA(Λ) from MDA(Υ_θ) by the fact that this latter is characterised by class $\mathcal{R}_{-\theta}$ with $0 < \theta < \infty$; see the remark after Theorem 5.1.17.

The second characterisation of MDA(Λ) is given in the following.

Theorem 5.1.20 (Characterisation II of MDA(Λ), Thm 3.3.27 [143])**.** *The distribution function F belongs to the maximum domain of attraction of Λ if and only if there exists some positive functions $\widetilde{a}$ such that the condition*

$$\lim_{x \uparrow x_F} \frac{\overline{F}(x + t\widetilde{a}(x))}{\overline{F}(x)} = e^{-t}, \quad t \in \mathbb{R}, \tag{5.1.23}$$

holds. A possible choice of $\widetilde{a}$ is the function a as given in (5.1.21).

Note that the function a in (5.1.21) is called *auxiliary function* for F. It is nothing but the *mean excess function* [143]:
$$a(x) = \mathbf{E}\{X - x \mid X > x\}, \quad x < x_F.$$

The above two Theorems 5.1.19 and 5.1.20 provide the main characterisations of the maximum domain of attraction of the Gumbel distribution with insight into how to choose normalising constants. However, one of the inconveniences is that this is not very simple to do because one will need to solve for equations as given in (5.1.20) which are usually complicated. For our later developments, we are interested in the following two properties. The first property is the monotone transformation described in [143, p.147]. It is stated in the following.

Proposition 5.1.21 (Embrechts et al. [143])**.** *Let Z_i be i.i.d. random variables having distribution F, and $M_n = \max_{i=1}^n X_i$. Let g be an increasing real function, denote $\widetilde{X}_i = g(X_i)$, and $\widetilde{M}_n = \max_{i=1}^n \widetilde{X}_i$. If $F \in MDA(\Lambda)$ with normalizing constant c_n and d_n, then*

$$\lim_{n \to \infty} \mathbf{P}\big(\widetilde{M}_n \leq g(c_n z + d_n)\big) = \Lambda(z), \quad z \in \mathbb{R}.$$

The second property that we shall describe below is due to Takahashi [155]. It provides necessary conditions for a distribution function to belong to MDA(Λ), and also proposes how to choose normalising constants.

Theorem 5.1.22 (Takahashi [155])**.** *Let F be a distribution function. Suppose that there exists constants $\omega > 0$, $l > 0$, $\eta > 0$ and $r \in \mathbb{R}$ such that*

$$\lim_{x \to \infty} \big(1 - F(x)\big) / \big(l x^r e^{-\eta x^\omega}\big) = 1. \tag{5.1.24}$$

For $\mu \in \mathbb{R}$ and $\sigma > 0$, let $F_* = F((x - \mu)/\sigma)$. Then, $F_* \in MDA(\Lambda)$ with normalizing constants $c_n^* = \sigma c_n$ and $d_n^* = \sigma d_n + \mu$, where

$$c_n = \frac{(\log n/\eta)^{\frac{1}{\omega} - 1}}{\omega \eta}, \text{ and}$$

$$d_n = \big(\frac{\log n}{\eta}\big)^{1/\omega} + \frac{\eta^{1/\omega}}{\omega^2} \frac{r(\log \log n - \log \eta) + \omega \log l}{(\log n)^{1 - \frac{1}{\omega}}}.$$

Remark *5.1.23.* In the paper [155] of Takahashi, the last term in the numerator of the expression of d_n is $\omega \log \omega$. After some verifications of his above result with several known distributions including normal and lognormal distributions, we found that this term must be $\omega \log l$ as it is stated above. In fact notations used in his paper are a for ω, and α for l. As a and α are apparently similar, we would guess that these two variables were probably confused during typing.

5.1.4 Limiting Joint Behaviour of Sum and Maximum

In addition to the limiting distributions of sums and maxima, the properties associated with the joint behaviour between the maximum and the sum has been also an important topic of the extreme value theory.

Darling 1952 [156] showed that if $\overline{F}$ is slowly varying, $\mathbf{E}\{S_n/M_n\} \to 1$ as $n \to \infty$. Extending the earlier result of [156], Maller and Resnick 1984 [157] showed:

Theorem 5.1.24 ([157]). $M_n/S_n \xrightarrow{\mathrm{P}} 1$ *as $n \to \infty$ if and only if $\overline{F} \in \mathcal{R}_0$.*

It means that if $\overline{F}$ is slowly varying (and so F does not have finite moments for any order $\varepsilon > 0$), the extreme term is of the same order as the sum. In that case the extreme term dominantly contributes to the sum while the remaining is asymptotically negligible.

In case that $\overline{F}$ is regularly varying with some index $-\alpha < 0$, i.e. F has finite moments of some fractional order $\varepsilon > 0$, Bingham and Teugels 1981 [158] showed that the extreme term only contributes a proportion to the sum.

Theorem 5.1.25 ([158]). *The following assertions are equivalent:*

(i) $\overline{F} \in \mathcal{R}_{-\alpha}$ for some $\alpha \in (0,1)$,

(ii) $M_n/S_n \xrightarrow{d} R$ as $n \to \infty$, where R has a non-degenerate distribution,

(iii) $\mathbf{E}\{S_n/M_n\} \to (1-\alpha)^{-1}$ as $n \to \infty$ for some $\alpha \in (0,1)$.

And for the case of $\alpha \in (1,2)$:

Theorem 5.1.26 ([158]). *Let $\mu = \mathbf{E}X_1$. The following assertions are equivalent:*

(i) $\overline{F} \in \mathcal{R}_{-\alpha}$ for some $\alpha \in (1,2)$,

(ii) $(S_n - (n-1)\mu)/M_n \xrightarrow{d} D$ as $n \to \infty$, where D has a non-degenerate distribution,

(iii) $\mathbf{E}\{(S_n - (n-1)\mu)/M_n\} \to c$ as $n \to \infty$ for some constant c.

Complementing to the above result of [158], Downey and Wright 1994 [159] showed

Theorem 5.1.27. *If either one of the following two conditions:*

(a) $\overline{F} \in \mathcal{R}_{-\alpha}$ for some $\alpha > 1$, or

(b) F has finite second moment

holds. Then

$$\mathbf{E}\left\{\frac{M_n}{S_n}\right\} = \frac{\mathbf{E}M_n}{\mathbf{E}S_n}\Big(1 + o(1)\Big), \quad as\ n \to \infty.$$

It follows that under suitable conditions, the expected ratio of the extreme term to the sum is asymptotically equal to the ratio of the expectations.

The above results and some related works provide information about the influence of the extreme term in the entire sum. In parallel to this view, the joint behaviour of the maximum and the sum has been studied in term of the limiting joint distribution. One of the first results of this topic was due to Chow and Teugels 1978 [160] for the case of i.i.d. random variables. Their conclusion is that under suitable conditions the maximum and the sum behave asymptotically independently as $n \to \infty$. It is given in the following.

Theorem 5.1.28 (Chow and Teugels [160]). *Let $a_n > 0$, $c_n > 0$, b_n, $d_n \in \mathbb{R}$, write*

$$(\widetilde{M}_n, \widetilde{S}_n) \equiv \left(\frac{M_n - d_n}{c_n}, \frac{S_n - b_n}{a_n} \right).$$

Then

$$\left(\frac{M_n - d_n}{c_n}, \frac{S_n - b_n}{a_n} \right) \xrightarrow{d} (U, V),$$

where neither U nor V is degenerate if and only if F belongs to both the domains of attraction of an extreme value distribution H and an α-stable law, i.e., $F \in \mathrm{MDA}(H) \cap \mathrm{D}(\alpha)$. The random variables U and V are independent unless $0 < \alpha < 2$, $\delta > -1$, and $H = \Upsilon_\alpha$. In the latter case, for $t \in R$, $v > 0$:

$$\mathbf{E}\{\exp(jt\widetilde{S}_n), \widetilde{M}_n \leq v\} = \phi_\alpha(t) \cdot \exp\left(\int_v^\infty e^{jtku} \mathrm{d}u^{-\alpha} \right)$$

where $\phi_\alpha(t)$ is the characteristic function of the α-stable distribution as given in (5.1.4) with $\gamma = 0$, and $k = \left(\mathrm{const} \cdot \frac{1+\delta}{2} \frac{2-\alpha}{\alpha} \right)^{1/\alpha}$.

It follows from Chow and Teugels [160] that if F has finite second moment, i.e. $F \in D(2)$, and if F belongs to the maximum domain of attraction of either Gumbel distribution Λ, or Fréchet distribution Υ_α with $\alpha \geq 2$, then the sum and the maximum are asymptotically independent as $n \to \infty$.

Anderson and Turkman [161] extended the above result of Chow and Teugels [160] to the case of stationary sequences with certain dependency conditions. Under suitable conditions of weak dependence, they showed that the asymptotic independence between the sum and the maximum is also obtained. Further, in their later work [162] appearing in 1995, they extended the above results and showed that under suitable conditions the asymptotic independence also holds for stationary sequences with distribution function which belongs to the domain of attraction (for sums) of an α-stable law of index $\alpha < 2$.

5.1.5 Application to Wireless Network Modelling

In previous sections, we obtained asymptotic behaviour of extreme events observed from n i.i.d. random variables as $n \to \infty$. But how should these results be applied to a wireless network? We can see that a scenario to which these results would be applied should fulfill two necessary conditions. First, it has to provide the *i.i.d.* condition among quantities to be observed. And second, the amount of quantities to be observed must be *infinitely large* standing for $n \to \infty$ condition.

In the wireless network modelling context, we can show here an example by considering a wireless network where more and more nodes are additionally deployed on a given geographical area in order to satisfy the need for capacity or coverage, such as hot-spot networks deployed for growing traffic demands, and ad-hoc / sensor wireless networks. This kind of network deployment is practically known as the network densification under which the total number of nodes N in the network may take very large values. Let $M_N = \max_{i=1,\ldots,N} P_i$ be the global maximum, and $I_N = \sum_{i=1,\ldots,N} P_i$ be the total interference. By taking appropriate assumptions so that received signal powers $\{P_i, i = 1, \ldots, N\}$ are i.i.d., and using the fact of network densification by which $N \to \infty$, one can apply above results to study the asymptotic behaviour of M_N, I_N, as well as of their joint distribution.

5.2 Stochastic Geometry

A wireless network is made up of communicating nodes which are spatially distributed in a plane or in higher dimensions. As we have seen in Chapter 2 the location of nodes is essential to the network modelling, especially for the analytical description of the signal strength, signal quality, and the interference which all depend on the relative spatial separation between nodes. For this reason, the modelling of the node spatial distribution is one of the main topics of wireless networking. Among different approaches, the spatial point process (p.p.) has received a lot of attention with many results and applications. Our attention in this section is focused on theoretical results of the field which are relevant to our purpose. We will provide a basic background on the spatial point processes with a focus on Poisson point processes which are required for an understanding of the Shot Noise field. Basic mathematical modelling of interference in wireless networks using Shot Noise field will be then presented. After that we will review some important results on the application of this mathematical tool to wireless networks.

5.2.1 Point Processes

Intuitively speaking, a spatial point process Φ is a *random* collection of "points" without accumulation in some metric space $\mathbb{S}$ [49]. Let $\delta_{\mathbf{x}}$ be the Dirac measure at $\mathbf{x} \in \mathbb{S}$, for $A \subset \mathbb{S}$:

$$\delta_{\mathbf{x}}(A) = \begin{cases} 1 & \text{if } \mathbf{x} \in A, \\ 0 & \text{if } \mathbf{x} \notin A. \end{cases}$$

The point process Φ can be represented as a point measure on $\mathbb{S}$ given as

$$\Phi = \sum_i \delta_{\mathbf{x}_i}. \tag{5.2.1}$$

Here $\mathbf{x}_i$ is a *random* variable taking value in $\mathbb{S}$, i.e. a point, and the random collection $\{\mathbf{x}_i\}$ represents the points of Φ. Then, Φ is a counting measure for which $\Phi(A)$ counts the number of points of Φ in set A. And a point process Φ is associated with an intensity measure Ξ defined as $\Xi(A) = \mathbf{E}\Phi(A)$ for $A \subset \mathbb{S}$ [11].

A spatial point process thus allows one to describe the location of nodes, seen as "points", which are randomly located in a wireless network according to some distribution. It is worth noting that the application of point processes is far beyond wireless networks. It is a well studied

branch in probability theory and especially is a powerful tool in statistics for modelling and analysing spatial data, for example in materials science, geography, and astronomy. An example showing the interest of point processes is the case where $\mathbb{S} = \mathbb{R}$. In this case, point processes model random events arriving at random times, such as user arrivals in queuing systems. In the remaining of this section we will consider $\mathbb{S} = \mathbb{R}^d$ with $d \geq 1$.

Similar to the fact that the distribution function of a random variable is completely charaterised by its *characteristic function*, a point process is characterised by its *Laplace functional* whose definition taken from Definition 1.2.1 in Baccelli and Blaszczyszyn [49] is given in the following.

Definition 5.2.1 (Laplace functional of point process)**.** *The Laplace functional $\mathcal{L}$ of a point process Φ is*

$$\mathcal{L}_{\Phi}(f) = \mathbf{E}\left\{ \exp\left(-\int_{\mathbb{R}^d} f(\mathbf{x})\Phi(\mathrm{d}\mathbf{x}) \right) \right\},$$

where f runs over the set of all non-negative functions on $\mathbb{R}^d$.

A special and useful case of point process is the Poisson point process. A point process Φ is Poisson if (i) for all bounded, disjoint sets $A_1, \ldots, A_k$ of $\mathbb{R}^d$, the random variables $\Phi(A_1), \ldots, \Phi(A_k)$ are independent, and (ii) for all set $A \subset \mathbb{R}^d$ the random variable $\Phi(A)$ is Poisson. Below, Ξ is a locally finite measure [1] on $\mathbb{R}^d$.

Definition 5.2.2 (Poisson p.p.)**.** *A Poisson point process Φ of intensity measure Ξ is defined by its finite-dimensional distributions*

$$\mathbf{P}(\Phi(A_1) = n_1, \ldots, \Phi(A_k) = n_k) = \prod_{i=1}^{k} \left(\frac{\Xi(A_i)^{n_i}}{n_i!} \exp(-\Xi(A_i)) \right). \tag{5.2.2}$$

If $\Xi(\mathrm{d}\mathbf{x}) = \lambda\mathrm{d}\mathbf{x}$ for λ a positive constant, we call Φ a homogeneous *Poisson point process, and call λ its* intensity parameter.

An interesting property of Poisson p.p. is that conditionally on the fact that there are n points located in a set A, i.e. $\Phi(A) = n$, then these n points are independently (and uniformly if Φ is homogeneous) distributed in A [11]. This property leads to many interesting results; especially it allows one to obtain the Laplace functional of a Poisson p.p. Φ given by Proposition 1.2.2 in [49]) as follows

Proposition 5.2.3. *The Laplace functional of a Poisson p.p. of intensity measure Ξ is*

$$\mathcal{L}_{\Phi}(f) = \exp\left(-\int_{\mathbb{R}^d} (1 - e^{-f(\mathbf{x})})\Xi(\mathrm{d}\mathbf{x}) \right). \tag{5.2.3}$$

Offering computational convenience, Poisson point processes form the most widely used class of point processes, especially for the modelling of different network quantities of interest. In the following, we will describe some operations which preserve the Poisson law. We refer to Baccelli and Blaszczyszyn [49] for technical details and proofs.

Definition 5.2.4 (Superposition of point processes)**.** *The superposition of point processes $\{\Phi_k\}$ is defined as the sum $\Phi = \sum_k \Phi_k$.*

---

[1] A measure μ is called *locally finite* if for every point $\mathbf{x}$ of the space there exists a neighbourhood $N_{\mathbf{x}}$ which is finite under μ, $\mu(N_{\mathbf{x}}) < \infty$. For example, any probability measure is locally finite since it assigns the unit measure to the whole probability space.

Proposition 5.2.5 (Prop 1.3.3 [49])**.** *The superposition of independent Poisson point processes with intensities Ξ_k is a Poisson p.p. with intensity measure $\Xi = \sum_k \Xi_k$ if and only if the latter is a locally finite measure.*

Unlike the superposition operation, the following operation preserves the Poisson law but "partitions" a point process. Consider a function $p : \mathbb{R}^d \mapsto [0, 1]$ and a p.p. Φ, we define:

Definition 5.2.6 (Thinning)**.** *The thinning of Φ with the retention function p is a p.p. given by*

$$\Phi^p = \sum_k \varepsilon_k \delta_{\mathbf{x}_k}, \tag{5.2.4}$$

where the random variables $\{\varepsilon_k\}$ take values $\{0, 1\}$, are independent given Φ, and

$$\mathbf{P}(\varepsilon_k = 1 \,|\, \Phi) = 1 - \mathbf{P}(\varepsilon_k = 0 \,|\, \Phi) = p(\mathbf{x}_k). \tag{5.2.5}$$

Proposition 5.2.7 (Prop 1.3.5 [49])**.** *The thinning of the Poisson p.p. of intensity measure Ξ with the retention probability p yields a Poisson p.p. of intensity measure $p\Xi$ with $(p\Xi)(A) = \int_A p(\mathbf{x})\Xi(\mathrm{d}\mathbf{x})$.*

In particular, we can easily see that if p is a constant function, i.e. $p(\mathbf{x}) = \rho$ for some constant $\rho \in [0, 1]$, and if the Poisson p.p. is homogeneous with intensity parameter λ, then the resulting Poisson p.p. is homogeneous with intensity parameter $\rho\lambda$. The above two operations seem straightforward but provide useful tools especially when one needs to study a heterogeneous network which is composed of some homogenous network layers such as co-existing macro-and-small cell networks. Even in the case of a homogenous network, algorithms used in cellular network such as those for node association or for neighbour cell selection require one to distinguish between the collection of candidate nodes from the remaining. In this case, one may consider the collection of the candidate nodes as a thinning of the whole network. We will talk about this again and again in many upcoming chapters.

5.2.2 Shot Noise Field

Point processes allow one to describe the location of nodes or points in the space. It is often the case that each node is associated with some information, for example the energies carried by particles in certain system, or the transmission powers of nodes in a wireless network. To describe this, the notion of *marked point processes* has been introduced. For a point process Φ defined on a space $\mathbb{R}^d$ with $d \geq 1$, consider that every point $\mathbf{x}_i$ of Φ is attached a random *mark* m_i which takes value in another space $\mathbb{R}^l$ with $l \geq 1$. The the collection of random pairs $(\mathbf{x}_i, m_i\}$ is called a *marked point process*, denoted by $\widetilde{\Phi}$. Similar to the representation (5.2.1) of the point process, the marked point process can be represented as the sum of Dirac measures

$$\widetilde{\Phi} = \sum_i \delta_{\mathbf{x}_i, m_i}, \tag{5.2.6}$$

where $\delta_{\mathbf{x}, m}$ is the Dirac measure on the Cartesian product $\mathbb{R}^d \times \mathbb{R}^l$, see Chapter 2 in [49].

Remark 5.2.8. It is observed in [49, p.23] that the representation (5.2.6) shows that the marked point process $\widetilde{\Phi}$ is a point process on the space $\mathbb{R}^d \times \mathbb{R}^l$. So, it has all properties of a point process, and this observation will be very useful in developing formulas for marked point processes.

The following definition, taken from Definition 2.1.1 in [49], specifies an important special case of marked point processes.

Definition 5.2.9. *A marked point process* $\widetilde{\Phi}$ *is said to be* independently marked *if:*

- *The marks* $\{m_i\}$ *are mutually independent given the location of the points* $\{\mathbf{x}_i\}$,

- *And the conditional distribution of the mark* m *attached to point* $\mathbf{x} \in \Phi$ *only depends on the location of this point* $\mathbf{x}$. *We denote by* $F_{\mathbf{x}}$ *the distribution of the mark associated to* $\mathbf{x}$.

Referring to Remark 5.2.8 where we say that a marked point process can be seen as a point process on the combining space, the following is an interesting result of the independently marked Poisson point process case, given by Corollary 2.1.2 in [49].

Proposition 5.2.10. *An independently marked Poisson point process* $\widetilde{\Phi}$ *with intensity measure* Ξ *on* $\mathbb{R}^d$ *and marks with distributions* $F_{\mathbf{x}}$ *on* $\mathbb{R}^l$ *is a Poisson point process on* $\mathbb{R}^d \times \mathbb{R}^l$ *with intensity measure* $\widetilde{\Xi}$ *given by*

$$\widetilde{\Xi}(A \times K) = \int_A \int_K F_{\mathbf{x}}(\mathrm{d}m) \Xi(\mathrm{d}\mathbf{x}) \tag{5.2.7}$$

for $A \subset \mathbb{R}^d$ *and* $K \subset \mathbb{R}^l$.

Given a marked point process $\widetilde{\Phi}$, a shot noise generated by $\widetilde{\Phi}$ is a non-negative vector random field $I_{\widetilde{\Phi}}(\mathbf{y})$ in $\mathbb{R}^k_+$ with $k \geq 1$ defined for all $\mathbf{y}$ in space $\mathbb{R}^{d'}$ with $d' \geq 1$, and is a functional of $\widetilde{\Phi}$. Its definition involves the following ingredients [49, §2.2.1]:

- The shot noise field is defined on $\mathbb{R}^{d'}$, i.e. for all $\mathbf{y} \in \mathbb{R}^{d'}$,

- The vector field takes values in $\mathbb{R}^k_+$, i.e. $I_{\widetilde{\Phi}}(\mathbf{y}) \in \mathbb{R}^k_+$,

- It is generated by the marked point process $\widetilde{\Phi}$ on $\mathbb{R}^d$ with marks in $\mathbb{R}^l$,

- It is associated with a non-negative response function $L = (L_1, \ldots, L_k) : \mathbb{R}^{d'} \times \mathbb{R}^d \times \mathbb{R}^l \mapsto \mathbb{R}^k_+$.

The shot noise field is then the result of a mapping of the marked point process $\widetilde{\Phi}$ to the "observing space" $\mathbb{R}^{d'}$ by the transfer function L; and the structure of the resulting shot noise field depends on this transfer function. Note that while the points of the point process Φ are mostly considered as "discrete" atoms in the space, the shot noise field is defined for the whole continuous space $\mathbb{R}^{d'}$.

On the shot noise field one may define different quantities, in the following we are interested in two quantities which are closely related to our later developments. These are the *additive shot noise* and the *extremal shot noise*.

Additive Shot Noise. With the above ingredients, we take the Definition 2.2.1 in [49] to define the additive shot noise.

Definition 5.2.11 (Additive Shot Noise). *Under the setting described above, the additive shot noise associated with the marked point process* $\widetilde{\Phi}$ *and the response function* L *is defined by*

$$I_{\widetilde{\Phi}}(\mathbf{y}) = (I_1(\mathbf{y}), \ldots, I_k(\mathbf{y})) = \int_{\mathbb{R}^d} \int_{\mathbb{R}^l} L(\mathbf{y}, \mathbf{x}, m) \widetilde{\Phi}(\mathrm{d}(\mathbf{x}, m)) = \sum_{(\mathbf{x}_i, m_i) \in \widetilde{\Phi}} L(\mathbf{y}, \mathbf{x}_i, m_i), \tag{5.2.8}$$

for $\mathbf{y} \in \mathbb{R}^{d'}$, *where the integral and the sum are evaluated component-wise for the vector response function* L.

Roughly speaking, the additive shot noise $I_{\widetilde{\Phi}}(\mathbf{y})$ at the observation point $\mathbf{y} \in \mathbb{R}^{d'}$ collects all the marks of the marked point process $\widetilde{\Phi}$ on space $\mathbb{R}^{d}$ through the "observation method" L, and then takes the total sum over the collected marks.

The additive shot noise $I_{\widetilde{\Phi}}(\mathbf{y})$ is nothing but a k-dimensional random variable. Therefore as usual we would like to determine its Laplace transform. By definition (5.2.8) we have

$$\mathcal{L}_{I_{\widetilde{\Phi}}(\mathbf{y})}(t_1, \ldots, t_k) = \mathbf{E}\Big\{ \exp\Big(-\sum_{i=1}^{k} t_i I_i(\mathbf{y}) \Big) \Big\}$$

$$= \mathbf{E}\Big\{ \exp\Big(-\int_{\mathbb{R}^d} \int_{\mathbb{R}^l} \sum_{i=1}^{k} t_i L_i(\mathbf{y}, \mathbf{x}, m) \widetilde{\Phi}(\mathrm{d}(\mathbf{x}, m)) \Big) \Big\}. \tag{5.2.9}$$

By the Remark 5.2.8, it turns out that the above Laplace transform of $I_{\widetilde{\Phi}}(\mathbf{y})$ is the Laplace functional of the point process $\widetilde{\Phi}$ on the space $\mathbb{R}^{d} \times \mathbb{R}^{l}$ at the input function $f(\mathbf{x}, m) = \sum_{i=1}^{k} t_i L_i(\mathbf{y}, \mathbf{x}, m)$, see Definition 5.2.1. Now if we consider that the point process $\widetilde{\Phi}$ is Poisson, then its intensity measure $\widetilde{\Xi}$ will be given by Proposition 5.2.10. Thus, using the formula for the Laplace functional of a Poisson point process as given by Proposition 5.2.3, we obtain

$$\mathcal{L}_{I_{\widetilde{\Phi}}(\mathbf{y})}(t_1, \ldots, t_k) = \exp\Big(-\int_{\mathbb{R}^d \times \mathbb{R}^l} (1 - e^{-f(\mathbf{x}, m)}) \widetilde{\Xi}(\mathrm{d}\mathbf{x}, \mathrm{d}m) \Big)$$

$$= \exp\Big(-\int_{\mathbb{R}^d} \int_{\mathbb{R}^l} \Big(1 - e^{-\sum_{i=1}^{k} t_i L_i(\mathbf{y}, \mathbf{x}, m)} \Big) F_{\mathbf{x}}(\mathrm{d}m) \Xi(\mathrm{d}\mathbf{x}) \Big). \tag{5.2.10}$$

This result forms the Proposition 2.2.4 in [49], and is stated below.

Theorem 5.2.12 (Laplace transform of additive shot noise). *Suppose that* $\widetilde{\Phi}$ *is an independently marked Poisson point process with intensity measure* Ξ *and mark distribution* $F_{\mathbf{x}}$. *Consider the additive shot noise* $I_{\widetilde{\Phi}}(\mathbf{y})$ *with response function* $L = (L_1, \ldots, L_k)$. *Then the Laplace transform of* $I_{\widetilde{\Phi}}(\mathbf{y})$ *is given by* (5.2.10).

This is an important result whose applications to the modelling of the interference in a wireless network will be discussed in the next subsection §5.2.3.

Extremal Shot Noise. Now we would like to determine the extremal term of the shot noise field. We define the extremal shot noise as follows, Definition 2.4.1 in [49].

Definition 5.2.13 (Extremal Shot Noise). *For the setting as described above, the extremal shot noise associated with the marked point process* $\widetilde{\Phi}$ *and the response function* L *is defined by*

$$M_{\widetilde{\Phi}}(\mathbf{y}) = (M_1(\mathbf{y}), \ldots, M_k(\mathbf{y})) = \max_{(\mathbf{x}_i, m_i) \in \widetilde{\Phi}} L(\mathbf{y}, \mathbf{x}_i, m_i), \quad \mathbf{y} \in \mathbb{R}^{d'}. \tag{5.2.11}$$

Similar to $I_{\widetilde{\Phi}}(\mathbf{y})$, $M_{\widetilde{\Phi}}(\mathbf{y})$ is a k-dimensional random variable. But more interestingly it is shown in [49, p.40] that the distribution function of $M_{\widetilde{\Phi}}(\mathbf{y})$ can be given explicitly. We have

$$\mathbf{P}(M_j(\mathbf{y}) \leq t_j, \forall j = 1..k) = \mathbf{P}(L_j(\mathbf{y}, \mathbf{x}_i, m_i) \leq t_j, \forall j = 1..k, (\mathbf{x}_i, m_i) \in \widetilde{\Phi})$$

$$= \mathbf{E}\Big\{ \prod_{(\mathbf{x}_i, m_i) \in \widetilde{\Phi}} \prod_{j=1}^{k} \mathbf{1}(L_j(\mathbf{y}, \mathbf{x}_i, m_i) \leq t_j) \Big\}$$

$$= \mathbf{E}\Big\{ \exp\Big(\sum_{(\mathbf{x}_i, m_i) \in \widetilde{\Phi}} \log\Big(\prod_{j=1}^{k} \mathbf{1}(L_j(\mathbf{y}, \mathbf{x}_i, m_i) \leq t_j)\Big)\Big)\Big\}$$

$$= \mathbf{E}\Big\{ \exp\Big(\int_{\mathbb{R}^d \times \mathbb{R}^l} \log\Big(\prod_{j=1}^{k} \mathbf{1}(L_j(\mathbf{y}, \mathbf{x}, m) \leq t_j)\Big) F_{\mathbf{x}}(\mathrm{d}m)\Xi(\mathrm{d}\mathbf{x})\Big)\Big\}.$$

Again this is the Laplace functional of $\widetilde{\Phi}$ at the input function

$$f(\mathbf{x}, m) = -\log\Big(\prod_{j=1}^{k} \mathbf{1}(L_j(\mathbf{y}, \mathbf{x}, m) \leq t_j)\Big).$$

If consider that $\widetilde{\Phi}$ is independently marked Poisson point process, then by Proposition 5.2.3, we obtain [49, Prop.2.4.2]:

Proposition 5.2.14. *Suppose that $\widetilde{\Phi}$ is an independently marked Poisson point process with intensity measure Ξ and mark distribution $F_{\mathbf{x}}$. Consider the extremal shot noise $M_{\widetilde{\Phi}}(\mathbf{y})$ as defined in* (5.2.11). *Then*

$$\mathbf{P}(M_1(\mathbf{y}) \leq t_1, \ldots, M_k(\mathbf{y}) \leq t_k)$$

$$= \exp\Big(- \int_{\mathbb{R}^d \times \mathbb{R}^l} \Big(1 - \prod_{j=1}^{k} \mathbf{1}(L_j(\mathbf{y}, \mathbf{x}, m) \leq t_j)\Big) F_{\mathbf{x}}(\mathrm{d}m)\Xi(\mathrm{d}\mathbf{x})\Big). \quad (5.2.12)$$

In particular, for $k = 1$,

$$\mathbf{P}(M(\mathbf{y}) \leq t) = \exp\Big(- \int_{\mathbb{R}^d \times \mathbb{R}^l} \mathbf{1}(L(\mathbf{y}, \mathbf{x}, m) > t) F_{\mathbf{x}}(\mathrm{d}m)\Xi(\mathrm{d}\mathbf{x})\Big). \quad (5.2.13)$$

5.2.3   Application to Wireless Link Modelling

Point processes provide a mathematical tool to model the spatial aspect of a system, and by parameterising it with marks we are able to quantify more quantities of the interest via a shot noise field generated by a marked point process. As we agree that the above framework and results are general, the spatial distribution of nodes in a wireless network is a particular case which can be suitably studied with this mathematical tool. Our attention in the sequel is reserved for applications of the field to settings which correspond to common characteristics of wireless networks.

In Chapter 2 we see that the signal power received at a location $\mathbf{y} \in \mathbb{R}^2$ from a transmitting node located at $\mathbf{x}_i$ of the two-dimensional Euclidean plane is given by (2.1.12) as:

$$P_i(\mathbf{y}) = \frac{p_i}{l(|\mathbf{y} - \mathbf{x}_i|)},$$

where p_i is the virtual transmission power associated with node $\mathbf{x}_i$ and only depending on this latter, while the path loss function l takes values in $\mathbb{R}_+$ and only depends on the transmitter-receiver spatial separation $|\mathbf{y} - \mathbf{x}_i|$, see §2.1. The interference field within such a context corresponds completely to a shot noise which is defined with the following ingredients:

- The shot noise field is defined on $\mathbb{R}^2$, i.e. $d' = 2$, and takes values in $\mathbb{R}_+$, i.e. $k = 1$,
- It is generated by the independently marked Poisson point process $\widetilde{\Phi} = \{(\mathbf{x}_i, p_i)\}$ where the points $\{\mathbf{x}_i\}$ are on $\mathbb{R}^2$ and marks $\{p_i\}$ take values in $\mathbb{R}_+$,
- It is associated with a scalar non-negative response function defined as $L(\mathbf{x}, \mathbf{y}, p) = p/l(|\mathbf{x} - \mathbf{y}|)$, for $\mathbf{x}, \mathbf{y} \in \mathbb{R}^2$, and $p \in \mathbb{R}_+$.

In particular, often l is a power law of the distance expressible as $l(|\mathbf{y} - \mathbf{x}_i|) = l(|\mathbf{y} - \mathbf{x}_i|)^\beta$ for some path loss exponent $\beta \geq 2$, see §2.1.

Within this setting, the total interference power received at location $\mathbf{y}$ is given as

$$I(\mathbf{y}) = \sum_i P_i(\mathbf{y}) = \sum_i \frac{p_i}{l(|\mathbf{x}_i - \mathbf{y}|)}.$$

This turns out to be the additive shot noise $I_{\widetilde{\Phi}}(\mathbf{y})$ generated by $\widetilde{\Phi}$ and associated to the response function L. Applying Theorem 5.2.12 for the the above setting, we obtain immediately the Laplace transform of $I(\mathbf{y}) = I_{\widetilde{\Phi}}(\mathbf{y})$ as follows.

Corollary 5.2.15. *The Laplace transform of the received interference $I(\mathbf{y})$ is*

$$\mathcal{L}_I(t) = \exp\left(-2\pi\lambda \int_0^\infty r\left(1 - \mathcal{L}_p\left(\frac{t}{l(r)}\right)\right) dr\right), \tag{5.2.14}$$

where $\mathcal{L}_p(t) = \mathbf{E}\{e^{-tp}\}$ is the Laplace transform of the transmission power (i.e. marks p_i).

Here we observe that the Laplace transform of the interference is independent of the receiver's location $\mathbf{y}$. We can simply obtain its characteristic function. Write

$$\phi_I(w) = \mathbf{E}\{\exp(jwI)\}, \quad w \in \mathbb{R},$$

then

$$\phi_I(w) = \mathcal{L}_I(-jw) = \exp\left(-2\pi\lambda \int_0^\infty r\left(1 - \mathcal{L}_p(\frac{-jw}{l(r)})\right) dr\right). \tag{5.2.15}$$

Now, if we consider that the path loss function l is a power law of the distance with exponent β, the characteristic function of I will be equal to

$$\phi_I(w) = \exp\left(-2\pi\lambda \int_0^\infty r\left(1 - \mathbf{E}\left\{\exp(\frac{jwp}{r^\beta})\right\}\right) dr\right),$$

where the expectation is taken over p. Using the change of variable $t = |w|r^{-\beta}$ for the integral and let $\alpha = 2/\beta$, we obtain

$$\int_0^\infty \left(1 - \mathbf{E}\left\{\exp\left(\frac{jwp}{r^\beta}\right)\right\}\right) r\,dr = \frac{\alpha|w|^\alpha}{2} \int_0^\infty \frac{1 - \mathbf{E}\{e^{j\,\mathrm{sign}(w)tp}\}}{t^{\alpha+1}} dt, \tag{5.2.16}$$

which, by special integral formula, is reduced to

$$\int_0^\infty \frac{1 - \mathbf{E}\{e^{j\operatorname{sign}(w)tp}\}}{t^{\alpha+1}}\mathrm{d}t = -\mathbf{E}\{p^\alpha\}\Gamma(-\alpha)e^{-j\operatorname{sign}(w)\frac{\pi\alpha}{2}},$$

where $\Gamma(\cdot)$ denotes the Gamma function. And thereby:

$$\phi_I(w) = \exp\Big(-\delta|w|^\alpha\big(1 - j\operatorname{sign}(w)\tan(\frac{\pi\alpha}{2})\big)\Big), \tag{5.2.17}$$

where $\delta = \pi\lambda\mathbf{E}\{p^\alpha\}\Gamma(1-\alpha)\cos(\frac{\pi\alpha}{2})$. As a result, (5.2.17) shows that the total interference I is an α-stable distribution with index $\alpha = 2/\beta$, see Theorem 5.1.4. This forms a main result of Win et al. [9]. It follows that, under the assumption of unbounded power-law path loss, the interference is Gaussian only if $\beta = 2$ while most of the case is $\beta > 2$ and consequently I is heavier-tailed than it was often assumed, see §2.4. The heavy-tailed behaviour of the interference under the ubbounded power law path loss model was also confirmed by Inaltekin et al. [76].

5.3   Level Crossings of Stochastic Processes

In radio communications, the communication quality depends closely on the received signal quality of the radio link. Especially, the service may be interrupted when the signal quality is worse than some critical level so that received information is not correctly decoded. As we have seen in Chapter 2, radio transmissions are sensitive to the propagation condition and is subject to random variations. This makes the signal quality behave as a stochastic process. The question is thus to understand and to characterise its properties, in particular, in terms of the fluctuation of its amplitude with respect to some threshold level.

It turns out that the above question is in the domain of extreme properties of random processes, especially the so-called *level crossing theory* of stationary processes. This study domain is concerned with random variables associated with crossings of a stochastic process of some level. Its first milestone dates back to the middle of the last century with fundamental works of Rice [12, 13], and of Kac and Slepian [14]. It has been further investigated and its results were quite fully summarised in Cramér and Leadbetter 1967 [163] and in Leadbetter 1983 [149].

This section by no means provides a whole picture of the level crossing theory and its applications, but it is aimed at first summarising some theoretical foundations and then showing some applications to mobile radio communication which will be used to develop our results in subsequent chapters.

5.3.1   Level Crossings of Stationary Gaussian Processes

In this subsection, we shall describe some fundamental results of the level crossing theory. Herein, we consider $X(t)$ a real-valued stationary normal process of continuous parameter t ('time') of *zero mean* and *unit variance*. We assume that $X(t)$ is not identically equal to any fixed level γ during any interval of t. Write $R_X(\tau)$ the autocorrelation function of $X(t)$. We restrict our attention here to some random variables associated with crossings of $X(t)$ of the level γ.

Let us begin with basic notation which can be found in Cramèr and Leadbetter [163]. For a given level γ, let $f(t)$ be some real-valued continuous function of t such that $f(t)$ is not identically

equal to γ in any subinterval. We say that f has an upcrossing of the level γ at t_0 if there exists $\epsilon > 0$ such that $f(t) \leq \gamma$ for $t \in (t_0 - \epsilon, t_0)$, and $f(t) \geq \gamma$ for $t \in (t_0, t_0 + \epsilon)$. A downcrossing of f is similarly defined by reserving inequalities in the above definition of an uncrossing to $f(t) \geq \gamma$ and $f(t) \leq \gamma$. Intuitively, since $f(t)$ is continuous and is not identically equal to γ in any subinterval, an upcrossing (a downcrossing, respectively) of the level γ at t_0 is described by the fact that $f(t) - \gamma$ changes sign from non-positive to non-negative (from non-negative to non-positive, respectively) when t goes from a left to a right neighbourhood of t_0, and $f(t_0) = \gamma$. And we say that $f(t)$ has a crossing of the level γ at t_0 if $f(t_0) = \gamma$ and that there exist t_1 and t_2 in a neighbourhood of t_0 with $t_1 < t_0 < t_2$ such that $(f(t_1) - \gamma)(f(t_2) - \gamma) < 0$.

The first question of interest is the mean number of crossings of $X(t)$ of the level γ. Write C_γ the number of crossings of $X(t)$ of the level γ during a unit time interval. $\mathbf{E}C_\gamma$ is clearly the mean number of crossing and is so-called *level crossing rate*. The following result was firstly obtained by the fundamental work of Rice 1958 [13], and its technical conditions have been weakened by, among others, Ivanov 1960 [164] and Ylvisaker 1965 [165]. It is summarised in [163, § 10.3] as follows:

Theorem 5.3.1 (Cramér and Leadbetter [163], p.194)**.** *With the notation developed and $X(t)$ defined as above:*

$$\mathbf{E}C_\gamma = \frac{1}{\pi}\sqrt{\frac{\lambda_2}{\lambda_0}}\exp\left(-\frac{\gamma^2}{2\lambda_0}\right), \tag{5.3.1}$$

with

$$\lambda_0 = R_X(0), \quad and \quad \lambda_2 = -R_X''(\tau)|_{\tau=0}.$$

$\mathbf{E}C_\gamma < +\infty$ *if and only if* $\lambda_2 < +\infty$.

The above last condition is equivalently stated that the level crossing rate is finite if and only if the autocorrelation function $R_X(\tau)$ of $X(t)$ has finite second derivative at the origin. According to Leadbetter et al. [149], this condition is satisfied if R_X admits the following form:

$$R_X(\tau) = 1 - \frac{\lambda_2\tau^2}{2} + o(\tau^2), \quad \text{as } \tau \to 0, \tag{5.3.2}$$

with finite λ_2.

Now let U_γ and D_γ be the number of upcrossings and downcrossings of $X(t)$ of the level γ during a unit time period. According to [163, §10.4], they are given as follows

Proposition 5.3.2 (Cramér and Leadbetter [163], p.197)**.** *With the same assumptions for the process $X(t)$, if $\lambda_2 < +\infty$:*

$$\mathbf{E}U_\gamma = \mathbf{E}D_\gamma = \frac{\mathbf{E}C_\gamma}{2}. \tag{5.3.3}$$

It means that when $\lambda_2 < +\infty$, the level crossing rate is equally shared between the up-level crossing rate and the down-level crossing rate.

We are now interested in another result related to crossings of the process $X(t)$ of a large level $\gamma \to \infty$ or of a small level $-\gamma \to -\infty$. In the following we provide results related to an upcrossing of a large level, the corresponding results of downcrossings of a small level will be directly obtainable by the evident relation $X(t) \geq \gamma \Leftrightarrow -X(t) \leq -\gamma$. The result that we shall show in the following gives the asymptotic trajectory of an up-excursion of $X(t)$ above a large level $\gamma \to \infty$. It was investigated in Rice [13], Kac and Slepian [14], Leadbetter et al. [149], and then was summarised in [16, 121, 166].

Theorem 5.3.3 (Leadbetter et al. [149], Thm. 10.4.2)**.** *With the process $X(t)$ described above. If its autocorrelation function $R_X(\tau)$ satisfies*

$$R_X''(\tau) = \lambda_2 + O(|\log|\tau||^{-a}) \quad \text{as } \tau \to 0 \tag{5.3.4}$$

with finite λ_2 for some $a > 1$, and

$$R_X(\tau) \to 0 \quad \text{as } \tau \to +\infty, \tag{5.3.5}$$

then, as $\gamma \to +\infty$, excursions of $X(t)$ above γ behave asymptotically as

$$X(t) \sim \gamma + \xi t - \gamma \frac{\lambda_2 t^2}{2}, \tag{5.3.6}$$

where ξ is a Rayleigh random variable of parameter $\sqrt{\lambda_2}$, i.e. the cdf of ξ is equal to

$$F_\xi(x) = 1 - \exp\left(-\frac{x^2}{2\lambda_2}\right). \tag{5.3.7}$$

Intuitively, trajectories of $X(t)$ above a large level γ behave asymptotically as parabolas with Rayleigh distributed parameter ξ. In [16], it was shown that the asymptotic behaviour has quite good agreement with the exact behaviour for $\gamma/\sqrt{\lambda_0} > 2$.

We obtained above the asymptotic distribution of the interval between an upcrossing and the next downcrossing. In the following we investigate the interval between an upcrossing and the kth subsequent upcrossing for $k = 1, 2, \ldots$. For this purpose, we consider the above stationary normal process $X(t)$ such that its autocorrelation function $R_X(\tau)$ satisfies the following two extra assumptions (Cramèr and Leadbetter [163, §12.1]):

$$R_X(\tau) = 1 - \frac{\lambda_2}{2!}\tau^2 + \frac{\lambda_4}{4!}\tau^4 + o(\tau^4) \tag{5.3.8}$$

with finite λ_2 and λ_4, as $\tau \to 0$, and

$$R_X(\tau) = O(\tau^{-a}) \tag{5.3.9}$$

for some $a > 0$, as $\tau \to +\infty$. The condition (5.3.8) implies that $X(t)$ has, with probability one, a continuous sample function derivative, and the condition (5.3.9) implies that the spectrum of $X(t)$ is everywhere continuous so that $X(t)$ is ergodic, see Cramèr and Leadbetter [163, §12.1].

Let $F_{2k}(t)$ be the distribution function of the interval t between an upcrossing and the kth subsequent upcrossing, and denote $\mu = \mathbf{E}U_\gamma$ which is the up-level crossing rate of $X(t)$ of the level γ.

Theorem 5.3.4 (Cramèr and Leadbetter [163],§12.4)**.** *With the assumptions and notation described above:*

$$\lim_{\gamma \to \infty} F_{2k}\left(\frac{t}{\mu}\right) = 1 - \left(\sum_{n=1}^{k} \frac{t^{n-1}}{(n-1)!}\right)e^{-t}, \quad k = 1, 2, \ldots. \tag{5.3.10}$$

The probability density function of this limiting distribution is

$$\frac{t^{k-1}}{(k-1)!}e^{-t}$$

with the mean k.

In particular, for $k = 1$ we obtain distribution of the time between two consecutive upcrossings:

$$\lim_{\gamma \to \infty} F_2 \left(\frac{t}{\mu} \right) = 1 - e^{-t}. \tag{5.3.11}$$

Another interesting property is related to the asymptotic Poisson character of the stream of upcrossings.

Theorem 5.3.5 (Cramèr and Leadbetter [163],p.258)**.** *Assume the conditions* (5.3.8) *and* (5.3.9)*. Let* $(a_1, b_1), \ldots, (a_j, b_j)$ *be disjoint time intervals depending on* γ *in such a way that*

$$b_i - a_i = \frac{\tau_i}{\mu}, \quad (\tau_i > 0),$$

j and $\tau_1, \ldots, \tau_j$ *being independent of* γ*. Let* $k_1, \ldots, k_j$ *be nonnegative integers independent of* γ*. Denote by* $U(a_i, b_i)$ *the number of upcrossings of* $X(t)$ *of the level* γ *during interval* (a_i, b_i)*. Then*

$$\lim_{\gamma \to \infty} \mathbf{P}(U(a_i, b_i) = k_i \text{ for } i = 1, \ldots, j) = \prod_{i=1}^{j} \frac{\tau_i^{k_i}}{k_i!} e^{-\tau_i}. \tag{5.3.12}$$

Hence, the stream of upcrossings behaves asymptotically as a Poisson process when γ tends to infinity.

5.3.2 Application to Mobile Radio Communication

Radio link outage refers to the situation where the communication link between a receiver and a transmitter is not reliable due to unsustainable quality of the radio link. Particularly, in digital radio communication, bit errors occur when the received signal quality is low. Some techniques such as redundancy coding or interleaving are often used to combat bit errors. Since the principle of these techniques is to correct erroneous bits by using redundancy bits correctly received, they are only effective when the bit error rate is still low. When the received signal quality is worse than a tolerable level for relatively long time, successive bits are erroneous and those error-fighting techniques do not help much. This could result in a link outage or service failure.

Outage is one of the main concerns of radio communication. It needs to be analytically characterised in order to develop appropriate system engineering solutions, for example for handover control, access point association, macro-diversity reception. By the random noise nature of the signal quality, it turns out that the level crossing theory is a suitable theoretical tool to study the link outage. In this subsection we shall focus on some applications of this theory to mobile radio communication with a particular interest in results which are related to our study of the mobility management.

To the best of our knowledge, one of the first applications of level crossing theory to mobile radio communication is due to Vijayan and Holtzman 1993 [121] for handover analysis. In particular, the minimum-duration outage concept was first mentioned and studied by Mandayam et al. [15, 16]. This concept incorporated a minimum duration in defining an outage event so that it is more appropriate and also general than instantaneous outage. This concept has received

increasing attention in the literature for the outage, capacity, and macro diversity analysis, see e.g. [166–169].

Let $P(t)$ be the signal strength received from the serving base station, $I(t)$ be the interference, and $N_0(t)$ be the thermal noise; all are received at time t. The signal quality Q expressed in term of the signal-to-interference-plus-noise ratio is a time-varying function given as (see Chapter 2):

$$Q(t) = \frac{P(t)}{N_0(t) + I(t)}.$$

An outage event is defined as the signal quality goes below a minimum required threshold u and stays below at least $\tau_{\min}$:

$$outage \triangleq \{Q(t) < u, \forall t \in [t_1, t_2], \text{ and } t_2 - t_1 \geq \tau_{\min}\}.$$

This is called *minimum-duration outage* which was introduced by Mandayam et al. [16]. The outage probability is defined as the fraction of time that the link is in outage given as:

$$P_{\text{out}} = \lim_{T \to +\infty} \frac{\text{Total outage time in } [0, T]}{T},$$

provided that the limit exists. To derive this outage probability, Mandayam et al. [16] also introduced the *frequency of outage* f_{out} which is defined as the rate of outage events:

$$f_{\text{out}} = \lim_{T \to +\infty} \frac{\text{Number of outage events during } [0, T]}{T},$$

provided that the limit exists. So far, all studies in the literature investigating this problem have taken a simplification that $N_0(t)$ and $I(t)$ are constant over t. In dB scale, the signal quality is expressible as $Q_{\text{dB}}(t) = P_{\text{dB}}(t) - [N_0(t) + I(t)]_{\text{dB}}$. For notational simplicity, in this section we ignore index $_{\text{dB}}$, so write $Q(t)$, $P(t)$, and $[N_0 + I]$ for the signal quality, signal strength, and noise plus interference expressed in dB scale.

The event that $Q(t)$ goes below u can be rewritten as

$$\begin{aligned} Q(t) &< u \\ \Leftrightarrow \mathbf{E}\{P(t)\} - P(t) &> \mathbf{E}\{P(t) - [N_0 + I]\} - u, \end{aligned}$$

Considering the effect of lognormal shadowing (see Chapter 2), and ignoring the variation of the distance from the mobile to the base station over a shot time, it was assumed that $P(t)$ (in dB scale) is a stationary Gaussian process. Then the process

$$X(t) := \mathbf{E}\{P(t)\} - P(t)$$

is a zero mean stationary Gaussian process. And

$$\gamma := \mathbf{E}\{P(t) - [N_0 + I]\} - u$$

is a constant. As a sequel, it turns out that level crossings of $Q(t)$ of the level u are described by those of stationary Gaussian process $X(t)$ of the level γ. In order to apply properties of level crossings of a normal process described in §5.3, $X(t)$ is assumed to admit the following

autocorrelation function

$$R_X(\tau) = \sigma_X^2 \exp\left(-\frac{1}{2}\left(\frac{v\tau}{d_c}\right)^2\right),$$

where v is the user's velocity and d_c is the decorrelation distance of the shadowing. This model was first proposed by Mandayam et al. [15] and was then supported by many later works including Graziosi and Santucci [166], Jiang and Davis [169]. It is close to the standard Gudmundson's model proposed by Gudmundson [41] in modelling the correlated shadowing, and satisfies all the conditions required for asymptotic properties presented in §5.3.

Denote by τ_{excur} the time duration that $X(t)$ continuously stays above γ, it will be determined by using Theorem 5.3.3 as follows. By (5.3.6), solve for equation $X(t) = \gamma$ and obtain two solutions, say t_1 and t_2. Then τ_{excur} is given by $|t_2 - t_1|$ which is equal to:

$$\tau_{\text{excur}} = \frac{2}{\gamma\lambda_2}\xi, \tag{5.3.13}$$

where ξ is a Rayleigh distributed random variable of parameter $\sqrt{\lambda_2}$. So the tail distribution of τ_{excur} is given by that of ξ as follows

$$\mathbf{P}(\tau_{\text{excur}} > \tau) = \overline{F}_\xi\left(\frac{\gamma\lambda_2}{2}\tau\right) = \exp\left(-\frac{\gamma^2\lambda_2}{8}\tau^2\right). \tag{5.3.14}$$

The outage duration, say τ_{out}, is a random variable related to τ_{excur} as

$$\tau_{\text{out}} = (\tau_{\text{excur}}|\tau_{\text{excur}} \geq \tau_{\min}).$$

We can directly obtain the average outage duration as follows

$$\begin{aligned}
\mathbf{E}\tau_{\text{out}} = \mathbf{E}\{\tau_{\text{excur}}|\tau_{\text{excur}} \geq \tau_{\min}\} &= \int_0^{+\infty} \overline{F}_{\tau_{\text{excur}}|\tau_{\text{excur}}\geq\tau_{\min}}(\tau)\mathrm{d}\tau \\
&= \tau_{\min} + \int_{\tau_{\min}}^{+\infty} \frac{\mathbf{P}(\tau_{\text{excur}} > \tau)}{\mathbf{P}(\tau_{\text{excur}} > \tau_{\min})}\mathrm{d}\tau \\
&= \tau_{\min} + \sqrt{\frac{\pi}{V}}\frac{\mathrm{Q}(\sqrt{2V}\tau_{\min})}{\mathbf{P}(\tau_{\text{excur}} > \tau_{\min})}, \tag{5.3.15}
\end{aligned}$$

where $V = \frac{\gamma^2\lambda_2}{8}$, and $\mathrm{Q}(\cdot)$ is the Q-function: $\mathrm{Q}(x) = \frac{1}{\sqrt{2\pi}}\int_x^\infty \exp(-\frac{x^2}{2})\mathrm{d}x$.

Now we derive the outage frequency. It is clear that the number of outages is equal to the number of up excursions which stay above the level γ at least $\tau_{\min}$. By the stationarity of process $X(t)$, the frequency of outage can be given as

$$f_{\text{out}} = \mathbf{E}U_\gamma \times \mathbf{P}(\tau_{\text{excur}} \geq \tau_{\min}). \tag{5.3.16}$$

where $\mathbf{E}U_\gamma$ is given according to Proposition 5.3.2.

Finally, by the stationarity of $X(t)$, the outage probability will be given as

$$P_{\text{out}} = f_{\text{out}} \times \mathbf{E}\tau_{\text{out}}, \tag{5.3.17}$$

which, by equations (5.3.16), (5.3.15), and (5.3.14), is equal to

$$P_{\text{out}} = \mathbf{E}U_\gamma \times \left(\tau_{\min}\exp(-V\tau_{\min}^2) + \sqrt{\frac{\pi}{V}}\mathrm{Q}(\sqrt{2V}\tau_{\min})\right). \tag{5.3.18}$$

5.4   Summary

Throughout this chapter we have described three mathematical tools with a restriction to results which are pertinent to our later development.

The results obtained with extreme value modelling provide insights in to asymptotic behaviours of extreme events. In particular, this framework can be applied to study the maximum and interference received from a number of nodes in a wireless network under appropriate scenarios. Stochastic Geometry provides detailed insights into the spatial structure of a wireless network. With a focus on Poisson point process and associated shot noise field, we have a handy mathematical tool for the computation of different quantities of interest, while obtain an exact mathematical representation of the distribution of the interference. These results will be intensively used in Part II for mathematical development, which will be then applied to Part III.

With the level crossing theory, we are interested in time-varying properties of quantities, precisely of the signal quality. We obtained asymptotic properties and showed their application in deriving analytical expressions of the minimum-duration outage in a mobile wireless network. These results will be used in Chapter 10.

Chapter 6

System Model and Conventions

This chapter factorises common assumptions and conventions which will be used throughout the remaining of this document, except Chapter 12.

6.1 Stochastic Wireless Link

Transmitting nodes are assumed to be equipped with omnidirectional antennas and transmit at power P_{tx}. The thermal noise average power N_0 is assumed constant, and it can be evaluated using (2.2.1).

The *signal strength* (also called *signal power*) received from node i is generally described by (2.1.12):

$$P_i(\mathbf{y}) = \frac{p_i}{l(|\mathbf{y} - \mathbf{x}_i|)},$$

with p_i denoting the virtual transmission power as given by (2.1.11):

$$p_i := A X_i,$$

where, regarding the notational simplification given in (2.3.2), throughout this document the variable A is given such that

$$10 \log_{10} A = P_{\text{tx,dB}} - L_{0,\text{dB}} - N_{0,\text{dB}}, \tag{6.1.1}$$

where $N_{0,\text{dB}}$ is the noise average power and $L_{0,\text{dB}}$ is the fixed-term path loss, both are expressed in decibel scale. Random variables $(X_i, i = 1, 2, \ldots)$ refer to shadowing, fading, or composite shadowing-fading, and are assumed independently and identically distributed, except where otherwise explicitly stated. Denote by F_X the distribution function of random variable $X = X_1$. In the time domain, we consider that $X_i(t)$ is wide-sense stationary and has auto-correlation function $R_X(\tau)$ with a finite second derivative at the origin for mathematical convenience.

Random variables $(p_i, i = 1, 2, \ldots)$ as given above are thus assumed i.i.d. Denote by F_p the distribution function of random variable $p = p_1$. For some results, it will be assumed that F_p admits a density function f_p.

In some particular context, the path loss function l is assumed to have the *typical decaying power law* as given by (2.1.10):

$$l(|\mathbf{y} - \mathbf{x}|) = |\mathbf{y} - \mathbf{x}|^{\beta},$$

with $\beta > 2$. In such a case, the signal strength is given as

$$P_i(\mathbf{y}) = p_i/(|\mathbf{y} - \mathbf{x}|)^{\beta}.$$

6.2   Spatial Distribution of Nodes

As shown from preceding chapters, the information about the spatial separation between receivers and transmitters is required to model the received signal power which is in turn a basic input of the interference and signal quality computation.

Traditionally, the spatial location of nodes is modelled by deterministic structures. A deterministic model requires complete information on the network structure or needs to be constrained to regular structures. A typical example is the well-known bee-hive structure of base station locations used in traditional cellular networks. One of the inconveniences is that it is expensive and time consuming to obtain precise information on the network, while it is not realistic enough to use a regular structure. It is even impossible when different systems including those with ad-hoc nature such as femtocell network are incorporated to provide ubiquitous services. Besides, in the mobile communication context, the location of a receiver such as a mobile user is often unknown to the network operator so that the relative spatial location of nodes compared to this user can not be deterministically known.

Often the spatial distribution of nodes is modelled as completely random according to some known distribution. The stochastic modelling of nodes by spatial distributions overcomes the aforementioned difficulties of a deterministic model. In the literature, *Poisson point processes* (see §5.2) have been intensively used for the mathematical description of nodes spatial distribution, such as [9, 70, 71, 74–76, 170] investigating the network interference, [171–175] investigating wireless connectivity and network coverage, [176–180] analysing packet throughput, and [181–184] addressing wireless link capacity.

It should be noted that, from the information-theoretic viewpoint, the homogeneous Poisson point process has maximum entropy among all homogeneous point processes with a given intensity [185]. It means that nodes are the least regular under the assumption that they are spatially distributed according to a homogeneous Poisson point process. Therefore, a Poisson point process and a regular grid structure of nodes are two extremes of reality where the location of nodes is decided through a network planning process to reduce co-channel interference and coverage holes. Fortunately, Andrews et al. [10] showed that a Poisson point process model of the nodes spatial distribution provides a reliable lower bound to reality whereas the grid model provides an upper bound that is equally loose. It means that modelling the spatial location of nodes as a Poisson point process can provide not only mathematical tractability but also accurate results.

With the above evidences, the spatial distribution of nodes will be modelled by a homogeneous Poisson point process with intensity λ in a two-dimensional Euclidean plane $\mathbb{R}^2$. The interference field within such a context corresponds completely to a shot noise which is defined with the following ingredients:

- The shot noise field is defined on $\mathbb{R}^2$, and takes values in $\mathbb{R}_+$.
- It is generated by the independently marked Poisson point process $\widetilde{\Phi} = \{(\mathbf{x}_i, p_i)\}$ where the points $\{\mathbf{x}_i\}$ are on $\mathbb{R}^2$ and marks $\{p_i\}$ take values in $\mathbb{R}_+$,
- It is associated with a scalar non-negative response function defined as $L(\mathbf{x}, \mathbf{y}, p) = p/l(|\mathbf{x} - \mathbf{y}|)$, for $\mathbf{x}$, $\mathbf{y} \in \mathbb{R}^2$, and $p \in \mathbb{R}_+$.

Results described in §5.2 thus can be directly applied.

6.3   Extremes of Wireless Links

Let Ω be the set of all the nodes in the network. Given a set of nodes $S \subset \Omega$, the *best signal quality* received from S at $\mathbf{y}$, denoted by $Y_S(\mathbf{y})$, is defined as

$$Y_S(\mathbf{y}) \stackrel{\text{def}}{=} \max_{i \in S} Q_i(\mathbf{y}). \tag{6.3.1}$$

Alternatively and naturally, we can also define the best signal quality of n nodes as

$$Y_n(\mathbf{y}) \stackrel{\text{def}}{=} \max_{i=1}^{n} Q_i(\mathbf{y}). \tag{6.3.2}$$

With regard to (2.3.3), the signal quality depends on the frequency reuse pattern, and so does the best signal quality. In the following, we have some observations on how the distribution of Y_S can be obtained.

Let us first consider a single-frequency network, i.e., all the nodes are allocated to the same frequency band, and denote

$$I(\mathbf{y}) = \sum_{i \in \Omega} P_i(\mathbf{y}) \tag{6.3.3}$$

which is the total signal power received at $\mathbf{y}$. By (2.3.3) and (6.3.1) we simply have

$$Y_S(\mathbf{y}) = \max_{i \in S} \left(\frac{P_i(\mathbf{y})}{1 + I(\mathbf{y}) - P_i(\mathbf{y})} \right), \tag{6.3.4}$$

where for all node $i \in \Omega$ we have $P_i(\mathbf{y}) < I(\mathbf{y})$, and $I(\mathbf{y})$ is the same for any $j \neq i$. Hence, by the fact that $x/(a-x)$ with a constant is an increasing function of $x < a$, (6.3.4) can be written as

$$Y_S(\mathbf{y}) = \frac{M_S(\mathbf{y})}{1 + I(\mathbf{y}) - M_S(\mathbf{y})}, \tag{6.3.5}$$

where

$$M_S(\mathbf{y}) \stackrel{\text{def}}{=} \max_{i \in S} P_i(\mathbf{y}) \tag{6.3.6}$$

is the maximum signal strength received at $\mathbf{y}$ from the set S. Equation (6.3.5) implies that in a single-frequency network, the distribution of the best signal quality Y_S can be determined by means of the joint distribution of M_S and I.

Let us now consider the case of a K-frequency network with $K > 1$, and assume that adjacent-channel interference is negligible compared to co-channel interference. It follows that nodes of different frequency bands do not interfere one another. Thus, for a given network topology $\mathcal{G}$, the SINRs received from nodes of different frequency bands are independent. In the context of

a random distribution of nodes, the SINRs received from nodes of different frequency bands are therefore conditionally independent given $\mathcal{G}$. Write cell set S as

$$S = \bigcup_{k=1}^{K} \{S_k \,:\, S_k \subset \Omega_k\},$$

with S_k denoting the subset of S allocated to frequency k. Let

$$Y_{S_k}(\mathbf{y}) = \max_{i \in S_k} Q_i(\mathbf{y})$$

be the best signal quality received at $\mathbf{y}$ from nodes which belong to S_k. The random variables $\{Y_{S_k}(\mathbf{y}), k = 1, ..., K\}$ are conditionally independent given $\mathcal{G}$. As a result,

$$\mathbf{P}(Y_S(\mathbf{y}) \leq \gamma \,|\, \mathcal{G}) = \prod_{k=1}^{K} \mathbf{P}(Y_{S_k}(\mathbf{y}) \leq \gamma \,|\, \mathcal{G}).$$

This means that the distribution of Y_S in the case of a multiple-frequency network can be obtained from that of a single-frequency network.

In light of that, our results will only deal with single-frequency networks (i.e. frequency reuse 1, see §3.2). In this context, the total interference is given by (6.3.3). For various uses latter, we define

$$I_S(\mathbf{y}) \stackrel{\text{def}}{=} \sum_{i \in S} P_i(\mathbf{y}), \quad \text{and} \quad I_n(\mathbf{y}) \stackrel{\text{def}}{=} \sum_{i=1}^{n} P_i(\mathbf{y}) \tag{6.3.7}$$

which are respectively the interference received from set S, and from n nodes. In addition, we define

$$M_n(\mathbf{y}) \stackrel{\text{def}}{=} \max_{i=1}^{n} P_i(\mathbf{y}) \tag{6.3.8}$$

to be the maximum signal strength received from n nodes. For notational simplicity, the location variable $\mathbf{y}$ appearing in $Y_S(\mathbf{y})$, $M_S(\mathbf{y})$, $I_S(\mathbf{y})$, $I(\mathbf{y})$ and in their alternative definitions will be omitted in case of no ambiguity.

6.4   Set of Observed Nodes

We now consider the set of nodes S from which extremes of wireless link are measured. In the subsequent chapters, we define S as a thinning with retention probability $0 \leq \rho \leq 1$ of some network area $B \subset \mathbb{R}^2$. To see the motivation behind this consideration, let us consider an example.

Example 6.4.1. *In cellular networks, the mobile station is provided with a neighbour cell list from which it searches for a handover target cell. The neighbour cell list is practically composed of N cell identifiers corresponding to N cells in the network. The mobile station picks k, $1 \leq k \leq N$, cell identifiers from the neighbour cell list and measures their signal quality, cf. Chapter 4. Under the assumptions that base stations are spatially distributed according to a homogeneous Poisson point process of intensity λ, consider B the geographic area which has in average N cells. The thinning of B with retention probability k/N has in average k cells, which can be seen as the set of cells picked out from the neighbour cell list.*

This example shows one of the practical applications, particularly of the mobility management, for which we come up with the situation of selecting a set of nodes from a network area. On the other hand, the above consideration for S is also motivated by the fact that the case where best signal quality is defined on network area B is just a particular case with $\rho = 1$.

Further, since the received signal strength depends closely on the distance from the observation location to transmitting node, the shape of B from which nodes are observed has a primary influence on the extremes of wireless links. As previously described, the broadcasting nature and distance-dependent path loss of wireless transmission lead to a disk-shaped interfering area around an observation point in a large-scale network. It is thus not uncommon that the observed network area B is assumed to be a disk centered at the observation location. In the remaining of the thesis, except some results developed for an arbitrary network area B, we assume that B is a disk-shaped network area.

6.5 Summary

The following assumptions will be considered in the remaining of the thesis, except in Chapter 12.

We consider a wireless network composed of a number of nodes. Nodes are assumed distributed on the two dimensional Euclidean plane according to a homogeneous Poisson point process of intensity λ. Denote by $\mathbf{x}_i$ the location of node i.

Nodes are equipped with omnidirectional antennas and transmit at power P_{tx}. The path loss function only depends on the spatial separation between receiver and transmitter, and is denoted by $l(\cdot)$. For some results, the typical far-field path loss function will be used. In this case, the path loss exponent is assumed equal to $\beta > 2$. For different uses, denote $\alpha = 2/\beta$.

The variables (X_i, $i = 1, 2, \ldots$) refer to shadowing, fading, or combining shadowing-fading effect. They are assumed independently and identically distributed according to a common distribution function F_X, except where otherwise explicitly stated. In the time domain, it is assumed that $X_i(t)$ is wide-sense stationary and that it has an auto-correlation function $R_X(\tau)$ with a finite second derivative at the origin.

Denote $p_i := AX_i$ random variable which is sometimes referred to as virtual transmission power. Denote by F_p its distribution function, and for some results it will be assumed that F_p admits a density function f_p.

The interference field is modelled as a shot noise defined on $\mathbb{R}^2$, taking value in $\mathbb{R}_+$, generated by an independently marked Poisson point process $\widetilde{\Phi} = \{(\mathbf{x}_i, p_i)\}$, and associated with a non-negative response function $L(\mathbf{x}, \mathbf{y}, p) = p/l(|\mathbf{x} - \mathbf{y}|)$ for $\mathbf{x}, \mathbf{y} \in \mathbb{R}^2$, and $p \in \mathbb{R}_+$.

We consider a single-frequency network, results for a multiple-frequency network can be directly obtained. The extremes of wireless links including the best signal quality Y_S, maximum signal strength M_S, and interference I_S are observed from a set of nodes S which is a thinning of a network area B with retention probability $\rho \in [0, 1]$. And B is assumed to be a disk-shaped network area, except where otherwise explicitly stated.

Part II

Wireless Link Modelling

Chapter 7

Stochastic Geometry Modelling of Wireless Links

7.1 Introduction

This chapter deals with the mathematical modelling of wireless links with a final purpose of deriving the distribution of the best signal quality. Under the assumptions described in Chapter 6, we treat this question from the perspective of using Stochastic Geometry.

Keeping in mind equation (6.3.5) which represents the best signal quality as a function of the interference and the maximum signal strength, we develop a framework in which the joint distribution of the interference and the maximum signal strength will be firstly studied, and thereby the distribution of the best signal quality is then derived. Besides, we obtain marginal distributions of the interference and of the maximum signal strength, and see that this framework allows to find back well-known results on the Poisson field interference and on the extremal shot noise.

In what follows, we develop in §7.2 the main lemma of the framework which provides the joint distribution of the interference I and the maximum signal strength M_S under a hybrid form, where S is a thinning with retention probability ρ of certain arbitrary network area B. Using this main lemma, we derive in §7.3 the joint distribution of I and M_S for more precise setting where B is a disk-shaped network area. We study therein necessary conditions for the existence of their joint density function. After presenting in §7.4 direct results and implication of the framework, we derive the distribution of the best signal quality in §7.5. Concluding remarks are provided in §7.6.

7.2 Main Lemma

Lemma 7.2.1. *Given $B \subset \mathbb{R}^2$, let S be a thinning of B with retention probability $\rho \in [0, 1]$. For $u \geq 0$ and $z \in \mathbb{C}$ with a non-negative real part, define:*

$$\mathcal{L}_{(I, M_S \leq u)}(z) \stackrel{\text{def}}{=} \mathbf{E}\{\mathbf{1}(M_S \leq u) \exp(-zI)\}. \tag{7.2.1}$$

Under the assumption of shot noise interference previously described:

$$\mathcal{L}_{(I,M_S \leq u)}(z) = \exp\left(-\lambda \int_{\mathbb{R}^2} \left(1 - \mathcal{L}_p\left(\frac{z}{l(|\mathbf{y} - \mathbf{x}|)}\right)\right) d\mathbf{x}\right.$$
$$\left. - \rho\lambda \int_B \mathbf{E}\left\{\mathbf{1}\left(\frac{p}{l(|\mathbf{y} - \mathbf{x}|)} > u\right) \exp\left(\frac{-zp}{l(|\mathbf{y} - \mathbf{x}|)}\right)\right\} d\mathbf{x}\right), \qquad (7.2.2)$$

where $\mathcal{L}_p(z) \stackrel{\text{def}}{=} \mathbf{E}\{\exp(-zp)\}$ which is the Laplace transform of the random variable $p = p_1$.

Proof. Under the provided assumptions, the nodes of set S are distributed in B according to a Poisson point process of intensity $\rho\lambda$ according to Proposition 5.2.7. Similarly, the nodes located in B but not retained in S are distributed B according to an independent Poisson point process of intensity $(1 - \rho)\lambda$. Thus, we can decompose the marked Poisson point process defined on $\mathbb{R}^2$ into three *independent* marked Poisson point processes such that

- The first $\widetilde{\Phi}_1$ is defined on B and has intensity $\rho\lambda$,
- The second $\widetilde{\Phi}_2$ is defined on B and has intensity $(1 - \rho)\lambda$,
- And the third $\widetilde{\Phi}_3$ is defined on $\overline{B} = \mathbb{R}^2 \setminus B$ and has intensity λ.

Note that for a node $i : i \notin S$, then $(\mathbf{x}_i, p_i) \in \widetilde{\Phi}_2 \cup \widetilde{\Phi}_3$.

We have:

$$\mathbf{E}\{\mathbf{1}(M_S \leq u)\exp(-zI)\} = \mathbf{E}\left\{\mathbf{1}(M_S \leq u)\exp\left(-z\sum_{i \in \Omega} P_i(\mathbf{y})\right)\right\}$$
$$= \mathbf{E}\left\{\exp\left(\sum_{i \in S}\left(\log \mathbf{1}(P_i(\mathbf{y}) \leq u) - zP_i(\mathbf{y})\right) - z\sum_{i \notin S} P_i(\mathbf{y})\right)\right\}$$
$$= \mathbf{E}\left\{\exp\left(\sum_{(\mathbf{x}_i,p_i)\in\widetilde{\Phi}_1}\left(\log \mathbf{1}(P_i(\mathbf{y}) \leq u) - zP_i(\mathbf{y})\right)\right.\right.$$
$$\left.\left. - z\sum_{(\mathbf{x}_i,p_i)\in\widetilde{\Phi}_2} P_i(\mathbf{y}) - z\sum_{(\mathbf{x}_i,p_i)\in\widetilde{\Phi}_3} P_i(\mathbf{y})\right)\right\}. \qquad (7.2.3)$$

Since $\widetilde{\Phi}_1$, $\widetilde{\Phi}_2$, and $\widetilde{\Phi}_3$ are independent as discussed above, apply Theorem 5.2.12 to each expectation on the right-hand side of (7.2.3) we obtain

$$\mathbf{E}\left\{\exp\left(\sum_{(\mathbf{x}_i,p_i)\in\widetilde{\Phi}_1} \log \mathbf{1}(P_i(\mathbf{y}) \leq u) - zP_i(\mathbf{y})\right)\right\}$$
$$= \exp\left(-\rho\lambda \int_B \left(1 - \mathbf{E}\left\{\mathbf{1}\left(\frac{p}{l(|\mathbf{y} - \mathbf{x}|)} \leq u\right) e^{\frac{-zp}{l(|\mathbf{y}-\mathbf{x}|)}}\right\}\right) d\mathbf{x}\right)$$
$$= \exp\left(-\rho\lambda \int_B \left(1 - \mathbf{E}\left\{\left(1 - \mathbf{1}\left(\frac{p}{l(|\mathbf{y} - \mathbf{x}|)} > u\right)\right) e^{\frac{-zp}{l(|\mathbf{y}-\mathbf{x}|)}}\right\}\right) d\mathbf{x}\right).$$
$$= \exp\left(-\rho\lambda \int_B \left(1 - \mathbf{E}\left\{e^{\frac{-zp}{l(|\mathbf{y}-\mathbf{x}|)}}\right\}\right) d\mathbf{x} - \rho\lambda \int_B \mathbf{E}\left\{\mathbf{1}\left(\frac{p}{l(|\mathbf{y} - \mathbf{x}|)} > u\right) e^{\frac{-zp}{l(|\mathbf{y}-\mathbf{x}|)}}\right\} d\mathbf{x}\right).$$
$$(7.2.4)$$

And

$$\mathbf{E}\Big\{\exp\Big(-z\sum_{(\mathbf{x}_i,p_i)\in\widetilde{\Phi}_2}P_i(\mathbf{y})\Big)\Big\}=\exp\Big(-(1-\rho)\lambda\int_B\Big(1-\mathbf{E}\Big\{e^{\frac{-zp}{l(|\mathbf{y}-\mathbf{x}|)}}\Big\}\Big)\mathrm{d}\mathbf{x}\Big). \quad (7.2.5)$$

$$\mathbf{E}\Big\{\exp\Big(-z\sum_{(\mathbf{x}_i,p_i)\in\widetilde{\Phi}_3}P_i(\mathbf{y})\Big)\Big\}=\exp\Big(-\lambda\int_{\overline{B}}\Big(1-\mathbf{E}\Big\{e^{\frac{-zp}{l(|\mathbf{y}-\mathbf{x}|)}}\Big\}\Big)\mathrm{d}\mathbf{x}\Big). \quad (7.2.6)$$

Substitute Equations (7.2.4), (7.2.5), and (7.2.6) into (7.2.3), we have

$$\begin{aligned}
\mathbf{E}\{\mathbf{1}(M_S\le u)\exp(-zI)\}=\exp\Big(&-\rho\lambda\int_B\Big(1-\mathbf{E}\Big\{e^{\frac{-zp}{l(|\mathbf{y}-\mathbf{x}|)}}\Big\}\Big)\,\mathrm{d}\mathbf{x}\\
&-(1-\rho)\lambda\int_B\Big(1-\mathbf{E}\Big\{e^{\frac{-zp}{l(|\mathbf{y}-\mathbf{x}|)}}\Big\}\Big)\mathrm{d}\mathbf{x}\\
&-\lambda\int_{\overline{B}}\Big(1-\mathbf{E}\Big\{e^{\frac{-zp}{l(|\mathbf{y}-\mathbf{x}|)}}\Big\}\Big)\mathrm{d}\mathbf{x}\\
&-\rho\lambda\int_B\mathbf{E}\Big\{\mathbf{1}\Big(\frac{p}{l(|\mathbf{y}-\mathbf{x}|)}>u\Big)e^{\frac{-zp}{l(|\mathbf{y}-\mathbf{x}|)}}\Big\}\mathrm{d}\mathbf{x}\Big). \quad (7.2.7)
\end{aligned}$$

Note that $\mathbf{E}\Big\{\exp\Big(\frac{-zp}{l(|\mathbf{y}-\mathbf{x}|)}\Big)\Big\}=\mathcal{L}_p\Big(\frac{z}{l(|\mathbf{y}-\mathbf{x}|)}\Big)$, we obtain:

$$\begin{aligned}
\mathbf{E}\{\mathbf{1}(M_S\le u)\exp(-zI)\}=\exp\Big(&-\lambda\int_{\mathbb{R}^2}\Big(1-\mathcal{L}_p(\frac{z}{l(|\mathbf{y}-\mathbf{x}|)})\Big)\mathrm{d}\mathbf{x}\\
&-\rho\lambda\int_B\mathbf{E}\Big\{\mathbf{1}\Big(\frac{p}{l(|\mathbf{y}-\mathbf{x}|)}>u\Big)e^{\frac{-zp}{l(|\mathbf{y}-\mathbf{x}|)}}\Big\}\mathrm{d}\mathbf{x}\Big). \qquad \square
\end{aligned}$$

We use Lemma 7.2.1 to develop further results in the subsequent sections.

7.3 Joint Distribution of Interference and Maximum Signal Strength

Lemma 7.2.1 provides a hybrid form of the joint distribution of I and M_S in the case where S is a thinning of an arbitrary network area B. In this section we study the joint distribution of I and M_S with the setting where B is a disk-shaped network area as described in Chapter 6.

7.3.1 Joint Distribution

The joint distribution of I and M_S for the case of a disk can be obtained from Lemma 7.2.1 as follows.

Proposition 7.3.1. *For $u\ge 0$ define:*

$$\phi_{(I,M_S\le u)}(w)\stackrel{\text{def}}{=}\mathbf{E}\{\mathbf{1}(M_S\le u)\exp(jwI)\},\quad\text{for }w\in\mathbb{R}. \quad (7.3.1)$$

Assume the same conditions of Lemma 7.2.1, and that B is a disk of radius R_B, $l(r)=r^\beta$ for $r\in\mathbb{R}_+$ and $\beta>2$. Let M_S and I be the maximum signal strength and the interference received

at the center of B. Then

$$\phi_{(I, M_S \leq u)}(w) = \exp\Big(- \delta|w|^\alpha \big(1 - j\text{sign}(w)\tan(\frac{\pi\alpha}{2})\big)$$
$$- \rho\pi\lambda\alpha|w|^\alpha \mathbf{E}\Big\{ \int_{\frac{\lfloor w \rfloor u}{p}}^{+\infty} \frac{\mathbf{1}(p \leq uR_B^\beta)e^{j\text{sign}(w)tp}}{t^{\alpha+1}} \text{d}t \Big\}$$
$$- \rho\pi\lambda\alpha|w|^\alpha \mathbf{E}\Big\{ \int_{\frac{\lfloor w \rfloor}{R_B^\beta}}^{+\infty} \frac{\mathbf{1}(p > uR_B^\beta)e^{j\text{sign}(w)tp}}{t^{\alpha+1}} \text{d}t \Big\}\Big), \tag{7.3.2}$$

where

$$\delta = c_\alpha\Gamma(1-\alpha)\cos(\frac{\pi\alpha}{2}), \tag{7.3.3}$$

with

$$c_\alpha = \pi\lambda\mathbf{E}\{p^\alpha\}. \tag{7.3.4}$$

Proof. By definition we have:

$$\phi_{(I, M_S \leq u)}(w) = \mathcal{L}_{(I, M_S \leq u)}(-jw).$$

Substitute $l(r) = r^\beta$ and $\text{d}\mathbf{x} = r\text{d}r\text{d}\theta$ into (7.2.2) of Lemma 7.2.1, we get

$$\phi_{(I, M_S \leq u)}(w) = \exp\Big(- 2\pi\lambda \int_0^{+\infty} \Big(1 - \mathbf{E}\Big\{\exp(\frac{jwp}{r^\beta})\Big\}\Big) r\text{d}r$$
$$- 2\pi\rho\lambda \int_0^{R_B} \mathbf{E}\Big\{\mathbf{1}(p > ur^\beta)\exp(\frac{jwp}{r^\beta})\Big\} r\text{d}r\Big). \tag{7.3.5}$$

Using the change of variable $t = |w|r^{-\beta}$ and $\alpha = 2/\beta$:

$$\int_0^{+\infty} \Big(1 - \mathbf{E}\Big\{\exp\Big(\frac{jwp}{r^\beta}\Big)\Big\}\Big) r\text{d}r = \frac{\alpha|w|^\alpha}{2} \int_0^{+\infty} \frac{1 - \mathbf{E}\{e^{j\text{sign}(w)tp}\}}{t^{\alpha+1}}\text{d}t. \tag{7.3.6}$$

Similarly,

$$\int_0^{R_B} \mathbf{E}\Big\{\mathbf{1}(p > ur^\beta)\exp(\frac{jwp}{r^\beta})\Big\} r\text{d}r = \frac{\alpha|w|^\alpha}{2} \int_{\frac{\lfloor w \rfloor}{R_B^\beta}}^{+\infty} \frac{\mathbf{E}\{\mathbf{1}(t > \frac{u|w|}{p})e^{j\text{sign}(w)tp}\}}{t^{\alpha+1}}\text{d}t. \tag{7.3.7}$$

In the following we simplify (7.3.6) and (7.3.7). For (7.3.6), for $0 < \alpha < 1$ we have:

$$\int_0^{+\infty} \frac{1 - e^{j\text{sign}(w)tp}}{t^{\alpha+1}}\text{d}t = -\Gamma(-\alpha)p^\alpha e^{-j\text{sign}(w)\frac{\pi\alpha}{2}}. \tag{7.3.8}$$

Taking expectations on both sides of (7.3.8), we get

$$\int_0^{+\infty} \frac{1 - \mathbf{E}\{e^{j\text{sign}(w)tp}\}}{t^{\alpha+1}}\text{d}t = -\mathbf{E}\{p^\alpha\}\Gamma(-\alpha)e^{-j\text{sign}(w)\frac{\pi\alpha}{2}}.$$

Substitute this back into (7.3.6), we obtain

$$2\pi\lambda \int_0^{+\infty} (1 - \mathbf{E}\{\exp(\frac{jwp}{r^\beta})\})r\text{d}r = \pi\lambda\mathbf{E}\{p^\alpha\}\Gamma(1-\alpha)(-jw)^\alpha. \tag{7.3.9}$$

Now we simplify (7.3.7). We simply have

$$\int_{\frac{|w|}{R_B^\beta}}^{+\infty} \frac{\mathbf{E}\{\mathbf{1}(t > \frac{u|w|}{p})e^{j\mathrm{sign}(w)tp}\}}{t^{\alpha+1}}\mathrm{d}t = \mathbf{E}\Big\{\int_{\frac{|w|}{R_B^\beta}}^{+\infty} \frac{\mathbf{1}(p > uR_B^\beta)e^{j\mathrm{sign}(w)tp}}{t^{\alpha+1}}\mathrm{d}t\Big\}$$

$$+ \mathbf{E}\Big\{\int_{\frac{|w|u}{p}}^{+\infty} \frac{\mathbf{1}(p \le uR_B^\beta)e^{j\mathrm{sign}(w)tp}}{t^{\alpha+1}}\mathrm{d}t\Big\}. \qquad (7.3.10)$$

Substitute this and (7.3.9) into (7.3.5), we obtain (7.3.2). $\qquad\qquad\square$

In many practical scenarios, the case where R_B is large may be of interest. For example, macro cellular networks are often deployed for scattered traffic areas and have a low density of base stations. Considering B_N as a disk with radius $R_N = \sqrt{N/(\pi\lambda)}$, which has in average N base stations; its radius increases as N increases. And so, one can consider that $R_N \approx \infty$ for some moderate or large value of N. Hence, it is worth considering the case where $B = \mathbb{R}^2$. It is directly obtained from Proposition 7.3.1 as follows.

Corollary 7.3.2. *Under the assumptions of Proposition 7.3.1, if $B = \mathbb{R}^2$ then:*

$$\phi_{(I,M_S\le u)}(w) = \exp\Big(-C_1|w|^\alpha\Big(1 - j\mathrm{sign}(w)\tan(\frac{\pi\alpha}{2})\Big) - C_2(w,u) + jC_3(w,u)\Big), \quad (7.3.11)$$

where $C_1 = (1-\rho)\delta$, and

$$C_2(w,u) = \rho\,c_\alpha\,\frac{{}_1F_2(-\frac{\alpha}{2};\frac{1}{2},1-\frac{\alpha}{2};-\frac{u^2w^2}{4})}{u^\alpha}, \qquad (7.3.12)$$

$$C_3(w,u) = \rho\,c_\alpha\,\frac{\alpha w}{1-\alpha}\frac{{}_1F_2(\frac{1-\alpha}{2};\frac{3}{2},\frac{3-\alpha}{2};-\frac{u^2w^2}{4})}{u^{\alpha-1}}, \qquad (7.3.13)$$

where δ and c_α are respectively given by (7.3.3) and (7.3.4), and ${}_1F_2$ denotes the hypergeometric function,

$${}_1F_2(a_1;b_1,b_2;z) := \sum_{n=0}^\infty \frac{(a_1)_n}{(b_1)_n(b_2)_n}\frac{z^n}{n!}, \quad \text{for } z \in \mathbb{C}, \qquad (7.3.14)$$

in which $(a)_n$ represents the Pochhammer symbol:

$$(a)_n := a(a+1)(a+2)\dots(a-n+1), \quad \text{and } (a)_0 = 1. \qquad (7.3.15)$$

Proof. Condition $B = \mathbb{R}^2$ induces $R_B = \infty$. Take this into account for (7.3.2), we have:

$$\mathbf{E}\Big\{\int_{\frac{|w|}{R_B^\beta}}^{+\infty} \frac{\mathbf{1}(p > uR_B^\beta)e^{j\mathrm{sign}(w)tp}}{t^{\alpha+1}}\mathrm{d}t\Big\} = 0, \qquad (7.3.16)$$

And

$$\mathbf{E}\Big\{\int_{\frac{|w|u}{p}}^{+\infty} \frac{\mathbf{1}(p \le uR_B^\beta)e^{j\mathrm{sign}(w)tp}}{t^{\alpha+1}}\mathrm{d}t\Big\} = \mathbf{E}\Big\{\int_{\frac{|w|u}{p}}^{+\infty} \frac{e^{j\mathrm{sign}(w)tp}}{t^{\alpha+1}}\mathrm{d}t\Big\}.$$

For $0 < \alpha < 1$, the integral on the right hand-side of this can be evaluated with help of a symbolic calculation software like Mathematica:

$$\int_{\frac{|w|u}{p}}^{+\infty} \frac{e^{j\operatorname{sign}(w)tp}}{t^{\alpha+1}} \mathrm{d}t = p^{\alpha}\Gamma(-\alpha)e^{-j\operatorname{sign}(w)\frac{\pi\alpha}{2}}$$

$$+ \frac{1}{\alpha}\Big(\frac{p}{|w|u}\Big)^{\alpha}\, {}_1F_2(-\frac{\alpha}{2};\frac{1}{2},1-\frac{\alpha}{2};-\frac{u^2w^2}{4})$$

$$- j\frac{wu}{1-\alpha}\Big(\frac{p}{|w|u}\Big)^{\alpha}\, {}_1F_2(\frac{1-\alpha}{2};\frac{3}{2},\frac{3-\alpha}{2};-\frac{u^2w^2}{4}).$$

Taking expectations on both sides, we obtain

$$\mathbf{E}\Big\{\int_{\frac{|w|u}{p}}^{+\infty} \frac{e^{j\operatorname{sign}(w)tp}}{t^{\alpha+1}} \mathrm{d}t\Big\} = \mathbf{E}\{p^{\alpha}\}\Gamma(-\alpha)e^{-j\operatorname{sign}(w)\frac{\pi\alpha}{2}} \tag{7.3.17}$$

$$+ \mathbf{E}\{p^{\alpha}\}\frac{{}_1F_2(-\frac{\alpha}{2};\frac{1}{2},1-\frac{\alpha}{2};-\frac{u^2w^2}{4})}{\alpha|w|^{\alpha}u^{\alpha}}$$

$$- j\mathbf{E}\{p^{\alpha}\}\frac{w}{1-\alpha}\frac{{}_1F_2(\frac{1-\alpha}{2};\frac{3}{2},\frac{3-\alpha}{2};-\frac{u^2w^2}{4})}{|w|^{\alpha}u^{\alpha-1}}. \tag{7.3.18}$$

Substituting (7.3.18) and (7.3.16) back to (7.3.2), we get (7.3.11). $\qquad\square$

7.3.2 Joint Density

We have identified the joint distribution of M_S and I in terms of hybrid Laplace transform, see Lemma 7.2.1, and hybrid characteristic function, see Proposition 7.3.1. In the following, we investigate their joint density function.

First of all, we would like to known under what condition (I, M_S) admits a joint density. We have the following theorem.

Theorem 7.3.3. *Assume that the conditions of Lemma 7.2.1 hold and that $l(r) = r^{\beta}$ for $r \in \mathbb{R}_+$, $\beta > 2$, and $0 < \mathbf{E}\{p_i^{\alpha}\} < \infty$. Then:*

(i) *$|\phi_{(I, M_S \leq u)}(w)|^q \in \mathbb{L}$ with respect to (w.r.t.) w for all $q = 1, 2, \ldots$, $\forall u > 0$.*

(ii) *If F_p admits a continuous density f_p, then $\frac{\partial}{\partial u}\phi_{(I, M_S \leq u)}(w)$ exists, and $|\frac{\partial}{\partial u}\phi_{(I, M_S \leq u)}(w)|^q \in \mathbb{L}$ w.r.t. w for all $q = 1, 2, \ldots$, $\forall u > 0$.*

where $\mathbb{L}$ denotes the space of absolutely integrable functions.

Proof. We begin with the proof of (i). Use (7.2.2) of Lemma 7.2.1:

$$\phi_{(I, M_S \leq u)}(w) = \mathcal{L}_{(I, M_S \leq u)}(-jw)$$

$$= \exp\Big(-2\pi\lambda\int_{\mathbb{R}_+}\Big(1 - \mathbf{E}\Big\{\exp(\frac{jwp}{l(r)})\Big\}\Big)r\mathrm{d}r$$

$$- \rho\lambda\int_B \mathbf{E}\Big\{\mathbf{1}(p > ul(|\mathbf{y} - \mathbf{x}|))\exp(\frac{jwp}{l(|\mathbf{y} - \mathbf{x}|)})\Big\}\mathrm{d}\mathbf{x}\Big). \tag{7.3.19}$$

It follows that

$$|\phi_{(I,M_S\leq u)}(w)|^q = \exp\Big(-2q\pi\lambda\int_{\mathbb{R}_+}\Big(1-\mathbf{E}\Big\{\cos(\frac{wp}{l(r)})\Big\}\Big)r\mathrm{d}r$$
$$-q\rho\lambda\int_B\mathbf{E}\Big\{\mathbf{1}(p>ul(|\mathbf{y}-\mathbf{x}|))\cos(\frac{wp}{l(|\mathbf{y}-\mathbf{x}|)})\Big\}\mathrm{d}\mathbf{x}\Big). \tag{7.3.20}$$

For the first term in the exponential, substituting $l(r)=r^\beta$ and noting that

$$\int_{\mathbb{R}_+}\Big(1-\mathbf{E}\Big\{\cos(\frac{wp}{r^\beta})\Big\}\Big)r\mathrm{d}r = \Re\Big\{\int_{\mathbb{R}_+}\Big(1-\mathbf{E}\Big\{\exp(\frac{jwp}{r^\beta})\Big\}\Big)r\mathrm{d}r\Big\},$$

we get from (7.3.9) that:

$$-2q\pi\lambda\int_{\mathbb{R}_+}\Big(1-\mathbf{E}\Big\{\cos(\frac{wp}{r^\beta})\Big\}\Big)r\mathrm{d}r = -q\pi\lambda\Gamma(1-\alpha)\cos(\frac{\pi\alpha}{2})\mathbf{E}\{p^\alpha\}|w|^\alpha. \tag{7.3.21}$$

For the second integral of (7.3.20), we have:

$$-\int_B\mathbf{E}\Big\{\mathbf{1}(p>ul(|\mathbf{y}-\mathbf{x}|))\cos(\frac{wp}{l(|\mathbf{y}-\mathbf{x}|)})\Big\}\mathrm{d}\mathbf{x}$$
$$=-\int_B\int_{ul(|\mathbf{y}-\mathbf{x}|)}^\infty\cos(\frac{wt}{l(|\mathbf{y}-\mathbf{x}|)})F_p(\mathrm{d}t)\mathrm{d}\mathbf{x}$$
$$=-\int_B\int_{ul(|\mathbf{y}-\mathbf{x}|)}^\infty\Big(1-1+\cos(\frac{wt}{l(|\mathbf{y}-\mathbf{x}|)})\Big)F_p(\mathrm{d}t)\mathrm{d}\mathbf{x}$$
$$=\int_B\int_{ul(|\mathbf{y}-\mathbf{x}|)}^\infty F_p(\mathrm{d}t)\mathrm{d}\mathbf{x}-\int_B\int_{ul(|\mathbf{y}-\mathbf{x}|)}^\infty\Big(1+\cos(\frac{wt}{l(|\mathbf{y}-\mathbf{x}|)})\Big)F_p(\mathrm{d}t)\mathrm{d}\mathbf{x},$$

where, since $1+\cos(\cdot)\geq 0$, we have:

$$-\int_B\mathbf{E}\{\mathbf{1}(p>ul(|\mathbf{y}-\mathbf{x}|))\cos(\frac{wp}{l(|\mathbf{y}-\mathbf{x}|)})\}\mathrm{d}\mathbf{x}\leq\int_B\int_{ul(|\mathbf{y}-\mathbf{x}|)}^\infty F_p(\mathrm{d}t)\mathrm{d}\mathbf{x}$$
$$\leq\int_{\mathbb{R}^2}\int_{ul(|\mathbf{y}-\mathbf{x}|)}^\infty F_p(\mathrm{d}t)\mathrm{d}\mathbf{x}$$
$$=2\pi\int_{\mathbb{R}_+}\Big(1-F_p(ur^\beta)\Big)r\mathrm{d}r. \tag{7.3.22}$$

Using an integration by parts with $1-F_p(ur^\beta)$ and $2r\mathrm{d}r$:

$$2\int_{\mathbb{R}_+}\Big(1-F_p(ur^\beta)\Big)r\mathrm{d}r = \int_0^\infty r^2\mathrm{d}F_p(ur^\beta) = \int_0^\infty(\frac{t}{u})^\alpha F_p(\mathrm{d}t) = \frac{\mathbf{E}\{p^\alpha\}}{u^\alpha}.$$

Taking this into account in (7.3.22), and then substituting (7.3.22) and (7.3.21) into (7.3.20), we get:

$$|\phi_{(I,M_S\leq u)}(w)|^q \leq \exp\Big(q\pi\lambda\rho u^{-\alpha}\mathbf{E}\{p^\alpha\}\Big)$$
$$\times\exp\Big(-q\pi\lambda\Gamma(1-\alpha)\cos(\frac{\pi\alpha}{2})\mathbf{E}\{p^\alpha\}|w|^\alpha\Big). \tag{7.3.23}$$

Under the condition that $\beta>2$, we have $0<\alpha<1$ and so $\cos(\frac{\pi\alpha}{2})>0$ and $\Gamma(1-\alpha)>0$. Hence, provided that $0<\mathbf{E}\{p^\alpha\}<\infty$, the right hand-side of (7.3.23) is integrable w.r.t. w, $\forall q=1,2,\ldots$, and $u>0$. This proves claim (i).

We now prove (ii). We first show that $\frac{\partial}{\partial u}\phi_{(I,M_S \leq u)}(w)$ exists for all $u > 0$. From (7.3.19), we can have that the differentiability of $\phi_{(I,M_S \leq u)}(w)$ w.r.t. u is implied by that of the second term in the exponential of (7.3.19) and that when the latter holds,

$$\frac{\partial}{\partial u}\phi_{(I,M_S \leq u)}(w)$$
$$= -\rho\lambda\phi_{(I,M_S \leq u)}(w)\frac{\partial}{\partial u}\int_B \mathbf{E}\left\{\mathbf{1}(p > ul(|\mathbf{y}-\mathbf{x}|))\exp\left(\frac{jwp}{l(|\mathbf{y}-\mathbf{x}|)}\right)\right\}\mathrm{d}\mathbf{x}, \quad (7.3.24)$$

where

$$\int_B \mathbf{E}\left\{\mathbf{1}(p > ul(|\mathbf{y}-\mathbf{x}|))\exp\left(\frac{jwp}{l(|\mathbf{y}-\mathbf{x}|)}\right)\right\}\mathrm{d}\mathbf{x} = \int_B \int_{ul(|\mathbf{y}-\mathbf{x}|)}^{\infty} e^{\frac{jwt}{l(|\mathbf{y}-\mathbf{x}|)}} F_p(\mathrm{d}t)\mathrm{d}\mathbf{x}. \quad (7.3.25)$$

Under the condition that F_p admits a continuous density f_p:

$$\frac{\partial}{\partial u}\int_{ul(|\mathbf{y}-\mathbf{x}|)}^{\infty} e^{\frac{jwt}{l(|\mathbf{y}-\mathbf{x}|)}} F_p(\mathrm{d}t) = \frac{\partial}{\partial u}\int_{ul(|\mathbf{y}-\mathbf{x}|)}^{\infty} e^{\frac{jwt}{l(|\mathbf{y}-\mathbf{x}|)}} f_p(t)\mathrm{d}t$$
$$= -e^{jwu}l(|\mathbf{y}-\mathbf{x}|)f_p(ul(|\mathbf{y}-\mathbf{x}|)),$$

and the last expression is continuous w.r.t. u. Taking this into account in (7.3.25), we have:

$$\frac{\partial}{\partial u}\int_B \mathbf{E}\left\{\mathbf{1}(p > ul(|\mathbf{y}-\mathbf{x}|))\exp\left(\frac{jwp}{l(|\mathbf{y}-\mathbf{x}|)}\right)\right\}\mathrm{d}\mathbf{x} = \int_B \frac{\partial}{\partial u}\int_{ul(|\mathbf{y}-\mathbf{x}|)}^{\infty} e^{\frac{jwt}{l(|\mathbf{y}-\mathbf{x}|)}} f_p(t)\mathrm{d}t\mathrm{d}\mathbf{x}$$
$$= -\int_B e^{jwu}l(|\mathbf{y}-\mathbf{x}|)f_p(ul(|\mathbf{y}-\mathbf{x}|))\mathrm{d}\mathbf{x}.$$

Thus under the above assumptions, $\frac{\partial}{\partial u}\phi_{(I,M_S \leq u)}(w)$ exists and

$$|\frac{\partial}{\partial u}\phi_{(I,M_S \leq u)}(w)|^q = |\rho\lambda\phi_{(I,M_S \leq u)}(w)|^q \times \left(\int_B l(|\mathbf{y}-\mathbf{x}|)f_p(ul(|\mathbf{y}-\mathbf{x}|))\mathrm{d}\mathbf{x}\right)^q. \quad (7.3.26)$$

Moreover, we have:

$$\int_B l(|\mathbf{y}-\mathbf{x}|)f_p(ul(|\mathbf{y}-\mathbf{x}|))\mathrm{d}\mathbf{x} \leq \int_{\mathbb{R}^2} l(|\mathbf{y}-\mathbf{x}|)f_p(ul(|\mathbf{y}-\mathbf{x}|))\mathrm{d}\mathbf{x}$$
$$= 2\pi\int_{R_+} r^{\beta} f_p(ur^{\beta})r\mathrm{d}r$$
$$= \pi\alpha u^{-\alpha-1}\int_{\mathbb{R}_+} t^{\alpha} f_p(t)\mathrm{d}t$$
$$= \pi\alpha u^{-\alpha-1}\mathbf{E}\{p^{\alpha}\} < \infty, \text{ provided that } \mathbf{E}\{p^{\alpha}\} < \infty.$$

We complete the proof of (ii) when taking this into account in (7.3.26) and using (i). $\qquad\square$

Corollary 7.3.4. *Assume that the conditions of Theorem 7.3.3 hold and that F_p admits a continuous density f_p. Then (I, M_S) admits a joint density $f_{(I,M_S)}(v, u)$ on $(\mathbb{R}_+^*)^2$ and the function $v \to f_{(I,M_S)}(v, u)$ is bounded, continuous, square-integrable. In addition, for all $u > 0$,*

$$f_{(I,M_S)}(v, u) = \int_{-\infty}^{+\infty} \frac{e^{-jwv}}{2\pi}\frac{\partial}{\partial u}\phi_{(I,M_S \leq u)}(w)\mathrm{d}w. \quad (7.3.27)$$

Proof. By definition,

$$\frac{\frac{\partial}{\partial u}\phi_{(I,M_S\le u)}(w)}{\frac{\partial}{\partial u}\phi_{(I,M_S\le u)}(0)} \tag{7.3.28}$$

is the characteristic function of I conditional on $M_S = u$. From (ii) of Theorem 7.3.3, for all $u > 0$, $w \to |\frac{\partial}{\partial u}\phi_{(I,M_S\le u)}(w)| \in \mathbb{L}$. So by Theorem 3 in [186, p.509], for all $u > 0$, the law of I conditional on $M_S = u$ admits a density and (I, M_S) hence admits a joint density $f_{(I,M_S)}(v, u)$ at v which is bounded and continuous w.r.t. v, and which is given by (7.3.27). Secondly, since $|\frac{\partial}{\partial u}\phi_{(I,M_S\le u)}(w)|^2 \in \mathbb{L}$ as shown by (ii) of Theorem 7.3.3, $f_{(I,M_S)}(v, u)$ is square-integrable w.r.t. v (see Remark A.1.5). □

The existence of the joint density requires the existence and integrability of $\frac{\partial}{\partial u}\phi_{(I,M_S\le u)}(w)$, which only hold for $u > 0$ according to Theorem 7.3.3. Note that u is a value of M_S and v is a value of I; since $M_S < I$, $u > 0$ implies $v > 0$. This leads to the joint density only existing on $(\mathbb{R}_+^*)^2$. Here we may ask why the integrability as stated in Theorem 7.3.3 only holds for $u > 0$. We have an answer for this question in Remark 7.4.1 in the next section.

7.4 Corollaries

In the following we show that the results developed above allow to directly obtain interesting results on the extremal shot noise M_S and on the total interference I.

7.4.1 Distribution of the Maximum Signal Strength

Using the fact that $\mathbf{P}(M_S \le u) = \mathcal{L}_{(I,M_S\le u)}(0)$, (see (7.2.1)), from (7.2.2) we get the cumulative distribution function of M_S:

$$F_{M_S}(u) = \exp\left(-\rho\lambda\int_B \left(1 - F_p(l(|\mathbf{y} - \mathbf{x}|)u)\right)\mathrm{d}\mathbf{x}\right). \tag{7.4.1}$$

We find back the well known result on the distribution of the max shot noise as given by Proposition 5.2.14 in Chapter 5.

Remark 7.4.1. When assuming that $F_p(0) < 1$ ($F_p(0) = 1$ corresponds to the case where the node's transmission power is 0 since the fading X_i satisfies $F_X(0) < 1$) and that $\rho\lambda > 0$, which will be done here and below, we get that

$$\int_B \left(1 - F_p(l(|y - x|)u)\right)\mathrm{d}\mathbf{x}|_{(u=0)} = \infty \quad \text{iff } B = \mathbb{R}^2.$$

Therefore, from (7.4.1) $F_{M_S}(0) = 0$ if and only if (iff) $B = \mathbb{R}^2$. Otherwise, $F_{M_S}(0) > 0$, which means that there is a mass of M_S at the origin, which is

$$F_{M_S}(0) = \exp\left(-\rho\lambda(1 - F_p(0))|B|\right), \tag{7.4.2}$$

with $|B|$ the Lebesgue measure of B. Due to this mass, the integrability in Theorem 7.3.3 only holds for $u > 0$.

Another interesting special case is when B is a disk of radius R_B and the path loss function is $l(r) = r^\beta$. In this case, F_{M_S} is given in closed-form as follows:

Corollary 7.4.2. *Under the conditions of Lemma 7.2.1, denote by M_S the maximum signal strength received at the center of a disk B of radius R_B. If the path loss function is $l(r) = r^\beta$ for $r \in \mathbb{R}_+$, then:*

$$F_{M_S}(u) = \exp\left(-\pi\rho\lambda R_B^2\left(1 - F_p(uR_B^\beta)\right) - \pi\rho\lambda\mathbf{E}\{\mathbf{1}(p \le uR_B^\beta)p^\alpha\}u^{-\alpha}\right), \qquad (7.4.3)$$

where $\alpha = 2/\beta$. In particular, if $B = \mathbb{R}^2$ then:

$$F_{M_S}(u) = \exp\left(-\pi\rho\lambda\mathbf{E}\{p^\alpha\}u^{-\alpha}\right). \qquad (7.4.4)$$

Remark *7.4.3.* The distribution of F_{M_S} as given by (7.4.4) is a Fréchet distribution with shape parameter α and scale parameter $(\pi\rho\lambda\mathbf{E}\{p^\alpha\})^{1/\alpha}$, see §5.1 in Chapter 5. Note that (7.4.4) is precisely the limit of (7.4.3) as $R_B \to +\infty$. So we can interpret this result as follows. Consider $B = \mathbb{R}^2$ as the limit of a sequence of disk-shaped network areas $(B_n, n = 1, 2, \ldots)$ with increasing radii R_n tending to $+\infty$ as $n \to +\infty$. Then the above result is intuitively stated as the maximum signal strength received at center of B_n tends in distribution to a Fréchet distribution as $n \to +\infty$. As a sequel, by abuse of vocabulary we say that the signal strength received at the centered of a disk-shaped network area belongs to the maximum domain of attraction of Fréchet distribution. In §5.1 of Chapter 5 we see that the Fréchet domain of attraction contains the most heavies-tail distributions among the three maximum domains of attraction. This implies that the signal strength received at the center of a disk is *very* heavy-tailed. How could we explain this phenomenon? For the moment, we observe that this is due to the unbounded power-law path loss $d^{-\beta}$ which creates very large values as the $d \to 0$, which happens when the disk *includes* the inner pole. For more insights, we refer to Chapter 8 where the inner pole of the disk is excluded.

Proof of Corollary 7.4.2. Substitute $l(r) = r^\beta$, $d\mathbf{x} = rdrd\theta$ into (7.4.1):

$$\int_B \left(1 - F_p(l(|\mathbf{y} - \mathbf{x}|)u)\right)d x = 2\pi \int_0^{R_B} \left(1 - F_p(ur^\beta)\right)rdr. \qquad (7.4.5)$$

An integration by parts with $1 - F_p(ur^\beta)$ and $2rdr$ yields

$$2\int_0^{R_B}\left(1 - F_p(ur^\beta)\right)rdr = R_B^2\left(1 - F_p(uR_B^\beta)\right) + \int_0^{R_B} r^2 dF_p(ur^\beta). \qquad (7.4.6)$$

where using the change of variable $t = ur^\beta$, we have:

$$\int_0^{R_B} r^2 dF_p(ur^\beta) = \int_0^{uR_B^\beta}\left(\frac{t}{u}\right)^{2/\beta}F_p(dt) = \frac{\mathbf{E}\{\mathbf{1}(p \le uR_B^\beta)p^\alpha\}}{u^\alpha}. \qquad (7.4.7)$$

Take (7.4.7) into account for Equations (7.4.6) and (7.4.5), we get (7.4.3). The proof for the case of $B = \mathbb{R}^2$ is straightforward. □

Here, note that for some constant $a > 0$:

- If p follows a Rayleigh distribution of parameter $\sigma > 0$:

$$\mathbf{E}\{\mathbf{1}(p \le a)p^\alpha\} = 2^{\frac{\alpha}{2}}\sigma^\alpha\left(\Gamma(1 + \frac{\alpha}{2}) - \Gamma(1 + \frac{\alpha}{2}, \frac{a^2}{2\sigma^2})\right),$$

where $\Gamma(z) \triangleq \int_0^\infty t^{z-1}e^{-t}\mathrm{d}t$ for $\Re(z) > 0$ is the gamma function, and $\Gamma(z,x) \triangleq \int_x^\infty t^{z-1}e^{-t}\mathrm{d}t$ is the upper incomplete gamma function.

- If p follows a gamma distribution of shape parameter $k > 0$ and scale parameter $\theta > 0$:

$$\mathbf{E}\{\mathbf{1}(p \leq a)p^\alpha\} = \theta^\alpha \frac{\Gamma(k+\alpha) - \Gamma(k+\alpha, a/\theta)}{\Gamma(k)}.$$

- If p follows a lognormal distribution of parameter $(\mu, \sigma > 0)$:

$$\mathbf{E}\{\mathbf{1}(p \leq a)p^\alpha\} = \frac{1}{2}\exp\left(\alpha\mu + \frac{\alpha^2\sigma^2}{2}\right)\mathrm{erfc}\left(\frac{\mu + \alpha\sigma^2 - \log(a)}{\sqrt{2}\sigma}\right).$$

7.4.2 Distribution of the Interference

The modelling of the network interference plays an important role in numerous problems of the network analysis and design such as capacity and outage analysis, modulation adaptation, and the design of interference mitigation techniques. It has been so far intensively investigated with very rich state-of-the-art, see §2.4 in Chapter 2. In the following we show that our framework allows to directly obtain the characteristic function of the interference.

Denote by

$$\phi_I(w) = \mathbf{E}\{\exp(jwI)\}, \quad \text{for } w \in \mathbb{R} \tag{7.4.8}$$

the characteristic function of I. By the definition given in (7.3.1), we see that $\phi_I(w) = \phi_{(I,M_S \leq +\infty)}(w)$. So using Proposition 7.3.1:

Corollary 7.4.4. *The characteristic function of the total interference generated by the shot noise field as described above is given by*

$$\phi_I(w) = \exp\left(-\delta|w|^\alpha\left(1 - j\mathrm{sign}(w)\tan(\frac{\pi\alpha}{2})\right)\right). \tag{7.4.9}$$

This is the characteristic function of a skewed α-stable random variable (see §5.1), and here we find back the same result recently developed by Win et al. [9], Inaltekin et al. [76] and summarised in §5.2.3 of Chapter 5.

7.5 Distribution of the Best Signal Quality

Using the results developed in §7.3 we derive in this section the distribution of the best signal quality. The following theorem gives its tail distribution function $\overline{F}_{Y_S}$.

Theorem 7.5.1. *Assume that the conditions of Theorem 7.3.3 hold and that F_p admits a continuous density f_p. Then for all $\gamma > 0$*

$$\overline{F}_{Y_S}(\gamma) = \frac{1}{2\pi}\int_{u=\gamma}^{+\infty}\int_{-\infty}^{+\infty}\phi_{(I,M_S \leq u)}(w)g(w,u)\mathrm{d}w\mathrm{d}u, \tag{7.5.1}$$

where

$$g(w,u) = e^{-jwu} - (1+\gamma^{-1})e^{jw(1-\frac{1+\gamma}{\gamma}u)} \tag{7.5.2}$$

and

$$\overline{F}_{Y_S}(0) = 1 - \exp\left(-\rho\lambda(1 - F_p(0))|B|\right).$$

Proof. The mass in 0 was evaluated in (7.4.2). Now let us consider $\gamma > 0$. Using (6.3.5), we have:

$$
\begin{aligned}
\overline{F}_{Y_S}(\gamma) &= \mathbf{P}\{\frac{M_S}{1+I-M_S} > \gamma) \\
&= \mathbf{P}\{M_S > \frac{\gamma}{1+\gamma}(1+I)) \\
&= \int_{v=\gamma}^{\infty} \int_{u=\frac{\gamma(1+v)}{1+\gamma}}^{v} f_{(I,M_S)}(v,u)\mathrm{d}u\mathrm{d}v, \\
&= \int_{v=\gamma}^{\infty} \int_{u=0}^{v} f_{(I,M_S)}(v,u)\mathrm{d}u\mathrm{d}v - \int_{v=\gamma}^{\infty} \int_{u=0}^{\frac{\gamma(1+v)}{1+\gamma}} f_{(I,M_S)}(v,u)\mathrm{d}u\mathrm{d}v. \quad (7.5.3)
\end{aligned}
$$

where $f_{(I,M_S)}$ is the joint density function of I and M_S, which exists at all points (i,m) with $m > 0$ according to Corollary 7.3.4.

For $u > 0$ let

$$h(v,u) := \int_0^u f_{(I,M_S)}(v,t)\mathrm{d}t + g_I(v)\mathbf{P}(M_S = 0), \quad (7.5.4)$$

where $g_I(v)$ is the density of I at v given that $M_S = 0$. Intuitively, h is the density of $(\mathbf{1}(M_S \le u)I)$. The characteristic function of $v \to h(v,u)$ is $\phi_{(I,M_S \le u)}(w)$. From Theorem 7.3.3, we have $\phi_{(I,M_S \le u)}(w) \in \mathbb{L}$ w.r.t. w for $u > 0$. So by the Fourier inversion theorem (Theorem A.1.4), we have:

$$h(v,u) = \frac{1}{2\pi}\int_{-\infty}^{\infty} e^{-jwv}\phi_{(I,M_S \le u)}(w)\mathrm{d}w.$$

Therefore

$$h(v,v) = \frac{1}{2\pi}\int_{-\infty}^{\infty} e^{-jwv}\phi_{(I,M_S \le v)}(w)\mathrm{d}w.$$

And so:

$$\int_{\gamma}^{\infty} h(v,v)\mathrm{d}v = \frac{1}{2\pi}\int_{\gamma}^{\infty}\int_{-\infty}^{\infty} e^{-jwv}\phi_{(I,M_S \le v)}(w)\mathrm{d}w\mathrm{d}v. \quad (7.5.5)$$

Similarly, we have:

$$h\left(v,\frac{\gamma(1+v)}{1+\gamma}\right) = \frac{1}{2\pi}\int_{-\infty}^{\infty} e^{-jwv}\phi_{(I,M_S \le \frac{\gamma(1+v)}{1+\gamma})}(w)\mathrm{d}w.$$

Hence

$$\int_{\gamma}^{\infty} h\left(v,\frac{\gamma(1+v)}{1+\gamma}\right)\mathrm{d}v = \frac{1}{2\pi}\int_{\gamma}^{\infty}\int_{-\infty}^{\infty} e^{-jwv}\phi_{(I,M_S \le \frac{\gamma(1+v)}{1+\gamma})}(w)\mathrm{d}w\mathrm{d}v.$$

Conducting the change of variable $x = \frac{\gamma(1+v)}{1+\gamma}$, we get:

$$\int_{\gamma}^{\infty} h\left(v,\frac{\gamma(1+v)}{1+\gamma}\right)\mathrm{d}v = \frac{1}{2\pi}\frac{1+\gamma}{\gamma}\int_{\gamma}^{\infty}\int_{-\infty}^{\infty} e^{-jw(\frac{1+\gamma}{\gamma}x-1)}\phi_{(I,M_S \le x)}(w)\mathrm{d}w\mathrm{d}x. \quad (7.5.6)$$

Moreover, by (7.5.4) we have:

$$\int_{\gamma}^{\infty}\int_{0}^{v} f_{(I,M_S)}(v,u)\mathrm{d}u\mathrm{d}v - \int_{\gamma}^{\infty}\int_{0}^{\frac{\gamma(1+v)}{1+\gamma}} f_{(I,M_S)}(v,u)\mathrm{d}u\mathrm{d}v$$

$$= \int_{\gamma}^{\infty} h(v,v)\mathrm{d}v - \int_{\gamma}^{\infty} h\left(v, \frac{\gamma(1+v)}{1+\gamma}\right)\mathrm{d}v.$$

Substituting (7.5.5) and (7.5.6) into this, then by (7.5.3) we get:

$$\overline{F}_{Y_S}(\gamma) = \frac{1}{2\pi}\int_{\gamma}^{+\infty}\int_{-\infty}^{+\infty} \phi_{(I,M_S\leq x)}(w)g(w,x)\mathrm{d}w\mathrm{d}x.$$

where

$$g(w,x) = \exp(-jwx) - \frac{1+\gamma}{\gamma}\exp\left(-jw\left(\frac{1+\gamma}{\gamma}x - 1\right)\right). \qquad \square$$

Corollary 7.5.2. *Under the assumptions of Theorem 7.3.3, if $B = \mathbb{R}^2$, then $\overline{F}_{Y_S}(0) = 1$, and*

$$\overline{F}_{Y_S}(\gamma) = \int_{u=\gamma}^{+\infty}\int_{w=0}^{+\infty} \frac{1}{\pi}\exp\left(-(C_1 w^{\alpha} + C_2(w,u))\right)$$

$$\times\left(-\frac{1+\gamma}{\gamma}\cos\left(C_1 w^{\alpha}\tan(\frac{\pi\alpha}{2}) + C_3(w,u) + C_4(w,u)\right)\right.$$

$$\left. + \cos\left(C_1 w^{\alpha}\tan(\frac{\pi\alpha}{2}) + C_3(w,u) - wu\right)\right)\mathrm{d}w\mathrm{d}u, \quad (7.5.7)$$

for $\gamma > 0$ where C_1, C_2, and C_3 are given in Corollary 7.3.2, and $C_4(w,u) = w(1 - \frac{1+\gamma}{\gamma}u)$.

Proof. From Theorem 7.5.1, $\overline{F}_{Y_S}$ is given by (7.5.1). For this, we have

$$\int_{-\infty}^{+\infty} \phi_{(I,M_S\leq u)}(w)g(w,u)\mathrm{d}w$$

$$= \int_{0}^{+\infty}\left(\phi_{(I,M_S\leq u)}(w)g(w,u) + \phi_{(I,M_S\leq u)}(-w,u)g(-w,u)\right)\mathrm{d}w, \quad (7.5.8)$$

where $\phi_{(I,M_S\leq u)}$ is given by Corollary 7.3.2 and g is given by (7.5.2). Thus, we have for $w \in [0,+\infty)$:

$$\phi_{(I,M_S\leq u)}(w,u)g(w,u) = \exp\left(-(C_1 w^{\alpha} + C_2(w,u))\right)$$

$$\times\left(\exp\left(j\left(C_1 w^{\alpha}\tan(\frac{\pi\alpha}{2}) + C_3(w,u) - wu\right)\right)\right.$$

$$\left. - \frac{1+\gamma}{\gamma}\exp\left(j\left(C_1 w^{\alpha}\tan(\frac{\pi\alpha}{2}) + C_3(w,u) + C_4(w,u)\right)\right)\right),$$

where $C_4(w,u) = w(1 - \frac{1+\gamma}{\gamma}u)$. Similarly, for $w \in [0, +\infty)$:

$$
\begin{aligned}
\phi_{(I,M_S \leq u)}(-w,u)g(-w,u) &= \exp\left(-(C_1 w^\alpha + C_2(w,u))\right) \\
&\times \left(\exp\left(-j\left(C_1 w^\alpha \tan(\frac{\pi\alpha}{2}) + C_3(w,u) - wu\right)\right) \right. \\
&\left. - \frac{1+\gamma}{\gamma} \exp\left(-j\left(C_1 w^\alpha \tan(\frac{\pi\alpha}{2}) + C_3(w,u) + C_4(w,u)\right)\right) \right).
\end{aligned}
$$

These result in

$$
\begin{aligned}
&\phi_{(I,M_S \leq u)}(w,u)g(w,u) + \phi_{(I,M_S \leq u)}(-w,u)g(-w,u) \\
&= 2\exp\left(-(C_1 w^\alpha + C_2(w,u))\right) \times \left(\cos\left(C_1 w^\alpha \tan(\frac{\pi\alpha}{2}) + C_3(w,u) - wu\right) \right. \\
&\left. - \frac{1+\gamma}{\gamma}\cos\left(C_1 w^\alpha \tan(\frac{\pi\alpha}{2}) + C_3(w,u) + C_4(w,u)\right) \right).
\end{aligned}
$$

Substitute this into (7.5.8), then by (7.5.1) we obtain (7.5.7). $\qquad\square$

7.6 Conclusion

In this chapter we have developed a framework for the distribution of the best signal quality in a wireless network.

Using an interference shot noise model, we first derived a hybrid Laplace transform of the joint distribution of the interference and the maximum signal strength by using prior results on the Laplace transform of an additive shot noise (Theorem 5.2.12 in Chapter 5).

This result was then used to develop results in the case where the observation network area is a disk centered at the observation point. We determined necessary conditions under which the joint density of the interference and the maximum signal strength exists, and derived their joint density. We observed that under the unbounded power-law path loss model, the inner pole around the observation point introduces a mass of the maximum signal strength at the origin, leading to the nonexistence of the discussed joint density at the origin.

Using the results developed for the joint distribution of the interference and the maximum signal strength, we derived the distribution of the best signal quality.

Besides, this framework allowed us to directly obtain marginal distributions of the interference and of the maximum signal strength. We showed that the network interference has a skewed α-stable distribution with $\alpha = 2/\beta$ where β is the path loss exponent. We also proved that the maximum signal strength received at the center of a disk-shaped network area belongs to the maximum domain of attraction of a Fréchet distribution independently of the type of fading.

These results are expected to enable various studies related to the stochastic modeling of wireless communication networks. In particular, an application of these results will be provided in Chapter 10.

Chapter 8

Heavy-Tail Asymptotics of Wireless Links

8.1 Introduction

Many quantities of interest of wireless link modelling are made up of a common and essential ingredient which is the received signal strength. Beside of the evident example that the interference is a sum of signal strengths, the extremal signal strength is given as max of signal strengths, and the best signal quality is expressed in term of the received signal strength by means of the interference and maximum signal strength as given in §6.3. The signal strength in its turn is composed of path loss and fading in which path loss is the dominant component, see Chapter 2.

In Chapter 2 we see that the path loss is typically modelled as a decaying power law $d^{-\beta}$ with positive path loss exponent β. The particularity of this model is that it has a singularity at the origin. This singularity sometimes introduces surprising effects, notably the physical impossibility which is the received power higher that the transmitted power, occurring when the distance d is close to zero. As proved in Chapter 7, it results in the interference behaving as an α-stable law with $\alpha < 2$ and the global maximum signal strength behaving as a Fréchet distribution, both are very heavy-tailed as discussed in §5.1. This gives rise to a curious question:

How does the path loss singularity impact the heavy-tailed asymptotics
of wireless links?

The interference and the maximum signal strength are precisely extremes of random signal strengths $(P_i, i = 1, 2, \ldots)$. Inspiring the mathematical modelling of extreme events as presented in §5.1, we are motivated in

Investigating the above question by using extreme value theory.

Precisely, basing on the set of assumptions described in Chapter 6, we introduces the following enhancements:

(a) The typical power-law path loss will be used under two models: unbounded and bounded. Let $R_{\min}$ be a real-valued constant, the typical distance-dependent model describes the path loss as $1/l(d) = (\max\{d, R_{\min}\})^{-\beta}$ for $d \in \mathbb{R}_+$ and where:

$$R_{\min} = 0, \quad \text{under } \textit{unbounded} \text{ path loss model},$$
$$R_{\min} > 0, \quad \text{under } \textit{bounded} \text{ path loss model}.$$

(b) The disk-shaped network area B is bounded by setting its outer radius $R_B < \infty$.

(c) Random variables $(X_i, i = 1, 2, \ldots)$ as described in Chapter 6 are assumed distributed according to a lognormal distribution of parameters $(0, \sigma_X)$ with $0 < \sigma_X < \infty$.

Within this context, the signal strength received at the center of B from a node i in B is

$$P_i = A \, X_i \, (\max\{d_i, R_{\min}\})^{-\beta},$$

where constant A is previously specified in Chapter 6, and d_i is the distance from the center of B to node i. Here we observe that studying the above two path loss models is *equivalent* to studying the unbounded model $d^{-\beta}$, for $d \in \mathbb{R}_+$, with disk B *including* and *excluding* the inner pole of radius $R_{\min}$. In other words, assume that the distance from the center of B to the closest node in B is $R_{\min}$, i.e. $d_i \geq R_{\min}$ for all nodes i, then we can study the bounded model by using the unbounded model and excluding the inner pole of radius $R_{\min} > 0$, and study the unbounded model by taking $R_{\min} = 0$.

For convenience when dealing with extreme value theory, we will use alternative notation of extremes of wireless link as introduced in §6.3, so denote:

$$M_n = \max_{i=1, \mathbf{x}_i \in B}^{n} P_i, \quad I_n = \sum_{i=1, \mathbf{x}_i \in B}^{n} P_i, \quad Y_n = \max_{i=1, \mathbf{x}_i \in B}^{n} Q_i,$$

to be respectively the maximum of signal strengths, the interference, and the best signal quality received at the center of B from n nodes which are randomly selected from B with equal probability.

In §8.2 we study the heavy-tailed behaviour of the signal strength P_i under both conditions with $R_{\min} = 0$ and $R_{\min} > 0$. We show that its tail distribution $\overline{F}_P$ is regularly varying with index $-\alpha < 0$ with $\alpha = 2/\beta$ under the unbounded path loss, while $\overline{F}_P$ is less heavy-tailed than a lognormal distribution under the bounded path loss. Theorem 8.3.2 in §8.3 and Proposition 8.4.1 in §8.4 show that P_i lies on both the domains of attraction of an extreme value distribution H and an α-stable law G_α, where H is a Fréchet distribution and G_α has parameter $\alpha < 2$ under unbounded path loss, while H is a Gumbel distribution and G_α is a Gaussian distribution under bounded path loss. Section 8.5 states that the asymptotic independence between M_n and I_n is obtained when the bounded path loss model is used. Its consequence is that the joint density of M_n and I_n can be approximated by the product of their marginal density function. Finally, §8.6 provides an approximation of the distribution of the best signal quality under bounded path loss condition.

8.2   Tail-equivalent Distribution of Signal Strength

We begin with the exact distribution of the signal strength.

Proposition 8.2.1. *Consider the setting described above, and let F_P be the cumulative distribution function of the signal strength P_i.*

(a) If $R_{\min} = 0$, then

$$F_P(x) = K_1(x) - a^{\frac{2}{\beta}} e^{\nu} x^{-\frac{2}{\beta}} K_3(x), \tag{8.2.1}$$

(b) If $R_{\min} > 0$, then

$$F_P(x) = c\left(a^{-\frac{2}{\beta}} K_1(x) - b^{-\frac{2}{\beta}} K_2(x) - e^{\nu} x^{-\frac{2}{\beta}} K_3(x) + e^{\nu} x^{-\frac{2}{\beta}} K_4(x)\right), \tag{8.2.2}$$

where $a = AR_B^{-\beta}$, $b = AR_{\min}^{-\beta}$, $c = A^{\frac{2}{\beta}}(R_B^2 - R_{\min}^2)^{-1}$, $\nu = 2\sigma_X^2/\beta^2$, and K_j, $j = 1, \ldots, 4$, refers to the cdf of a lognormal distribution of parameters (μ_j, σ_X), in which

$$\mu_1 = \log a, \quad \mu_2 = \log b, \quad \mu_3 = \mu_1 + 2\sigma_X^2/\beta, \quad \mu_4 = \mu_2 + 2\sigma_X^2/\beta.$$

Proof. The distribution of the distance d_i is given as follows:

$$F_D(d) = \mathbf{P}(d_i \leq d) = \sum_{n=0}^{+\infty} \mathbf{P}(d_i \leq d \mid N_B = n)\mathbf{P}(N_B = n), \tag{8.2.3}$$

where $\mathbf{P}(N_B = n)$ is the probability that there are N_B nodes in B. Under the assumption that nodes are spatially distributed according to a homogeneous Poisson point process with intensity λ, the number of nodes located in B is distributed according to a Poisson distribution with intensity $\lambda|B|$ and is given according to Definition 5.2.2:

$$\mathbf{P}(N_B = n) = e^{-\lambda|B|}\frac{(\lambda|B|)^n}{n!}. \tag{8.2.4}$$

In addition, as described in §5.2.1, under the assumption of homogeneous Poisson point process, conditionally on the fact that $N_B = n$ these n nodes are uniformly distributed in B. Thus

$$\mathbf{P}(d_i \leq d \mid N_B = n) = \frac{\pi d^2 - \pi R_{\min}^2}{\pi R_B^2 - \pi R_{\min}^2}.$$

As a sequel of this, we obtain

$$F_D(d) = \sum_{n=0}^{+\infty} \frac{\pi d^2 - \pi R_{\min}^2}{\pi R_B^2 - \pi R_{\min}^2} e^{-\lambda|B|}\frac{(\lambda|B|)^n}{n!} = \frac{d^2 - R_{\min}^2}{R_B^2 - R_{\min}^2}. \tag{8.2.5}$$

Let $U_i = Ad_i^{-\beta}$, for $\beta > 0$, its distribution is equal to:

$$F_U(u) = -c\left(u^{-\frac{2}{\beta}} - a^{-\frac{2}{\beta}}\right), \quad \text{for} \quad u \in [a, b],$$

where $c = A^{\frac{2}{\beta}}(R_B^2 - R_{\min}^2)^{-1}$, $a = AR_B^{-\beta}$, and $b = AR_{\min}^{-\beta}$. The density of U_i is

$$f_U(u) = (2c/\beta)u^{-1-2/\beta}.$$

Thus, the distribution F_P of the power P_i is equal to:

$$F_P(x) = \int_{u=a}^{b} F_X\left(\frac{x}{u}\right) f_U(u)\mathrm{d}u. \tag{8.2.6}$$

Substituting F_X as the lognormal distribution of parameters $(0, \sigma_X)$ and f_U given above into (8.2.6), after changing the variable such that $t = \log(\frac{x}{u})$, we have:

$$F_P(x) = \frac{c}{\beta}x^{-\frac{2}{\beta}}\left(\int_{\log(\frac{x}{b})}^{\log(\frac{x}{a})} e^{\frac{2t}{\beta}}\mathrm{d}t + \int_{\log(\frac{x}{b})}^{\log(\frac{x}{a})} e^{\frac{2t}{\beta}}\mathrm{erf}\left(\frac{t}{\sqrt{2}\sigma_X}\right)\mathrm{d}t\right)$$

where the first integral is straightforward. By doing an integration by parts of $\mathrm{erf}\left(\frac{t}{\sqrt{2}\sigma_X}\right)$ and $e^{\frac{2t}{\beta}}\mathrm{d}t$ for the second integral, we get:

$$F_P(x) = \frac{c}{\beta}x^{-\frac{2}{\beta}}\frac{\beta}{2}\left[e^{\frac{2t}{\beta}} + e^{\frac{2t}{\beta}}\mathrm{erf}\left(\frac{t}{\sqrt{2}\sigma_X}\right) - e^{\frac{2\sigma_X^2}{\beta^2}}\mathrm{erf}\left(\frac{t}{\sqrt{2}\sigma_X} - \frac{\sqrt{2}\sigma_X}{\beta}\right)\right]\Big|_{t=\log(\frac{x}{b})}^{\log(\frac{x}{a})}.$$

After some elementary simplifications, we can obtain:

$$F_P(x) = c\left(a^{-\frac{2}{\beta}}\left(\frac{1}{2} + \frac{1}{2}\mathrm{erf}\left(\frac{\log x - \mu_1}{\sqrt{2}\sigma_X}\right)\right) - b^{-\frac{2}{\beta}}\left(\frac{1}{2} + \frac{1}{2}\mathrm{erf}\left(\frac{\log x - \mu_2}{\sqrt{2}\sigma_X}\right)\right)\right.$$
$$\left. + e^{\nu}x^{-\frac{2}{\beta}}\left[-\frac{1}{2} - \frac{1}{2}\mathrm{erf}\left(\frac{\log x - \mu_3}{\sqrt{2}\sigma_X}\right) + \frac{1}{2} + \frac{1}{2}\mathrm{erf}\left(\frac{\log x - \mu_4}{\sqrt{2}\sigma_X}\right)\right]\right), \tag{8.2.7}$$

where $\nu = \frac{2\sigma_X^2}{\beta^2}$, $\mu_1 = \log a$, $\mu_3 = \mu_1 + 2\sigma_X^2/\beta$, $\mu_2 = \log b$, and $\mu_4 = \mu_2 + 2\sigma_X^2/\beta$.

Denote by K_j, $j = 1, ..., 4$, the lognormal distribution of parameters (μ_j, σ_X), $j = 1, ..., 4$. For $R_{\min} = 0$, we have $c = A^{\frac{2}{\beta}}R^{-2} = a^{\frac{2}{\beta}}$, $b = \infty$, and $\mu_2 = \mu_4 = \infty$. And so (8.2.7) is reduced to (8.2.1).

And for $R_{\min} > 0$, F_P as given in (8.2.7) can be rewritten as (8.2.2).   □

Denote $\overline{K}_j(x) = 1 - K_j(x)$. For case of $R_{\min} = 0$, we have from (8.2.1) that:

$$\overline{F}_P(x) = 1 - K_1(x) + a^{\frac{2}{\beta}}e^{\nu}x^{-\frac{2}{\beta}}K_3(x)$$
$$= \overline{K}_1(x) - a^{\frac{2}{\beta}}e^{\nu}x^{-\frac{2}{\beta}}\overline{K}_3(x) + a^{\frac{2}{\beta}}e^{\nu}x^{-\frac{2}{\beta}}. \tag{8.2.8}$$

Here we see that $\overline{F}_P(x)$ is a combination of lognormal distributions and a decaying power-law term.

Similarly, for $R_{\min} > 0$, observe that $c(a^{-\frac{2}{\beta}} - b^{-\frac{2}{\beta}}) = 1$, so from (8.2.2):

$$F_P(x) = c\left(a^{-\frac{2}{\beta}}[1 - \overline{K}_1(x)] - b^{-\frac{2}{\beta}}[1 - \overline{K}_2(x)] - e^{\nu}x^{-\frac{2}{\beta}}[1 - \overline{K}_3(x)] + e^{\nu}x^{-\frac{2}{\beta}}[1 - \overline{K}_4(x)]\right)$$
$$= 1 - c\left(a^{-\frac{2}{\beta}}\overline{K}_1(x) - b^{-\frac{2}{\beta}}\overline{K}_2(x) - e^{\nu}x^{-\frac{2}{\beta}}\overline{K}_3(x) + e^{\nu}x^{-\frac{2}{\beta}}\overline{K}_4(x)\right).$$

This yields the tail distribution $\overline{F}_P = 1 - F_P$:

$$\overline{F}_P(x) = c\left(a^{-\frac{2}{\beta}}\overline{K}_1(x) - b^{-\frac{2}{\beta}}\overline{K}_2(x) - e^{\nu}x^{-\frac{2}{\beta}}\overline{K}_3(x) + e^{\nu}x^{-\frac{2}{\beta}}\overline{K}_4(x)\right). \tag{8.2.9}$$

The tail distribution of P_i is now a combination (but not linear) of those of lognormal distributions. The behaviour of $\overline{F}_P$ at large x for the both cases is given in the following.

Theorem 8.2.2. *The signal strength P_i has the following tail equivalent distribution:*

(a) If $R_{\min} = 0$, denoting $\alpha = 2/\beta$, then

$$\overline{F}_P(x) \sim a^\alpha e^\nu x^{-\alpha}, \quad as \ x \to \infty. \tag{8.2.10}$$

(b) If $R_{\min} > 0$, then

$$\overline{F}_P(x) \sim \kappa \frac{\exp\left(-(\log x - \mu_2)^2/(2\sigma_X^2)\right)}{(\log x - \mu_2)^2/(2\sigma_X^2)} \tag{8.2.11a}$$

$$\sim \kappa \frac{2\sqrt{2\pi}\sigma_X \overline{K}_2(x)}{\log x - \mu_2}, \qquad as \ x \to \infty, \tag{8.2.11b}$$

where $\overline{K}_2(x) = 1 - K_2(x)$, and $\kappa = \frac{\sigma_X}{\sqrt{2\pi}\beta} \frac{R_{\min}^2}{R_B^2 - R_{\min}^2}$.

When $R_{\min} = 0$, we see from (8.2.10) that F_P is *regularly* varying with index $-\alpha < 0$. According to what discussed in §5.1.1 of Chapter 5, F_P in this case has *very heavy-tailed* behaviour. By contrast, in case $R_{\min} > 0$, the tail distribution of the signal strength P_i is close to that of K_2 and it decays more rapidly, as given by (8.2.11b). Since K_2 is a lognormal distribution which belongs to the family of rapidly varying functions, F_P can only be of *rapidly* varying type. This difference between two cases implies that the singularity of the path loss model has decisive influence on the tail behaviour of the received signal strength. We also see that the decaying power-law path loss is the dominant component by the fact that even when the inner pole is excluded from the disk, the tail of F_P is still determined by that of the signal strength received from the most inner ring which is K_2 as given by (8.2.11b). Theorem 8.2.2 as so provides us useful insights into the heavy-tailed asymptotics of F_P with respect to the singularity of the path loss model. And again it confirms the discussion in Remark 7.4.3 of Chapter 7. In the next section, we investigate more asymptotic properties using this theorem.

Proof of Theorem 8.2.2. The tail distribution of lognormal distribution is given as

$$\overline{K}_j(x) = \frac{1}{2} \operatorname{erfc}\left(\frac{\log x - \mu_j}{\sqrt{2}\sigma_X}\right).$$

An asymptotic expansion of $\operatorname{erfc}(x)$ for large x [43, 7.1.23] gives us:

$$\overline{K}_j(x) \sim \frac{\sigma_X}{\sqrt{2\pi}(\log x - \mu_j)} \exp\left(-\frac{(\log x - \mu_j)^2}{2\sigma_X^2}\right), \quad as \ x \to \infty, \tag{8.2.12}$$

for $j = 1, \ldots, 4$. In the following we use this asymptotic expansion for the proof.

We begin now with the proof of (a). It can be easily seen that for $\beta > 0$:

$$\frac{\exp\left(-\frac{(\log x - \mu_1)^2}{2\sigma_X^2}\right)}{(\log x - \mu_1)} = o(x^{-\frac{2}{\beta}}), \quad as \ x \to \infty,$$

which leads to $\overline{K}_1(x) = o(x^{-\frac{2}{\beta}})$. And

$$\frac{\exp\left(-\frac{(\log x - \mu_3)^2}{2\sigma_X^2}\right)}{(\log x - \mu_3)} = o(1), \quad \text{as } x \to \infty,$$

leading to $x^{-\frac{2}{\beta}}\overline{K}_3(x) = o(x^{-\frac{2}{\beta}})$. As a result, by (8.2.8) we get (8.2.10).

Now we prove (b). Using (8.2.12):

$$\overline{K}_3(x) \sim \frac{\sigma_X}{\sqrt{2\pi}(\log x - \mu_3)} \exp\left(-\frac{(\log x - \mu_3)^2}{2\sigma_X^2}\right), \quad \text{as } x \to \infty, \qquad (8.2.13)$$

in which the first term is simplified as follows

$$\frac{1}{\log x - \mu_3} = \frac{1}{\left(\log x - \mu_1 - \frac{2\sigma_X^2}{\beta}\right)} = \frac{1}{\log x - \mu_1} \frac{1}{1 - \frac{2\sigma_X^2}{\beta(\log x - \mu_1)}},$$

which, after a Taylor expansion of the last term on the right-hand side, is reduced to

$$\frac{1}{\log x - \mu_3} \sim \frac{1}{\log x - \mu_1}\left(1 + \frac{2\sigma_X^2}{\beta}\frac{1}{(\log x - \mu_1)}\right), \quad \text{as } x \to \infty. \qquad (8.2.14)$$

And the second term of (8.2.13) is simplified as follows

$$\begin{aligned}
\exp\left(-\frac{(\log x - \mu_3)^2}{2\sigma_X^2}\right) &= \exp\left(-\frac{(\log x - \mu_1 - \frac{2\sigma_X^2}{\beta})^2}{2\sigma_X^2}\right) \\
&= \exp\left(-\frac{2\sigma_X^2}{\beta^2}\right)\exp\left(\frac{2}{\beta}(\log x - \mu_1)\right)\exp\left(-\frac{(\log x - \mu_1)^2}{2\sigma_X^2}\right) \\
&= e^{-\nu}a^{-\frac{2}{\beta}}x^{\frac{2}{\beta}}\exp\left(-\frac{(\log x - \mu_1)^2}{2\sigma_X^2}\right).
\end{aligned} \qquad (8.2.15)$$

Substitute (8.2.14) and (8.2.15) into (8.2.13) we obtain

$$\begin{aligned}
\overline{K}_3(x) &\sim \frac{\sigma_X a^{-\frac{2}{\beta}}e^{-\nu}x^{\frac{2}{\beta}}}{\sqrt{2\pi}(\log x - \mu_1)}\left(1 + \frac{2\sigma_X^2}{\beta}\frac{1}{(\log x - \mu_1)}\right)\exp\left(-\frac{(\log x - \mu_1)^2}{2\sigma_X^2}\right) \\
&= \frac{a^{-\frac{2}{\beta}}}{e^{\nu}x^{-\frac{2}{\beta}}}\left(\frac{\sigma_X}{\sqrt{2\pi}}\frac{\exp\left(-\frac{(\log x - \mu_1)^2}{2\sigma_X^2}\right)}{(\log x - \mu_1)} + \sqrt{\frac{2}{\pi}}\frac{\sigma_X^3}{\beta}\frac{\exp\left(-\frac{(\log x - \mu_1)^2}{2\sigma_X^2}\right)}{(\log x - \mu_1)^2}\right),
\end{aligned} \qquad (8.2.16)$$

in which, using (8.2.12):

$$\frac{\sigma_X}{\sqrt{2\pi}}\frac{\exp\left(-\frac{(\log x - \mu_1)^2}{2\sigma_X^2}\right)}{(\log x - \mu_1)} \sim \overline{K}_1(x), \quad \text{as } x \to \infty.$$

Take this into account for (8.2.16), we get

$$e^{\nu}x^{-\frac{2}{\beta}}\overline{K}_3(x) \sim a^{-\frac{2}{\beta}}\left(\overline{K}_1(x) + \sqrt{\frac{2}{\pi}}\frac{\sigma_X^3}{\beta}\frac{\exp\left(-\frac{(\log x - \mu_1)^2}{2\sigma_X^2}\right)}{(\log x - \mu_1)^2}\right), \quad \text{as } x \to \infty.$$

This leads to

$$a^{-\frac{2}{\beta}}\overline{K}_1(x) - e^{\nu}x^{-\frac{2}{\beta}}\overline{K}_3(x) \sim -\sqrt{\frac{2}{\pi}}\frac{a^{-\frac{2}{\beta}}\sigma_X^3}{\beta}\frac{\exp\left(-\frac{(\log x - \mu_1)^2}{2\sigma_X^2}\right)}{(\log x - \mu_1)^2}, \quad \text{as } x \to \infty. \qquad (8.2.17)$$

In the same manner, we have

$$b^{-\frac{2}{\beta}}\overline{K}_2(x) - e^{\nu}x^{-\frac{2}{\beta}}\overline{K}_4(x) \sim -\sqrt{\frac{2}{\pi}}\frac{b^{-\frac{2}{\beta}}\sigma_X^3}{\beta}\frac{\exp\left(-\frac{(\log x - \mu_2)^2}{2\sigma_X^2}\right)}{(\log x - \mu_2)^2}, \quad \text{as } x \to \infty. \qquad (8.2.18)$$

A substitution of (8.2.17) and (8.2.18) into (8.2.9) results in

$$\overline{F}_P(x) \sim \sqrt{\frac{2}{\pi}}\frac{c\sigma_X^3}{\beta}\left(b^{-\frac{2}{\beta}}\frac{\exp\left(-(\log x - \mu_2)^2/(2\sigma_X^2)\right)}{(\log x - \mu_2)^2}\right.$$
$$\left. - a^{-\frac{2}{\beta}}\frac{\exp\left(-(\log x - \mu_1)^2/(2\sigma_X^2)\right)}{(\log x - \mu_1)^2}\right). \quad (8.2.19)$$

Moreover, $b > a$ yields $\mu_2 - \mu_1 = \log(b/a) > 0$. Then, we have the following result for large x:

$$\frac{\exp\left(-\frac{(\log x - \mu_1)^2}{2\sigma_X^2}\right)/(\log x - \mu_1)^2}{\exp\left(-\frac{(\log x - \mu_2)^2}{2\sigma_X^2}\right)/(\log x - \mu_2)^2} = \left(\frac{\log x - \mu_2}{\log x - \mu_1}\right)^2 e^{\frac{\mu_2^2 - \mu_1^2}{2\sigma_X^2}}x^{-\frac{\mu_2 - \mu_1}{\sigma_X^2}} \to 0, \quad \text{as } x \to \infty.$$

Taking this into account in (8.2.19), finally we have:

$$\overline{F}_P(x) \sim \kappa\frac{\exp\left(-(\log x - \mu_2)^2/(2\sigma_X^2)\right)}{\left((\log x - \mu_2)/(\sqrt{2}\sigma_X)\right)^2} \sim 2\sqrt{2\pi}\sigma_X\kappa\frac{\overline{K}_2(x)}{\log x - \mu_2}, \quad \text{as } x \to \infty, \qquad (8.2.20)$$

where $\kappa := \frac{\sigma_X}{\sqrt{2\pi}\beta}\frac{R_{\min}^2}{R_B^2 - R_{\min}^2}$. $\qquad\qquad\qquad\qquad\qquad\qquad\qquad\qquad\qquad\qquad\qquad\qquad\qquad\qquad$ □

8.3 Asymptotic Distribution of Maximum Signal Strength

Under the studied system model, $(P_i, i = 1, 2, \ldots)$ are i.i.d., and so the cumulative distribution function (cdf) F_{M_n} and probability density function (pdf) f_{M_n} of M_n are easily obtained as follows.

Corollary 8.3.1. *The cdf and the pdf of M_n, for $n \geq 1$, are given respectively by:*

$$\begin{aligned} F_{M_n}(x) &= F_P^n(x), & (8.3.1) \\ f_{M_n}(x) &= n f_P(x) F_P^{n-1}(x), & (8.3.2) \end{aligned}$$

where $F_P(x)$ is given by Proposition 8.2.1, and f_P is the pdf of P_i, $f_P(x) = \mathrm{d}F_P(x)/\mathrm{d}x$.

Nonetheless, in §5.1 of Chapter 5 we see that the asymptotic distribution of a normalised maximum of i.i.d. random variables when exists must have one of the three known distributions: Fréchet, Weibull, or Gumbel distribution. More importantly, the heavy-tail behaviour of the

underlying distribution decides the type of its maximum domain of attraction. With the information provided by Theorem 8.2.2, we are interested in asymptotic properties of M_n by using extreme value theory.

Theorem 8.3.2. *Under the setting described above,*

(a) *If $R_{\min} = 0$, then*
$$c_n^{-1}(M_n - d_n) \overset{d}{\to} \Upsilon_\alpha(x), \quad as\ n \to \infty, \tag{8.3.3}$$

where Υ_α is the standard Fréchet distribution of parameter $\alpha = 2/\beta$, and normalising constants can be chosen such that

$$\overline{F}_P(c_n) = 1/n, \quad d_n = 0, \tag{8.3.4}$$

where $\overline{F}_P$ is given by (8.2.8).

(b) *If $R_{\min} > 0$, then*
$$c_n^{-1}(M_n - d_n) \overset{d}{\to} \Lambda, \quad as\ n \to \infty, \tag{8.3.5}$$

where Λ is the standard Gumbel distribution, and a possible choice of c_n and d_n is:

$$
\begin{aligned}
c_n &= \sigma_X (2 \log n)^{-\frac{1}{2}} d_n, \\
d_n &= \exp\left(\mu_2 + \sigma_X \left(\sqrt{2 \log n} + \frac{-\log \log n + \log \kappa}{\sqrt{2 \log n}} \right) \right),
\end{aligned}
\tag{8.3.6}
$$

with κ given by Theorem 8.2.2.

Proof. The proof of (a) is simple. By (a) of Theorem 8.2.2, $\overline{F}_P$ is regularly varying with index $-\alpha < 0$. The proof then follows Theorem 5.1.17.

Now is the proof of (b). Let $g(t) = e^{\sqrt{2}\sigma_X t + \mu_2}$ be a real function defined on $\mathbb{R}$, g is increasing with t. Let $\widetilde{P}_i$ be the random variable such that $P_i = g(\widetilde{P}_i)$. By (8.2.11a) of Theorem 8.2.2, the tail distribution $\overline{F}_{\widetilde{P}}$ is given by:

$$\overline{F}_{\widetilde{P}_i}(x) = \mathbf{P}(g(\widetilde{P}) \le g(x)) = \overline{F}_P\left(e^{\sqrt{2}\sigma_X x + \mu_2} \right) \sim \kappa x^{-2} e^{-x^2}, \quad as\ x \to \infty. \tag{8.3.7}$$

By (8.3.7), $F_{\widetilde{P}}$ satisfies Theorem 5.1.22 with constants $l = \kappa$, $r = -2$, $\eta = 1$, and $\omega = 2$. So, $F_{\widetilde{P}} \in \mathrm{MDA}(\Lambda)$ with the following normalising constants:

$$
\begin{aligned}
c_n^* &= \frac{(\log n/\eta)^{\frac{1}{\omega}-1}}{\omega \eta} = \frac{1}{2}(\log n)^{-\frac{1}{2}}, \\
d_n^* &= \left(\frac{\log n}{\eta} \right)^{1/\omega} + \frac{\eta^{1/\omega}}{\omega^2} \frac{r(\log \log n - \log \eta) + \omega \log l}{(\log n)^{1 - \frac{1}{\omega}}} \\
&= (\log n)^{\frac{1}{2}} + \frac{1}{2} \frac{(-\log \log n + \log \kappa)}{(\log n)^{\frac{1}{2}}}.
\end{aligned}
\tag{8.3.8}
$$

Then, by Proposition 5.1.21, we have

$$\lim_{n \to \infty} \mathbf{P}\left(M_n \le g(c_n^* x + d_n^*) \right) = \Lambda(x), \quad x \in \mathbb{R}.$$

By a Taylor expansion of $\exp(\sqrt{2}\sigma_X c_n^* x)$, we have:

$$\lim_{n\to\infty} \mathbf{P}\left(e^{-(\sqrt{2}\sigma_X d_n^* + \mu_2)} M_n \leq 1 + \sqrt{2}\sigma_X c_n^* x + o(c_n^*)\right) = \Lambda(x).$$

Since $c_n^* \to 0$ when $n \to \infty$, we have

$$\frac{M_n - e^{\sqrt{2}\sigma_X d_n^* + \mu_2}}{\sqrt{2}\sigma_X c_n^* e^{\sqrt{2}\sigma_X d_n^* + \mu_2}} \xrightarrow{d} \Lambda, \qquad \text{as } n \to \infty. \tag{8.3.9}$$

Substituting c_n^* and d_n^* from (8.3.8) into (8.3.9), we obtain c_n and d_n for (8.3.6). The conditions $R_B < \infty$, $R_{\min} > 0$ and $\sigma_X > 0$ provide $\kappa > 0$. This leads to $d_n > 0$, and consequently, $c_n > 0$. $\qquad\qquad\square$

To this end, Theorem 8.3.2 concludes our previous discussions about the asymptotic behaviour of F_P. According to (a) of Theorem 8.3.2, in case of disk with inner pole, or equivalently of unbounded path loss, F_P belongs to the maximum domain of attraction of Fréchet distribution. Note that here the network domain B is bounded, i.e. $R_B < +\infty$, and that the distribution of M_n is asymptotically of Fréchet type as the number of nodes measured from this bounded area tends to infinity, i.e. $n \to \infty$. The fact that the number of nodes increases freely within a bounded network area refers to a network densification scenario. This result therefore complements Corollary 7.4.2 in Chapter 7 according to which F_P belongs to the maximum domain of attraction of the Fréchet distribution under a network extension scenario. Precisely, Corollary 7.4.2 states that the maximum of signal strength *is* a Fréchet distribution as the outer radius of the measured network domain tending to infinity, i.e. $R_B \to +\infty$. The fact of increasing the radius of the network domain corresponds to a network extension scenario. So, under the unbounded decaying power-law path loss condition, $F_P \in \text{MDA}(\Upsilon_\alpha)$ for both scenarios: network densification, and network extension.

On the other hand, in case of a disk *excluding* the inner pole, or equivalently of bounded path loss, F_P belongs to the maximum domain of attraction of Gumbel distribution. This is dominantly imposed by the heavy-tailed behaviour of the lognormal distribution X_i as given by Theorem 8.2.2. And this property holds for a network densification scenario, i.e. $n \to \infty$ in a bounded domain B.

Theorem 8.3.2 provides asymptotic properties when $n \to \infty$. In practical applications, n is the number of nodes, and so it should only take moderate values. It is thus useful to evaluate the convergence speed of asymptotic limits. In the following we will evaluate the convergence speed of $c_n^{-1}(M_n - d_n) \xrightarrow{d} \Lambda$, and do this by using simulations. We will measure the discrepancy using a symmetrised version of the Kullback-Leibler divergence (the so-called Jensen-Shannon divergence (JSdiv)), see Appendix A.2 for more information.

Denote $\widetilde{M}_n \equiv c_n^{-1}(M_n - d_n)$ with constants given by (8.3.6). Let us start with some numerical evaluations of the convergence of $\widetilde{M}_n$ to its limiting distribution. Figure 8.1(a) shows $F_{\widetilde{M}_n}$ for different n and compares to empirical simulation results. As expected the analytical distributions obtained by (8.3.1) of Corollary 8.3.1 match with the empirical distributions for all n. Figure 8.1(b) plots the analytical distribution and its limiting distribution, i.e. the Gumbel distribution Λ. There is a discrepancy in the negative regime (see the circled region in Figure 8.1(b)). It is worth pointing out that as a maximum of signal strengths, $M_n \geq 0$ and thus $\widetilde{M}_n \geq -d_n/c_n = -\sqrt{2\log n}/\sigma_X$ since $\widetilde{M}_n = (M_n - d_n)/c_n$. This means that $F_{\widetilde{M}_n}(x) = 0$,

(a) Analytical vs. Empirical CDFs

(b) Analytical vs. Limiting CDFs
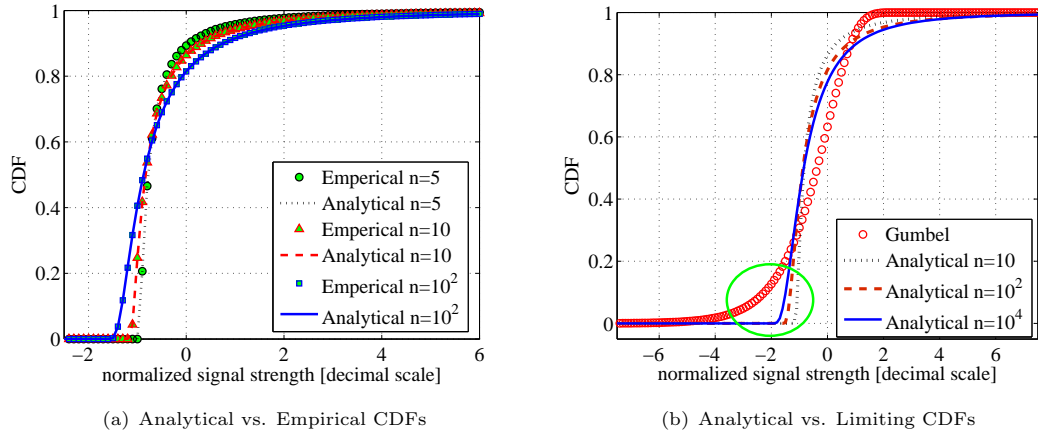
FIGURE 8.1: CDF of $\widetilde{M}_n$ under different n: $\sigma_{\mathrm{dB}} = 8$, $\beta = 3$.

(a) Under different σ_{dB}: $\beta = 3$

(b) Under different β: $\sigma_{\mathrm{dB}} = 8$
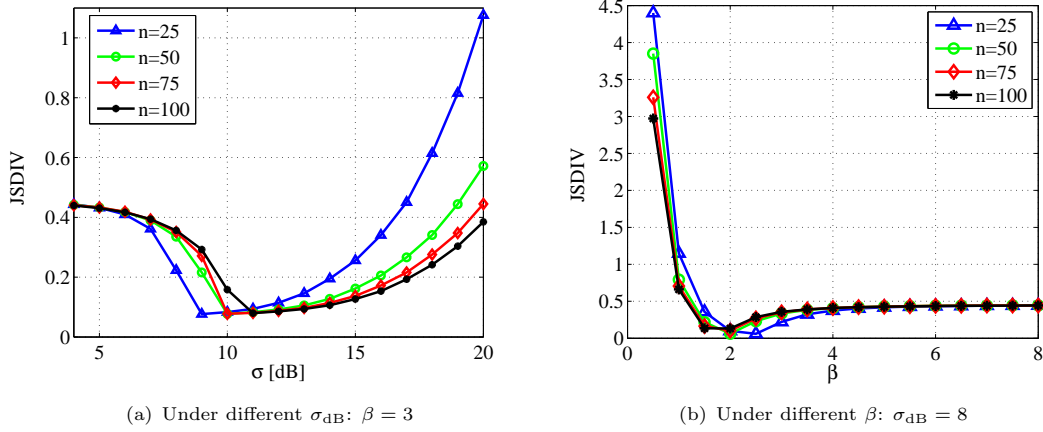
FIGURE 8.2: Jensen-Shannon divergence between $\widetilde{M}_n$ and Λ.

$\forall x \le -\sqrt{2 \log n}/\sigma_X$, whereas $\Lambda(x) > 0$, $\forall x > -\infty$. This explains the gap observed for n small. This dissimilarity should have limited impact as long as we only deal with positive values of M_n (respectively, $\widetilde{M}_n \ge -\sqrt{2 \log n}/\sigma_X$).

We now study the symmetrised divergence between the analytical and limiting distributions of $\widetilde{M}_n$ for some moderate values of n and under different σ_{dB} and β. The convergence is best for σ_{dB} around 10 dB and β around two to four. For practical systems, σ_{dB} is approx. 8 dB and $2 < \beta \le 4$. We compute the Jensen-Shannon divergence for $\beta = 3$ and $\sigma_{\mathrm{dB}} = 8$ and plot the results in Figure 8.2(a) and (b), respectively. For these (and other) values (within the range given above) of σ_{dB} and β, $\widetilde{M}_n$ and Λ have low divergence.

8.4 Asymptotic Distribution of the Interference

The interference I_n is nothing but sum of i.i.d. random variables (P_i, $i = 1, \ldots, n$). Similar to the maximum of signal strengths M_n, the fluctuation of I_n is determined by the tail behaviour

of F_P. Using Theorem 8.2.2 and theoretical support provided in §5.1.2, we obtain the following asymptotic distribution of I_n.

Proposition 8.4.1. *Under the setting described above*

(a) If $R_{\min} = 0$ and $\beta > 1$, then $F_P \in D(\alpha)$ with $\alpha = 2/\beta$, i.e.,

$$a_n^{-1}(I_n - b_n) \xrightarrow{d} G_\alpha, \qquad as \ n \to \infty, \tag{8.4.1}$$

where G_α is an α-stable law, and normalising constants can be chosen such that

$$\overline{F}_P(a_n) = 1/n, \quad b_n = n \left(a_n F_P(a_n) - \int_0^{a_n} F_P(x) \mathrm{d}x \right), \tag{8.4.2}$$

with $\overline{F}_P$ and F_P respectively given by (8.2.8) and (8.2.1). In particular, we can choose $b_n = 0$ if $\beta > 2$.

(b) If $R_{\min} > 0$, then $F_P \in D(2)$, i.e.,

$$a_n^{-1}(I_n - b_n) \xrightarrow{d} \Phi, \qquad as \ n \to \infty, \tag{8.4.3}$$

where Φ is the standard Gaussian distribution, and

$$a_n = \sqrt{n \operatorname{var}(P_i)}, \quad b_n = n \mathbf{E} P_i. \tag{8.4.4}$$

Proof. By (a) of Theorem 8.2.2, $\overline{F}_P$ is regularly varying with index $-\alpha$. Thus, the proof of (a) follows (b) of Theorem 5.1.6. In addition, the normalising constants in (8.4.1) are given according to Proposition 5.1.8 and Proposition 5.1.9.

For (b), under the considered setting, we have $d_i \geq R_{\min} > 0$. So

$$
\begin{aligned}
\mathbf{E} P_i = \mathbf{E}\{A d_i^{-\beta} X_i\} &\leq \left(A R_{\min}^{-\beta} \right) \mathbf{E} X_i, \\
\operatorname{var}(P_i) = \operatorname{var}(A d_i^{-\beta} X_i) &\leq \left(A R_{\min}^{-\beta} \right)^2 \operatorname{var}(X_i),
\end{aligned}
$$

where note that for X_i distributed according to a lognormal distribution of parameters $(0, \sigma_X)$, $\mathbf{E} X_i = \exp(\sigma_X^2/2)$ and $\operatorname{var}(X_i) = (e^{\sigma_X^2} - 1)e^{\sigma_X^2}$ which are finite under the assumption that $\sigma_X < \infty$. As a result, $\mathbf{E} P_i < \infty$, $\operatorname{var}(P_i) < \infty$, and so

$$\mathbf{E}\{P_i^2\} = \mathbf{E}\{P_i\}^2 + \operatorname{var}(X_i)^2 < \infty.$$

Thus P_i belongs to the domain of attraction of the Gaussian distribution according to *(a)* of Corollary 5.1.7. Finally, constants a_n and b_n are given by the general central limit theorem, Theorem 5.1.10. $\qquad \square$

Proposition 8.4.1 tells us that to obtain Gaussian interference, we have to use bounded path loss model or to exclude the inner pole around the observation point. Otherwise, it is asymptotically an α-stable law with $\alpha = 2/\beta < 2$ which is heavier-tailed. This is explained by the fact that when $R_{\min} = 0$, i.e. including the inner pole or using unbounded path loss, there is a dominant component at the origin in the sum which violates the condition for a convergence to the Gaussian distribution. This result is in light with Corollary 7.4.4 in Chapter 7.

Above we determined the asymptotic distribution of the partial interference I_n. For completeness, we have the following result of the total interference I.

Proposition 8.4.2. *Relax the condition of lognormal X_i from the setting described above, denote by I the total interference. For $R_{\min} \geq 0$:*

(a) *The characteristic function ϕ_I of I is equal to*

$$\phi_I(w) = \exp\left(-\pi\lambda\alpha(A|w|)^\alpha \int_0^{\frac{A|w|}{R_{\min}^\beta}} \frac{1 - \phi_X(\mathrm{sign}(w)t)}{t^{\alpha+1}} \mathrm{d}t\right),\qquad (8.4.5)$$

where $\alpha = 2/\beta$, and ϕ_X is the characteristic function of X_i.

(b) *$|\phi_I(w)|^q \in \mathbb{L}$ for all $q = 1, 2, \ldots$, where $\mathbb{L}$ is the space of absolutely integrable functions.*

(c) *If $R_{\min} > 0$ and if $AR_{\min}^{-\beta}$ is large, then ϕ_I admits the following approximation*

$$\phi_I(w) \approx \exp\left(-\delta|w|^\alpha \left(1 - j\,\mathrm{sign}(w)\tan\left(\frac{\pi\alpha}{2}\right)\right)\right),\qquad (8.4.6)$$

where δ is as given by (7.3.3):

$$\delta = c_\alpha\Gamma(1 - \alpha)\cos(\pi\alpha/2),$$

with c_α given by (7.3.4):

$$c_\alpha = \pi\lambda A^\alpha \mathbf{E}\{X_i^\alpha\},$$

and with $\Gamma(\cdot)$ denoting the gamma function.

Proof. Under the assumptions of the theorem, the interference field can be modeled as a shot noise defined on $\mathbb{R}^2$ excluding the inner disk of radius $R_{\min}$. Hence, using Theorem 5.2.12, the Laplace transform of I is given by:

$$\mathcal{L}_I(z) = \exp\left(-2\pi\lambda \int_{R_{\min}}^\infty \left(1 - \mathbf{E}\{e^{-\frac{zAX_i}{r^\beta}}\}\right)r\mathrm{d}r\right).\qquad (8.4.7)$$

Noting that

$$\phi_I(w) = \mathcal{L}_I(-jw), \quad w \in \mathbb{R},$$

we have from (8.4.7) that:

$$\phi_I(w) = \exp\left(-2\pi\lambda \int_{R_{\min}}^\infty (1 - \mathbf{E}\{e^{\frac{jwAX_i}{r^\beta}}\})r\mathrm{d}r\right).\qquad (8.4.8)$$

Using the change of variable $t = |w|Ar^{-\beta}$, we obtain

$$\int_{R_{\min}}^{+\infty} \left(1 - \mathbf{E}\left\{\exp\left(\frac{jwAX_i}{r^\beta}\right)\right\}\right)r\mathrm{d}r = \frac{(A|w|)^{2/\beta}}{\beta} \int_0^{\frac{A|w|}{R_{\min}^\beta}} \frac{1 - \mathbf{E}\{e^{j\,\mathrm{sign}(w)tX_i}\}}{t^{2/\beta+1}}\mathrm{d}t,\qquad (8.4.9)$$

where $\mathbf{E}\{\exp(j\,\mathrm{sign}(w)tX_i)\} = \phi_X(\mathrm{sign}(w)t)$. So, substituting this into (8.4.8), we get the first part of the Proposition 8.4.2.

From (8.4.5), for all $q = 1, 2, \ldots$, we have:

$$|\phi_I(w)|^q = \exp\left(-q\pi\lambda\alpha(A|w|)^\alpha \mathbf{E}\left\{\int_0^{\frac{A|w|}{R_{\min}^\beta}} \frac{1 - \cos(tX_i)}{t^{\alpha+1}} \mathrm{d}t\right\}\right). \tag{8.4.10}$$

Since $1 - \cos(tX_i) \geq 0$, $\forall t \in \mathbb{R}$, we have

$$\mathbf{E}\left\{\int_0^{\frac{A|w|}{R_{\min}^\beta}} \frac{1 - \cos(tX_i)}{t^{\alpha+1}} \mathrm{d}t\right\} \geq 0. \tag{8.4.11}$$

Therefore

$$|\phi_I(w)|^q \leq \exp(-\mathrm{const} \times |w|^\alpha), \tag{8.4.12}$$

where const is some positive constant, and hence the right hand-side of this is an absolutely integrable function. This proves the second assertion of Proposition 8.4.2.

Under the assumption that $AR_{\min}^{-\beta} \approx \infty$, ϕ_I can be approximated by:

$$\phi_I(w) \approx \exp\left(-\pi\lambda\alpha(A|w|)^\alpha \int_0^\infty \frac{1 - \phi_X(\mathrm{sign}(w)t)}{t^{\alpha+1}} \mathrm{d}t\right). \tag{8.4.13}$$

For $0 < \alpha < 1$, we have

$$\int_0^\infty \frac{1 - e^{j\mathrm{sign}(w)tX_i}}{t^{\alpha+1}} \mathrm{d}t = -\Gamma(-\alpha)X_i^\alpha e^{-j\mathrm{sign}(w)\frac{\pi\alpha}{2}} \tag{8.4.14}$$

Taking expectations on both sides, we get

$$\begin{aligned}
\int_0^{+\infty} \frac{1 - \mathbf{E}\{e^{j\mathrm{sign}(w)tX_i}\}}{t^{\alpha+1}} \mathrm{d}t &= -\mathbf{E}\{X_i^\alpha\}\Gamma(-\alpha)e^{-j\mathrm{sign}(w)\frac{\pi\alpha}{2}} \\
&= \mathbf{E}\{X_i^\alpha\}\frac{\Gamma(1-\alpha)}{\alpha}\cos\left(\frac{\pi\alpha}{2}\right)\left(1 - j\mathrm{sign}(w)\tan\left(\frac{\pi\alpha}{2}\right)\right).
\end{aligned}$$

Substituting this into (8.4.13), we obtain (8.4.6). Alternatively, we can prove the assertion (c) by noting that the condition $AR_{\min}^{-\beta} \approx +\infty$ implies that $R_{\min} \approx 0$. And so the total interference in this case is approximately equal to the total interference received from the whole plane $\mathbb{R}^2$ whose characteristic function is given by Corollary 7.4.4 in Chapter 7. □

8.5 Asymptotic Joint Distribution of Interference and Maximum Signal Strength

Theorem 8.3.2 and Proposition 8.4.1 conclude that F_P lies on both the domains of attraction of an extreme value distribution H and an α-stable law G_α. In particular, if $R_{\min} > 0$, then $H = \Lambda$ and $G_\alpha = \Phi$. Hence, by Theorem 5.1.28 we have the following result:

Corollary 8.5.1. *Assume the setting described above, and that $R_{\min} > 0$. Denote:*

$$\widetilde{I}_n \equiv \frac{I_n - b_n}{a_n}, \quad and \quad \widetilde{M}_n \equiv \frac{M_n - d_n}{c_n}, \tag{8.5.1}$$
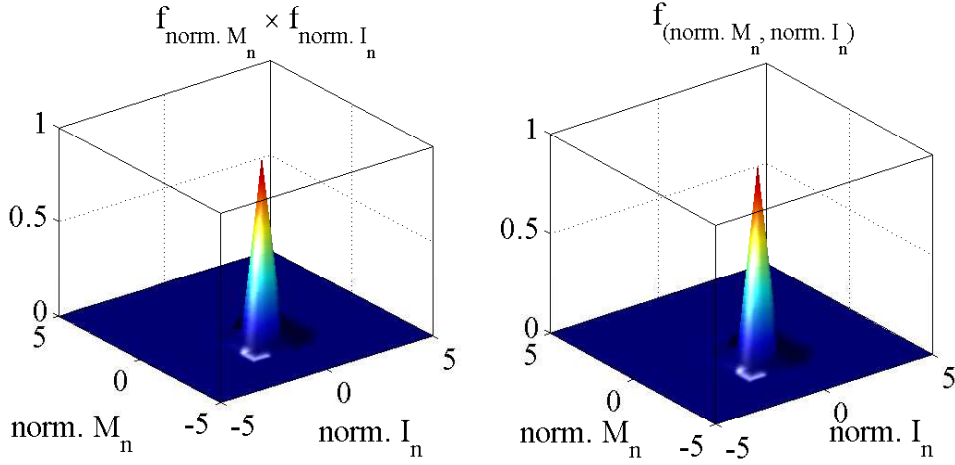
FIGURE 8.3: Example of joint densities of $\widetilde{M}_n$ and $\widetilde{I}_n$: $n = 50$, $\sigma_{\mathrm{dB}} = 8$, $\beta = 3$. Here, norm. M_n refers to $\widetilde{M}_n$, while norm. I_n refers to $\widetilde{I}_n$.

(a) Under different σ_{dB}: $\beta = 3$ (b) Under different β: $\sigma_{\mathrm{dB}} = 8$
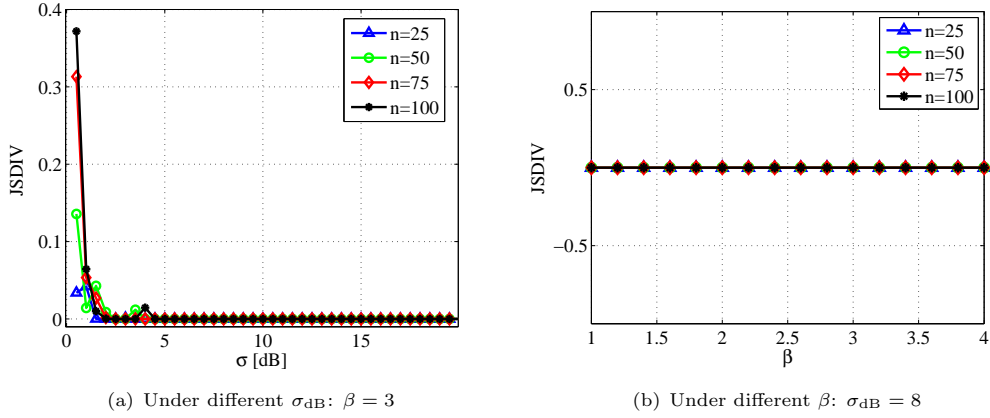
FIGURE 8.4: Jensen-Shannon divergence between $f_{(\widetilde{M}_n, \widetilde{I}_n)}$ and $f_{\widetilde{M}_n} \times f_{\widetilde{I}_n}$.

with a_n and b_n given by (8.4.4), and c_n and d_n given by (8.3.6). Then

$$\left(\widetilde{M}_n, \widetilde{I}_n\right) \xrightarrow{d} \left(\Lambda, \Phi\right), \quad as \ n \to \infty, \tag{8.5.2}$$

and where the coordinates Λ and Φ are independent.   □

In case $R_{\min} = 0$, by (a) of Theorem 8.3.2 and (a) of Proposition 8.4.1) $F_P \in \mathrm{MDA}(\Upsilon_\alpha) \cap \mathrm{D}(\alpha)$ with $\alpha < 2$. Thus, according to Theorem 5.1.28, we cannot have the asymptotic independence between M_n and I_n.

The total interference I can be written as $I = I_n + I_n^{\mathrm{c}}$ where I_n^{c} denotes the complement of I_n in I. Under the consider setting, I_n and I_n^{c} are independent. The asymptotic independence between M_n and I_n induces the asymptotic independence between M_n and I. This observation is stated in the following corollary.

Corollary 8.5.2. *Under the conditions of Corollary 8.5.1, M_n and I are asymptotically independent as $n \to \infty$.*   □

For practical applications, we follows the same treatment of §8.3 to evaluate the convergence speed of the asymptotic independence. We do this by measuring the (dis)similarity between the empirical joint distribution, $\mathbf{P}(\widetilde{M}_n \leq u, \widetilde{I}_n \leq v)$, and the product of the empirical marginal distributions, $\mathbf{P}(\widetilde{M}_n \leq u) \times \mathbf{P}(\widetilde{I}_n \leq v)$. Figure 8.3 shows an example with $n = 50$, $\beta = 3$ and $\sigma_{\mathrm{dB}} = 8$. We see that these two density functions are very similar. Figure 8.4 compares these two density functions for different values of σ_{dB} and β. Within the range defined above, the divergence between the two distributions is again small. Comparing Figure 8.2 and Figure 8.4, one can conclude that even if the convergence of $\widetilde{M}_n \xrightarrow{d} \Lambda$ remains slow, $\widetilde{M}_n$ and $\widetilde{I}_n$ quickly become uncorrelated. Thus, the independence between M_n and I_n holds for moderate values of n. So:

Corollary 8.5.3. *Under the conditions of Corollary 8.5.1, (M_n, I_n), and (M_n, I) admit the following approximations for moderate or large n:*

$$f_{(M_n, I_n)}(u, v) \quad \approx \quad f_{M_n}(u) \times f_{I_n}(v), \tag{8.5.3}$$

$$f_{(M_n, I)}(u, v) \quad \approx \quad f_{M_n}(u) \times f_I(v), \tag{8.5.4}$$

where f_{M_n}, f_{I_n}, and f_I are respectively the pdf of M_n, I_n, and I.

The asymptotic independence facilitates a wide range of studies involving the total interference and the maximum signal strength. This result will be used in the coming sub-section to derive the distribution of the best signal quality.

8.6 Distribution of the Best Signal Quality

Using the asymptotic properties developed above, we can derive the distribution of the best signal quality. It is given as follows.

Theorem 8.6.1. *Under the the setting described above, assume that $R_{\min} > 0$ and $AR_{\min}^{-\beta}$ is large. Then the tail distribution of Y_n admits the following approximation:*

$$\overline{F}_{Y_n}(\gamma) \approx \int_\gamma^\infty \Big\{ f_{M_n}(u) \int_0^\infty \frac{2}{\pi w} e^{-\delta w^\alpha} \sin\big(w \frac{u - \gamma}{2\gamma}\big)$$

$$\times \cos\big(wu + w\frac{u - \gamma}{2\gamma} - \delta w^\alpha \tan\frac{\pi\alpha}{2}\big) \mathrm{d}w \Big\} \mathrm{d}u. \tag{8.6.1}$$

Proof. Similar to the proof of Theorem 7.5.1, using (6.3.5) in §6.3, we have:

$$\mathbf{P}(Y_n > \gamma) \quad = \quad \mathbf{P}\left(M_n/(1 + I - M_n) > \gamma\right)$$

$$= \quad \mathbf{P}\left(I < \frac{1 + \gamma}{\gamma} M_n - 1\right)$$

$$= \quad \int_0^\infty \int_u^{\frac{1+\gamma}{\gamma} u - 1} f_{(I, M_n)}(v, u) \mathrm{d}v \mathrm{d}u. \tag{8.6.2}$$

Under the conditions of Theorem 8.6.1, M_n and I are asymptotically independent and their joint density admits an approximation given according to Corollary 8.5.3. So, substitute (8.5.4) into (8.6.2), we have:

$$\mathbf{P}(Y_n \geq \gamma) \approx \int_0^\infty f_{M_n}(u) \int_0^\infty h(v, u) f_I(v) \mathrm{d}v \mathrm{d}u, \tag{8.6.3}$$

where

$$h(v,u) = \mathbf{1}\left(v \le \frac{(1+\gamma)u}{\gamma} - 1\right)\mathbf{1}(v \ge u) = \begin{cases} 1 & \text{if } v \in [u, \frac{1+\gamma}{\gamma}u - 1] \text{ and } u > \gamma \\ 0 & \text{otherwise} \end{cases}. \tag{8.6.4}$$

It is easily seen that $h(v,u)$ is square-integrable with respect to v, and its Fourier transform w.r.t. v is given by:

$$\widehat{h}(\frac{w}{2\pi}, u) = \begin{cases} 0 & \text{if } u \le \gamma \\ \int_u^{\frac{1+\gamma}{\gamma}u-1} e^{-jwv}dv & \text{if } u > \gamma \end{cases} \tag{8.6.5}$$

which yields:

$$\widehat{h}(\frac{w}{2\pi}, u) = \begin{cases} 0 & \text{if } u \le \gamma \\ \frac{1}{jw}\left(e^{-jwu} - e^{jw\left(1-\frac{1+\gamma}{\gamma}u\right)}\right) & \text{if } u > \gamma \end{cases}. \tag{8.6.6}$$

Besides, according to Proposition 8.4.2 we have that $\phi_I \in \mathbb{L}$ and $\phi_I \in \mathbb{L}^2$, where $\mathbb{L}^2$ is the space of square integrable functions. And so, by Theorem 3 in [186, Chap. 15], f_I is bounded continuous and square integrable. Hence, applying the Plancherel-Parseval theorem to the inner integral of (8.6.3), we have

$$\int_0^\infty h(v,u)f_I(v)dv = \int_{-\infty}^\infty \widehat{h}(-w,u)\widehat{f_I}(w)dw, \tag{8.6.7}$$

where $\widehat{f_I}(w)$ is the Fourier transform of $f_I(v)$. Take (8.6.6) into account for (8.6.7) and (8.6.3), we have:

$$\overline{F}_{Y_n}(\gamma) = \int_\gamma^\infty \left\{ f_{M_n}(u) \int_{-\infty}^\infty \widehat{h}(-w,u)\widehat{f_I}(w)dw \right\}du, \tag{8.6.8}$$

where we further have

$$\begin{aligned} \int_{-\infty}^\infty \widehat{h}(-w,u)\widehat{f_I}(w)dw &= \frac{1}{2\pi}\int_{-\infty}^{+\infty} \widehat{h}(-\frac{w}{2\pi},u)\widehat{f_I}(\frac{w}{2\pi})dw \\ &= \frac{1}{2\pi}\int_0^{+\infty}\left(\widehat{h}(\frac{w}{2\pi},u)\widehat{f_I}(\frac{-w}{2\pi}) + \widehat{h}(\frac{-w}{2\pi},u)\widehat{f_I}(\frac{w}{2\pi})\right)dw. \end{aligned} \tag{8.6.9}$$

Note that

$$\widehat{f_I}(\frac{w}{2\pi}) = \phi_I(-w). \tag{8.6.10}$$

And under the assumption that $AR_{\min}^{-\beta} \approx \infty$, ϕ_I is approximated by (8.4.6). Thus, by (8.4.6) and (8.6.6), we have for $w \in [0, +\infty)$:

$$\begin{aligned} \widehat{h}(\frac{w}{2\pi}, u)\widehat{f_I}(-\frac{w}{2\pi}) \approx \frac{e^{-\delta w^\alpha}}{jw}\bigg(&\exp\left(j\left(-wu + \delta w^\alpha \tan\frac{\pi\alpha}{2}\right)\right) \\ &- \exp\left(-j\left(-w + w\frac{1+\gamma}{\gamma}u - \delta w^\alpha \tan\frac{\pi\alpha}{2}\right)\right)\bigg), \end{aligned} \tag{8.6.11}$$

and

$$\begin{aligned} \widehat{h}(-\frac{w}{2\pi}, u)\widehat{f_I}(\frac{w}{2\pi}) \approx \frac{e^{-\delta w^\alpha}}{jw}\bigg(&-\exp\left(-j\left(-wu + \delta w^\alpha \tan\frac{\pi\alpha}{2}\right)\right) \\ &+ \exp\left(j\left(-w + w\frac{1+\gamma}{\gamma}u - \delta w^\alpha \tan\frac{\pi\alpha}{2}\right)\right)\bigg). \end{aligned} \tag{8.6.12}$$

By (8.6.11) and (8.6.12), we get

$$\frac{1}{2\pi}\left(\widehat{h}(\frac{w}{2\pi},u)\widehat{f}_I(\frac{-w}{2\pi}) + \widehat{h}(\frac{-w}{2\pi},u)\widehat{f}_I(\frac{w}{2\pi})\right) \tag{8.6.13}$$

$$\approx \frac{e^{-\delta w^{\alpha}}}{\pi w}\left(\sin(-wu + \delta w^{\alpha}\tan\frac{\pi\alpha}{2}) + \sin(-w + w\frac{1+\gamma}{\gamma}u - \delta w^{\alpha}\tan\frac{\pi\alpha}{2})\right)$$

$$= \frac{2e^{-\delta w^{\alpha}}}{\pi w}\sin\left(w\frac{u-\gamma}{2\gamma}\right) \times \cos\left(wu + w\frac{u-\gamma}{2\gamma} - \delta w^{\alpha}\tan\frac{\pi\alpha}{2}\right). \tag{8.6.14}$$

Substitute the above (8.6.14) into (8.6.9) and then into (8.6.8), we have (8.6.1). □

The approximation of $\overline{F}_{Y_n}$ as given by Theorem 8.6.1 takes effect on two approximations:

  (i) The asymptotic density function of (M_n, I) as given in Corollary 8.5.3,
  (ii) And the approximation of ϕ_I as given by Proposition 8.4.2.

This approximation of $\overline{F}_{Y_n}$ will be validated by simulation and used in Chapter 11.

8.7   Conclusion

We investigated the heavy-tail asymptotics of wireless links under both unbounded and bounded path loss models. The singularity of the decaying power-law path loss model results in different asymptotic behaviours of wireless links.

In case of unbounded path loss, the signal strength is regularly varying, leading to very heavy-tailed interference and maximum signal strength. Moreover, due the common dominant component corresponding to the singularity of the path loss, interference and maximum of signal strengths behave dependently even after undergoing appropriate normalisation.

By contrast, in case of bounded path loss, the signal strength is rapidly varying and its tail behaviour is rather determined by that of the underlying lognormal shadowing. Thereby, it lies on the domains of attraction of the Gumbel distribution and Gaussian distribution. More importantly we obtain in this case the asymptotic independence of the interference and maximum of signal strengths. This allows for an approximation of the distribution of the best signal quality which is analytically less complex than its exact form previously developed in Chapter 7.

Finally, we observe that the above asymptotic properties of extremes of wireless links are obtained as the number of measured nodes increases freely within a bounded network area. This scenario corresponds to a network densification context. The results should be consequently suitable for such a network densification scenario. This observation opens applications to dense small cell networks as the one presented in Chapter 11.

Chapter 9

Some Properties of Level Crossings of a Stationary Process

9.1 Introduction

The contribution of many authors has established a fundamental of level crossings of stationary processes with important results such as those summarised in §5.3. They have important applications to the mobile communication networking such as the one shown in §5.3.2. In particular, celebrated results firstly provided by Rice [12, 13], Kac and Slepian [14] give us the exact formulation of the mean level crossing rate (Theorem 5.3.1), the asymptotic trajectory of excursions above a large level (Theorem 5.3.3), as well as the Poisson process of up-crossings (Theorem 5.3.5). However, different applications give rise to new questions, and they require for more investigations of this theoretical topic. In particular, in wireless communications, fluctuations of wireless link signal with respect to a low level or with respect to a high level are all critical to the communication quality and to network designs. While the asymptotic property of up-excursions above a very *large* level was investigated and formulated in Theorem 5.3.3,

How do up-excursions behave above a very small level?

is still an open question. In addition, since results as we have seen in §5.3 concern with properties of level crossings of one level, another important question remains:

What are properties of level crossings of several adjacent levels?

This chapter is aimed at investigating these two questions by considering a stationary normal process $X(t)$. With appropriate conditions specified for the autocorrelation function $R_X(\tau)$ of $X(t)$, we show in §9.2 that the length of up-excursions above a small level $-\gamma$ is asymptotically an exponential distribution with rate equal to $\mathbf{E}U_{-\gamma}$ as $-\gamma \to -\infty$.

For the above second question, we develop in §9.3 some properties associated with crossings of $X(t)$ of two adjacent large levels γ_1 and $\gamma_2 \geq \gamma_1$. We obtain the mean number of crossings of $X(t)$ of level γ_2, and the distribution of the length of up-excursions above γ_2, given that $X(t)$

has an up-excursion above γ_1 as $\gamma_1 \to +\infty$. An application with the probability of successive excursions of $X(t)$ during some given time window is then derived in §9.3.3 to show the interest of the developed results.

9.2   Excursions Above a Small Level

Given a very small level $-\gamma \to -\infty$, we are interested in the time τ_u of an up-excursion of the process $X(t)$ above the level $-\gamma$. We investigate its limiting distribution by assuming that the stationary normal process $X(t)$ admits an autocorrelation function $R_X(\tau)$ satisfying condition (5.3.8)

$$R_X(\tau) = 1 - \frac{\lambda_2}{2!}\tau^2 + \frac{\lambda_4}{4!}\tau^4 + o(\tau^4) \tag{9.2.1}$$

with finite λ_2 and λ_4, as $\tau \to 0$, and satisfying condition (5.3.9)

$$R_X(\tau) = O(\tau^{-a}) \tag{9.2.2}$$

for some $a > 0$, as $\tau \to \infty$.

Let t_2 be the time between a downcrossing to the next downcrossing of level $-\gamma$. With the conditions stated above, its limiting distribution as $-\gamma \to -\infty$ is given according to Theorem 5.3.4 in §5.3 for $k = 1$:

$$F_2(t) = 1 - e^{-\mu t}, \quad \text{as } -\gamma \to -\infty \tag{9.2.3}$$

with $\mu = \mathbf{E}D_{-\gamma}$ which is the mean downcrossing rate of level $-\gamma$. By Proposition 5.3.2 we can write $\mu = \mathbf{E}U_{-\gamma}$.

Let τ_d be the time between a downcrossing and the next upcrossing of the level $-\gamma$. Then the time τ_u of the up-excursion above $-\gamma$ is precisely the interval from the upcrossing to the next downcrossing of $X(t)$ of the level $-\gamma$. It is clear that τ_u is a random variable given as

$$\tau_u = (t_2 - \tau_d \,|\, t_2 \geq \tau_d).$$

But t_2 as given by (9.2.3) is an exponential distribution with rate μ. By the memorylessness property of the exponential distributions, τ_u is an exponential distribution with rate μ. This is stated in the following.

Theorem 9.2.1. *With the process $X(t)$ described above, under the conditions (9.2.1) and (9.2.2), the time τ_u of an up-excursion of $X(t)$ above a very small level $-\gamma < 0$ is asymptotically an exponential distribution of rate $\mu = \mathbf{E}U_{-\gamma}$, i.e.*

$$\mathbf{P}(\tau_u \leq \tau) = 1 - e^{-\mu\tau}, \quad as \ -\gamma \to -\infty.$$

By Proposition 5.3.2 and Theorem 5.3.1 we have that

$$\mu = \mathbf{E}U_{-\gamma} = \frac{1}{2\pi}\sqrt{\frac{\lambda_2}{\lambda_0}} \exp\left(-\frac{\gamma^2}{2\lambda_0}\right),$$

which tends to zero. As a sequel, $\mathbf{P}(\tau_u \leq \tau)$ is approximatively equal to zero as $-\gamma \to -\infty$ for all τ less than infinity as $-\gamma \to -\infty$. It means that the process $X(t)$ stays most of the time

above a very low level. Whereas, by Theorem 5.3.3, the length of an up-excursion above a very large level γ behaves asymptotically as a Rayleigh distribution of parameter

$$\frac{2}{\gamma\sqrt{\lambda_2}}$$

(see (5.3.13)) which tends to zero as $\gamma \to \infty$. Thus, $\mathbf{P}(\tau_u \leq \tau)$ is approximatively equal to zero as $\gamma \to \infty$ for all τ higher than zero. This means that $X(t)$ stays above a very large level for a very short interval.

The above difference leads to another distinctness between up-excursions of high level γ and of small level $-\gamma$. In the case of up-excursions above $\gamma \to +\infty$, the length of up-excursions is very small and their trajectory is approximated by parabolas according to Theorem 5.3.3. By contrast, we do not have any information about the trajectory of up-excursions above a level $-\gamma \to -\infty$ except their length given according to Theorem 9.2.1. In fact, the condition (9.2.2) suggests that it is not possible to 'predict' $X(t_0 + T)$ from $X(t_0)$ when $T \to \infty$. Since the length of up-excursions above $-\gamma$ is very long as discussed above, (9.2.2) does not allow us to have enough information about the trajectory of $X(t)$ above a very small level $-\gamma$.

9.3 Crossings of Adjacent High Levels

Till now we have concerned with crossings of a stationary normal process $X(t)$ of one level. In this section we investigate some properties associated with crossings of $X(t)$ of several adjacent high levels. In the sequel, we assume that the autocorrelation function $R_X(\tau)$ of $X(t)$ satisfies condition (9.2.2), and condition (5.3.4) which is

$$R_X''(\tau) = \lambda_2 + O(|\log|\tau||^{-a}) \quad \text{as } \tau \to 0 \tag{9.3.1}$$

with finite λ_2 for some $a > 1$. Note that here we relax the assumption in (9.2.1) used in §9.2 that $R_X(\tau)$ has a finite fourth derivative at the origin.

9.3.1 Mean Number of Crossings of Successive Levels

Given that $X(t)$ has an up-excursion above a high level γ_1 with length $T_1 \geq \tau_1$ for some τ_1, we investigate the mean number of crossings of $X(t)$ of a level $\gamma_2 \geq \gamma_1$, in particular we study this quantity as $\gamma_1 \to +\infty$.

Under the conditions (9.2.2) and (9.3.1), by Theorem 5.3.3 an up-excursion of $X(t)$ above the level γ_1 behaves asymptotically as

$$X(t) \sim \gamma_1 + \xi t - \gamma_1 \frac{\lambda_2 t^2}{2}, \quad \text{as } \gamma_1 \to +\infty,$$

where ξ is a Rayleigh random variable of parameter $\sqrt{\lambda_2}$. This suggests that $X(t)$ stays above γ_1 during time interval $[0, T_1]$ with

$$T_1 = \frac{2}{\gamma_1 \lambda_2}\xi, \tag{9.3.2}$$

and behaves as a downwards parabola. During this time interval $[0, T_1]$, $X(t)$ will have one up-crossing of level γ_2 if

$$\gamma_1 + \xi t - \gamma_1 \frac{\lambda_2 t^2}{2} > \gamma_2, \tag{9.3.3}$$

and will have zero up-crossing of level γ_2 otherwise. Here, $X(t)$ will have a tangency with the level γ_2 if $\Delta = 0$, and this tangency is not considered as an up-crossing. Solving for the quadratic inequality

$$-\gamma_1 \frac{\lambda_2 t^2}{2} + \xi t - (\gamma_2 - \gamma_1) > 0$$

with discriminant

$$\Delta = \xi^2 - 2\gamma_1 \lambda_2 (\gamma_2 - \gamma_1), \tag{9.3.4}$$

we obtain

$$(\# \text{ up-crossings of } X(t) \text{ of } \gamma_2 \,|\, X(t) \geq \gamma_1) = \begin{cases} 1 & \text{if } \Delta > 0 \\ 0 & \text{if } \Delta \leq 0 \end{cases}.$$

Hence, the mean number of up-crossings of $X(t)$ of level $\gamma_2 \geq \gamma_1$ during $[0, T_1]$ given that $X(t)$ has an up-excursion above γ_1 with length $T_1 \geq \tau_1$ is

$$\mathbf{E}\{\# \text{ up-crossings of } X(t) \text{ of } \gamma_2 \,|\, X(t) \geq \gamma_1 \text{ with } T_1 \geq \tau_1\} = \mathbf{P}(\Delta > 0 \,|\, T_1 \geq \tau_1)$$

$$= \mathbf{P}(\xi^2 > 2\gamma_1 \lambda_2 (\gamma_2 - \gamma_1) \,|\, \xi \geq \frac{\gamma_1 \lambda_2}{2} \tau_1)$$

$$= \frac{\mathbf{P}\left(\xi^2 > \max\left(2\gamma_1 \lambda_2 (\gamma_2 - \gamma_1), (\frac{\gamma_1 \lambda_2}{2} \tau_1)^2\right)\right)}{\mathbf{P}\left(\xi \geq \frac{\gamma_1 \lambda_2}{2} \tau_1\right)},$$

as $\gamma_1 \to +\infty$. With ξ a Rayleigh distribution of parameter $\sqrt{\lambda_2}$, ξ^2 is an exponential distribution of intensity $1/(2\lambda_2)$:

$$\mathbf{P}(\xi^2 \leq x) = 1 - \exp\left(-\frac{x}{2\lambda_2}\right).$$

Hence,

$$\mathbf{P}\left(\xi^2 > \max\{2\gamma_1 \lambda_2 (\gamma_2 - \gamma_1), (\frac{\gamma_1 \lambda_2}{2} \tau_1)^2\}\right) = \exp\left(-\max\{\gamma_1 (\gamma_2 - \gamma_1), \frac{\gamma_1^2 \lambda_2}{8} \tau_1^2\}\right)$$

$$= \exp(-V \max\{(\tau_1^*)^2, \tau_1^2\})$$

where

$$V := \frac{\gamma_1^2 \lambda_2}{8}, \tag{9.3.5}$$

and

$$\tau_1^* := \sqrt{\frac{\gamma_1 (\gamma_2 - \gamma_1)}{V}} = \sqrt{\frac{8(\gamma_2 - \gamma_1)}{\gamma_1 \lambda_2}}, \tag{9.3.6}$$

We have the following conclusion

Theorem 9.3.1. *With the process $X(t)$ described above, assume that $R_X(t)$ satisfies conditions (9.3.1) and (9.2.2). Then, for $\gamma_2 \geq \gamma_1$*

$$\mathbf{E}\{\# \text{ up-crossings of } X(t) \text{ of } \gamma_2 \,|\, X(t) \geq \gamma_1 \text{ with } T_1 \geq \tau_1\} = \frac{\exp\left(-V \max\{(\tau_1^*)^2, \tau_1^2\}\right)}{\exp\left(-V \tau_1^2\right)},$$

as $\gamma_1 \to +\infty$ with V given in (9.3.5) and τ_1^* given in (9.3.6).

In particular, if the up-excursion of $X(t)$ above γ_1 is long enough so that $\tau_1 > \tau_1^*$, then there will be one up-crossing of $X(t)$ of the level γ_2 with probability one. Motivated by this, we call τ_1^* the '*critical length*' of an up-excursion above γ_1.

An interesting application of the above result is for the case of $\tau_1 = 0$. Denote by $U_{\gamma_2|\gamma_1}$ the number of up-crossings of $X(t)$ of level γ_2 given that $X(t)$ is above γ_1. Then $U_{\gamma_2|\gamma_1}$ is equal to $\mathbf{E}\{\# \text{ up-crossings of } X(t) \text{ of } \gamma_2 \,|\, X(t) \geq \gamma_1 \text{ with } T_1 \geq \tau_1\}$ for $\tau_1 = 0$. So:

Corollary 9.3.2. *With the notation described above and hypothesis of Theorem 9.3.1:*

$$\mathbf{E}U_{\gamma_2|\gamma_1} = \exp(-\gamma_1(\gamma_2 - \gamma_1)) \quad as \ \gamma_1 \to +\infty. \tag{9.3.7}$$

During the up-excursion of $X(t)$ above γ_1, if $X(t)$ has an up-crossing of γ_2, then $X(t)$ will have a down-crossing of γ_2 by the parabola property of $X(t)$ as $\gamma_1 \to +\infty$. Hence, denoting $D_{\gamma_2|\gamma_1}$ to be the number of down-crossings of $X(t)$ of the level γ_2 given that $X(t)$ has an up-excursion above γ_1, it is obvious that

$$\mathbf{E}D_{\gamma_2|\gamma_1} = \mathbf{E}U_{\gamma_2|\gamma_1},$$

and the mean number of crossings is

$$\mathbf{E}C_{\gamma_2|\gamma_1} = 2\,\mathbf{E}U_{\gamma_2|\gamma_1},$$

as $\gamma_1 \to +\infty$.

Above we obtained the mean number of a up-crossings (and down-crossings, crossings) of an adjacent level γ_2 given an up-excursion above a lower level $\gamma_1 \to +\infty$. Using these results, we can also obtain the mean up-crossing rate (and also mean down-crossing rate, mean crossing rate) of $(X(t)|X(t) \geq \gamma_1 \text{ with } T_1 \geq \tau_1)$ of the level $\gamma_2 \geq \gamma_1$ as $\gamma_1 \to +\infty$ by noting that the up-crossing rate is given as the ratio of number of up-crossings divided by the time duration T_1. Taking the expectation of this ratio for T_1 from τ_1 to infinity, we obtain the mean up-crossing rate without any difficulty. Nevertheless, we prefer to not provide it here. The reason is that such a mean up-crossing rate does not provide meaningful information, and it may even introduce ambiguity. In fact, a mean crossing rate should give the mean number of crossings when it is multiplied by a time duration, whereas in our case we know that $(X(t)|X(t) \geq \gamma_1)$ can have at most only one up-crossing of γ_2 for all time durations T_1.

9.3.2 Length of Excursions Above Successive Levels

Using the notation described above, we devote to this subsection the distribution of the length, say T_2, of an up-excursion of $X(t)$ above the level $\gamma_2 \geq \gamma_1$ given that $X(t)$ has an up-excursion above γ_1 with length $T_1 \geq \tau_1$, as $\gamma_1 \to +\infty$. The conditional length T_2 is the length of the time interval during with the inequality (9.3.3) holds:

$$(T_2 \,|\, X(t) \geq \gamma_1 \text{ with } T_1 \geq \tau_1) = \begin{cases} \frac{2\sqrt{\Delta}}{\gamma_1 \lambda_2} & \text{if } \Delta > 0 \,|\, T_1 \geq \tau_1 \\ 0 & \text{if } \Delta \leq 0 \,|\, T_1 \geq \tau_1 \end{cases},$$

with Δ given in (9.3.4). Hence,

$$
\begin{aligned}
\mathbf{P}(T_2 = 0 \,|\, X(t) \geq \gamma_1 \text{ with } T_1 \geq \tau_1) &= \mathbf{P}(\Delta \leq 0 \,|\, T_1 \geq \tau_1) \\
&= \mathbf{P}\left(\xi^2 \leq 2\gamma_1\lambda_2(\gamma_2 - \gamma_1) \,\Big|\, \xi \geq \frac{\gamma_1\lambda_2}{2}\tau_1 \right) \\
&= \frac{\mathbf{P}((\frac{\gamma_1\lambda_2}{2}\tau_1)^2 \leq \xi^2 \leq 2\gamma_1\lambda_2(\gamma_2 - \gamma_1))}{\mathbf{P}(\xi \geq \frac{\gamma_1\lambda_2}{2}\tau_1)},
\end{aligned}
$$

which, by the Rayleigh distribution of ξ, reduces to

$$
\mathbf{P}(T_2 = 0 \,|\, X(t) \geq \gamma_1 \text{ with } T_1 \geq \tau_1) = \mathbf{1}\left(\tau_1 \leq \tau_1^*\right)\left(1 - \frac{e^{-V(\tau_1^*)^2}}{e^{-V\tau_1^2}} \right) \tag{9.3.8}
$$

with V given in Theorem 9.3.1, and τ_1^* is the critical length given in (9.3.6). Similarly, for all $\tau \geq 0$

$$
\begin{aligned}
\mathbf{P}(T_2 > \tau \,|\, X(t) \geq \gamma_1 \text{ with } T_1 \geq \tau_1) &= \mathbf{P}\left(\frac{2\sqrt{\Delta}}{\gamma_1\lambda_2} > \tau \,\Big|\, T_1 \geq \tau_1 \right) \\
&= \mathbf{P}\left(\xi^2 > (\frac{\gamma_1\lambda_2}{2}\tau)^2 + 2\gamma_1\lambda_2(\gamma_2 - \gamma_1) \,\Big|\, \xi \geq \frac{\gamma_1\lambda_2}{2}\tau_1 \right) \\
&= \frac{\mathbf{P}(\xi^2 > \max\{(\frac{\gamma_1\lambda_2}{2}\tau)^2 + 2\gamma_1\lambda_2(\gamma_2 - \gamma_1), (\frac{\gamma_1\lambda_2}{2}\tau_1)^2\})}{\mathbf{P}(\xi \geq \frac{\gamma_1\lambda_2}{2}\tau_1)},
\end{aligned}
$$

which is finally equal to

$$
\mathbf{P}(T_2 > \tau \,|\, X(t) \geq \gamma_1 \text{ with } T_1 \geq \tau_1) = \frac{\exp\left(-V \max\{\tau^2 + (\tau_1^*)^2, \tau_1^2\}\right)}{\exp(-V\tau_1^2)}. \tag{9.3.9}
$$

We conclude the above results in the following

Proposition 9.3.3. *With the notation described above and the conditions of Theorem 9.3.1, the distribution of the length T_2 of an up-excursion of $X(t)$ above γ_2 given that $X(t)$ has an up-excursion above $\gamma_1 \leq \gamma_2$ with length $T_1 \geq \tau_1$ is determined jointly by (9.3.8) and (9.3.9) as $\gamma_1 \to +\infty$.*

9.3.3 Applications

The following application shows the interest of the results developed above. Using the notation and conditions described within §9.3, for two fixed levels γ_1 and $\gamma_2 \geq \gamma_1$, we are interested in successive up-excursions of $X(t)$ above γ_1 and above γ_2 during some time window $[0, T]$. Specifically, we determine the following probability

$$
P := \mathbf{P}(X(t) \geq \gamma_1 \text{ with } T_1 \geq \tau_1 \text{ and } X(t) \geq \gamma_2 \text{ with } T_2 \geq \tau_2 \text{ for } t \in [0, T]).
$$

This is precisely given by

$$
P = \frac{\mathbf{E}\{\text{total time of } X(t) \geq \gamma_1 \text{ with } T_1 \geq \tau_1 \text{ and } X(t) \geq \gamma_2 \text{ with } T_2 \geq \tau_2, \, t \in [0, T]\}}{T},
$$

by the stationarity of $X(t)$. Of course, the main concern here is due to the numerator. Putting

$$T_2^* = (T_2 \,|\, X(t) \geq \gamma_1 \text{ with } T_1 \geq \tau_1),$$

where, according to the notation described above, T_2 is the length of an up-excursion of $X(t)$ above γ_2. We have

$$
\begin{aligned}
\mathbf{E}\{&\text{total time of } X(t) \geq \gamma_1 \text{ with } T_1 \geq \tau_1 \text{ and } X(t) \geq \gamma_2 \text{ with } T_2 \geq \tau_2,\ t \in [0, T]\}\\
&=\mathbf{E}\{\# \text{ excursions above } \gamma_1 \text{ with } T_1 \geq \tau_1 \text{ for } t \in [0, T]\}\\
&\quad \times \mathbf{E}\{\# \text{ excursions above } \gamma_2 \text{ with } T_2 \geq \tau_2 \,|\, X(t) \geq \gamma_1 \text{ with } T_1 \geq \tau_1\}\\
&\quad \times \mathbf{E}\{T_2^* \,|\, T_2^* \geq \tau_2\}.
\end{aligned}
\tag{9.3.10}
$$

We shall determine the three terms on the right hand side of this equation in the following. Firstly we have

$$
\begin{aligned}
\mathbf{E}\{\# \text{ excursions above } \gamma_1 &\text{ with } T_1 \geq \tau_1 \text{ for } t \in [0, T]\}\\
&= \mathbf{E}\{\# \text{ up-crossings of } \gamma_1 \text{ during } [0, T]\} \times \mathbf{P}(T_1 \geq \tau_1)\\
&= T \cdot \mathbf{E}U_{\gamma_1} \cdot \exp(-V\tau_1^2), \quad \text{as } \gamma_1 \to +\infty,
\end{aligned}
\tag{9.3.11}
$$

which is obtainable with T_1 given in (9.3.2), where $\mathbf{E}U_{\gamma_1}$ is the mean up-crossing rate of level γ_1 given according to Proposition 5.3.2.

For the second term on the right-hand side of (9.3.10),

$$
\begin{aligned}
\mathbf{E}\{\# \text{ excursions above } \gamma_2 &\text{ with } T_2 \geq \tau_2 \,|\, X(t) \geq \gamma_1 \text{ with } T_1 \geq \tau_1\}\\
&=\mathbf{E}\{\# \text{ up-crossings of } \gamma_2 \,|\, X(t) \geq \gamma_1 \text{ with } T_1 \geq \tau_1\}\\
&\quad \times \mathbf{P}(T_2 \geq \tau_2 \,|\, X(t) \geq \gamma_1 \text{ with } T_1 \geq \tau_1),
\end{aligned}
$$

in which the first term on the right hand side is the mean number of up-crossings of $X(t)$ of level γ_2 given that $X(t)$ has an up-excursion above γ_1 with length $T_1 \geq \tau_1$, it is given according to Theorem 9.3.1; and the second term on the right-hand side is given as

$$
\begin{aligned}
\mathbf{P}(T_2 \geq \tau_2 \,&|\, X(t) \geq \gamma_1 \text{ with } T_1 \geq \tau_1)\\
&= \mathbf{P}(T_2 > \tau_2 \,|\, X(t) \geq \gamma_1 \text{ with } T_1 \geq \tau_1) + \mathbf{P}(T_2 = \tau_2 \,|\, X(t) \geq \gamma_1 \text{ with } T_1 \geq \tau_1)\\
&= \frac{e^{-V \max\{\tau_2^2 + (\tau_1^*)^2,\, \tau_1^2\}}}{e^{-V\tau_1^2}} + \mathbf{1}(\tau_2 = 0)\mathbf{1}(\tau_1 \leq \tau_1^*)\left(1 - \frac{e^{-V(\tau_1^*)^2}}{e^{-V\tau_1^2}}\right)
\end{aligned}
\tag{9.3.12}
$$

which is obtainable by Proposition 9.3.3. So

$$
\begin{aligned}
\mathbf{E}\{\# &\text{ excursions above } \gamma_2 \text{ with } T_2 \geq \tau_2 \,|\, X(t) \geq \gamma_1 \text{ with } T_1 \geq \tau_1\}\\
&= \frac{e^{-V \max\{(\tau_1^*)^2,\, \tau_1^2\}}}{e^{-V\tau_1^2}} \left(\frac{e^{-V \max\{\tau_2^2 + (\tau_1^*)^2,\, \tau_1^2\}}}{e^{-V\tau_1^2}} + \mathbf{1}(\tau_2 = 0)\mathbf{1}(\tau_1 \leq \tau_1^*)\left(1 - \frac{e^{-V(\tau_1^*)^2}}{e^{-V\tau_1^2}}\right)\right)
\end{aligned}
\tag{9.3.13}
$$

Finally we derive the last term on the right-hand side of (9.3.10).

$$\mathbf{E}\{T_2^* \,|\, T_2^* \geq \tau_2\} = \tau_2 + \int_{\tau_2}^\infty \frac{\mathbf{P}(T_2^* > \tau)}{\mathbf{P}(T_2^* \geq \tau_2)}\, d\tau \tag{9.3.14}$$

where by (9.3.9) we have

$$\int_{\tau_2}^{\infty} \mathbf{P}(T_2^* > \tau) \mathrm{d}\tau = \int_{\tau_2}^{\infty} \frac{e^{-V \max\{\tau^2 + (\tau_1^*)^2, \tau_1^2\}}}{e^{-V \tau_1^2}} \mathrm{d}\tau.$$

For this we distinguish between two cases with $\tau_1 \leq \tau_1^*$ and $\tau_1 > \tau_1^*$. (i) For the case with $\tau_1 \leq \tau_1^*$,

$$\int_{\tau_2}^{\infty} \mathbf{P}(T_2^* > \tau) \mathrm{d}\tau = \int_{\tau_2}^{\infty} \frac{e^{-V(\tau^2 + (\tau_1^*)^2)}}{e^{-V \tau_1^2}} \mathrm{d}\tau = \frac{e^{-V(\tau_1^*)^2}}{e^{-V \tau_1^2}} \sqrt{\frac{\pi}{4V}} \mathrm{erfc}(\sqrt{V} \tau_2). \tag{9.3.15}$$

And (ii) for the case with $\tau_1 > \tau_1^*$, let us denote by τ_2^* the solution of

$$\tau^2 + (\tau_1^*)^2 = \tau_1^2,$$

it means that

$$\tau_2^* = \sqrt{\tau_1^2 - (\tau_1^*)^2}. \tag{9.3.16}$$

Then

$$\int_{\tau_2}^{\infty} \mathbf{P}(T_2^* > \tau) \mathrm{d}\tau = \mathbf{1}(\tau_2 < \tau_2^*) \int_{\tau_2}^{\tau_2^*} \mathrm{d}\tau + \int_{\max\{\tau_2^*, \tau_2\}}^{\infty} \frac{e^{-V(\tau^2 + (\tau_1^*)^2)}}{e^{-V \tau_1^2}} \mathrm{d}\tau$$

$$= \mathbf{1}(\tau_2 < \tau_2^*)(\tau_2^* - \tau_2) + \frac{e^{-V(\tau_1^*)^2}}{e^{-V \tau_1^2}} \sqrt{\frac{\pi}{4V}} \mathrm{erfc}(\sqrt{V} \max\{\tau_2^*, \tau_2\}). \tag{9.3.17}$$

So, $\mathbf{E}\{T_2^* \mid T_2^* \geq \tau_2\}$ is given according to (9.3.14) with $\mathbf{P}(T_2^* \geq \tau_2)$ given by (9.3.12), and $\int_{\tau_2}^{\infty} \mathbf{P}(T_2^* > \tau) \mathrm{d}\tau$ given by (9.3.15) in case $\tau_1 \leq \tau_1^*$, and given by (9.3.17) in case in case $\tau_1 > \tau_1^*$.

By substituting (9.3.11), (9.3.13), and (9.3.14) into (9.3.10), we obtain the probability of the question. For ease of illustration, we present the final result for different possibilities of τ_1 and τ_2

- For $\tau_1 \leq \tau_1^*$ and $\tau_2 = 0$:

$$P = \mathbf{E}\{U_{\gamma_1}\} e^{-V(\tau_1^*)^2} \sqrt{\frac{\pi}{4V}}. \tag{9.3.18}$$

- For $\tau_1 \leq \tau_1^*$, and $\tau_2 > 0$:

$$P = \mathbf{E}\{U_{\gamma_1}\} e^{-2V(\tau_1^*)^2} \frac{e^{-V \tau_2^2}}{e^{-V \tau_1^2}} \left(\tau_2 + \sqrt{\frac{\pi}{4V}} \frac{\mathrm{erfc}(\sqrt{V} \tau_2)}{e^{-V \tau_2^2}} \right). \tag{9.3.19}$$

- For $\tau_1 > \tau_1^*$ and $\tau_2 \geq \tau_2^*$. We have $\tau_1^2 \leq \tau_2^2 + (\tau_1^*)^2$. Then

$$P = \mathbf{E}\{U_{\gamma_1}\} e^{-V(\tau_1^*)^2} e^{-V \tau_2^2} \left(\tau_2 + \sqrt{\frac{\pi}{4V}} \frac{\mathrm{erfc}(\sqrt{V} \tau_2)}{e^{-V \tau_2^2}} \right). \tag{9.3.20}$$

- For $\tau_1 > \tau_1^*$ and $\tau_2 < \tau_2^*$. We have $\tau_1^2 > \tau_2^2 + (\tau_1^*)^2$. Then

$$P = \mathbf{E}\{U_{\gamma_1}\} e^{-V \tau_1^2} \left(\tau_2^* + \frac{e^{-V(\tau_1^*)^2}}{e^{-V \tau_1^2}} \sqrt{\frac{\pi}{4V}} \frac{\mathrm{erfc}(\sqrt{V} \tau_2)}{e^{-V(\tau_2^*)^2}} \right). \tag{9.3.21}$$

9.4 Conclusion

In this chapter we investigated some properties of level crossings of a stationary normal process. We showed that the length of up-excursions above a very small level $-\gamma$ is asymptotically an exponential distribution as $-\gamma \to -\infty$. Besides the analytical simple expression provided by the exponential distributions, this result clarifies the difference between up-excursions above a small level and above a large level in that a stationary normal process stays most of the time above a very small level, while it stays during every short intervals above a very large level. The mean number of crossings as well as the length of up-excursions above adjacent high level were also obtained. These results allow us to derive the probability of successive excursions above adjacent levels during a time window, which will be used in Chapter 10 for the analysis of handover measurement.

Part III

Mobility Management

Chapter 10

Handover Measurement: Analysis and Applications to LTE

10.1 Introduction

In mobile cellular networks, a user may travel across different cells during a service. Handover which switches the user's connection from one cell to another is an essential function. Technology advancement is expected to minimise service interruption and to provide seamless handover. As we have seen in Chapter 4, a handover procedure includes two functions which are handover *measurement* and handover *decision-execution*. The measurement function is responsible for finding the a suitable neighbouring cell for handover. Handover decision-execution is made upon the measurement function. It decides whether or not to execute a handover to the candidate neighbouring cell provided by the measurement function, and in that case it coordinates multi-party handshaking between the user and cell sites to have handover execution fast and transparent. In mobile-assisted network-controlled handover, which is recommended by all cellular standards for its operational scalability and effectiveness, the mobile is in charge of the handover measurement function. It measures the signal quality of neighbouring cells, and reports the measurement result to the network to make a handover decision.

It is clear that the quality of the handover target cell is directly determined by handover measurement. Moreover, the handover measurement is performed during the active state (also called connected-mode) of the mobile, its impact on the on-going service is inevitable. Advanced wireless broadband systems such as 3G and 4G allow adjacent cells operating in a common frequency band, and thereby enable the measurement of several neighbouring cells simultaneously. This results in enhanced handover measurement. Its efficiency is primarily determined by the number of cells that the mobile is able to measure simultaneously during a measurement period, which is called mobile's *measurement capability*, namely k. For example, a LTE-compliant terminal is required be able to measure eight cells in each period, see §4.1.

Handover is an important topic and has received a lot of investigations. But our literature review summarised in §4.3 shows that most of prior arts addressed the handover control problem of the handover decision function. The handover measurement function has received less attention and most investigations and analysis are given by simulations. While a handover control problem

can be studied conventionally in a simplified model of two cells in which a handover decision is made by assigning the mobile to one of them, the handover measurement problem involves a more complex system in which the signal quality of best cell among a large number of cells needs to be determined. This often incurs modeling and analysis difficulty especially when stochastic parameters are introduced to better describe a wireless network. Moreover, cellular standards introduce many parameters to control the handover measurement operation trying to reduce the impact of this function on the system performance, for example 3GPP specifies a dozen of measurement reporting events for 3G networks, and many for LTE as summarised in Table 3.4. This makes the analysis of handover measurement more complex. Therefore, some basic questions remain to be answered. Most importantly,

What are unified impacts of handover measurement controlling parameters on the system performance?

In particular, how optimal is the current suggestion that $k = 8$ of LTE standard considering that the handover measurement in LTE is no longer supported by a neighbour cell list? There lacks a unified model and analytical study of the handover measurement which is essential to network design and optimisation. With this observation,

This chapter establishes a generalised framework for the system analysis and probabilistic aspects of handover measurement.

Using the results of the best signal quality developed in Chapters 7 and 8, and those of level crossings developed in Chapter 9, this chapter will bring the following main contributions:

- A generalised model is developed to characterise the handover measurement and to facilitate network analysis and performance evaluation.
- The probability of the key events is derived under interference-limited condition in a multicell system: suitable target found, service failure, scanning triggering, and scanning withdrawal taking into account the nature of digital communication. Analytical results of the above are known fundamental but challenging.
- Using the above results, we investigate the handover measurement in LTE with respect to its requirements on measurement capability and system setting.

Section 10.2 describes the system model. Section 10.3 formulates the key probabilistic events of a handover measurement process. Section 10.4 is devoted to developing analytical results of the formulated key events. Section 10.5 describes state diagrams developed for handover measurement, and Section 10.6 defines performance metrics using the proposed state diagram. Section 10.7 applies the proposed framework to study the handover measurement in LTE and presents its results. Finally, Section 10.8 provides some concluding remarks.

10.2   System Description

The system is assumed to be entirely described by the assumptions presented in Chapter 6 with the following precision.

Wireless Link Model. The random variables $\{X_i, i = 1, 2, \ldots\}$ refer to shadowing, and are assumed lognormal expressible as

$$X_i = 10^{Z_i/10}, \tag{10.2.1}$$

where the random variables $\{Z_i, i = 1, 2, \ldots\}$ are independently and identically distributed according to a Gaussian distribution with zero mean and standard deviation $0 < \sigma_Z < \infty$. Within this context, fast fading is averaged out as it usually varies much faster than that of handover decision process. Handover algorithms are hard to respond to short-term fading as the delay involved in BS switching is often much larger than the time scale of short-term fading, cf §2.1.

The typical distance-dependent path loss is considered and is expressible as (cf. Chapter 8):

$$l(d) = (\max(d, R_{\min}))^{\beta}, \quad \text{for } d \in \mathbb{R}_+,$$

where $R_{\min}$ is some non-negative constant, and β is the path loss exponent.

The signal quality expressed in signal-to-interference-plus-noise ratio is given according to (2.3.3):

$$Q_i = P_i/(1 + I_i), \tag{10.2.2}$$

where P_i is the signal strength of cell i, and $I_i = \sum_{j \neq i} P_j$ is the interference created by other cells to the signal of cell i.

In the time domain, we consider that $Z_i(t)$ is stationary with auto-correlation function $R_Z(\tau)$ satisfying condition (5.3.9)

$$R_Z(\tau) = O(\tau^{-a})$$

for some $a > 0$, as $\tau \to \infty$, and condition (5.3.4) which is

$$R_Z''(\tau) = \lambda_2 + O(|\log|\tau||^{-a}) \quad \text{as } \tau \to 0$$

with finite λ_2 for some $a > 1$. For different uses later, for some time-varying process $W(t)$, we denote

$$D_W(\gamma, \tau, [t_a, t_b]) \triangleq \{W(t) < \gamma, \forall t \in [t_0, t_0 + \Delta_t] \text{ with } \Delta_t \geq \tau \text{ and } t_0 + \tau \in [t_a, t_b]\}.$$

to be an excursion of W below level γ with minimum-duration τ, considering time window $[t_a, t_b]$. Similarly, denote

$$U_W(\gamma, \tau, [t_a, t_b]) \triangleq \{W(t) > \gamma, \forall t \in [t_0, t_0 + \Delta_t] \text{ with } \Delta_t \geq \tau \text{ and } t_0 + \tau \in [t_a, t_b]\}.$$

to be an excursion W above level γ with minimum-duration τ, considering time window $[t_a, t_b]$. In the above definitions, the starting time t_0 of the crossing event does not necessarily belong to the time window $[t_a, t_b]$. Besides, the strictly inequalities $<$ and $>$ can be replaced by inequalities $\leq$ and $\geq$, respectively, without change of results. We refer to §5.3 for more details on level crossing properties of a time-varying process.

Handover Measurement Procedure. The handover measurement, also called (neighbour cell) *scanning*, as described in §4.1 is generalised in Figure 10.1. The mobile starts scanning neighbouring cells as soon as the triggering condition is satisfied. Later on, it needs a certain time
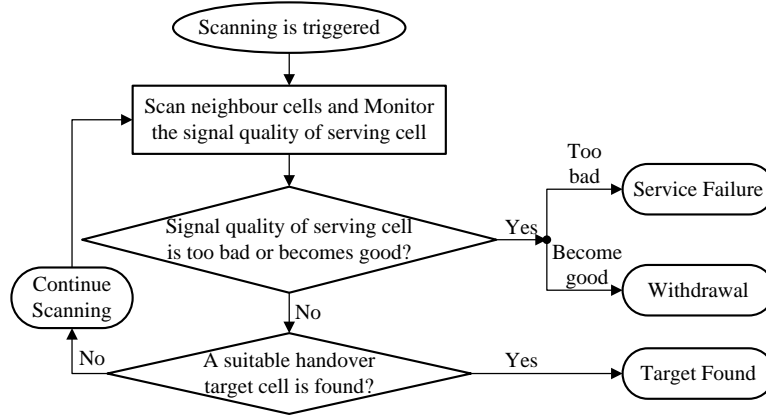
FIGURE 10.1: Procedure of handover measurement

duration to successfully measure the signal quality of a neighbouring cell. This time duration is so-called *measurement period* denoted by T_{meas}. During each measurement period $[(m-1)T_{\text{meas}}, mT_{\text{meas}}]$, for $m = 1, 2, \ldots$ where $m = 1$ corresponds to the first measurement after the scanning is triggered, the mobile measures the signal quality of k neighbouring cells where k is the mobile's measurement capacity. And it obtains the signal quality of neighbouring cells at discrete times $m \times T_{\text{meas}}$. For notational simplicity, in case of no ambiguity, we will use m and $m\,T_{\text{meas}}$ interchangeably, and use $[m-1, m]$ to refer to the measurement period $[(m-1)T_{\text{meas}}, mT_{\text{meas}}]$.

During the measurement of neighbouring cells, the on-going service continuously undergoes the fluctuations of the serving cell's signal quality, leading to different possible outcomes. In fact, the signal quality of the serving cell affects the on-going user's service in a time scale as short as one time slot which is usually much smaller than T_{meas}. During each measurement period $[m-1, m]$, if the signal quality of the serving cell becomes good enough, the mobile may withdraw the scanning to reduce the scanning overheads. If the signal quality of the serving cell is too bad, the scanning ends in *failure* as a call drop or service interrupt occurs. In this case, the mobile will perform a link reestablishment procedure for the service recovery purpose, see e.g. §3.3 for the Radio Link Reestablishment in LTE. If the scanning identifies a *suitable handover target*, the scanning ends in *success*. Otherwise, the mobile will continue the scanning and keep monitoring the signal quality received from the serving cell.

10.3 Basic Formulation

10.3.1 Suitable Handover Target Found

A *suitable* handover target is a candidate neighbouring cell to which the serving base station decides whether or not to handover the mobile. The *suitable* handover target becomes the *final* handover target in the case that a handover execution is to be done.

A suitable handover target needs to satisfy *necessary* conditions of a handover target. The necessary condition considered here is that the signal quality of the suitable handover target must be better than a required threshold γ_{req}. The handover decision process may consider more criteria to refine the selection depending on the control algorithm used by the base station,

for example the current load of the candidate handover target, or the relative signal quality between the candidate handover target and the serving cell. Here we deal with the handover measurement function whose role is to *find a suitable handover target* and prevent service failure, criteria for handover decision process are thus not of our interest here.

Since in each measurement period a mobile scans k cells and the cell with best signal quality is preferable, the event of having a suitable handover target found at moment m can be defined by:

$$findtarget_m(k) \triangleq \{Y_k \geq \gamma_{\text{req}}\}, \tag{10.3.1}$$

where

$$Y_k \triangleq \max_{i=1,\cdots,k} Q_i \tag{10.3.2}$$

denotes the best signal quality received from the k cells scanned.

10.3.2 Service Failure

In wireless communications, the signal usually undergoes time-varying fading and other impairments like interference such that its instantaneous amplitude fluctuates. This results in bit and burst errors when the signal quality is low. Techniques such as redundancy coding, automatic repeat request (ARQ) and hybrid-ARQ (see §3.2) are often used to maintain the communication reliability. These techniques are however effective to recover data only when the *bit error rate* is relatively low. When the SINR stays below a minimum allowable level, say γ_{min}, for long time, successive bits and successive bursts are erroneous, those error-fighting techniques do not help any more, leading to a service failure. For instance, LTE considers that a radio link failure is to be detected if a maximum number of retransmissions (under ARQ or H-ARQ mechanism) is reached, see §3.3. Therefore, it is more appropriate and also general to incorporate a minimum duration τ_{min} when characterising the event, see §5.3.2. A service failure during $[m-1, m]$ is thus defined by an excursion of the serving cell's signal quality below the minimum tolerable level γ_{min} with minimum-duration τ_{min}:

$$fail_m \triangleq D_{Q_0}(\gamma_{\text{min}}, \tau_{\text{min}}, [m-1, m]), \tag{10.3.3}$$

where $Q_0(t)$ denotes the SINR received from the serving cell at time t. In Figure 10.2, the serving cell's signal quality is below γ_{min} during duration τ_{min} and a service failure occurs at D. Note that when $\tau_{\text{min}} = 0$, the definition in (10.3.3) corresponds to an instantaneous SINR outage.

10.3.3 Scanning Trigger

Handover measurement introduces overheads such as gaps in data transmission or mobile's resource consumption (see §4.1). It is thus helpful to only perform a handover measurement when the signal quality of the serving cell is really bad. It is possible that the SINR may cross and stay below or above a threshold only for a very short duration. Thus, to predict with high probability the *future* signal quality of the serving cell, the handover measurement should be triggered only if the serving cell's signal quality is *worse than* threshold γ_{t} for a certain period τ_{t}. But note that if these two parameters are not appropriately configured, it may happen that a service failure occurs before the handover measurement initiation; and in this case the mobile is not be able to perform a handover measurement but it has to conduct a link reestablishment
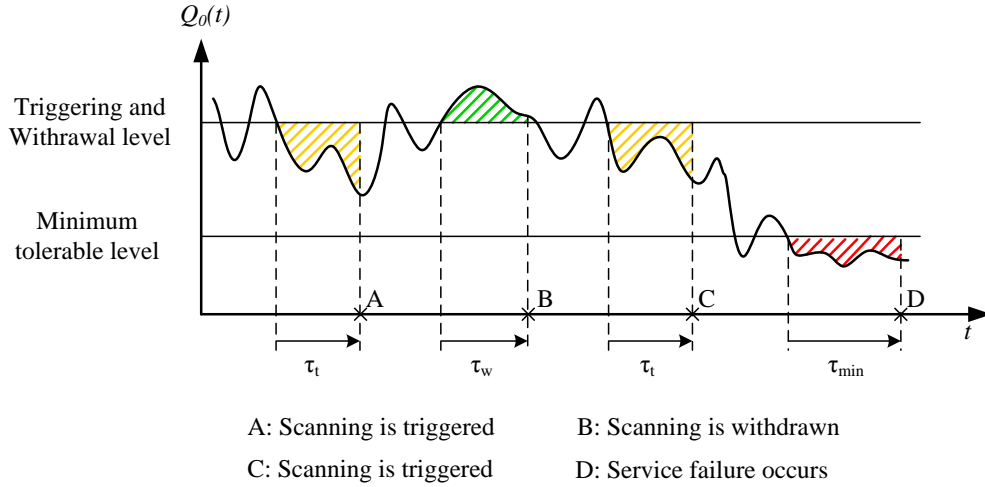
FIGURE 10.2: Level crossing events

procedure. Therefore, the handover measurement is triggered during period $[m-1, m]$ if the serving cell's signal quality is worse than threshold γ_t during at least τ_t *and if* no service failure occurs during this period:

$$trig_m \triangleq D_{Q_0}(\gamma_t, \tau_t, [m-1, m]) \land \neg fail_m, \qquad (10.3.4)$$

where $\land$ and $\neg$ stand for logical AND and logical NEGATION, respectively. It is thus obvious that γ_t must be set higher than $\gamma_{\min}$.

In Figure 10.2, the handover measurement is triggered at A. After that, the serving cell's signal quality appears bad again which triggers another scanning process at C.

10.3.4   Scanning Withdrawal

Similarly, the handover measurement should be withdrawn when the signal quality of serving cell becomes back good. Precisely, it should be withdrawn if the serving cell's signal quality is better than a threshold γ_w for a certain period τ_w. So, the event of scanning withdrawal during period $[m-1, m]$ is expressible as:

$$wdraw_m \triangleq U_{Q_0}(\gamma_w, \tau_w, [m-1, m]). \qquad (10.3.5)$$

In Figure 10.2 where we consider $\gamma_w = \gamma_t$, and $\tau_w = \tau_t$, $Q_0(t)$ crosses over γ_t and stays above during a duration longer than τ_t, the scanning process is canceled at B.

10.4   Analytical Development

This section is reserved to the development of the probability of events which are formulated in §10.3, including: $(Y_k \geq \gamma_{\mathrm{req}})$, $fail_m$, $trig_m$, and $wdraw_m$. We determine these event probabilities in the following structure. First, we derive $\mathbf{P}(Y_k \geq \gamma)$ for some constant γ by using theoretical

results developed in Chapter 7 and Chapter 8. Next, we deal with $\mathbf{P}(fail_m)$ in §10.4.2. Then, the analogy between down-crossing events $trig_m$ and $fail_m$ will allow us to obtain $\mathbf{P}(trig_m)$ in §10.4.3. Finally, we determine $\mathbf{P}(wdraw_m)$ in §10.4.4.

10.4.1 Probability of Finding a Suitable Cell

To determine the probability of $\mathbf{P}(Y_k \geq \gamma)$, one needs to define the set of candidate cells from which k cells are taken. By today's cellular standards, there are two different cases: *limited* candidate set and *unlimited* candidate set. In the former, a mobile only scans neighbouring cells belonging to a pre-defined set which includes a limited number of potential candidates, say N_{cell} cells. This set in practice corresponds to the neighbour cell list as used in GSM, WCDMA, and WiMAX with $N_{\text{cell}} = 32$, see §4.2. In the unlimited candidate set, the mobile is allowed to scan any cell in the network. However, a network may have a very large number of cells, scanning without restriction would introduce unsupportable overheads. Therefore, new broadband cellular systems use a set of, say N_{CSID}, cell synchronisation identities (CSID) which allow a mobile to identify and measure cells more easily. This set of N_{CSID} CSIDs are shared among all the cells such that two cells having the same CSID need to be spatially separated enough to avoid any confusion. When required to scan k cells, the mobile just picks k out of the total N_{CSID} CSIDs and conduct standardised cell synchronisation and measurement. An example system using this mechanism is LTE that defines 504 physical cell identifiers (PCI) which serve as CSIDs. The mobile performs the cell measurement autonomously without need of a pre-configured cell set like the neighbour cell list used in predecessor systems, see §3.3 and Chapter 4 for more information.

Denote by B the network area of the candidate set. Then B is a bounded area in the case of limited candidate set, whereas $B = \mathbb{R}^2$ in the case of unlimited candidate set. By the results of Chapter 7 and Chapter 8, we determine $\mathbf{P}(Y_k \geq \gamma)$ for both cases.

Case $B = \mathbb{R}^2$. The set of neighbouring cells which are scanned through a selection of k out of the total N_{CSID} CSIDs is precisely a thinning S_k of $B = \mathbb{R}^2$ with retention probability equal to

$$\rho_k = k/N_{\text{CSID}}. \tag{10.4.1}$$

Note that the set S_k may have more than k cells, and this efficiently describes the real situation where the mobile may detect several cells which have the same CSID. For this reason, LTE defines the automatic neighbour relation (ANR) table to convert a reported physical cell identifier to a unique cell global identifier (see §3.3).

Hence, (10.3.2) is equivalent to

$$Y_k \equiv \max_{i \in S_k} Q_i. \tag{10.4.2}$$

and as a result

$$\mathbf{P}(Y_k > \gamma) = \overline{F}_{Y_k}(\gamma), \tag{10.4.3}$$

where $\overline{F}_{Y_k}(\cdot)$ is the tail distribution function of Y_k. Here, Y_k is the best signal quality received from a thinning of the whole network $B = \mathbb{R}^2$ with retention probability ρ_k. Consider the unbounded distance-dependent path loss function $l(d) = d^\beta$, i.e. $R_{\min} = 0$, the tail distribution

of Y_k is precisely given by Corollary 7.5.2 in Chapter 7, and is depicted in the following:

$$\mathbf{P}(Y_k > \gamma) = \int_\gamma^{+\infty} \int_0^{+\infty} \frac{\exp\left(-C_1 w^\alpha - C_2(w, u)\right)}{\pi}\left[-\frac{1+\gamma}{\gamma}\right.$$

$$\times \cos\left(C_1 w^\alpha \tan(\frac{\pi\alpha}{2}) + C_3(w, u) + C_4(w, u)\right)$$

$$\left. + \cos\left(C_1 w^\alpha \tan(\frac{\pi\alpha}{2}) + C_3(w, u) - wu\right)\right] dw du, \qquad (10.4.4)$$

where constants as given therein are applied here for X_i as a lognormal random variable, so: $\alpha = 2/\beta$, and

$$
\begin{aligned}
C_1 &= (1-\rho_k)\delta, \\
C_2(w, u) &= \rho_k c_\alpha \frac{{}_1F_2(-\frac{\alpha}{2}; \frac{1}{2}, 1 - \frac{\alpha}{2}; -\frac{u^2 w^2}{4})}{u^\alpha}, \\
C_3(w, u) &= \rho_k c_\alpha \frac{\alpha w}{1 - \alpha} \frac{{}_1F_2(\frac{1-\alpha}{2}; \frac{3}{2}, \frac{3-\alpha}{2}; -\frac{u^2 w^2}{4})}{u^{\alpha-1}}, \\
C_4(w, u) &= w(1 - u(1+\gamma)/\gamma),
\end{aligned}
$$

in which $\Gamma(\cdot)$ denotes the gamma function, ${}_1F_2$ denotes the hypergeometric function (see Chapter 7), and constant δ is as given by (7.3.3):

$$\delta = c_\alpha \Gamma(1 - \alpha) \cos(\pi\alpha/2),$$

where c_α is as given by (7.3.4):

$$c_\alpha := \pi\lambda \mathbf{E}\{p^\alpha\} = \pi\lambda\mathbf{E}\{(A\,X_i)^\alpha\} = \pi\lambda A^\alpha \exp\left(\alpha^2 \sigma_X^2/2\right),$$

with $\sigma_X = \sigma_Z \frac{\log 10}{10}$. Simulation results in §10.7 show its accuracy.

Case $B \subsetneq \mathbb{R}^2$. We consider two different possibilities: scattered networks like rural macro cellular networks where inter-site distance is large such that the intensity λ is small, and dense networks like urban small cell networks where a large number of cells are deployed to support dense traffic such that λ is large. Consider $\widehat{B}$ a disk-shaped network area with radius

$$R_{\widehat{B}} = \sqrt{N_{\text{cell}}/(\pi\lambda)}. \qquad (10.4.5)$$

Under the Poisson point process assumption of the base station spatial distribution, $\widehat{B}$ has on average N_{cell} BSs. In light of that, we can approximate the region of the N_{cell} neighbouring cells by $\widehat{B}$.

For small λ and N_{cell} is relatively large, we can have $R_{\widehat{B}} \approx \infty$, i.e., $\widehat{B}$ can be approximated by $\mathbb{R}^2$. Similarly, let S_k be a thinning on $\widehat{B}$ with retention probability

$$\rho_k = k/N_{\text{cell}} \qquad (10.4.6)$$

such that S_k has on average k cells. The probability of finding a target cell can be well approximated by (10.4.4).

For large λ (and so the approximation $R_{\widehat{B}} \approx \infty$ may be not applicable), it turns out that the results developed in Chapter 8 for dense networks are applicable. Assume the bounded distance-dependent path loss model by considering $R_{\min} > 0$, and assume that $AR_{\min}^{-\beta}$ is large. Then Theorem 8.6.1 in Chapter 8 is applicable and gives us:

$$\mathbf{P}(Y_k > \gamma) \approx \int_\gamma^\infty \Big\{ f_{M_k}(u) \int_0^\infty \frac{2}{\pi w} e^{-\delta w^\alpha} \sin\big(w\frac{u-\gamma}{2\gamma}\big)$$
$$\times \cos\big(wu + w\frac{u-\gamma}{2\gamma} - \delta w^\alpha \tan\frac{\pi\alpha}{2}\big) \mathrm{d}w \Big\} \mathrm{d}u, \quad (10.4.7)$$

where δ is given under (10.4.4), and f_{M_k} is the probability density function of the maximum signal strength $M_k = \max_{i=1}^k P_i$ and is given by Corollary 8.3.1:

$$f_{M_k}(x) = k \cdot f_P(x) \cdot F_P^{k-1}(x), \quad \text{for } k \geq 1, \qquad (10.4.8)$$

with F_P denoting the cumulative density function of the signal strength received from a cell in $\widehat{B}$ for the case of bounded path loss model, its exact expression is given by (8.2.2) of Proposition 8.2.1:

$$F_P(x) = c\left(a^{-\frac{2}{\beta}} K_1(x) - b^{-\frac{2}{\beta}} K_2(x) - e^{\lambda_2} x^{-\frac{2}{\beta}} K_3(x) + e^{\lambda_2} x^{-\frac{2}{\beta}} K_4(x)\right),$$

where $a = AR_{\widehat{B}}^{-\beta}$, $b = AR_{\min}^{-\beta}$, $c = A^{\frac{2}{\beta}}(R_{\widehat{B}}^2 - R_{\min}^2)^{-1}$, $\lambda_2 = 2\sigma_Z^2/\beta^2$, and K_j, $j = 1, \ldots, 4$, refers to the cdf of a lognormal distribution of parameters (μ_j, σ_X), in which

$$\mu_1 = \log a, \quad \mu_2 = \log b, \quad \mu_3 = \mu_1 + 2\sigma_X^2/\beta, \quad \mu_4 = \mu_2 + 2\sigma_X^2/\beta.$$

and $f_P(x) = \mathrm{d}F_P(x)/\mathrm{d}x$. It is observed in §11.5 of Chapter 11 that (10.4.7) is a good approximation. This completes the discussion.

10.4.2 Probability of Service Failure $\mathbf{P}(fail_m)$

In the definition (10.3.3), by noting that $P_i = AX_i/l(d)$, $Q_0(t) < \gamma_{\min}$ is re-written as $Z(t) < \hat{\gamma}_{\min}(t)$ where

$$\hat{\gamma}_{\min}(t) = 10\log_{10}\left(\gamma_{\min} \frac{l(d(t))}{A}(1 + I(t))\right)$$

is a time-varying level. As a sequel, the excursions of non-stationary process $Q_0(t)$ below the fixed level $\gamma_{\min}$ can be represented by the excursions of the stationary normal process $Z(t)$ below the time-varying level $\hat{\gamma}_{\min}(t)$. Let $T_{\min}$ be the length of an excursion of $Z(t)$ below level $\hat{\gamma}_{\min}(t)$, $fail_m$ is thus expressible as an excursion of $Z(t)$ below the level $\hat{\gamma}_{\min}(t)$ with $T_{\min}$ longer than $\tau_{\min}$, i.e.,

$$fail_m \equiv \{\text{excursion of } Z(t) \text{ below } \hat{\gamma}_{\min}(t) \text{ with } T_{\min} \geq \tau_{\min},$$
$$\text{for } t \in [(m-1)T_{\text{meas}} - \tau_{\min}, mT_{\text{meas}}]\}, \quad (10.4.9)$$

where the considered time window is $[(m-1)T_{\text{meas}} - \tau_{\min}, mT_{\text{meas}}]$ since the failure will occur at a moment $t_0 + \tau_{\min}$ anterior to $(m-1)T_{\text{meas}}$ if the excursion starts at a moment $t_0 < (m-1)T_{\text{meas}} - \tau_{\min}$. In practice, $\tau_{\min}$ and T_{meas} are typically about a few hundreds of milliseconds (see, §4.1). The interval $T_{\text{meas}} + \tau_{\min}$ is very short so that we consider that wherein the distance

between the mobile and its serving BS is constant, i.e.

$$d(t) \approx d_m, \tag{10.4.10}$$

for $t \in [(m-1)T_{\text{meas}} - \tau_{\min}, mT_{\text{meas}}]$. In addition, if consider that the interference is constant, say I, we have that $\hat{\gamma}_{\min}(t) \approx \hat{\gamma}_{\min}$ which is a constant and is equal to

$$\hat{\gamma}_{\min} := 10 \log_{10} \left(\gamma_{\min} \frac{l(d_m)}{A} (1+I) \right), \tag{10.4.11}$$

for $t \in [(m-1)T_{\text{meas}} - \tau_{\min}, mT_{\text{meas}}]$. Thus, by the stationarity of $Z(t)$, for constant $\hat{\gamma}_{\min}$ and all intervals $[t_1, t_2]$, we have:

$$\mathbf{P}(\text{excursions of } Z(t) \text{ below } \hat{\gamma}_{\min} \text{ with } T_{\min} \geq \tau_{\min}, \text{ for } t \in [t_1, t_2])$$
$$= \mathbf{P}(\text{excursions of } Z(t) \text{ below } \hat{\gamma}_{\min} \text{ with } T_{\min} \geq \tau_{\min}).$$

With the conditions previously described for $R_Z(\tau)$, the probability of excursions of $Zt(t)$ below $\hat{\gamma}_{\min}$ with length $T \geq \tau_{\min}$ is given by (5.3.18). Hence

$$\mathbf{P}(fail_m \,|\, I(t) = x, d(t) = d_m) = \mathbf{P}(\text{excursions of } Z(t) \text{ below } \hat{\gamma}_{\min} \text{ with } T_{\min} \geq \tau_{\min})$$
$$= \mathbf{E}\{D_{\hat{\gamma}_{\min}}\} \left(\tau_{\min} e^{-V_{\min}\tau_{\min}^2} + \sqrt{\frac{\pi}{V_{\min}}} \mathrm{Q}(\sqrt{2V_{\min}}\tau_{\min}) \right), \tag{10.4.12}$$

where $\mathrm{Q}(x) = \int_x^\infty \frac{\exp(-t^2/2)}{\sqrt{2\pi}}\mathrm{d}t$ is the Q-function, $\mathbf{E}D_{\hat{\gamma}_{\min}}$ is the average down-level crossing rate of $Z(t)$ of the level $\hat{\gamma}_{\min}$ and is given by Proposition 5.3.2:

$$\mathbf{E}\{D_{\hat{\gamma}_{\min}}\} = \frac{\sqrt{\lambda_2}}{2\pi\sigma_Z} \exp\left(-\frac{\hat{\gamma}_{\min}^2}{2\sigma_Z^2} \right),$$

and where $V_{\min} = \frac{\hat{\gamma}_{\min}^2 \lambda_2}{8}$. Note that the interference behaves as a random variable, and under the system model described in Section 10.2, it can be modeled as a shot noise and has the characteristic function given by Corollary 7.4.4 in case $R_{\min} = 0$, and by Proposition 8.4.2 in case $R_{\min} > 0$. So:

$$\phi_I(w) = \exp\left(-\delta|w|^\alpha[1 - j\,\mathrm{sign}(w)\tan(\frac{\pi\alpha}{2})] \right),$$

where δ is given by (7.3.3) and is depicted under (10.4.4). Consider that $\beta > 2$, we have $0 < \alpha < 1$ such that $\phi_I(w)$ is absolutely integrable. By Feller [186, Thm.3, p.509], the pdf of I is thus given by:

$$f_I(x) = \frac{1}{2\pi} \int_{-\infty}^{+\infty} e^{-jwx}\phi_I(w)\mathrm{d}w = \frac{1}{\pi} \int_0^\infty e^{-\delta w^\alpha} \cos\left(\delta \tan(\frac{\pi\alpha}{2})w^\alpha - xw \right)\mathrm{d}w.$$

Hence, a more general expression of the service failure probability with random interference $I(t)$ than that of (10.4.12) is obtainable:

$$\mathbf{P}(fail_m \,|\, d(t) = d_m) = \int_0^\infty \mathbf{P}(fail_m \,|\, I(t) = x, d(t) = d_m)f_I(x)\mathrm{d}x$$
$$= \int_0^\infty \int_0^\infty \mathbf{E}\{D_{\hat{\gamma}_{\min}}\} \left(\tau_{\min} e^{-V_{\min}\tau_{\min}^2} + \sqrt{\frac{\pi}{V_{\min}}} \mathrm{Q}(\sqrt{2V_{\min}}\tau_{\min}) \right)$$
$$\times \frac{e^{-\delta w^\alpha}}{\pi} \cos\left(\delta \tan(\frac{\pi\alpha}{2})w^\alpha - xw \right)\mathrm{d}w\mathrm{d}x. \tag{10.4.13}$$

Under the approximation (10.4.10) that $d(t)$ is approximately constant in time interval $T_{\text{meas}} + \tau_{\text{min}}$, we have $\mathbf{P}(fail_m)$ given by (10.4.13).

Remark 10.4.1. If one may consider users moving at very high speeds such that $d(t)$ changes significantly during a time interval $T_{\text{meas}} + \tau_{\text{min}}$, $\mathbf{P}(fail_m)$ is then given by:

$$\int_{(m-1)\cdot T_{\text{meas}} - \tau_{\text{min}}}^{m \cdot T_{\text{meas}}} \int_0^\infty \mathbf{P}(fail_m \,|\, I(t) = x, d(t)) f_I(x)\mathrm{d}x \cdot f_d(t)\mathrm{d}t$$

which requires the pdf of $d(t)$, denoted by $f_d(t)$. This needs for an appropriate mobility model which is omitted here for simplification.

10.4.3 Probability of Scanning Trigger $\mathbf{P}(trig_m)$

By the definition of the scanning trigger event $trig_m$ given in (10.3.4), we have:

$$
\begin{aligned}
\mathbf{P}(trig_m) =& \mathbf{P}(D_{Q_0}(\gamma_{\text{t}}, \tau_{\text{t}}, [m-1, m]) \wedge \neg fail_m) \\
=& \mathbf{P}(D_{Q_0}(\gamma_{\text{t}}, \tau_{\text{t}}, [m-1, m])) - \mathbf{P}(D_{Q_0}(\gamma_{\text{t}}, \tau_{\text{t}}, [m-1, m]) \wedge fail_m), \quad (10.4.14)
\end{aligned}
$$

in which, by the analogy between $D_{Q_0}(\gamma_{\text{t}}, \tau_{\text{t}}, [m-1, m])$ and $D_{Q_0}(\gamma_{\text{min}}, \tau_{\text{min}}, [m-1, m])$, the first term on the right-hand side can be directly obtained from the result of §10.4.2 considering requirements γ_{t} and τ_{t}. Precisely, denote

$$\hat{\gamma}_{\text{t}}(t) = 10 \log_{10}\left(\gamma_{\text{t}} \frac{l(d(t))}{A} (1 + I(t))\right).$$

Then, the excursions of non-stationary process $Q_0(t)$ below the fixed level γ_{t} is represented by the excursions of the stationary normal process $Z(t)$ below the time-varying level $\hat{\gamma}_{\text{t}}(t)$. Let T_{t} be the length of an excursion of $Z(t)$ below level $\hat{\gamma}_{\text{t}}(t)$, we have

$$
\begin{aligned}
D_{Q_0}(\gamma_{\text{t}}, \tau_{\text{t}}, [m-1, m]) \equiv \{&\text{excursion of } Z(t) \text{ below } \hat{\gamma}_{\text{t}}(t) \text{ with } T_{\text{t}} \geq \tau_{\text{t}}, \\
&\text{for } t \in [(m-1)T_{\text{meas}} - \tau_{\text{t}}, \, mT_{\text{meas}}]\}. \quad (10.4.15)
\end{aligned}
$$

Since the interval $\tau_{\text{t}} + T_{\text{meas}}$ is small, assume that the condition (10.4.10) holds for $t \in [(m-1)T_{\text{meas}} - \tau_{\text{t}}, \, mT_{\text{meas}}]$. So, similarly to (10.4.13), we obtain:

$$
\begin{aligned}
\mathbf{P}(D_{Q_0}(\gamma_{\text{t}}, \tau_{\text{t}}, [m-1, m]) \,|\, d(t) = d_m) =& \int_0^\infty \int_0^\infty \mathbf{E}\{D_{\hat{\gamma}_{\text{t}}}\} \left(\tau_{\text{t}} e^{-V_{\text{t}} \tau_{\text{t}}^2} + \sqrt{\frac{\pi}{V_{\text{t}}}} Q(\sqrt{2V_{\text{t}}} \tau_{\text{t}})\right) \\
&\times \frac{e^{-\delta w^\alpha}}{\pi} \cos\left(\delta \tan(\frac{\pi \alpha}{2}) w^\alpha - xw\right) \mathrm{d}w\mathrm{d}x, \quad (10.4.16)
\end{aligned}
$$

where $\mathbf{E}\{D_{\hat{\gamma}_{\text{t}}}\}$ is the average down-crossing rate of $Z(t)$ of the level $\hat{\gamma}_{\text{t}}$ given according to Proposition 5.3.2, $V_{\text{t}} = \frac{\hat{\gamma}_{\text{t}}^2 \lambda_2}{8}$, and

$$\hat{\gamma}_{\text{t}} := \hat{\gamma}_{\text{t}}(d(t) = d_m) = 10 \log_{10}\left(\gamma_{\text{t}} \frac{l(d_m)}{A} (1 + I)\right). \quad (10.4.17)$$

Now, we derive the second term on the right hand-side of (10.4.14). Using (10.4.9) and (10.4.15), we get

$$\mathbf{P}\big(D_{Q_0}(\gamma_{\mathrm{t}}, \tau_{\mathrm{t}}, [m-1, m]) \wedge \mathit{fail}_m \,|\, I(t) = x, d(t) = d_m\big)$$
$$= \mathbf{P}\big(Z(t) \leq \hat{\gamma}_{\min} \text{ with } T_{\min} \geq \tau_{\min}, \text{ and } Z(t) < \hat{\gamma}_{\mathrm{t}} \text{ with } T_{\mathrm{t}} \geq \tau_{\mathrm{t}},$$
$$\text{for } t \in [(m-1)T_{\mathrm{meas}} - \tau_{\mathrm{t}}, mT_{\mathrm{meas}}]\big).$$

This turns out to be the probability of successive excursions of two adjacent levels which is developed in §9.3.3. Precisely, represent the down-excursions by the up-excursions thanks to an inversion of signs and obtain

$$\mathbf{P}\big(D_{Q_0}(\gamma_{\mathrm{t}}, \tau_{\mathrm{t}}, [m-1, m]) \wedge \mathit{fail}_m \,|\, I(t) = x, d(t) = d_m\big)$$
$$= \mathbf{P}\big(- Z(t) \geq -\hat{\gamma}_{\min} \text{ with } T_{\min} \geq \tau_{\min}, \text{ and } - Z(t) > -\hat{\gamma}_{\mathrm{t}} \text{ with } T_{\mathrm{t}} \geq \tau_{\mathrm{t}},$$
$$\text{for } t \in [(m-1)T_{\mathrm{meas}} - \tau_{\mathrm{t}}, mT_{\mathrm{meas}}]\big),$$

where $-Z(t)$ is still a stationary normal process; and where, using (10.4.11), (10.4.17), and that $\gamma_{\mathrm{t}} \geq \gamma_{\min}$, we have $-\hat{\gamma}_{\mathrm{t}} \leq -\hat{\gamma}_{\min}$. Depending on requirements made for $\tau_{\min}$ and τ_{t}, $\mathbf{P}\big(D_{Q_0}(\gamma_{\mathrm{t}}, \tau_{\mathrm{t}}, [m-1, m]) \wedge \mathit{fail}_m \,|\, I(t) = x, d(t) = d_m\big)$ is given by either (9.3.18), (9.3.19), (9.3.20), or (9.3.21). Finally, considering the random interference, similarly to (10.4.16) we get

$$\mathbf{P}\big(D_{Q_0}(\gamma_{\mathrm{t}}, \tau_{\mathrm{t}}, [m-1, m]) \wedge \mathit{fail}_m \,|\, d(t) = d_m\big)$$
$$= \int_0^\infty \mathbf{P}\big(D_{Q_0}(\gamma_{\mathrm{t}}, \tau_{\mathrm{t}}, [m-1, m]) \wedge \mathit{fail}_m \,|\, I(t) = x, d(t) = d_m\big) f_I(x)\mathrm{d}x. \quad (10.4.18)$$

Substitute this and (10.4.16) into (10.4.14), we obtain the probability of the scanning trigger $\mathbf{P}(\mathit{trig}_m)$ under the assumption that (10.4.10) holds for $t \in [(m-1)T_{\mathrm{meas}} - \tau_{\mathrm{t}}, mT_{\mathrm{meas}}]$.

10.4.4 Probability of Scanning Withdrawal $\mathbf{P}(\mathit{wdraw}_m)$

The probability of wdraw_m defined in (10.3.5) can be obtained by following the same technique used in §10.4.2. Note that $Q_0(t) \geq \gamma_{\mathrm{w}}$ is equivalently represented as $Z(t) \geq \hat{\gamma}_{\mathrm{w}}(t)$ with

$$\hat{\gamma}_{\mathrm{w}}(t) = 10 \log_{10}\Big(\gamma_{\mathrm{w}} \frac{l(d(t))}{A}\big(1 + I(t)\big)\Big).$$

The scanning withdrawal wdraw_m is then expressible as an up-excursion of $Z(t)$ above the level $\hat{\gamma}_{\mathrm{w}}(t)$ with length $T_{\mathrm{w}} \geq \tau_{\mathrm{w}}$. By stationarity of $Z(t)$

$$\mathbf{P}(\mathit{wdraw}_m \,|\, I(t) = x, d(t) = d_m) = \mathbf{P}(\text{excursions of } Z(t) \text{ above } \hat{\gamma}_{\mathrm{w}} \text{ with } T_{\mathrm{w}} \geq \tau_{\mathrm{w}}),$$

with $\hat{\gamma}_{\mathrm{w}} := 10 \log_{10}(\gamma_{\mathrm{w}} l(d_m)(1 + I)/A)$. Under the conditions specified for $R_Z(\tau)$, we have from (5.3.18) in §5.3.2 that

$$\mathbf{P}(\mathit{wdraw}_m | I(t) = x_0, d(t) = d_m) = \mathbf{E}\{U_{\hat{\gamma}_{\mathrm{w}}}\}\left(\tau_{\mathrm{w}} e^{-V_{\mathrm{w}}\tau_{\mathrm{w}}^2} + \sqrt{\frac{\pi}{V_{\mathrm{w}}}} \mathrm{Q}(\sqrt{2V_{\mathrm{w}}}\tau_{\mathrm{w}})\right)$$

where $\mathbf{E}U_{\hat{\gamma}_{\mathrm{w}}}$ is the average up-crossing rate of $Z(t)$ of the level $\hat{\gamma}_{\mathrm{w}}$ given according to Proposition 5.3.2, and $V_{\mathrm{w}} = \frac{\hat{\gamma}_{\mathrm{w}}^2 \lambda_2}{8}$. Similarly to (10.4.13), using the pdf of the interference I provided in

§10.4.2 we obtain a more general expression:

$$\mathbf{P}(wdraw_m \,|\, d(t) = d_m) = \int_0^\infty \int_0^\infty \mathbf{E}\{U_{\hat{\gamma}_\mathrm{w}}\} \left(\tau_\mathrm{w} e^{-V_\mathrm{w}\tau_\mathrm{w}^2} + \sqrt{\frac{\pi}{V_\mathrm{w}}} \mathrm{Q}(\sqrt{2V_\mathrm{w}}\tau_\mathrm{w}) \right)$$

$$\times \frac{e^{-\delta w^\alpha}}{\pi} \cos\left(\delta \tan(\frac{\pi\alpha}{2})w^\alpha - xw \right) \mathrm{d}w \mathrm{d}x. \quad (10.4.19)$$

Assume that the condition (10.4.10) holds for $t \in [(m-1)T_\mathrm{meas} - \tau_\mathrm{w}, \, mT_\mathrm{meas}]$, $\mathbf{P}(wdraw_m)$ given by (10.4.19).

10.5   State Diagram

The mobile performs the handover measurement function during its connected-mode (i.e. the mobile has an active connection). In the connected-mode, the mobile's activities related to the mobility management are described by four states which are involved in a diagram as shown in Figure 10.3. Essentially, two states `Scan` and `NoScan` describe whether the mobile is scanning neighbouring cells or not. And two states `Fail` and `CellSwitch` describe whether the mobile is encountering a service failure or whether it is being switched to another cell. For ease of analytical development, we number the four states from one to four as illustrated in Figure 10.3. In this diagram, the transition from state i, for $i = 1, \ldots, 4$, at moment $m-1$ to state j, for $j = 1, \ldots, 4$, at moment m is described by its probability denoted as $\pi_m(i, j)$.

From state `NoScan` at moment $m-1$, in the next moment m the mobile will start a handover measurement procedure and enter into state `Scan` if the specified triggering condition holds; or the mobile will enter into state `Fail` if it encounters a service failure during period $[m-1, m]$. Otherwise, it will remain in state `NoScan`. Note that the mobile does not scan neighbouring cells when being in state `NoScan`, leading to no handover target to be identified. As a consequence, excluding the case that the network forces the mobile to connect to an another cell, there is no transition between `NoScan` and `CellSwitch`. This says that reducing scanning overheads by increasing the state probability of `NoScan` will increase the risk of service failures due to no-target-found problem. The transition probabilities $\pi_m(1, j)$, for $j = 1, \ldots, 4$, are given as follows:

$$\begin{aligned}
\pi_m(1, 2) &= \mathbf{P}(trig_m), \\
\pi_m(1, 3) &= 0, \\
\pi_m(1, 4) &= \mathbf{P}(fail_m), \\
\pi_m(1, 1) &= 1 - \pi_m(1, 2) - \pi_m(1, 4).
\end{aligned} \quad (10.5.1)$$

In state `Scan`, the mobile performs the handover measurement function as previously described in §10.2. Hence, according to the procedure described in Figure 10.1, the probability of transitions from state `Scan` to the other states can be obtained in the following:

$$\begin{aligned}
\pi_m(2, 1) &= \mathbf{P}(wdraw_m), \\
\pi_m(2, 4) &= \mathbf{P}(fail_m), \\
\pi_m(2, 3) &= (1 - \pi_m(2, 1) - \pi_m(2, 4)) \times \mathbf{P}(Y_k \geq \gamma_\mathrm{req}), \\
\pi_m(2, 2) &= (1 - \pi_m(2, 1) - \pi_m(2, 4)) \times \mathbf{P}(Y_k < \gamma_\mathrm{req}),
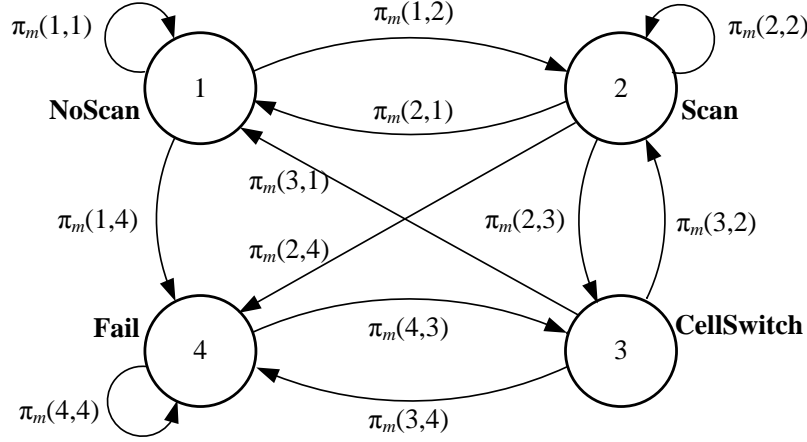\end{aligned} \quad (10.5.2)$$

FIGURE 10.3: State diagram of the mobile in connected-mode

where $\mathbf{P}(Y_k \geq \gamma_{\mathrm{req}})$ is the probability of finding a suitable handover target with Y_k referring to the the signal quality of neighbouring cells scanned during one measurement period, cf §10.3.

In state `CellSwitch`, the mobile is switched to the identified target cell. If the signal quality of the new serving cell is too bad, or if the connection switching procedure (i.e. handover execution) is not successful, the mobile may encounter a service failure during period $[m-1,\, m]$. In this case, the mobile enters into state `Fail`. Also depending on the signal quality of the new serving cell, if the triggering condition holds the mobile will enter into state `Scan` and scan neighbouring cells, otherwise the mobile will enter into state `NoScan`. Thus, the transition probabilities from state `CellSwitch` are given as

$$
\begin{aligned}
\pi_m(3,2) &= \mathbf{P}(trig_m^*), \\
\pi_m(3,4) &= \mathbf{P}(fail_m^*), \\
\pi_m(3,1) &= 1 - \pi_m(3,2) - \pi_m(3,4),
\end{aligned}
\tag{10.5.3}
$$

where the events $trig_m^*$ and $fail_m^*$ refer to scanning triggering and service failure considering the signal quality of the new serving cell, namely Q_0^*.

In state `Fail`, the mobile conducts a network entry or a link reestablishment procedure to recover the on-going service from interruption. The mobile scans all possible neighbouring cells. And in the case that a suitable cell is found, the process will continue by entering into state `CellSwitch` in which the mobile connects to the identified cell. Obviously, the signal quality of the suitable cell is required to be better than the minimum tolerable level γ_{min}. Otherwise, the mobile continues to scan for a suitable cell, and during which the service is still in failure status. So:

$$
\begin{aligned}
\pi_m(4,3) &= \mathbf{P}(Y_k \geq \gamma_{\mathrm{min}}), \\
\pi_m(4,4) &= 1 - \pi_m(4,3).
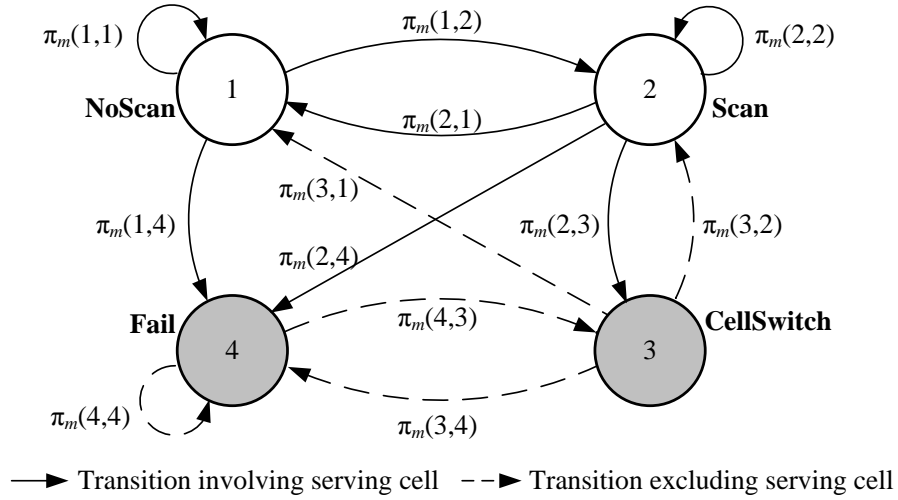\end{aligned}
\tag{10.5.4}
$$

FIGURE 10.4: State diagram of the mobile in connected mode with different transitions

Obviously, the above state diagram is associated with its transition matrix which is given by

$$\mathbf{N}_m = \begin{pmatrix} \pi_m(1,1) & \pi_m(1,2) & 0 & \pi_m(1,4) \\ \pi_m(2,1) & \pi_m(2,2) & \pi_m(2,3) & \pi_m(2,4) \\ \pi_m(3,1) & \pi_m(3,2) & 0 & \pi_m(3,4) \\ 0 & 0 & \pi_m(4,3) & \pi_m(4,4) \end{pmatrix}. \tag{10.5.5}$$

Let $\mathbf{N}^m = \mathbf{N}_1 \times \mathbf{N}_2 \times \cdots \times \mathbf{N}_m$. It is clear that $\mathbf{N}^m(i,j)$ is the transition probability from state i at moment 0 to state j at moment m.

Above we have the state diagram of the mobile in connected-mode. Our final purpose is the state diagram of the handover measurement. Note that the mobile is connected to the current serving cell when being in one of two states `NoScan` and `Scan`. By contrast, it is not the case when the mobile is in two `CellSwitch` and `Fail`. As a sequel, as seen from the above description, the transitions from states `NoScan` and `Scan`, $\pi_m(1,j)$ and $\pi_m(2,j)$, depend on the signal quality of the (current) serving cell, whereas transitions from states `CellSwitch` and `Fail`, $\pi_m(3,j)$ and $\pi_m(4,j)$, do not since they occur after the connection with the (current) serving cell was interrupted (in case of service failure) or was released (in case of cell switching). Therefore, it is useful to distinguish between two types of states as shown in Figure 10.4 where `CellSwitch` and `Fail` are grey-coloured. And it is also convenient to distinguish between two types of transitions which are shown as solid-line and dash-line connections. The solid-line connections are used for transitions which are a result of the signal quality of the current serving cell, while the dash-line connections are used for transitions which are not decided by the signal quality of the current serving cell.

As described above, the mobile only performs the handover measurement function when it is in state `Scan`. Two states `CellSwitch` and `Fail` are outcomes of the handover measurement. Moreover, the handover measurement is performed within one cell, i.e. within the current serving cell. It does not involve transitions which occur out of the current serving cell. As a result, `CellSwitch` and `Fail` are absorbing states, and the state diagram of the handover measurement is obtained from Figure 10.4 by excluding dash-line transitions as given in Figure 10.5. Thereby,
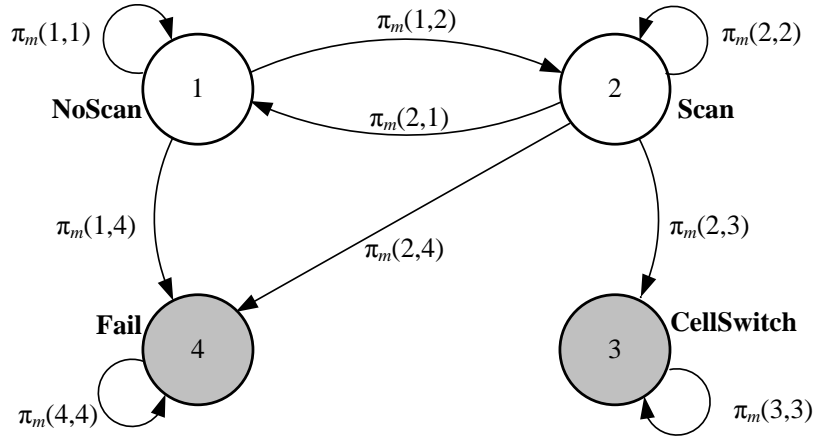
FIGURE 10.5: State diagram of the mobile in handover measurement

the transition matrix of the handover measurement is given by

$$\mathbf{M}_m = \begin{pmatrix} \pi_m(1,1) & \pi_m(1,2) & 0 & \pi_m(1,4) \\ \pi_m(2,1) & \pi_m(2,2) & \pi_m(2,3) & \pi_m(2,4) \\ 0 & 0 & 1 & 0 \\ 0 & 0 & 0 & 1 \end{pmatrix}. \tag{10.5.6}$$

Let $\mathbf{M}^m = \mathbf{M}_1 \times \mathbf{M}_2 \times \cdots \times \mathbf{M}_m$. $\mathbf{M}^m(i,j)$ is the transition probability of the handover measurement from state i at moment 0 to state j at moment m.

10.6 Performance Metrics of HO Measurement

By the above discussion, a handover measurement can have two outcomes which are *failure* if a service failure occurs during the handover measurement, and *success* if a suitable handover target found. Let D be the time duration during which a mobile has an active connection with one cell. Let $L = \lceil D/T_{\mathrm{meas}} \rceil$, where $\lceil x \rceil$ gives the smallest integer greater than real number x. The variable L is the number of measurement periods that a mobile carries out during its connected mode within one cell. Hence, the probability of *handover measurement failure*, denoted by $\mathcal{F}$, is given as

$$\mathcal{F} = \mathbf{M}^L(2,4),$$

and the probability of *handover measurement success*, denoted by $\mathcal{S}$ is

$$\mathcal{S} = \mathbf{M}^L(2,3),$$

It is clear that $\mathcal{F}$ and $\mathcal{S}$ are functions of all parameters including the terminal's measurement capability k, system specification T_{meas}, control parameters γ_{t}, τ_{t}, γ_{w}, and τ_{w}, as well as requirements γ_{req}, γ_{min}, and τ_{min}. Note that the duration D can be studied as a deterministic constant or as a random variable. In the latter case, the above metrics should be given accordingly as

$$\mathcal{F} = \int_0^\infty \mathbf{M}^{\lceil t/T_{\mathrm{meas}} \rceil}(2,4) F_D(\mathrm{d}t),$$

$$\mathcal{S} = \int_0^\infty \mathbf{M}^{\lceil t/T_{\text{meas}} \rceil}(2,3) F_D(\mathrm{d}t),$$

where F_D is the distribution of D which is often assumed an exponential distribution. Intuitively, $\mathcal{F}$ represents the probability that a service failure occurs before a suitable cell is identified, and $\mathcal{S}$ indicates the probability that the system enters into the handover decision-execution phase. It is desirable to minimise $\mathcal{F}$ and to maximise $\mathcal{S}$. In particular, one can enhance $\mathcal{S}$ by increasing the transition probability $\pi_m(2,3)$, which is in turn achievable by setting low handover target required level γ_{req}. However, this results in handover targets with low signal quality. Therefore, it is necessary to assess the target cell quality when the handover measurement is in success. Since a suitable target cell is given by the best cell among k cells scanned and provided that its signal quality is better than γ_{req}, the expectation of the resulting signal quality is thus given as

$$\mathbf{E}\{Y_k|Y_k \geq \gamma_{\text{req}}\} = \gamma_{\text{req}} + \int_{\gamma_{\text{req}}}^\infty \frac{\overline{F}_{Y_k}(y)\mathrm{d}y}{\overline{F}_{Y_k}(\gamma_{\text{req}})},$$

with tail distribution $\overline{F}_{Y_k}$ of Y_k. Hence, the performance of the handover measurement is also measurable by the *target cell quality* defined as

$$\mathcal{Q} = \mathcal{S} \times \mathbf{E}\{Y_k|Y_k \geq \gamma_{\text{req}}\}.$$

10.7 Application to LTE Handover Measurement

Using the above framework, we investigate the handover measurement in LTE, in particular we study the impact of the mobile's measurement capability k on the system performance. As described in Chapter 4, a User Equipment (UE) in a LTE network measures neighbouring cells as soon as it enters in connected-mode. This setting corresponds to triggering level and withdrawal level set to infinity, $\gamma_{\text{t}} = +\infty$, and $\gamma_{\text{w}} = +\infty$, so that $\mathbf{P}\{wdraw_m\} = 0$ according to the scanning withdrawal formulated in (10.3.5), and that

$$\mathbf{P}(trig_m) = 1 - \mathbf{P}(fail_m)$$

according to (10.4.14) for all m. This leads to $\pi_m(1,1) = 0$ according to (10.5.1). The transition matrix of the LTE handover measurement thus reduces to

$$\mathbf{M}_m = \begin{pmatrix} 0 & \pi_m(1,2) & 0 & \pi_m(1,4) \\ 0 & \pi_m(2,2) & \pi_m(2,3) & \pi_m(2,4) \\ 0 & 0 & 1 & 0 \\ 0 & 0 & 0 & 1 \end{pmatrix}.$$

Hence, for an integer $L \geq 1$, we can easily obtain

$$\mathcal{F} = \mathbf{M}^L(2,4) = \sum_{m=1}^L \left(\pi_m(2,4) \prod_{i=1}^{m-1} \pi_i(2,2) \right).$$

$$\mathcal{S} = \mathbf{M}^L(2,3) = \sum_{m=1}^L \left(\pi_m(2,3) \prod_{i=1}^{m-1} \pi_i(2,2) \right).$$

TABLE 10.1: Evaluation parameters

	Parameter	Assumption
Scenario	Environment	Urban macro cell
	Path loss (d in m)	$L(d) = 15.3 + 37.6 \log_{10} d$
	User's velocity	$v = 10$ m/s
BS	Transmission power	$P_{\text{BS}} = 43$ dBm
	Antenna pattern	Omnidirectional
	Cell radius	$R = 700$ m
Shadowing	Standard deviation	$\sigma_Z = 10$ dB
	Decorr. distance	$d_c = 50$ m
Noise	Noise density	$= -174$ dBm/Hz
	UE noise figure	$N_{\text{F}} = 9$ dB
Service	Min outage duration	$\tau_{\min} = 200$ ms
	Min allowable level	$\gamma_{\min} = -20$ to -5 dB
Measurement	Measurement period	$T_{\text{meas}} = 200$ ms
	Handover margin	$\Delta_{\text{HO}} = 2$ dB
	Required threshold	$\gamma_{\text{req}} = \gamma_{\min} + \Delta_{\text{HO}}$
	Triggering level	$\gamma_{\text{t}} = +\infty$
	Withdrawal level	$\gamma_{\text{w}} = +\infty$

Since the LTE standard assumes that UEs perform the handover measurement autonomously using 504 physical cell identifiers (PCIs) without need of a neighbour cell list, see §3.3, the probability of finding a suitable handover target $\mathbf{P}(\mathit{findtarget}_m(k))$ is given by (10.4.4) with retention probability $\rho_k = k/N_{\text{CSID}}$ where $N_{\text{CSID}} = 504$.

10.7.1   Evaluation Scenario

System parameters are summarised in Table 10.1 following 3GPP recommendations provided in 3GPP TR 36.942 [26], 3GPP TS 36.133 [47] for an urban macro cellular deployment of LTE networks. The network density λ is set for simulation corresponding to hexagonal cellular layout of 3GPP's standard scenario so that $\lambda = 2/(3\sqrt{3}R^2)$ BS/m². In lognormal shadowing, the autocorrelation proposed in the literature as described in §5.3.2 is used

$$R_Z(\tau) = \sigma_Z^2 \exp\left(-\frac{1}{2}\left(\frac{v\tau}{d_c}\right)^2\right),$$

where v is the user's velocity, and d_c is the decorrelation distance. This model satisfies conditions required in §10.2. Its second spectral λ_2 is given by

$$\lambda_2 = -R_Z''(\tau)|_{(\tau=0)} = (\sigma_Z v/d_c)^2.$$

The minimum allowable level $\gamma_{\min}$ and minimum-outage duration $\tau_{\min}$ were set according to the condition of a *radio link failure* specified by LTE standard. As described in "Radio Link Failure" in §3.3, when the downlink radio link quality estimated over the last 200 ms period becomes worse than a threshold Qout, Layer 1 of the UE shall send an *out-of-sync* indication to higher layers. Upon receiving N310 consecutive *out-of-sync* indications from Layer 1, the UE

will start timer T310. And upon the expiry of this timer, the UE considers radio link failure to be detected. It can be consequently concluded that a radio link failure occurs if the signal quality of the serving cell is worse than $\gamma_{\min} = \text{Qout}$ during at least

$$\tau_{\min} = 200[\text{ms}] \cdot \text{N310} + \text{T310}.$$

Following parameters specified in 3GPP TS 36.133 [47, §A.6], N310 = 1 and T310 = 0. This yields $\tau_{\min} = 200$ ms. The threshold Qout is defined in 3GPP TS 36.133 [47, §7.6.1] as the level at which the downlink radio link cannot be reliably received and corresponds to 10% block error rate of Physical Downlink Control CHannel (PDCCH). From 3GPP TR 36.942 [26, §A.2], Qout is as small as -10 dB. In simulation, some more settings of $\gamma_{\min}$ were evaluated as summarised in Table 10.1.

LTE uses two policies with *relative* and *absolute* requirements to control the handover measurement as specified in 3GPP TS 36.331 [101] and summarised in Table 3.4. These two policies were investigated in our numerical evaluation. In the former, γ_{req} is required to be higher than the minimum tolerable level $\gamma_{\min}$ by a handover margin Δ_{HO} such that $\gamma_{\text{req}} = \gamma_{\min} + \Delta_{\text{HO}}$. In the latter, γ_{req} is on a fixed absolute level.

Regarding user's mobility, we considered 100 mobile users in the serving cell and each of them moves away from the serving BS at velocity v in a random direction generated according to a uniform distribution on $(-\pi, \pi]$. This scenario has been considered as the most critical circumstance 3GPP TR 36.942 [26] and WiMAX Forum [27].

10.7.2   Result

A computer simulation was built with the above parameter setting in order to check the accuracy of the models developed in §10.4. The interference field was generated according to a Poisson point process with intensity λ in a 100 km^2 region, and the serving base station is located at the center of this region. The auto-correlated shadowing was generated as the output of an infinite impulse response filter with input Gaussian noise of standard deviation σ_Z.
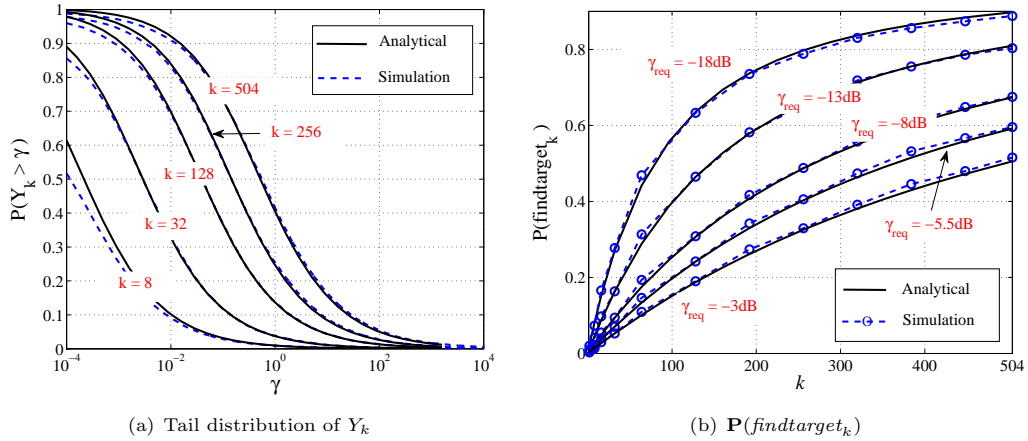

(a) Tail distribution of Y_k

(b) $\mathbf{P}(\mathit{findtarget}_k)$

FIGURE 10.6: Analytical expression against simulation result of $\overline{F}_k$
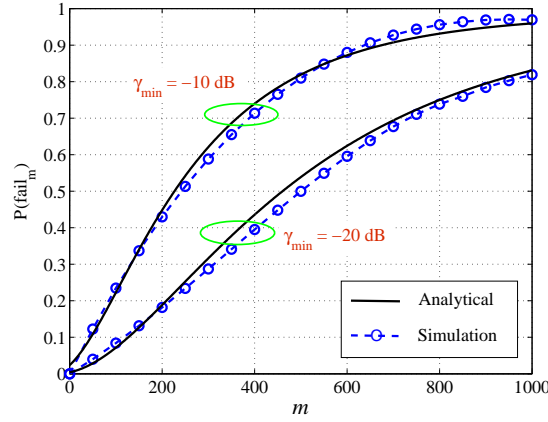
FIGURE 10.7: Validation of level crossing analysis

(a) Under *relative* threshold: $\gamma_{\mathrm{req}} = \gamma_{\min} + \Delta_{\mathrm{HO}}$ (b) Under *absolute* threshold: $\gamma_{\min} = -20$ dB
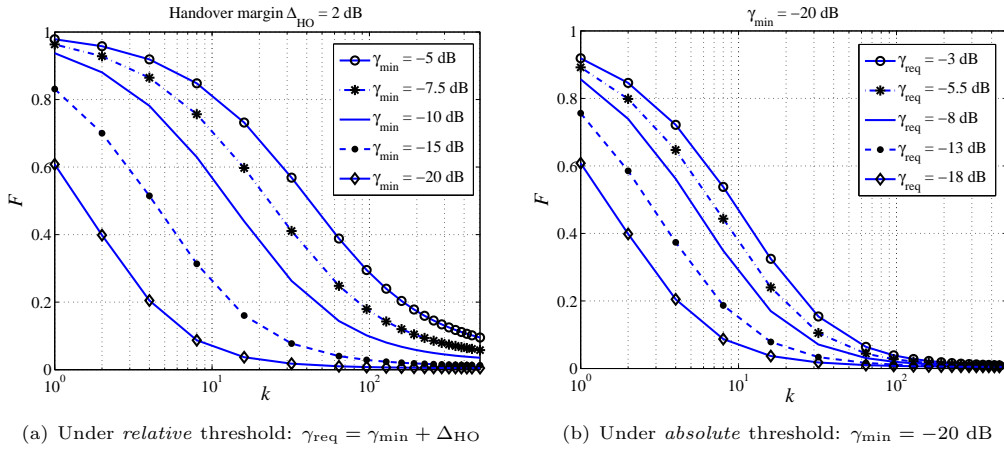
FIGURE 10.8: Handover measurement failure probability $\mathcal{F}$

First, Figure 10.6 verifies our analytical model against computer simulation. Figure 10.6(a) plots the tail distribution of the best signal quality $\overline{F}_{Y_k}$ of (10.4.4), which corresponds to common LTE setting described above, and Figure 10.6(b) plots the probability of suitable target found $\mathbf{P}(findtarget_m(k))$ obtained from the corresponding tail distribution $\overline{F}_{Y_k}$. The agreement of the proposed analytical results with simulation illustrates the accuracy of modelling the best signal quality Y_k defined in (10.3.2) by the maximum of SINRs received from the thinning S_k proposed in (10.4.2).

Figure 10.7 checks the analytical framework based on level crossing analysis which was used to derive the probabilities of service failure, scanning triggering, and scanning withdrawal. Results show that both the analytical model and the simulation provide agreed results of the probability of service failure $\mathbf{P}(fail_m)$ in both settings.

With the accuracy provided by the proposed analytical framework, we investigate numerical results of the defined performance metrics. Figure 10.8 indicates that high measurement capability k reduces the handover measurement failure probability $\mathcal{F}$. It also indicates the dependence of $\mathcal{F}$ on the minimum tolerable level $\gamma_{\min}$ and on the handover target required level γ_{req}, respectively. Comparing Figure 10.8(b) and Figure 10.8(a), absolute requirement policy shows better robustness than relative requirement policy to different system configurations. This is explained

(a) Under *relative* threshold, $\gamma_{\text{req}} = \gamma_{\text{min}} + \Delta_{\text{HO}}$

(b) Under *absolute* threshold, $\gamma_{\text{min}} = -20$ dB
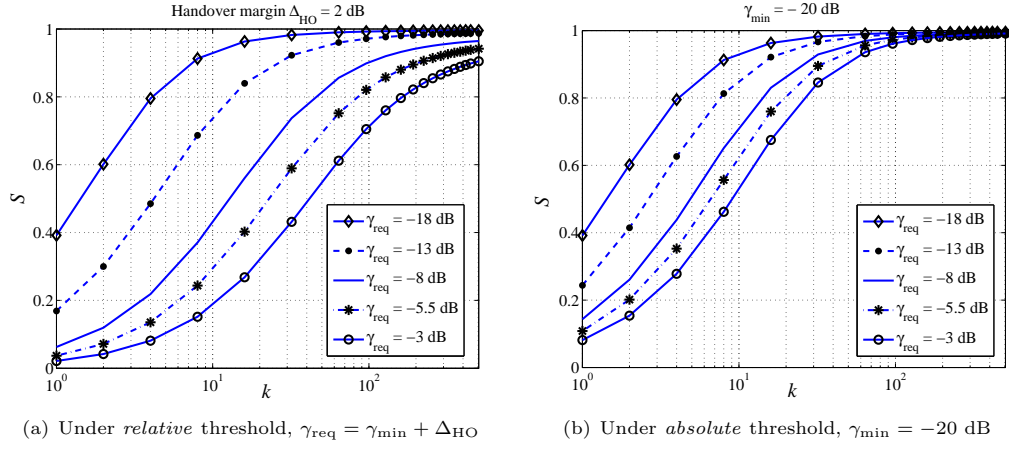
FIGURE 10.9: Handover measurement success probability $\mathcal{S}$
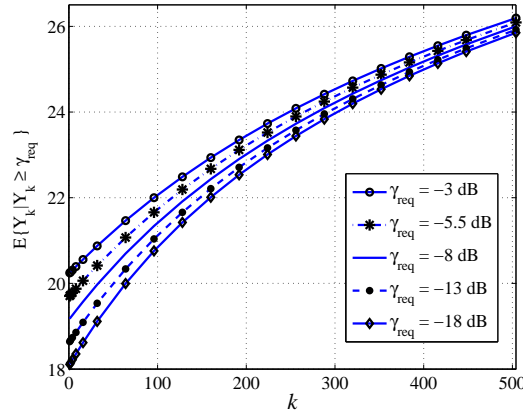
FIGURE 10.10: Plots of $\mathbf{E}\{Y_k | Y_k \geq \gamma_{\text{req}}\}$.

by a fixed lower minimum tolerable level γ_{min} used in the absolute requirement policy than that used in the relative requirement policy. Figure 10.8(b) shows that increasing the measurement capability k to the order of 10^2 improves the performance very marginally. Besides, we can see that the current LTE requirement of the UE's measurement capability with $k = 8$ is insufficient for reliable handover measurement performance (here LTE does not use a pre-defined neighbour cell list).

Low handover target required level γ_{req} reduces the handover measurement failure $\mathcal{F}$, c.f. Figure 10.8, and improves the handover measurement success $\mathcal{S}$, c.f. Figure 10.9. However, lower γ_{req} reduces the resulting signal quality of the target cell $\mathbf{E}\{Y_k | Y_k \geq \gamma_{\text{req}}\}$ as shown by Figure 10.10. Figure 10.11 presents the combining results of these two effects on the target cell signal quality $\mathcal{Q}$. In Figure 10.11(a) which plots the target cell quality $\mathcal{Q}$ under the relative requirement scheme, lower minimum tolerable level γ_{min} (and so lower γ_{req}) always results in higher target cell quality $\mathcal{Q}$. On the other hand, Figure 10.11(b) shows a crossing point between the curves when the measurement capability k is in-between 10 and 16 under the absolute requirement scheme, in which given large k, the target cell quality $\mathcal{Q}$ can be generally enhanced by higher handover target required level γ_{req}. However, for small measurement capability k, it is better to maintain low γ_{req}. Figure 10.11 helps the network operator appropriately setting

(a) Under *relative* threshold (b) Under *absolute* threshold
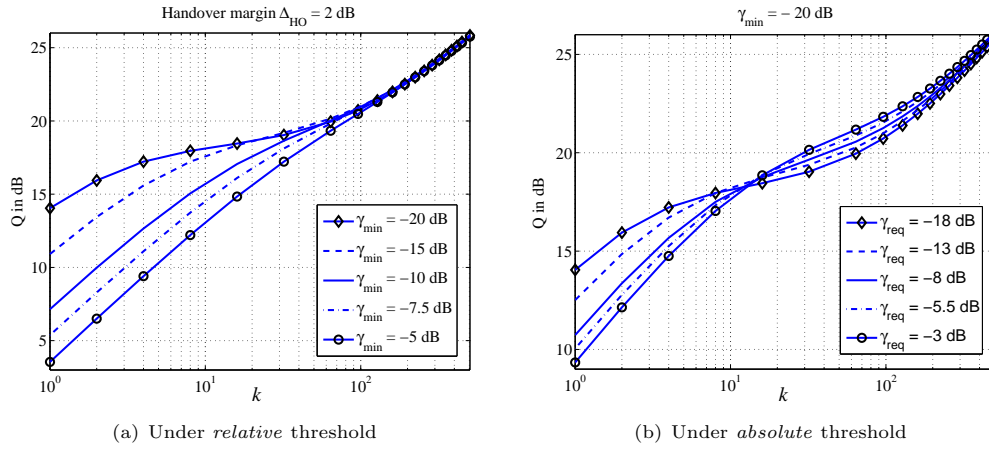
FIGURE 10.11: Asymptotic target cell quality $\mathcal{Q}$

the handover target required level γ_{req} according to the UE's measurement capability so as to obtain the best performance.

10.8   Concluding Remarks

We investigated the handover measurement in a mobile cellular network with fundamental establishment in the probabilistic aspects and system modelling. A handover measurement is basically characterised by four key probabilistic events including (i) suitable handover target found, (ii) service failure, (iii) scanning triggering, and (iv) scanning withdrawal. Using the mathematical results developed in previous chapters, we were able to derive the probability of these key events in a multicell system. In particular, (ii)-(iv) were formulated as minimum-duration outage of the SINR, and were derived under interference-limited condition which are in fact more general and realistic and can cover the commonly used instantaneous SINR outage as special case.

The operation of handover measurement can be modelled by a state diagram which is able to describe the temporal evolution of the handover measurement as well as the system dynamics in terms of user's mobility and autocorrelated shadowing. This generalised framework provides analytical insights into the unified influence of the control parameters to the system performance in terms of service failure, handover measurement success (equivalent to handover probability), as well as the quality of handover target.

We also investigated an application of the above framework to the handover measurement in LTE. Results indicated that the LTE's current requirement for UE measurement capability with $k = 8$ seems insufficient for reliable handover measurement performance without using a neighbour cell list. More applications of the frameworks to other systems such as WiMAX are reserved for a future work.

Chapter 11

Autonomous Cell Scanning For Data Small Cell Networks

11.1 Introduction

Motivation of data small cell networks. By the early 1990's, the second generation of cellular networks which uses digital communications greatly enhanced the network capacity and reduced the power consumption of the mobile handset, see Chapter 3. This substantially reduced the communication cost and more importantly made the mobile telephone service explosively accessible to the main-stream mobile market all over the world. Nonetheless, in parallel with the success of the second cellular network generation in providing high quality mobile voice service, the Internet with wireline broadband access has shown its great advantage compared to mobile communication in bringing the end users very enriching information communication services including rich Web, data transfers, and multimedia services. This has introduced the mobile communication networking a big challenge of significantly increasing the network capacity to provide the end users with wireline broadband-equivalent services over the mobile communication. Moreover, the strong competition of the telecommunications industry has lead to declining *average revenue per user* (ARPU) of voice service overtime [187, 188], as well as it has required network operators to enable more and more data applications. These all have created an endless operator-push user-pull game where the operators need to continually introduce new broadband wireless services to satisfy the users who continue to express higher demands.

Besides, the tremendous growth of the Internet with business models basing on it have introduced more and more applications which are mostly throughput-greedy and need frequent updates from the end user such as online multimedia services, YouTube, eBay, and Facebook. Paradoxically, the (wireline broadband) Internet is not able to satisfy this high frequent update requirement due to its nature of wired connection. As a result, there has been high demand from the end users for anytime and anywhere available mobile coverage service.

Today's macro cellular systems have become saturated in capacity, though installing a new macro base station is more and more difficult due to various problems from installation agreement acquisition, regulation, to technical reasons. Also due to the difficulty in installing a new macro base station, today mobile cellular networks is not yet able to provide 100%-coverage, and this

generally results in potential coverage holes and dead zones. Therefore, a new network design / architecture is critically required for the mobile networking so as to be able to provide high capacity as well as ubiquitous mobile service.

To enhance network capacity and satisfy user demand of broadband services, it is known that [189–193]

> *Reducing cell size is one of the most effective approaches to improve the network capacity and coverage.*

On the other hand, a small cell only needs lightweight antennas. It helps to replace bulky roof top base stations by small boxes set on building facade, on public furniture or indoor. Small cells can even be installed by end users (e.g. femtocells, see §3.2). This greatly facilitates the network deployment. The small cell network architecture is therefore truly promising to enhance the network capacity as well as to effectively cope with coverage holes [193, 194].

Pervasive small cell networks have shown a great potential. For example, Willcom has deployed small cell systems in Japan [195], and Vodafone has recently launched home 3G femtocell networks in the UK in 2009 [196]. The proven business opportunity of small cell networking has attracted the attention of industry, research community, as well as standardisation bodies. For this reason, the standardisation of small cell networks is being supported by 3GPP from the basis of its advancement in Home NodeB (for WCDMA) and Home eNodeB (for LTE) specification [197], some specification series include 3GPP TS 36.300 [6], 3GPP TR 32.821 [198], 3GPP TS 25.467 [199], 3GPP TS 22.220 [200].

Challenges of small cell networking. It can be immediately observed that reducing cell size to increase the spatial reuse for supporting dense traffic will induce a large number of cells in the same geographical area. Secondly, end users can set up small cells by their own means [2, 188]. This makes small cell locations and coverage areas more random and unpredictable than traditional mobile cellular networks. Therefore,

> *High-density and randomness are the two basic characteristics of small cell networks.*

The above characteristics have introduced technical challenges that require new studies beyond those for macro and micro cellular networks. The main issues concern spectrum sharing and interference mitigation, capacity analysis, network self-organisation, and mobility management [2, 192, 193]. Among those technical concerns, it is realised that [2, Chapter 7]

> *Mobility management is one of the most challenging issues of small cell networking.*

Following existing cellular network standards, it is expected that small cell networking will also use mobile-assisted handover without need of specific mobility management mechanism. However, due to the aforementioned characteristics of high-density and randomness, the real implementation will involve many questions since current assumptions made for macro cell networks should be not valid. In particular, the configuration of neighbour cell list will not scale anymore to support a large number of small cells which are potentially neighbouring to a cell [201] and even more whose location is quite dynamic. In addition, it is believed that small cells may be added / removed or powered on / off frequently [192] for the network capacity and power

saving purposes. This requires quick adaptation of the neighbour cell list which will generate much expenses. Therefore, using neighbor cell list is not an effective solution for the mobility management in small cell networks.

Proposed solution. As we have seen in Chapter 4, wideband technologies such as WCDMA, WiMAX, and LTE use a set of cell synchronisation identities (CSID) which help a mobile identify cells in the air interface so as to measure the cell's radio condition. There are 512 primary scrambling codes (PSC) in WCDMA, 114 pseudo-noise (PN) sequences in WiMAX, and 504 physical cell identities (PCI) in LTE. By using a predefined set of codes, these wideband technologies can support more autonomous cell measurement conducted by the mobile, for example in WCDMA and LTE networks the mobile performs intra-frequency cell measurement without explicit control from the network. Besides, in a small cell network where a large number of cells are deployed in a geographical area, it is highly probable that the mobile receives strong pilot signal from many cells such that it can identify and measure those cells. These capabilities are enabling factors by which

We propose and study autonomous cell scanning for the mobility
management in dense small cell networks.

Under this scheme, the mobile simply conducts a scanning of a number of cells whose CSIDs are randomly selected with equal probability from the whole CSID set of the underlying cellular standard. The cell which has the best signal quality among those scanned is then selected at the handover target. This autonomous scanning scheme is able to simplify the network configuration and operation by avoiding the configuration of the conventional neighbor cell list.

Further, we show that the autonomous scanning is subject to an optimisation problem in which the number of cells to be scanned is a necessary tradeoff parameter to maximise the user's data throughput. Using the theoretical result developed in Chapter 8 for the distribution of the best signal quality in a dense network, we investigate this optimisation problem. Evaluation results show that under a common scenario of small cell networks, performing autonomous scanning with 30 cells is effective.

11.2 Autonomous Cell Scanning

In §11.1 we have seen that broadband cellular systems and high-density characteristic of small cell networks are an enabler for autonomous cell scanning. In fact, the mobile is able to identify and then measure a neighbour cell if it is provided a priori the cell synchronisation identity (CSID), and if the cell pilot signal is strong enough, see Chapter 4. In the current cellular standards, there are only 512 CSIDs (i.e. primary scrambling codes) in WCDMA, 504 CSIDs (i.e. physical cell identities) in LTE, and 114 CSIDs (i.e. pseudo noise sequences) in WiMAX shared within the network. Since there is a large number of cells within a limited area, it is very likely that a mobile will be able to scan a neighbour cell regardless of which CSID has been selected out from the whole set. As a result, the proposed autonomous cell scanning is as follows:

(1) When a mobile gets admitted to the network, the first serving cell provides the mobile the whole set of CSIDs used in the network. The mobile then keeps this information in its memory.

(2) To find a handover target, the mobile randomly selects a set of n CSIDs from its memory and conducts the standardised scanning procedure of the underlying cellular system.

(3) The mobile finally selects the cell with the *best* received signal quality as the handover target.

To perform this simple scanning scheme, the mobile needs to be specified how many cells it should scan. In the next sections, we will analyze how the number of cells to be scanned n impacts the user's quality of service so as to determine an optimal number of cells to be scanned.

11.3   Network Assumption

The randomness of small cell locations should be suitably modelled by a Poisson point process, see §6.2 in Chapter 2. On the other hand, regarding the concluding remarks of Chapter 8, the asymptotic properties of the wireless link signal quality developed therein should be effective for dense systems like small cell networks. In light of that, we follow the network assumptions and use theoretical tools developed in Chapter 8 to study the autonomous cell scanning with the following precisions. Firstly, it is assumed that the mobile is able to synchronise and scan any cell located in a disk-shaped network area B centered at the user with radius R_B such that $0 < R_B < \infty$. The attenuation of the radio signal strength is due to lognormal shadowing and bounded distance-dependent path loss as given in Chapter 8 such that the signal strength received from a cell i is:

$$P_i = A\, X_i \, (\max\{d_i, R_{\min}\})^{-\beta},$$

where $R_{\min}$ is a strictly positive constant, $R_{\min} > 0$, and $X_i = 10^{Z_i/10}$ with Z_i being a normal random variable of zero mean and standard deviation σ_Z. The random variable

$$Y_n = \max_{i=1,\mathbf{x}_i \in B}^{n} Q_i$$

as defined in Chapter 8 will be used to refer to the best signal quality received from n cells located in the network area B.

It is assumed that the mobile may follow a scanning procedure either *with* or *without* measurement gap depending on the underlying cellular standard, see Figure 4.1 in §4.1. Denote by s the time duration needed to scan one neighbour cell. For the case where the underlying technology allows the mobile scanning k cells in parallel during a certain measurement period T_{meas}, see §4.1, we will prefer to use the *equivalent* scanning time such that $s = T_{\mathrm{meas}}/k$ for the merit that the impact of the number of cells to be scanned n will be better observed.

11.4   Optimisation Problem

The optimisation problem has to take into account the two contrary effects due to the number of cells to be scanned. On one hand, the more number of cells to be scanned, the better is the signal quality of the best cell, and hence the better the data throughput obtained by the mobile user. On the other hand, scanning can have a linear cost in the number of scanned cells, which is detrimental to the throughput obtained by the mobile. Let us quantify these two effects using the notation and tools previously developed in Chapter 8. Let W be the average cell bandwidth

available per mobile and assume that it is a constant. Under the assumption of additive white Gaussian noise channel, the maximum capacity C_n that the mobile can achieve by selecting the best among n randomly scanned cells is

$$C_n = W \log(1 + Y_n). \tag{11.4.1}$$

Hence

$$\mathbf{E}C_n = W\mathbf{E}\{\log(1 + Y_n)\} = W \int_{\gamma=0}^{\infty} \log(1 + \gamma) f_{Y_n}(\gamma) \mathrm{d}\gamma,$$

where f_{Y_n} is the density of Y_n. Using a simple integration by parts of $\log(1 + \gamma)$ and $f_{Y_n}(\gamma)\mathrm{d}\gamma = -\mathrm{d}\overline{F}_{Y_n}(\gamma)$, this reduces to

$$\mathbf{E}C_n = W \int_{\gamma=0}^{\infty} \frac{\overline{F}_{Y_n}(\gamma)}{1 + \gamma} \mathrm{d}\gamma,$$

where the tail distribution function $\overline{F}_{Y_n}$ of Y_n. Under the above network assumption, $\overline{F}_{Y_n}$ is given by Theorem 8.6.1 in Chapter 8.

Note that $\mathbf{E}C_n$ is the expected throughput from the best cell. Since Y_n is the maximum signal quality of the n cells, Y_n increases with n and so does C_n. Hence, the mobile should scan as many cells as possible. However, on the other hand, if scanning many cells, the mobile will consume much time in scanning and thus have less time for data transmission with the serving cell. A typical situation is that where the scanning time increases proportionally with the number of cells scanned and where the data transmission is suspended. This for instance happens if the underlying cellular technology uses a *scanning with measurement gap* mechanism as described in §4.1 of Chapter 4. Another scenario is that of *scanning without measurement gap* which is also described in Chapter 4: here scanning can be performed in parallel to data transmission so that no transmission gap occurs.

Let T_{data} be the average time during which the mobile stays in the tagged cell and receives data from it. Let $T_{\mathrm{gap}}(n)$ be the duration of the suspension of data transmission due to the gap introduced by scanning n cells, referring to Figure 4.1 we have

$$T_{\mathrm{gap}}(n) = \begin{cases} s \times n & \text{if scanning } with \text{ measurement gap,} \\ 0 & \text{if scanning } without \text{ measurement gap.} \end{cases} \tag{11.4.2}$$

Finally, let $\mathbf{E}C_0$ be the average throughput received from the serving cell when no scanning at all is performed (this would be the case if the mobile would pick as serving cell one of the cells at random). The gain of scanning n cells can be quantified by the following metric, that we will call the *acceleration*:

$$\begin{aligned} \rho_n \quad &\triangleq \quad \frac{T_{\mathrm{data}} \cdot \mathbf{E}C_n}{T_{\mathrm{data}} \cdot \mathbf{E}C_0 + T_{\mathrm{gap}}(n) \cdot \mathbf{E}C_0} \\ &= \quad \frac{T_{\mathrm{data}}}{T_{\mathrm{data}} + T_{\mathrm{gap}}(n)} \times \frac{\mathbf{E}C_n}{\mathbf{E}C_0}. \end{aligned} \tag{11.4.3}$$

In this definition, $T_{\mathrm{data}} \cdot \mathbf{E}C_n$ (resp. $T_{\mathrm{data}} \cdot \mathbf{E}C_0 + T_{\mathrm{gap}}(n) \cdot \mathbf{E}C_0$)) is the expected amount of data transmitted when scanning n cells (resp. doing no scanning at all). We aim at finding the value of n that maximises the acceleration ρ_n.

It is clear that $T_{\mathrm{data}}/(T_{\mathrm{data}} + T_{\mathrm{gap}}(n)) = 1$ when (i) $T_{\mathrm{data}} \to \infty$, i.e., the mobile stays in and receives data from the tagged cell forever, or (ii) $T_{\mathrm{gap}}(n) = 0$, i.e., scanning without measurement

gap. In these cases, ρ_n increases with n and the mobile "should" scan as many cells as possible. However, ρ_n is often concave and the reward of scanning then decreases. To characterise this, we introduce a *growth factor g* defined as follows:

$$g_n \triangleq \frac{\rho_n}{\rho_{n-1}} = \frac{T_{\text{data}} + T_{\text{gap}}(n-1)}{T_{\text{data}} + T_{\text{gap}}(n)} \times \frac{\mathbf{E}C_n}{\mathbf{E}\{C_{n-1}\}}. \tag{11.4.4}$$

Special cases as those considered above can be cast within a general framework which consists in finding the value of n that maximises ρ_n under the constraint that $g_n \geq 1 + \Delta_g$, where $\Delta_g > 0$ is a threshold.

11.5   Result

In the following, we show how to apply the above results to find the optimal n. We adopt system parameters of WCDMA standard for the evaluation purpose. Parameters are summarised in Table 11.1. One hundred omni-directional small cell base stations are deployed in a square domain of 1 km $\times$ 1 km. The network density is thus equal to:

$$\lambda = 10^{-4} \text{ small base stations/m}^2.$$

It is assumed that any cell synchronisation identifier can be found in a radius $R_B = 1$ km. We take $R_{\min}$ equal to 2 metres. The propagation path loss is based on by the picocell path loss model recommended by ETSI TR 101.112 [202]:

$$l_{[\text{dB}]}(d) = 37 + 30 \log_{10}(\max\{d, R_{\min}\}) + 18.3 f^{(\frac{f+2}{f+1} - 0.46)},$$

where d is the distance from the base station in metres, f the number of penetrated floors in the propagation path. For indoor office environments, $f = 4$ is the default value [27]; however, here, the small cell network is assumed to be deployed in a general domain including outdoor urban areas where there are less penetrated walls and floors. So, we use $f = 3$ in our numerical study. So, the fixed-term path loss is:

$$L_{0,\text{dB}} = 37 + 18.3 f^{(\frac{f+2}{f+1} - 0.46)}.$$

It is assumed that the total transmission power including the antenna gain of each small cell base station is $P_{\text{tx,dB}} = 2$ dB. So, the path loss exponent β and parameter A are respectively given by according to (2.1.10) and (6.1.1) as follows:

$$\beta = 3, \quad \text{and} \quad A_{\text{dB}} = P_{\text{tx,dB}} - L_{0,\text{dB}} - N_{0,\text{dB}},$$

where the received noise power N_0 at the mobile reception antenna is computed with the effective bandwidth $W = 3.84 \times 10^6$ Hz, ambiance temperature $T_0 = 290$ K which results in noise density of -174 dBm/Hz, and noise figure at the terminal $N_{\text{F,dB}} = 7$ dB.

Finally, shadowing is modelled as a random variable with lognormal distribution with an underlying Gaussian distribution of zero mean and 8 dB standard deviation. And it is assumed that the mobile is capable of scanning eight identified cells within 200 ms [105]. So, the average time needed to scan one cell is given by $s = 25$ ms.

TABLE 11.1: Evaluation parameters

Parameter	Assumption
Environment	Urban pico cell
Antenna pattern	Omnidirectional
Path loss	Outdoor pico pathloss
BS tx power	$P_{\text{tx}} = 2$ dB
Bounding distance	$R_{\min} = 2$ metres
Network density	$\lambda = 100/\text{km}^2$
Shadowing std. dev.	$\sigma_Z = 8$ dB
Bandwidth	$W = 3.84$ MHz
UE noise figure	$N_{\text{F}} = 7$ dB
Noise density	-174 dBm/Hz
Measurement scheme	*with* and *without* gaps
Measurement capability	8 cells / 200 ms
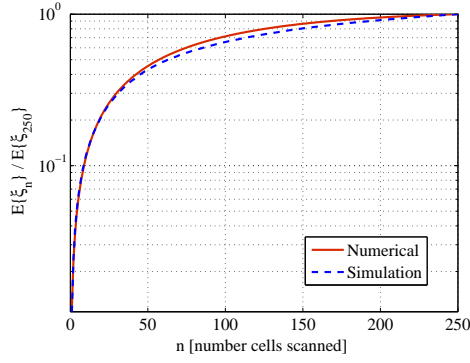
(a) Plot of $\frac{\mathbf{E}C_n}{\max_k \mathbf{E}\{C_k\}}$
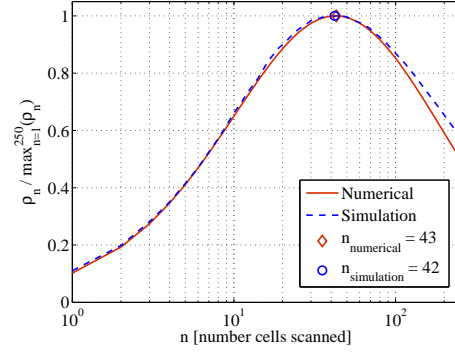
(b) Plot of $\frac{\rho_n}{\max_k \rho_k}$, $T_{\text{data}} = 0.5$ second
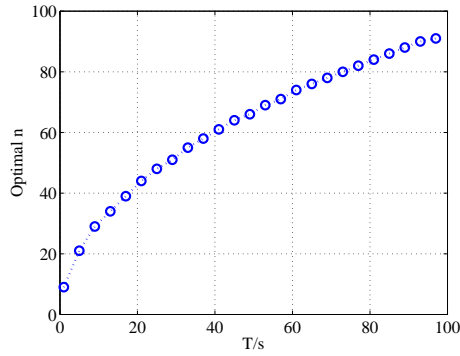
(c) Optimal number of cells to be scanned
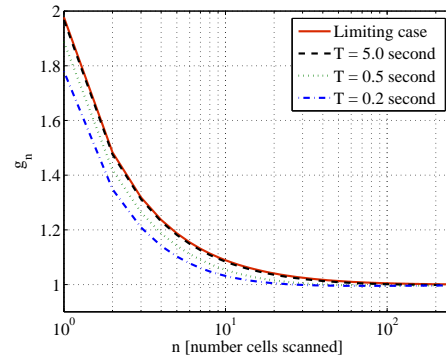
(d) Growth factor g_n under different T_{data}

FIGURE 11.1: Numerical results in the random cell scanning optimisation.

In order to check the accuracy of the approximations used in Chapter 8 for the tail distribution function $\overline{F}_{Y_n}$ of Y_n, a simulation was built with the above parameter setting. The interference field was generated according to a Poisson point process of intensity λ in a region of raidus $R_\infty = 100$ km. For a number n, the maximum of SINR received from n base stations which are randomly selected from the disk B of radius R_B was computed. After that, the expectation of

the maximal capacity $\mathbf{EC}_n$ received from the n selected BSs was evaluated.

In Figure 11.1(a), the expectation of the maximal throughput $\mathbf{EC}_n$ for different n is plotted, as obtained through the analytical model and simulation. The agreement between model and simulation is quite evident. As shown in Figure 11.1(a), $\mathbf{EC}_n$ increases with n, though the increasing rate is slow down as n increases. Note that in Figure 11.1(a), $\mathbf{EC}_n$ is plotted after normalisation by $\mathbf{E}\{C_{250}\}$.

Figure 11.1(b) gives an example of acceleration ρ_n for $T_{\text{data}} = 0.5$ second and $T_{\text{gap}}(n) = n \times 25$ ms. In the plot, ρ_n is normalised by its maximum. Here, an agreement between model and simulation is also obtained. We see that ρ_n first increases rapidly with n, attains its maximum at $n = 42$ by simulation and $n = 43$ by model, and then decays.

Next, using the model we compute the optimal number of cells to be scanned and the growth factor g_n for different T_{data}. Note that in (11.4.3), the factor $T_{\text{data}}/(T_{\text{data}} + T_{\text{gap}}(n))$ can be re-written as:

$$\frac{T_{\text{data}}}{T_{\text{data}} + T_{\text{gap}}(n)} = \frac{1}{1 + n \times s/T_{\text{data}}} \quad \text{for} \quad \begin{cases} T_{\text{data}} < \infty, \\ T_{\text{gap}}(n) = n \times s \end{cases} .$$

It is clear that this factor also depends on the ratio T_{data}/s. Figure 11.1(c) plots the optimal n for different values of T_{data}/s. Larger T_{data}/s will drive the optimal n towards larger values. Since T_{data} can be roughly estimated as the mobile residence time in a cell, which is proportional to the cell diameter divided by the user speed, this can be rephrased by stating that the faster the mobile, the smaller T_{data} and thus the fewer cells the mobile should scan.

Finally, Figure 11.1(d) plots the growth factor g_n with different T_{data}. In Figure 11.1(d), the "limiting case" corresponds to the case when $T_{\text{data}} \to \infty$ or $T_{\text{gap}}(n) = 0$. We see that g_n is quite stable with respect to the variation of T_{data}. Besides, g_n flattens out at about 30 cells for a wide range of T_{data}. Therefore, in practice this value can be taken as a recommended number of cells to be scanned in the system.

11.6   Concluding Remarks

The randomness and high-density characteristics of small cell networks require for new logic in implementation of the standardised mobility management mechanism. In this chapter, we propose *Autonomous Cell Scanning* which is preferable for underlying broadband cellular systems. This solution is desirable as firstly it avoids the conventional neighbour cell list which is known ineffective for dense small cell networks. And on the other hand this scheme is supported by our theoretical basis for an optimal network performance in term of the user's throughput. By numerical study with a common WCDMA system setting, it is suggested that a mobile should perform autonomous scanning with 30 cells to achieve effective performance. Additionally, simulation results demonstrate that the asymptotic properties developed in Chapter 8 provide a good degree of accuracy. We expect that this confirmation would encourage its future applications.

Chapter 12

Neighbour Cell List Self-Optimisation

12.1 Introduction

As we have seen from previous chapters, most of cellular standards use mobile-assisted network-controlled handover in which the mobile measures the pilot channel signal quality of neighbouring cells and reports the measurement result to the network. The network bases on the reported measurement result to initiate a handover to that cell (see, Chapter 4). To measure neighbouring cells, the mobile needs to be provided with information on the pilot channels of potential neighbouring cells (e.g., cell synchronisation information, pilot channel frequency). If this information is not provided by the network, the mobiles have to spend longer time to acquire it via scanning through all possibilities. Therefore, in today's commercial cellular networks (i.e. except LTE networks), a list of neighbouring cells as handover candidates is configured for each cell. This list contains information of the selected handover candidates and is sent to all mobiles connected to the cell. The mobiles then only need to monitor the pilot signal quality of the cells comprised in the neighbour cell list of the serving cell, see §4.2 in Chapter 4.

Therefore, the neighbour cell list has an important influence on the performance of the mobility management. It needs to contain a sufficiently large number of potential neighbouring cells to ensure that any mobile in the serving cell can find at least one handover target when its own signal deteriorates. However, as the mobile measurement capability is often limited, the mobile needs to cycle through neighbouring cells of the neighbour cell list. A long list thus firstly results in delays in finding a suitable handover target, resulting in call drops especially when the user moves at high speed as shown in Chapter 10. More importantly, when an averaging of several measurement epochs is required to filter out estimation errors and achieve higher estimation precision such as Layer 3 filtering (4.1.1) described in Chapter 4, cycling neighbouring cells of a long neighbour cell list results in long time separation between two successive measurements of the same neghbouring cell. This leads to less correlation between measurements, paradoxically resulting in low measurement accuracy [134]. This measurement error may cause call drops in the new serving cell immediately after the handover execution due bad prediction of its signal quality (This is described in Chapter 10 by transition $\pi_m(3,4)$ from state `CellSwitch` to state `Fail` of Figure 10.3).
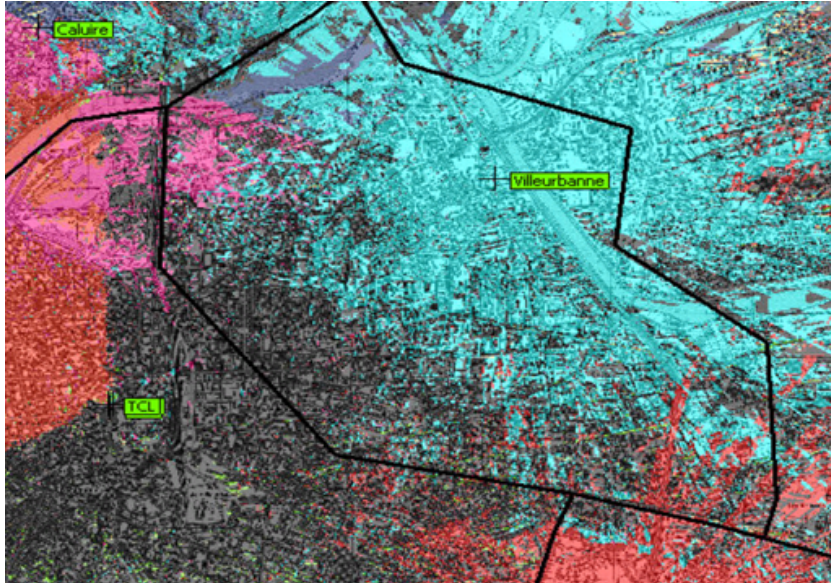
FIGURE 12.1: Example of cell coverage in Lyon city obtained by propagation simulation on actual 3D map.

While it might appear easy to configure a neighbour cell list by simply looking at the cell topology and selecting all cells overlapping with the cell of interest, it is not as straightforward in reality. This is mainly due to the fact that the real radio coverage is unknown, it depends strongly on the environment which can only be modelled to some degree in radio simulations. Although analytical models are able to obtain some mathematical generalisation of the radio environment by modelling propagation effects by probability laws, such as the modelling of shadowing by a lognormal distribution, they are hard to provide any certain information about the presence of buildings, trees, and moving objects, etc. in a precise area. And within a precise context, these unpredicted objects have strong effects on the coverage and may create coverage holes which results in high call dropping rate. Figure 12.1 gives an example of cell coverage in Lyon city, France, obtained from a best server map. In this example, cells are mapped to different colours, and we observe that cell layouts are far from hexagonal and that the overlap between cells creates numerous small coverage islands. Changes in the environment due to for example newly constructed buildings cannot easily be taken into account. Thus, an accurate prediction of the cell coverage is hard and also might not be valid anymore after some time.

Nowadays, the neighbour cell list is still manually configured at the beginning of the network deployment by means of planning tools, and is manually updated when new cells are installed. During this manual configuration the cell coverage and the neighbour relation are predicted using static information such base station locations, antenna patterns, and received signal maps (obtained through driver-tests). Due to the sensibility and the dynamic of the radio propagation condition, these static predictions of the cell coverage are more or less inaccurate [134], and cannot take into account changes in the radio conditions and indoor coverage. Therefore,

The manual configuration and optimisation of neighbour cell lists is a big every-day operator's concern

which requires a lot of efforts for the network operator, resulting in considerable operational expenses. Conceptually, a self-optimisation solution uses direct measurements of the actual radio

environment and network event statistics, it is thus capable of providing real cell coverage without generating operation expenses while being able to follow changes in the radio environment. Besides, using updated real cell coverage and event statistics allows a self-optimisation algorithm to generate effective neighbour cell lists which are short enough to enhance the measurement accuracy while remove unfavorable neighbouring cells [134]. A self-optimisation approach is hence able to overcome drawbacks and difficulties of the manual configuration. In light of that, the Next Generation Mobile Network (NGMN) alliance recently specified neighbour cell list self-optimisation as a required use-case [110], and described its benefits to the network operator [203].

The automatic configuration and dynamic optimisation of neighbour cell lists have therefore received a lot of attention of operators as well as industrial research centers. Prior works in this field as summarised in §4.3.3 contributed several valuable concepts, mostly the one for automatically configuring and optimising neighbour cell lists with field measurements despite some limitations in realising the concept which will be discussed here-below. Besides, the concept of using test frequencies to discover cells not currently comprised in the neighbour cell list is also helpful to the design of a self-optimisation solution. This concept will be used in our solution for the same purpose of cell discovery. Nevertheless, some important drawbacks in prior works did not allow for a true self-optimisation solution. It is clear that an effective formulation of the optimal neighbour cell list should be important in order to design appropriate optimisation solutions and algorithms. However, it was only addressed by Parodi et al. [138], whereas their definition of the optimal neighbour cell list would be not effective in reality. Therein, the best neighbour list is the one that comprises all and only all the actual neighbours which really overlap with the serving cell. It often happens in reality that there may be a large number of cells overlapping with the serving cell (as it was also realised by Soldani and Ore [137] which is summarised in §4.3.3). Thus, adding all the overlapping cells will create a very long list which can generate call droppings due to long scanning time and reduce the measurement accuracy [134]. Second, when realising the proposed concepts, the prior works mostly based on cell coverage prediction models and used static thresholds which limit the performance and the ability to adapt to dynamic changes in the radio environment.

A key element of the neighbour cell list configuration is reliable information on the cell coverage. In a real network, the best way to obtain accurate coverage information is to continuously perform measurements of the radio signals. The most efficient way to achieve this is to let the network entities such as mobile stations and base stations perform measurements during operation. In light of that,

We propose a measurement-based self-optimisation solution

which uses live measurements to *self-configure* the initial neighbour cell list, and to continuously *self-optimise* the neighbour cell list of a cell during operation. This chapter brings the following contributions:

- A complete optimisation procedure which self-configures an initial neighbour cell list and continuously self-optimises the neighbour cell list.
- An efficient method which does not generate additional overheads by using cell statistics measured by the base station for the initial self-configuration, and using the mobile-reported measurement, which is available by the standard requirement, for the self-optimisation.

- An efficient self-optimisation algorithm avoiding static constraints and computing the neighbour cell list from live measurements. It frees the operator from a manual collection of the network information (e.g. drive-tests), and allows the neighbour cell list adapting to dynamic changes in the network and its environment.

These contributions will be detailed in the following structure. Section 12.2 describes the concept of the proposed method consisting of a self-configuration phase for initialisation of the neighbour cell list followed by an ongoing self-optimisation process. The self-configuration method used for initialisation is described in §12.3. Therein, neighbours are identified and measured at the serving base station by using the existing antenna gain of the serving base station. Then, a predefined number of neighbours with the best received pilot signal quality are selected as the initial neighbour cell list. The ongoing self-optimisation process is described in §12.4. During the network operation, connected mobiles measure neighbours pilot signal and report results to the serving base station. Then the neighbour cell list is optimised such that it maximises the probability of finding a handover target. Section 12.5 presents the performance evaluation using simulations based on a real network deployment scenario. The simulation results show that the proposed solution achieves a high success rate of handover target scanning, and the self-optimisation algorithm converges quickly. Concluding remarks are given in §12.6.

12.2   Concept

The concept of the proposed neighbour cell list self-optimisation method is conceived on the basis of the following questions:

- What is the definition of an optimal neighbour cell list?
- What measurement statistics are needed and how can they be obtained?
- How can potential neighbours be discovered that are not currently included in the neighbour cell list?

The objective of the neighbour cell list is to assist mobile stations in finding a suitable handover target. As discussed in §10.3 of Chapter 10, a neighbouring cell is considered as a suitable handover target for a mobile if its pilot signal quality received by the mobile is higher than a minimum requirement $P_{\min}$, for example $P_{\min,E_c/I_0} = -20$ dB in WCDMA [105]. In addition, the information obtained by measurements of the pilot signals of neighbouring cells must be of good statistical confidence. The shorter the neighbour cell list is, the more frequent the neighbouring cells can be measured, which results in a higher confidence in the measurements. In reality, the maximum size of the neighbour cell list is limited by the standard, such as to 32 cells as specified by 3GPP, see §4.2 in Chapter 4. From the above considerations, *the optimal neighbour cell list is defined as the one that has the least cells within the standardised allowable number (e.g., 32), and maximises the probability of finding a handover target.* Here the probability of finding a handover target is defined as the probability that at any location in the serving cell the mobile finds at least one suitable handover target from the neighbour cell list.

The measurement statistics needed are the indicators that are used for the handover target selection such as signal-to-interference-plus-noise ratio SINR in GSM, and chip-energy-to-interference ratio E_c/I_0 in WCDMA. Since this information is only available when the network is operational

but not in the planning phase, the proposed optimisation method is composed of two phases: self-configuration for the network initialisation, and ongoing self-optimisation during the network operation, c.f., Figure 12.2.

When the network is newly deployed, neighbours are identified and measured by each base station on the downlink band. The neighbour cell list of each cell is then initialised using a self-configuration algorithm based on the collected measurements. This phase is also applied to self-configure an initial neighbour cell list of a new cell that is installed when the network is already operating.

During the network operation, connected mobiles are instructed to perform measurements using standardised scanning procedures, and report results to the serving base station. This phase of collecting measurement statistics also deals with the cell discovery. In broadband systems such as WCDMA, and LTE, mobiles are capable of detecting and reporting cells even when they are not comprised in the current neighbour cell list [105, 204]. Note that this capability of measuring new cells does not weaken the importance of the neighbour cell list since, as mentioned in the Introduction and in Chapter 4, the mobiles need longer time to measure an unidentified neighbouring cell. Measuring new cells is not mandatory but can occur when a measurement opportunity appears to the mobile. For multi-carriers networks like GSM, the cell discovery can be done by using the test-frequency concept proposed by Magnusson and Olofsson [135] as previously described. It follows that some of all the frequency carriers in the system are added to a frequency list so that mobiles perform the discovery and measurement of cells allocated to those test frequency carriers. This should be performed now and then in an iterative manner so as to allow mobiles discovering cells over all frequency carriers.

The collected measurement statistics are then used by a self-optimisation algorithm implemented in the base station to continuously refine the neighbour cell list. The update of the current neighbour cell list with the self-configured or self-optimised neighbour cell list can be totally automatic, or with the intervention of the operator to allow the introduction of additional specific policies (for example to remove prohibitive cells is not performed fully autonomously).
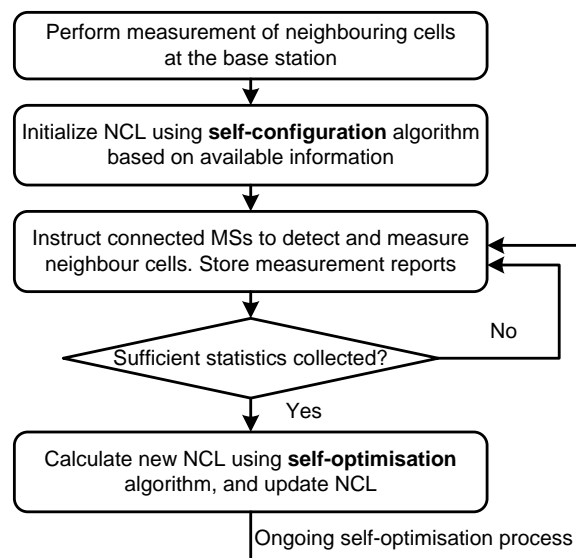

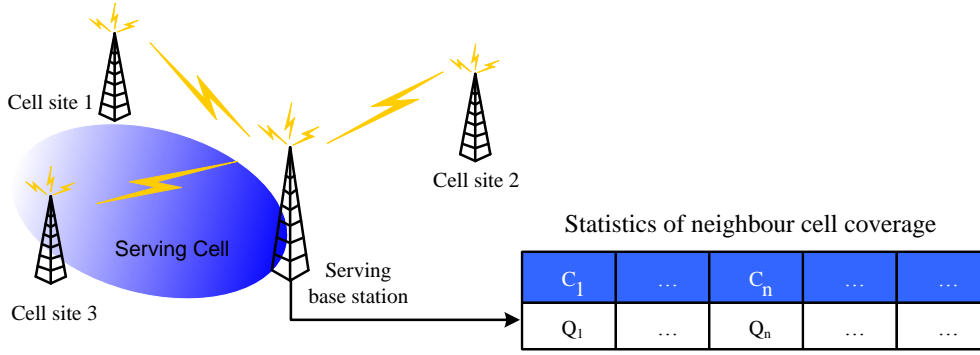FIGURE 12.2: Principle of neighbour cell list self-organisation

FIGURE 12.3: Neighbours statistics retrieval for self-configuration

12.3 Neighbour Cell List Self-Configuration

Just after the network planning phase, no measurement from mobiles are available, neighbouring cells are identified based on measurements performed by each base station. This is done by using the existing sectorised antenna of the serving base station to scan the downlink band and measure identified cells as illustrated in Figure 12.3. Then a predefined number of neighbours with the best received pilot quality are included in the neighbour cell list.

The serving base station's antenna gain supports the measurements of neighbouring cells in the direction of the sector coverage, and thereby helps to detect neighbouring cells which overlap with the sectorised serving cell.

This approach does not require the operator to provision information on neighbouring cells, and thereby reduces the deployment costs. However, its disadvantage is that the neighbours pilot signal quality can not be measured in the whole serving cell coverage area. This is why further measurements by the mobiles are required. These measurements become available during operation and are used in the ongoing self-optimisation process described next.

12.4 Neighbour Cell List Self-Optimisation

12.4.1 Neighbours Statistics Retrieval

During the scanning procedure, the connected mobiles measure the pilot signal of neighbours currently in the neighbour cell list. In parallel, potential neighbours are detected and measured by the mobiles according to the principle explained in §12.2. This means that the mobiles perform measurements of neighbours that are either detected during the scanning procedure, or are identified during scanning of test frequencies. The mobiles then send measurement reports to their serving base station as illustrated in Figure 12.4.

The serving base station stores a measurement statistics table whose structure is given in Table 12.1. The table columns are neighbouring cells identifiers, and the table rows are measurement reports sent by mobiles. The value at row i and column j represents the pilot signal quality of cell jth received by a mobile reporting the measurement ith.
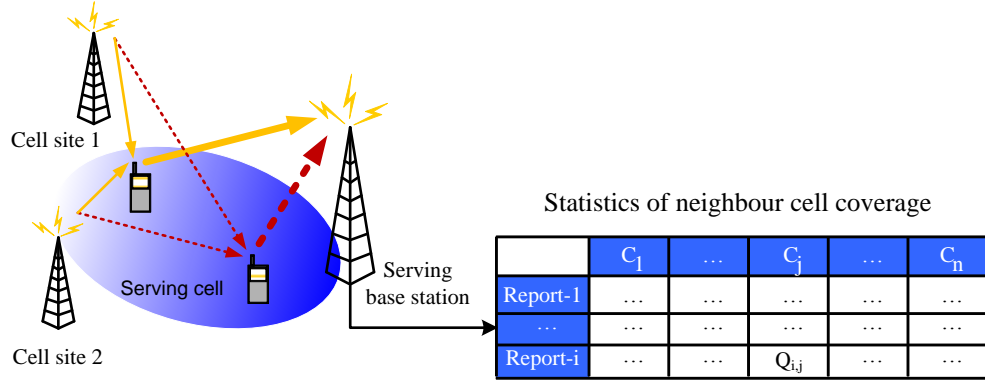
FIGURE 12.4: Neighbours statistics retrieval for self-optimisation

Whenever a measurement report is received, the statistics table **S** is updated according Algorithm 12.1. It follows that a new row will be added to the current statistics table. If this measurement report contains cells that are not currently present in the table columns, one new column is added for each new reported cell. After that, for the recently added row, columns corresponding to the reported cells are filled with the corresponding reported values.

TABLE 12.1: Structure of statistics table **S**

	CellID 1st	$\cdots$	**CellID jth**	$\cdots$	**CellID nth**	
Report 1st $\rightarrow$	$\cdots$	$\cdots$	$\cdots$	$\cdots$	$\cdots$	$\leftarrow$ Row 0th
Report ith $\rightarrow$	$\cdots$	$\cdots$	$\mathbf{S}[i,j]$	$\cdots$	$\cdots$	$\leftarrow$ Row ith

Each row of the statistics table reflects the coverage of neighbouring cells at the reported measured location. Any mobile may send several measurement reports during a scanning procedure, and these may correspond to different measured locations in the serving cell (due to user's mobility). Therefore, only the measurement reports are relevant while the identifier of the mobiles performing the measurements is not stored. Besides, old measurements may be not valid anymore due to potential changes in the radio environment. Thus, at some point, older rows can be removed from the statistics table.

12.4.2 Self-Optimisation Algorithm

The proposed self-optimisation algorithm is presented in Algorithm 12.2. The objective of the algorithm is to select neighbouring cells such that the resulting neighbour cell list maximises the number of locations at which there is at least one suitable target cell from the neighbour cell list available.

The input includes the statistics table, the minimum requirement of the pilot signal quality $P_{\min}$, and the maximum allowable size $N_{\max}$. The "`for`" loop in lines 4-9 cycles through the number of locations (i.e., number of table rows), m_j, at which neighbouring cell j is a suitable handover target.

Algorithm 12.1: Add measurement report to statistics table

Input: MeasReport = $[(\text{CellID}_j, Q_j), j = 1, 2, \ldots]$;	**1**
statistics table **S**;	
initialisation	**2**
$m \leftarrow$ number of rows in **S**;	**3**
$n \leftarrow$ number of columns in **S**;	**4**
CurrentCellIDs $\leftarrow$ **S**$[0, *]$;	**5**
ReportCellIDs $\leftarrow [\text{CellID}_j, j = 1, 2, \ldots]$;	**6**
end	**7**
add row $(m + 1)$th to **S**;	**8**
S$[m + 1, *] \leftarrow -\infty$;	**9**
foreach CellID_j *of* ReportCellIDs **do**	**10**
if $\text{CellID}_j \in$ CurrentCellIDs **then**	**11**
$j^* = \textbf{find}$ index of CellID_j in CurrentCellIDs;	**12**
S$[m + 1, j^*] \leftarrow Q_j$;	**13**
else	**14**
add column $(n + 1)$th to **S**;	**15**
S$[0, n + 1] \leftarrow \text{CellID}_j$;	**16**
S$[1 \ldots m, n + 1] \leftarrow -\infty$;	**17**
S$[m + 1, n + 1] \leftarrow Q_j$;	**18**
add CellID_j to CurrentCellIDs;	**19**
$n \leftarrow n + 1$;	**20**
end	**21**
end	**22**

Between the remaining neighbouring cells in table **S**, the cell corresponding to column j^* (line 11) is the best one that maximises the number of locations covered by the neighbour cell list, and thus is added to the neighbour cell list (line 12). The case of $\max_j(m_j) = 0$ ("`else`" in line 17) means that all the remaining neighbouring cells in table **S** do not cover any location of the serving cell with acceptable signal quality. Adding any of these cells will not improve the neighbour cell list. In this case, the resulted neighbour cell list is the best one that maximises the probability of finding handover target, and so the algorithm terminates (lines 18 and 21).

When the neighbouring cell identified by column j^* is included in the neighbour cell list (line 12), this column j^* and the corresponding rows can be removed (by line 16, and 14, resp.). The cell identified by column j^* ensures that the mobiles will find at least one suitable handover target at the locations (i.e., rows) that satisfy the "`if`" condition in line 14. As the objective is to find the shortest neighbour cell list that covers a maximum number of locations, only the locations that are still not covered by the current neighbour cell list are considered in the next rounds.

12.5   Simulation

A cellular network deployment in Phoenix in the United States was used for the simulation, from which cell locations and antenna orientations were extracted. The size of the simulated scenario is 16 km × 16 km and includes 120 macrocell sectors. We adopt system parameters of WCDMA standard for the evaluation purpose, from which parameters are summarised in Table 12.2. The

---

Algorithm 12.2: Self-optimisation algorithm

Input: statistics table, $P_{\min}$, $N_{\max}$;	1
initialisation: $\mathbf{S}$ = statistics table; NCL = $\varnothing$;	2
while $N_{\max}$ > *size of NCL* **do**	3
foreach *column j of* $\mathbf{S}$ **do**	4
$m_j = 0$;	5
foreach *row i of* $\mathbf{S}$ **do**	6
if $\mathbf{S}[i,j] \geq P_{\min}$ **then** $m_j \leftarrow m_j + 1$;	7
end	8
end	9
if $\max_j(m_j) > 0$ **then**	10
$j^* = \arg\max(m_j)$;	11
add cell identified by column j^* to the NCL;	12
foreach *row i of* $\mathbf{S}$ **do**	13
if $\mathbf{S}[i,j^*] \geq P_{\min}$ **then** remove row i from $\mathbf{S}$;	14
end	15
remove column j^* from $\mathbf{S}$;	16
else	17
to *(21)*;	18
end	19
end	20
return *NCL*	21

TABLE 12.2: Evaluation parameters

Parameter	Assumption
Scenario	Macrocell in Phoenix, US
Antenna pattern	Tri-sector directional
Path loss (d in m)	$l(d) = 28 + 35\log_{10}(d)$
BS tx power	$P_{\text{tx}} = 20$ W (43 dBm)
Bounding distance	$R_{\min} = 5$ metres
Shadowing std. dev.	$\sigma_Z = 8$ dB
Inter-cell correlation	0.5
Effective bandwidth	$W = 3.84$ MHz
UE noise figure	$N_{\text{F}} = 7$ dB
Noise density	-174 dBm/Hz
Handover hysteresis	$\Delta_{\text{HO}} = 2$ dB
Minimum level	CPICH $\text{E}_{\text{c}}/\text{I}_0 \geq -20$ dB
Measurement capability	8 cells / 200 ms
User's speed	$v = 5 \rightarrow 50$ m/s

propagation path loss for a typical macrocell deployment in urban environment is modelled as

$$l_{[\text{dB}]}(d) = 28 + 35\log_{10} d, \tag{12.5.1}$$

where d is the distance from the base station in metres. Shadow fading in dB scale is modelled as random variable Z with normal distribution with 8 dB standard deviation and a correlation of 0.5 between different sites.

It is assumed that the total transmit power for each base station is $P_{\text{tx}} = 20$ W per sector,
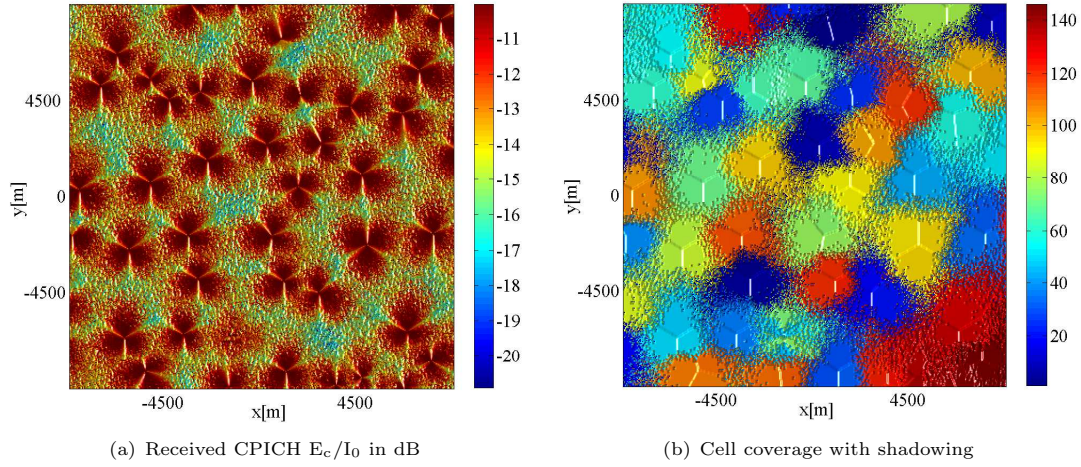
(a) Received CPICH E_c/I_0 in dB

(b) Cell coverage with shadowing

FIGURE 12.5: Simulation scenario.

where 10% of this power is allocated to a pilot channel $P_{tx,pilot}$. Each macrocell transmits via a sectorised antenna with a gain pattern as recommended by 3GPP TR 25.942 [52]:

$$G_{[dB]}(\theta) = G_{max} - \min\left(12\left(\frac{\theta}{\theta^*}\right)^2, G_s\right), \quad -\pi < \theta \leq \pi, \tag{12.5.2}$$

where $\theta^* = 70\pi/180$ is the angle where the gain pattern is 3 dB down from peak, the maximum gain is $G_{max} = 16$ dB, and $G_s = 20$ dB.

For any location in the considered scenario the received power from a base station j can be calculated based on (12.5.1) as

$$P_{rx[dBm]} = P_{tx[dBm]} + G_{[dB]}(\theta) - l_{[dB]}(d) + Z. \tag{12.5.3}$$

The received noise power N_0 at the mobile reception antenna is given by (2.2.1) in Chapter 2 with the noise figure at the terminal $N_{F,dB} = 7$ dB, the effective bandwidth $W = 3.84 \times 10^6$ Hz, and ambiance temperature $T_0 = 290$ K which results in noise density of -174 dBm/Hz.

For each location in the scenario, an E_c/I_0 can be calculated. The pilot E_c/I_0 is defined in 3GPP as the ratio of the received energy per pseudo-noise chip for the CPICH to the total received power spectral density at the UE antenna connector. It can be calculated for a UE connected to the mth cell as

$$\text{CPICH } E_c/I_{0_i} = \frac{P_{rx,pilot,i}}{N_0 + \sum_j P_{rx,j}}, \tag{12.5.4}$$

where $P_{rx,pilot,i}$ denotes the pilot power received from cell i, $P_{rx,j}$ is the total received power of cell j including data and pilot. The pilot minimum requirement for the UE is CPICH $E_c/I_0 \geq -20$ dB [105]. In the scenario considered, this requirement results in a nearly 100% coverage of the area. Figure 12.5(a) shows an example of the highest received pilot E_c/I_0, and Figure 12.5(b) shows the corresponding coverage regions based on received pilot E_c/I_0 for the sectors within the simulated area. It is assumed that the UE is capable of measuring CPICH of 8 identified cells (i.e., cells in the neighbour cell list) within 200 ms [105].
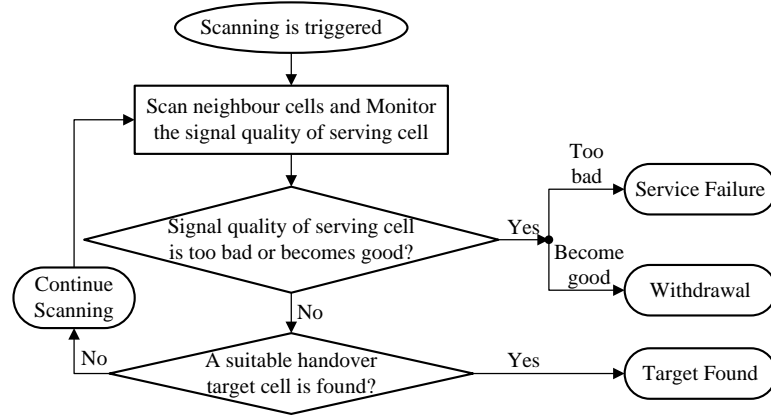
FIGURE 12.6: Procedure of handover measurement.

For the neighbour cell list performance evaluation, mobiles are randomly placed in the simulated area, and move in the network. Each mobile moves at a given speed and changes its direction after each simulated time step (see, e.g., [205, 206]). User's speeds between 5 m/s and 50 m/s are considered. If the signal quality received from the serving cell falls below the scanning trigger threshold, the mobile starts scanning cells comprised in the neighbour cell list. The scanning with handover target selection process is similar to that discussed in Chapter 10 and is shown in Figure 12.6. The handover hysteresis margin was set to 2 dB.
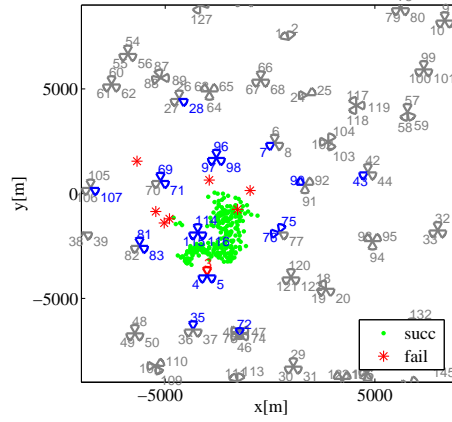
The quality of the neighbour cell list is assessed by the success rate of handover target scanning defined as ratio of the number of mobiles finding a suitable handover target to the total number of mobiles finding a suitable handover target plus the number of mobiles which did not find a suitable handover target (resulting in a call drop):

$$success \ rate = \frac{\text{number of TargetFounds}}{\text{number of TargetFounds + Failures}}. \tag{12.5.5}$$

Note that after finding a handover target, the mobile enters into the handover decision-execution phase whose outcome depends on the handover algorithm but is not impacted by the neighbour cell list. Therefore, only the handover target scanning phase is used to assess the neighbour cell list quality, the handover execution phase is not taken into the neighbour cell list performance evaluation.

12.5.1 Performance

An example of neighbour cell list optimisation and handover target scanning is shown in Figure 12.7 for the serving cell 3. Figure 12.7(a) shows the results directly after initialisation with a neighbour cell list computed by the self-configuration algorithm, and Figure 12.7(b) shows the results with the neighbour cell list that is computed by the self-optimisation algorithm. The optimised neighbour cell list has 21 cells. For comparison, a cell list size of 21 was also used for the self-configuration algorithm. In Figure 12.7, cells comprised in the NCLs are blue-coloured. Comparing Figure 12.7(a) and 12.7(b), the self-optimisation method can improve the success rate of 85% from the self-configuration to 97.3%. It is shown that three cells 7, 96 and 98 make the difference between the two NCLs. By using mobile-reported measurements, the self-optimisation
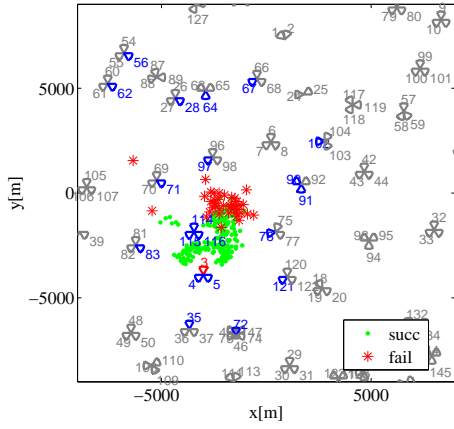
(a) *succ rate* = 85% with self-configured NCL   (b) *succ rate* = 97.3% with self-optimised NCL

FIGURE 12.7: Examples of scanning with computed NCLs. User's speed $v = 20$ m/s
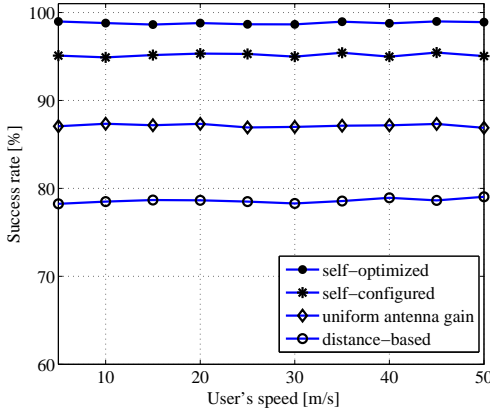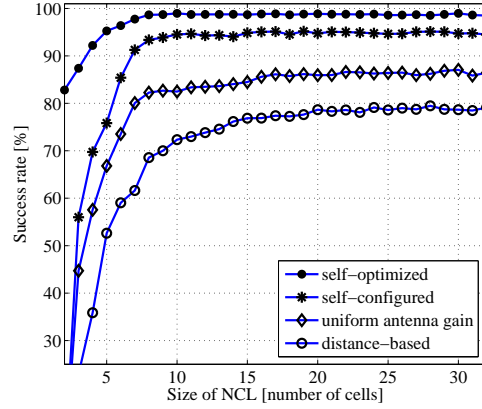

(a) Under different user's speeds   (b) Under different list sizes: $v = 20$m/s

FIGURE 12.8: Performance evaluation. Simulation with 20 serving cells.

algorithm included these three cells, and thereby eliminates call drops close to these neighbouring cells.

For more general results, the handover target scanning with NCLs to be evaluated is simulated in 20 serving cells, and the average success rate of each simulated neighbour cell list is computed. The self-configuration method is compared to two other methods. The first one is a distance-based method that configures a neighbour cell list by selecting a number of the closest neighbouring cell sites. And the second one is similar to the proposed self-configuration method except that the measurements are performed using a separate antenna with uniform gain pattern. These benchmarking methods are marked in Figure 12.8(a) & 12.8(b) as "distance-based" and "uniform antenna gain", respectively. Note that, as discussed in §12.1 and §4.3.3, self-optimisation concepts in the literature are not realised with live measurements like the proposed approach, but with static configuration information. Therefore, no directly comparable benchmark is available. Instead, the self-optimisation method is compared with the best self-configuration method for its performance.

Figure 12.8(a) shows the performance with different user's speeds v. It is shown that with a measurement speed of 8 cells/200ms as in WCDMA, the user's speed does not have much impact on the success rate. It is also shown that the proposed self-configuration method is better than two benchmarking methods, and the self-optimisation method performs best.

Figure 12.8(b) shows the performance with different list sizes. We see that all the NCLs give better performance for longer lists within the maximum allowed size, $N_{max} = 32$. This is thanks to the relatively high measurement speed in WCDMA. In some case where measurement speed is low, if the neighbour cell list is too long the connection between the mobile and the serving may be lost before finding a suitable handover target. It is also clear from Figure 12.8(b) that the proposed self-configuration method is better than two benchmarking methods, and the self-optimisation again performs best. It is shown that the success rates flatten out at about 10 neighbours. From this point on, the performance of the self-optimised neighbour cell list approaches a success rate close to 100%, while the configured NCLs have lower flat performance and are not further improved because having limited knowledge about the neighbouring cells coverage prevents the configuration methods from adding useful neighbouring cells.

12.5.2   Convergence Speed of the Self-Optimisation Method

A further important aspect that was evaluated is the convergence speed of the self-optimisation method. This provides information on from which point the self-optimisation method provides reliable performances that outperform the self-configuration method used for initialisation. Figure 12.9 shows the achievable performance for different numbers of reported measurements. It is shown that the more measurements are available, the better the quality of the self-optimised neighbour cell list is, since more reliable information about the neighbouring cell coverage is available.

At about 3000 measurements, the self-optimisation algorithm provides a success rate about 95%. And at 6000 available measurements, the success rate attains 99%. Since the self-configuration achieves an average performance of approximately 95% when the neighbour cell list size is sufficient large as shown in Figure 12.8(b), it makes sense to switch to the neighbour cell list obtained from the self-optimisation algorithm once more than approximately 3000 measurement are available. From this point on, the self-optimised neighbour cell list provides improved performance.

12.6   Conclusion

A method for automatically optimising a neighbour cell list was presented. The proposed approach consists of a self-configuration phase for initialisation, followed by a switch to a self-optimisation phase once sufficient measurements are reported by connected mobile stations. For initialisation, the measurements-based self-configuration method achieved the best performance of approximately 95% in success rate of handover target scanning with 10 or more neighbouring cells. The success rate is further improved by switching to a neighbour cell list obtained by the proposed self-optimisation method. It was shown that a switch to a self-optimised neighbour cell list can improve the performance once more than approximately 3000 measurements reports are collected, and a near maximum performance of around 99% success rate is achieved after more than around 6000 measurements reports are available. The proposed solutions are simple
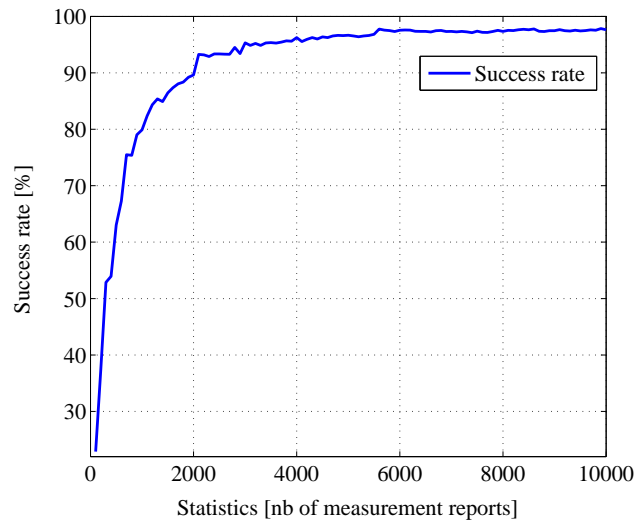
FIGURE 12.9: Convergence speed. User speed $v = 20$ m/s

but efficient by using true measurement-based self-optimisation algorithms. These suggest that the optimisation of NCLs can be automated, which will help to reduce operational expenses in future cellular networks.

Part IV

Appendices

Appendix A

Probability

A.1 Characteristic Function and Uniqueness Property

The following definition and properties are taken from Chapter 15 in Feller [186].

Definition A.1.1. *Let X be a random variable with probability distribution F. The characteristic function of F (or of X) is the function ϕ defined for real w by*

$$\phi(w) = \int_{-\infty}^{+\infty} e^{jxw} F(\mathrm{d}x).$$

Theorem A.1.2 (Uniqueness). *Distinct probability distributions have distinct characteristic functions.*

Theorem A.1.3 (Continuity theorem). *In order that a sequence $\{F_n\}$ of probability distributions converges to a probability distribution F, it is necessary and sufficient that the sequence $\{\phi_n\}$ of their characteristic functions converges pointwise to a limit ϕ, and that ϕ is continuous at the origin. In this case, ϕ is the characteristic function of F. (Hence ϕ is continuous everywhere and the convergence $\phi_n \to \phi$ is uniform in every finite interval.)*

Theorem A.1.4 (Fourier inversion). *Let ϕ be the characteristic function of the distribution function F and suppose that $\phi \in \mathbb{L}$ (i.e. ϕ is absolutely integrable). Then F has a bounded continuous density f given by*

$$f(x) = \frac{1}{2\pi} \int_{-\infty}^{+\infty} e^{-jxw} \phi(w) \mathrm{d}w.$$

Remark A.1.5 (Plancherel identity). Let the distribution F have a density f and characteristic function ϕ. Then $|\phi|^2 \in \mathbb{L}$ iff $f^2 \in \mathbb{L}$, and in this case

$$\int_{-\infty}^{+\infty} f^2(x) \mathrm{d}x = \frac{1}{2\pi} \int_{-\infty}^{+\infty} |\phi(w)|^2 \mathrm{d}w.$$

A.2   Kullback-Leibler and Jensen-Shannon Divergences

For some distributions F and G on the same probability space S, the Kullback-Leibler divergence [207, 208] of G from F, denoted by and $\mathrm{KLdiv}(F, G)$, is defined as follows:

$$\mathrm{KLdiv}(F, G) = \int_S \mathrm{d}F \log \frac{\mathrm{d}F}{\mathrm{d}G}. \tag{A.2.1}$$

For example if F and G are continuous distributions on $\mathbb{R}$ and admit densities f and g, respectively, then:

$$\mathrm{KLdiv}(F, G) = \int_{-\infty}^{\infty} f(x) \log \frac{f(x)}{g(x)} \mathrm{d}x.$$

Jensen-Shannon divergence [209], denoted by $\mathrm{JSdiv}(F, G)$, is a symmetrized version of the Kullback-Leibler divergence. It is defined as follows:

$$\mathrm{JSdiv}(F, G) = \frac{1}{2}\mathrm{KLdiv}(F, M) + \frac{1}{2}\mathrm{KLdiv}(G, M), \tag{A.2.2}$$

where

$$M = \frac{1}{2}(F + G).$$

Appendix B

Résumé Etendu

Une liaison sans fil entre un émetteur et un récepteur est soumise à des variations dans la fréquence, le temps, et l'espace. La puissance reçue du signal est traditionnellement caractérisée par une superposition de trois composantes appelées l'affaiblissement de parcours, l'effet de masque, et les évanouissements rapides (respectivement appelées *path loss*, *shadowing*, et *fast-fading* en anglais). L'affaiblissement de parcours décrit l'atténuation de puissance due à la propagation des ondes radios dans l'espace libre. Il est généralement exprimé sous une fonction déterministe de la distance de parcours. L'effet de masque représente des variations de la puissance du signal due à des obstacles entre le transmetteur et le récepteur qui peuvent affaiblir ou renforcer le signal par la réflexion, la diffraction, la diffusion, et la réfraction du signal transmis. Les évanouissements rapides sont générés par le mouvement relatif du récepteur et aussi par la réception multi-trajet du signal original. L'effet de masque et les évanouissements rapides sont convenablement caractérisés par des lois probabilistes [7, 8]. Pour une raison simpliste, ci-après nous allons appeler "fading" pour dire l'effet de masque, et les évanouissements rapides.

Dans un réseau sans fil, l'interférence se produit lorsque plusieurs nœuds transmettent simultanément en utilisant une même ressource radio, par exemple sur une même bande de fréquence. La qualité de communication est principalement déterminée par la qualité du signal exprimée en

termes du rapport signal à interférence et bruit (souvent appelé SINR pour *signal-to-interference-plus-noise ratio*). Cela pousse à rechercher des états où chaque récepteur se connecte à l'émetteur qui lui donne la meilleure qualité du signal. La meilleure qualité du signal est donc une information fondamentale à l'évaluation de nombreuses quantités d'intérêt, ainsi qu'à la conception et l'optimisation du réseau.

> *La **première contribution** de la thèse est la modélisation des liaisons*
> *sans fil avec des résultats principaux concentrés sur la distribution de la*
> *meilleure qualité du signal.*

Dans l'établissement de ces résultats, nous obtenons une variété des résultats et des observations intéressants sur les liaisons sans fil [1], en particulier sur l'interférence et le maximum des puissances reçues de plusieurs nœuds. Les résultats sont présentés dans la première partie (Part I) de la thèse. Afin de mieux présenter notre approche et les résultats, prenons un exemple concret. Considérons n émetteur à partir desquelles un récepteur reçoit des puissances $(P_1, P_2, \ldots, P_n)$. La puissance d'interférence que les autres émetteurs interfèrent le signal d'un émetteur i est ainsi donnée comme $I_i = P_1 + \cdots + P_{i-1} + P_{i+1} + \cdots + P_n$. La qualité du signal reçu de l'émetteur i est donc $Q_i = P_i/(N_0 + I_i)$ où N_0 représente la puissance du bruit thermique. La meilleure qualité du signal parmi ces n émetteurs est donnée comme $Y_n = \max(Q_1, \ldots, Q_n)$. Rappelons que la puissance reçue P_i inclut l'effet de masque, et les évanouissements rapides qui sont considérés aléatoires. Les puissances reçues $\{P_i\}$ sont donc aléatoires. De cet effet, les variables $(Q_1, Q_2, \ldots, Q_n)$ sont aléatoires et en plus dépendent les uns les autres en raison des ingrédients communs $(I_i, i = 1, \ldots, n)$. Ainsi, l'obtention de la distribution de Y_n n'est pas tout-à-fait facile. En notant $I = P_1 + \cdots + P_n$, il est clair que $I_i = I - P_i$, ce qui conduit à $Q_i = P_i/(N_0 + I - P_i)$. Avec une simple observation, nous pouvons voir que $Y_n = M_n/(N_0 + I - M_n)$ où nous notons M_n le maximum des puissances reçues des n émetteurs, soit $M_n = \max(P_1, \ldots, P_n)$. Cela signifie que l'émetteur qui donne la puissance maximale du signal va offrir aussi la meilleure qualité du signal. Plus important, cela suggère que nous pouvons dériver la distribution de la meilleure qualité du signal Y_n par la distribution conjointe du maximum des puissances reçues M_n et l'interférence totale I. C'est l'idée directrice tout au long de notre travail.

---

[1] *"Remember that happiness is a way of travel - not a destination."* M. Roy Goodman.

Afin de développer notre idée ci-dessus, nous avons besoin tout d'abord de l'information concernant la répartition (ou distribution) spatiale des nœuds dans le réseau. Cela permet de modéliser la puissance reçue qui dépend de la distance entre chaque paire d'émetteur-récepteur. Dans la littérature, il existe deux approches pour obtenir cette information: soit en utilisant un modèle déterministe, soit en utilisant un modèle stochastique. Un modèle déterministe nécessite une information complète de la structure du réseau ou doit être contraint à une topologie régulière, comme la grille ou des structures hexagonales. Il en résulte des coûts pour obtenir des informations précises sur le réseau, et également des difficultés dans la généralisation mathématique [9, 10]. Un modèle trop idéalisé fondé sur des structures régulières est aussi pratiquement moins intéressant. La distribution spatiale des nœuds est donc souvent traitée comme aléatoire selon certains processus ponctuel. Bien qu'un modèle stochastique n'est pas en mesure de décrire les emplacements des nœuds précisément, il donne un même niveau de précision que donne un modèle déterministe [10], en plus il peut nous fournir un certain degré de généralisation mathématique et est particulièrement adapté à des analyses au niveau de système. En particulier, les processus ponctuels poissonniens facilitent des développements mathématiques [11], ils ont été intensivement utilisés pour modéliser la distribution spatiale des nœuds dans un réseau sans fil, et ont permis d'obtenir des formes closes des quantités importantes d'un réseau sans fil par exemple l'inteférence [49, 72] (voir §6.2 pour plus de détails). En utilisant ce modèle, nos résultats sont comme suit.

- Dans le **chapitre 7**, nous obtenons les formules exactes de la distribution conjointe de la puissance maximale reçue d'un domaine sous forme un disque B et l'interférence totale, ainsi que la distribution de la meilleur qualité du signal. Quelques observations retirées sont comme suit. Sous un modèle d'affaiblissement de parcours non-borné avec l'exposant d'affaiblissement β donné comme $d^{-\beta}$ où d est la distance de parcours, le maximum des puissances reçues de l'ensemble du réseau suit une distribution de Fréchet, et l'interférence totale suit une loi α-stable où le facteur caractéristique est $\alpha = 2/\beta$, indépendamment du type de fading. Cela signifie que la puissance maximale et l'interférence totale appartient à la famille des lois à queue lourde. Nous avons aussi montré que dans des conditions bien

déterminées, leur distribution conjointe existe partout du plan euclidien à deux dimensions, sauf à l'origine si B est borné. (Ce travail a été réalisé en collaboration avec François Baccelli, et a été publié dans la conférence WiOPT 2010.)

- Dans le **chapitre 8**, nous montrons que la singularité de la fonction d'affaiblissement de parcours décide la propriété à queue lourde de la distribution de la puissance reçue. Dans le cas d'un modèle d'affaiblissement de parcours borné, la puissance reçue est de type à variation régulière, qui est en effet une distribution à queue très lourde. En conséquence, l'interférence et le maximum des puissances reçues sont des distributions à queue très lourde. Ceci s'explique par la composante dominante créée par la singularité de la fonction d'affaiblissement de parcours. Cette composante dominante en plus renforce la dépendance entre l'interférence et la puissance maximale. En revanche, en cas où la fonction d'affaiblissement de parcours est bornée, la queue de la distribution de la puissance reçue est principalement imposée par le type de fading. Particulièrement, en cas d'un fading lognormale, la puissance reçue appartient à la fois les domaines d'attraction d'une distribution de Gumbel et d'une distribution gaussienne. Cela signifie que la queue de la distribution de la puissance reçue est moins lourde qu'en cas de l'affaiblissement non-borné. Cette propriété nous donne l'indépendance asymptotique entre le maximum des puissances reçues et l'interférence lors que le nombre des émetteurs observés tend vers l'infini. Cela nous permet d'obtenir une approximation de la distribution de la meilleure qualité du signal, qui est analytiquement plus simple que sa formulation exacte que nous avons obtenue dans le chapitre 7. (Ce travail a été fait avec François Baccelli, Laurent Thomas, et Chung Chen Shue, et a été publié dans le jounral EURASIP JWCN 2010.)

Maintenant, nous nous intéressons à des variations temporelles des liaisons sans fil. Dans le domaine temporel, la puissance et la qualité d'une liaison sans fil souvent franchissent des seuils en raison des variations au cours du temps. Il nécessite donc certains mécanismes pour contrôler le fonctionnement du réseau en faisant face à des situations où la puissance / la qualité du signal est trop basse ou très élevée. Par exemple, lorsque la qualité du signal est trop faible tels qu'elle reste en dessous d'un niveau bas, la communication devient non fiable, nécessitant une commutation de

la communication à un autre émetteur. Comprendre les propriétés associées aux franchissements des seuils des liaisons sans fil est depuis longtemps un sujet important. Il est connu sous la théorie "level crossing" des processus stochastiques qui a été étudiée depuis le milieu du siècle dernier avec les premiers travaux publiés par Rice [12, 13], et par Kac and Slepian [14]. Pour un processus gaussien stationnaire $X(t)$ où t représente le "temps", ils ont contribué des résultats fondamentaux sur le nombre moyen de franchissements d'un seuil, et la trajectoire asymptotique de $X(t)$ au-dessus d'un seuil très haut qui tend vers l'infini. L'application de ces résultats à la communication radio mobile a attiré beaucoup d'attention, surtout depuis que le papier de Mandayam [15] ait apparu en 1996, et ait été républié en 1998 dans [16]. Toutefois, l'introduction de nouveaux mécanismes de contrôle dans les réseaux cellulaires émergents nécessite plus d'études de ce sujet.

> La **deuxième contribution** *de cette thèse est une investigation de*
> *certaines propriétés de franchissement de seuils d'un processus gaussien*
> *stationnaire.*

Considérant un processus gaussien stationnaire, nous étudions l'intervalle de temps pendant lequel le processus $X(t)$ reste au-dessus d'un seuil très faible, et étudions ensuite des propriétés associées au franchissement de $X(t)$ de plusieurs seuils adjacents.

- Dans le **chapitre 9**, nous montrons que l'intervalle de temps pendant lequel $X(t)$ reste au-dessus d'un seuil très bas suit une distribution exponentielle de taux égal au taux moyen des franchissements de ce seuil (aussi appelé "*mean level-crossing rate*"). Cela complète le résultat bien connu de [14] montrant que l'intervalle pendant lequel $X(t)$ reste au-dessus d'un seuil très haut suit une distribution de Rayleigh (voir §5.3). Ensuite, nous nous intéressons au franchissement de $X(t)$ de plusieurs seuils adjacents. Conditionnellement sur le fait que $X(t)$ ait un franchissement au-dessus d'un seuil donné γ_1, nous obtenons alors le nombre moyen de franchissements, et puis la distribution de l'intervalle de temps des franchissements de $X(t)$ d'un certain seuil $\gamma_2 > \gamma_1$ quand γ_1 tend vers $+\infty$. Ces résultats ont ensuite appliqués à l'analyse et l'optimisation de la gestion de mobilité dans

les réseaux cellulaires 3GPP *Long Term Evolution* (LTE). (Ce travail a été réalisé pendant

l'achèvement de la mémoire de thèse. Il fait l'objet une future publication.)

Les résultats ci-dessus devraient avoir diverses implications. Dans le cadre de cette thèse, nous

nous intéressons à leurs applications à la gestion de mobilité dans les réseaux cellulaires. Nous

allons tout d'abord aborder une vue générale du concept de réseau cellulaire et de la nécessité

d'un mécanisme de gestion de mobilité. Fondamentalement, afin de garantir un niveau de qualité

de communication sans fil, il est nécessaire de maintenir une qualité suffisamment bonne de la

liaison radio. Comme la qualité du signal est en effet le rapport signal à interférence et bruit, il

nécessite de limiter l'interférence à un niveau relativement faible, ce qui en conséquence signifie

que seulement un nombre limité des nœuds sont autorisés à transmettre simultanément. Ceci

peut être faisable dans une situation de la radiodiffusion où il n'y a qu'une seule communication

à sens unique d'un émetteur à une population de récepteurs, tels que les systèmes de télévision

radio, ou une note conférence donnée par un professeur à un grand nombre d'étudiants dans

un grand amphithéâtre. Mais se pose le problème quand beaucoup de nœuds ont besoin de

transmettre. Pour mieux illustrer le problème, prenons l'exemple d'un exercice de brainstorming

entre les étudiants guidé par un professeur. Chaque étudiant est invité à présenter son idée au

groupe, et le professeur peut lui donner des commentaires et en même temps animer l'activité

du groupe. Si le groupe a trop d'étudiants, la possibilité pour chaque étudiant de présenter son

idée devient faible. L'idée ici est de séparer la classe en plusieurs groupes de telle manière que

chaque groupe soit affecté un professeur et travaille dans une salle séparée. Cette réorganisation

donne l'opportunité à chaque élève de montrer son idée, bien sûr au coût d'une augmentation

du nombre de professeurs. C'est aussi la logique derrière le concept des réseaux cellulaires qui

utilise un certain nombre de stations de base spatialement éloignées pour fournir des services

de communication à une région. La zone géographique où la qualité du signal d'une station de

base est meilleure que celle de toute autre station de base et est mieux qu'un niveau requis est

appelé une cellule (radio). Une station mobile dans une cellule est garantie des communications

avec la station de base de cette cellule. Mais la situation ici est plus compliquée que l'exemple

d'exercice de brainstorming ci-dessus. Un utilisateur mobile peut se déplacer en traversant

plusieurs cellules lors d'une communication (par exemple un appel téléphonique). Il faut donc un mécanisme permettant de faire automatiquement la commutation d'une cellule à une autre de manière transparente à l'utilisateur. Ceci est réalisé par une procédure appelée la gestion de mobilité, ou encore *handover* en anglais. Il consiste en deux fonctions: (i) la détermination d'une station de base avec laquelle la station mobile obtient la meilleure qualité du signal, puis (ii) la commutation de la connexion de la station de base en cours à celle de meilleure qualité du signal, appelée station targette ou cellule targette. La première fonction s'agit de mesurer la qualité du signal des stations de base voisines, elle est appelée *handover measurement*, alors que la deuxième fonction est appelée *handover decision-execution*. La fonction de handover measurement décide la qualité du signal de la station targette, et aussi elle impacte la qualité du service pendant la mesure, tandis que la fonction de handover decision-execution est responsable de la fiabilité de la commutation d'appels. Ces deux fonctions ont donc des impacts très importants sur la qualité de service en termes d'interruption d'appels et la dégradation de débit. La fonction de handover decision-execution a été intensivement étudiée avec une littérature très riche, y compris l'optimisation des paramètres qui sont utilisés par le procédure de handover, le contrôle optimal de handover qui sert à décider de faire ou non une commutation d'appel, et la conception du protocole qui sert à faire une commutation fiable et rapide. Au contraire, la fonction de handover measurement a reçu moins d'attention. Même aujourd'hui on a tendance à implicitement mentionner la fonction de handover decision-execution quand parler de handover, tout en oubliant la fonction de handover measurement. En plus, la plupart des travaux antérieurs sur cette fonction étaient basés sur des simulations et ont seulement investi un certain aspect spécifique (voir §4.3). Il manque un modèle unifié et aussi suffisamment générique pour étudier cette fonction dans différents normes des réseaux cellulaires.

> La **troisième contribution** *de cette thèse est l'analyse et*
> *l'optimisation de la fonction de handover measurement dans les réseaux*
> *cellulaires.*

En principe, plus de cellules sont mesurées, plus de chance la station mobile peut trouver une bonne cellule targette. C'est tellement évident comme une situation où plus de candidats nous examinons pour un poste de travail, plus de chance nous pouvons trouver un employé compétent.

Mais le temps requis pour la mesure des cellules (ou pour les entretiens avec les candidats) est une question. Non seulement un temps de mesure plus long introduit plus de coût, mais aussi plus important il est souvent la cause des interruptions d'appels car la qualité du signal de la cellule serveuse devient mauvaise pendant que la station mobile mesure d'autres cellules. Savoir quand à démarrer la mesure, et comment à la faire de manière optimale sont des questions critiques. Nous utilisons les résultats développés dans les chapitres précédents pour investir cette fonction de handover measurement.

- Dans le **chapitre 10**, nous développons un modèle analytique de handover measurement avec une caractérisation des principaux événements probabilistes dans un système de multi-cellules sous la condition de l'interférence. Le fonctionnement global de la procédure de handover measurement impliquant tous les paramètres de contrôle est décrit par un diagramme d'état markovien, qui permet de déterminer différentes quantités d'intérêt de handover measurement. Une application de ce modèle à la spécification actuelle de réseau 3GPP LTE la nécessité d'une amélioration de la capacité de mesure du terminal de cette norme cellulaire. (Ce travail a été réalisé avec Chung Shue Chen et Laurent Thomas, et avec le conseiller de François Baccelli. Une partie de ce travail a été présentée en conférence ICC 2011)

- Dans le **chapitre 11**, nous proposons une solution d'implémentation efficace des mécanismes de gestion de mobilité standardisés pour les réseaux denses de petites cellules (aussi appelés réseaux pico cellulaires denses). Cette solution, qui est ainsi appelée la *mesure autonome des cellules voisines*, permet de faire face à une des questions les plus difficiles de ce type de réseaux [192]. Les résultats suggèrent que dans un cadre de figure typique, la station mobile peut effectuer la mesure autonome de 30 cellules voisines pour atteindre une performance efficace en termes du débit effectif maximal. (Ce travail a été fait avec François Baccelli, Laurent Thomas, et Chung Chen Shue, et a été publié dans le journal EURASIP JWCN 2010.)

- Dans le **chapitre 12**, nous nous concentrons sur un élément problématique de la fonction de handover measurement qui est utilisée dans les réseaux cellulaires déployés d'aujourd'hui.

Il s'agit de la liste des cellules voisines (appelée *neighbour cell list* en anglais). Afin d'introduire cet élément, prenons à nouveau l'exemple ci-dessus de la concurrence pour un poste de travail. Au lieu d'interroger tous les candidats, nous pouvons tout d'abord sélectionner uniquement ceux qui sont admissibles et ont des compétences potentielles à notre travail, puis entretenir chacun d'entre eux pour mieux examiner. Cela permet d'économiser du temps, et il fournit un résultat équivalent si la liste courte est convenablement choisie. La liste des cellules voisines utilisée dans les réseaux cellulaires est similaire à cette courte liste de candidats à l'emploi. La station mobile effectue une mesure des cellules qui sont comprises dans la liste des cellules voisines préconfigurée pour sa cellule serveuse. La performance de handover measurement dépend par conséquence de la configuration de la liste des cellules voisines. Le problème est que la couverture réelle des cellules radios est très sensible à l'environnement alentour, il est difficile de la récupérer à une bonne précision. Ainsi, une bonne configuration de la liste des cellules voisines est une préoccupation quotidienne, et génère des coûts à l'opérateur dans l'opération du réseau. Dans ce chapitre, nous proposons une solution d'auto-optimisation des listes de cellules voisines. Premiers avantages de la solution proposée est qu'elle libère tous les abstractions mathématiques [2] et les opérations manuelles de l'opérateur, tout en générant des listes de cellules voisines optimisées sans introduire de coûts. Les résultats de simulation avec un déploiement réel de réseau confirment son efficacité. (Ce travail a été fait avec Holger Claussen, et a été publié dans la conférence de PIMRC 2010.)

Les résultats ci-dessus sont de nature diverse et leur développement nécessite de différents outils mathématiques. La première partie (Part I) de la thèse est réservée aux notions de base. Chapitre 2 décrit les propriétés de base des liaisons sans fil, y compris une revue de littérature sur le domaine. Chapitre 3 décrit le concept de réseau cellulaire, de son histoire à une brève description technique, et son évolution actuelle. Ces deux chapitres peuvent être ignorés pour un lecteur qui est déjà familier avec ces éléments de base. Chapitre 4 décrit en plus de détails des aspects différents de la gestion de mobilité, y compris son état-de-l'art. Lecteur est recommandé de

---

[2] *"As far as the laws of mathematics refer to reality, they are not certain; and as far as they are certain, they do not refer to reality."* Geometry and Experience, 1921, ALBERT EINSTEIN.

prendre au moins une lecture rapide de §4.1 et §4.2 avant d'entrer dans la troisième partie (Part III). Chapitre 5 décrit brièvement trois théories mathématiques: §5.1 décrit la théorie des valeurs extrêmes [143, 149] et elle est nécessaire pour le chapitre 8, §5.2 décrit la géométrie stochastique [49] et elle est nécessaire pour le chapitre 7, et enfin §5.3 décrit la théorie des franchissements de seuil des processus gaussiens [163] et elle est nécessaire pour le chapitre 9. Chapitre 6 résume les hypothèses qui sont utilisées tout au long de la thèse; lecture de ce chapitre est donc fortement recommandée avant d'aller à n'importe quel chapitre ultérieur, sauf le chapitre 12. La deuxième partie (Part II) porte sur la modélisation des liaisons sans fil, les résultats de cette partie sont utilisés dans la troisième partie (Part III). Toutefois, ceux qui s'intéressent à l'optimisation de gestion de mobilité sans être intéressé par trop de développements mathématiques peuvent commencer la troisième partie considérant que des résultats mathématiques qui y sont utilisés sont déjà prouvés.

Bibliography

[1] M. Etoh, editor. *Next generation mobile systems: 3G and beyond*. Wiley, 2005.

[2] J. Zhang and G. De la Roche. *Femtocells : Technologies and Deployment*. John Wiley & Sons, 1st edition, Dec. 2009.

[3] R. Steele, P. Gould, and C. C. Lee. *GSM, cdmaOne and 3G Systems*. John Wiley & Sons, Inc. New York, NY, USA, 2000.

[4] 3GPP TS 36.211. Evolved Universal Terrestrial Radio Access (E-UTRA): Physical channels and modulation. Tech. Spec. v10.0.0, Dec. 2010.

[5] S. Sesia, I. Toufik, and M. Baker, editors. *LTE - The UMTS Long Term Evolution: From Theory to Practice*. John Wiley & Sons, 2009.

[6] 3GPP TS 36.300. Evolved Universal Terrestrial Radio Access (E-UTRA) and Evolved Universal Terrestrial Radio Access Network (E-UTRAN) - Overall description: Stage 2. Tech. Spec. v9.4.0, June 2010.

[7] X. Lagrange, editor. *Les Réseaux Radiomobiles*. Hermès Science Publication, 2000. ISBN 2-7462-0110-0.

[8] Theodore S. Rappaport. *Wireless Communications: Principles and Practice*. Prentice Hall, 2nd edition, Jan 2002.

[9] Moe Z. Win, Pedro C. Pinto, and Lawrence A. Shepp. A mathematical theory of network interference and its applications. *Proceedings of the IEEE*, 97(2):205–230, Feb. 2009.

[10] J.G. Andrews, F. Baccelli, and R.K. Ganti. A tractable approach to coverage and rate in cellular networks. *Arxiv preprint arXiv:1009.0516*, (version 2):26, Feb 2011.

[11] M. Haenggi, J. G. Andrews, F. Baccelli, O. Dousse, and M. Franceschetti. Stochastic geometry and random graphs for the analysis and design of wireless networks. *IEEE J. Sel. Areas Commun.*, 27(7):1029 –1046, Sep. 2009. ISSN 0733-8716.

[12] S. O. Rice. Mathematical analysis of random noise. *Bell Syst. Tech. J.*, 24:46–156, 1945.

[13] S. O. Rice. Distribution of the duration of fades in radio transmission: Gaussian noise model. *Bell Syst. Tech. J*, 37(3):581–635, 1958.

[14] M. Kac and D. Slepian. Large excursions of Gaussian processes. *The Annals of Mathematical Statistics*, 30(4):1215–1228, 1959. ISSN 0003-4851.

[15] N.B. Mandayam, P.-C. Chen, and J.M. Holtzman. Minimum duration outage for cellular systems: a level crossing analysis. In *IEEE 46th Vehicular Technology Conference, VTC '96*, volume 2, pages 879–883, May 1996.

[16] N.B. Mandayam, P.-C. Chen, and J.M. Holtzman. Minimum duration outage for CDMA cellular systems: A level crossing analysis. *Wireless Personal Communications, Springer Netherlands*, 7 (2-3):135–146, Aug. 1998.

[17] J.D. Parsons and P.J.D. Parsons. *The mobile radio propagation channel*. Pentech Press London, 1992.

[18] M.F. Iskander and Z. Yun. Propagation prediction models for wireless communication systems. *IEEE Trans. Microw. Theory Tech.*, 50(3):662–673, 2002.

[19] J. Walfisch and H.L. Bertoni. A theoretical model of UHF propagation in urban environments. *IEEE Trans. Antennas Propag.*, 36(12):1788–1796, Dec. 1988.

[20] G. Liang and H.L. Bertoni. A new approach to 3-d ray tracing for propagation prediction in cities. *IEEE Trans. Antennas Propag.*, 46(6):853 –863, Jun 1998. ISSN 0018-926X.

[21] S.Y. Seidel and T.S. Rappaport. Site-specific propagation prediction for wireless in-building personal communication system design. *IEEE Trans. Veh. Technol.*, 43(4):879 –891, nov 1994. ISSN 0018-9545.

[22] D. Tse and P. Viswanath. *Fundamentals of Wireless Communication*. Cambridge University Press, June 2005.

[23] M. Hata. Empirical formula for propagation loss in land mobile radio services. *IEEE Trans. Veh. Technol.*, 29(3):317–325, Aug. 1980.

[24] J. Okumura et al. Field strength and its variability in VHF and UHF land mobile radio service. *Rev. Elect. Commun. Lab*, 16(9-10):825–873, 1968.

[25] COST 231. *Digital mobile radio towards future generation systems.* European Commission, 1999. ISBN: 92-828-5416-7.

[26] 3GPP TR 36.942. Evolved Universal Terrestrial Radio Access (E-UTRA): Radio Frequency (RF) System Scenarios. Tech. Rep. v8.2.0, June 2010.

[27] WiMAX Forum. WiMAX Systems Evaluation Methodology. Spec. v2.1, July 2008.

[28] W.C. Lee. *Mobile Communications Engineering.* McGraw-Hill Professional, 1982.

[29] A. Abdi and M. Kaveh. On the utility of gamma PDF in modeling shadow fading (slow fading). *IEEE 49th Vehicular Technology Conference, VTC '99*, 3:2308–2312, Jul 1999.

[30] A.J. Coulson, A.G. Williamson, and R.G. Vaughan. A statistical basis for lognormal shadowing effects in multipath fading channels. *IEEE Trans. Commun.*, 46(4):494–502, Apr 1998. ISSN 0090-6778.

[31] I.M. Kostic. Analytical approach to performance analysis for channel subject to shadowing and fading. *IEE Proceedings on Communications*, 152(6):821–827, Dec. 2005. ISSN 1350-2425.

[32] W.R. Braun and U. Dersch. A physical mobile radio channel model. *IEEE Trans. Veh. Technol.*, 40(2):472–482, 1991.

[33] S.Nadarajah and S. Kotz. A class of generalized models for shadowed fading channels. *Wirel. Pers. Commun.*, 43(4):1113–1120, 2007. ISSN 0929-6212.

[34] V. Erceg, L.J. Greenstein, S.Y. Tjandra, S.R. Parkoff, A. Gupta, B. Kulic, A.A. Julius, and R. Bianchi. An empirically based path loss model for wireless channels in suburban environments. *IEEE J. Sel. Areas Commun.*, 17(7):1205, 1999.

[35] S. Ghassemzadeh, L. Greenstein, A. Kavcic, T. Sveinsson, and V. Tarokh. An empirical indoor path loss model for ultra-wideband channels. *Journal of Communications and Networks*, 5(4): 303–308, 2003.

[36] J. Salo, L. Vuokko, H.M. El-Sallabi, and P. Vainikainen. Shadow fading revisited. *IEEE 63rd Vehicular Technology Conference, VTC 2006-Spring*, 6:2843–2847, May 2006. ISSN 1550-2252.

[37] A. Goldsmith. *Wireless Communications.* Cambridge University Press, 2005.

[38] W.C. Jakes and D.C. Cox. *Microwave mobile communications.* Wiley-IEEE Press, 1994.

[39] G. L. Stuber. *Principles of mobile communication.* Springer Netherlands, 2001.

[40] A.J. Goldsmith and J. Greenstein. A measurement-based model for predicting coverage areas of urban microcells. *IEEE J. Sel. Areas Commun.*, 11(7):1013, 1993.

[41] M. Gudmundson. Correlation model for shadow fading in mobile radio systems. *Electronics Letters*, 27(23):2145–2146, Nov. 1991. ISSN 0013-5194.

[42] R. H. Clarke. A statistical theory of mobile-radio reception. *Bell Syst. Tech. J.*, 47(6):957–1000, 1968.

[43] M. Abramowitz and I. A. Stegun. *Handbook of Mathematical Functions.* Dover Publ. Inc, 10 edition, 1972.

[44] S.A. Fechtel and H. Meyr. Matched filter bound for trellis-coded transmission over frequency-selective fading channels with diversity. *European Transactions on Telecommunications*, 4(3): 343–354, 1993.

[45] X. Lagrange, P. Godlewski, and Tabbane S. *Réseaux GSM.* Hermès Sciences Publication, 5e édition revue et augmentée edition, 2000.

[46] WiMAX Forum. Mobile WiMAX - Part 1: A Technical overview and Performance evaluation. Tech. rep., Mar. 2006.

[47] 3GPP TS 36.133. Evolved Universal Terrestrial Radio Access (E-UTRA): Requirements for support of radio resource management (Release 9). Tech. Spec. v9.4.0, June 2010.

[48] IEEE 802.16m. IEEE 802.16m System Requirements. Technical Report 802.16m-07/002r6, IEEE 802.16m, Sept. 2008.

[49] F. Baccelli and B. Blaszczyszyn. Stochastic Geometry and Wireless Networks, Volume I - Theory. *Foundations and Trends ® in Networking*, 3(3-4):249–449, 2009. ISSN 1554-057X.

[50] Mustafa Ergen. *Mobile Broadband - Including WiMAX and LTE.* Springer, 1st edition, Feb. 2009.

[51] Leon W. Couch. *Digital and Analog Communication Systems.* Prentice Hall, 7th edition, July 2006.

[52] 3GPP TR 25.942. Radio frequency (RF) system scenarios (release 9). Tech. Spec. v9.0.0, Dec. 2009.

[53] A.J. Viterbi. *Advances in communication systems: theory and applications.* Academic Press, 1975.

[54] I.M.I. Habbab, M. Kavehrad, and C.-E.W. Sundberg. Aloha with capture over slow and fast fading radio channels with coding and diversity. *IEEE J. Sel. Areas Commun.*, 7(1):79 –88, Jan. 1989. ISSN 0733-8716.

[55] J. Cheng and N.C. Beaulieu. Accurate ds-cdma bit-error probability calculation in rayleigh fading. *IEEE Trans. Wireless Commun.*, 1(1):3 –15, Jan. 2002. ISSN 1536-1276.

[56] N.C. Beaulieu and A.A. Abu-Dayya. Bandwidth efficient qpsk in cochannel interference and fading. *IEEE Trans. Commun.*, 43(9):2464 –2474, Sept. 1995. ISSN 0090-6778.

[57] B. C. Jones and D. J. Skellern. Interference distributions in microcell ensembles. *Sixth IEEE International Symposium on Personal, Indoor and Mobile Radio Communications, PIMRC '95*, 3: 1372–, Sept. 1995.

[58] F. Santucci, M. Pratesi, M. Ruggieri, and F. Graziosi. A general analysis of signal strength handover algorithms with cochannel interference. *IEEE Trans. Commun.*, 48(2):231–241, Feb 2000. ISSN 0090-6778.

[59] Jaeweon Cho and Daehyoung Hong. Statistical model of downlink interference for the performance evaluation of cdma systems. *IEEE Commun. Lett.*, 6(11):494–496, Nov. 2002. ISSN 1089-7798.

[60] Yuh-Ren Tsai. Spatial correlation models for total co-channel interference and carrier-to-interference ratio in mobile cellular systems. *IEEE Trans. Wireless Commun.*, 5(10):2752–2759, Oct. 2006. ISSN 1536-1276.

[61] L. Fenton. The sum of log-normal probability distributions in scatter transmission systems. *IRE Transactions on Communications Systems*, 8(1):57–67, March 1960. ISSN 0096-2244.

[62] S.C. Schwartz and Y.S. Yeh. On the distribution function and moments of power sums with log-normal components. *Bell Syst. Tech. J*, 61(7):1441–1462, 1982.

[63] N.C. Beaulieu and Qiong Xie. An optimal lognormal approximation to lognormal sum distributions. *IEEE Trans. Veh. Technol.*, 53(2):479–489, Mar. 2004. ISSN 0018-9545.

[64] J. Wu, NB Mehta, and J. Zhang. Flexible lognormal sum approximation method. *IEEE GLOBE-COM 2005*, 6:3413–3417, 2005.

[65] G.V. Trunk and S.F. George. Detection of targets in non-gaussian sea clutter. *IEEE Trans. Aerosp. Electron. Syst.*, AES-6(5):620 –628, Sept. 1970. ISSN 0018-9251.

[66] G.V. Trunk. Further results on the detection of targets in non-gaussian sea clutter. *IEEE Trans. Aerosp. Electron. Syst.*, AES-7(3):553 –556, May 1971. ISSN 0018-9251.

[67] J. Ilow, D. Hatzinakos, and A.N. Venetsanopoulos. Performance of fh ss radio networks with interference modeled as a mixture of gaussian and alpha-stable noise. *IEEE Trans. Commun.*, 46 (4):509 –520, Apr. 1998. ISSN 0090-6778.

[68] M. Shao and C.L. Nikias. Signal processing with fractional lower order moments: stable processes and their applications. *Proceedings of the IEEE*, 81(7):986–1010, Jul 1993. ISSN 0018-9219.

[69] C.L. Nikias and M. Shao. *Signal processing with alpha-stable distributions and applications*. Wiley-Interscience, 1995.

[70] J. Ilow and D. Hatzinakos. Analytic alpha-stable noise modeling in a poisson field of interferers or scatterers. *IEEE Trans. Signal Process.*, 46(6):1601–1611, Jun 1998. ISSN 1053-587X.

[71] Xueshi Yang and A.P. Petropulu. Co-channel interference modeling and analysis in a poisson field of interferers in wireless communications. *IEEE Trans. Signal Process.*, 51(1):64–76, Jan. 2003. ISSN 1053-587X.

[72] F. Baccelli and B. Blaszczyszyn. Stochastic Geometry and Wireless Networks, Volume II - Applications. *Foundations and Trends® in Networking*, 4(1-2):1–312, 2009.

[73] M. Haenggi and R.K. Ganti. Interference in large wireless networks. *Foundations and Trends ® in Networking*, 3(2):127–248, 2008. ISSN 1554-057X.

[74] R.J. Fontana. An insight into uwb interference from a shot noise perspective. *IEEE Conference on Ultra Wideband Systems and Technologies*, pages 309–313, 2002.

[75] E. Salbaroli and A. Zanella. Interference Analysis in a Poisson Field of Nodes of Finite Area. *IEEE Trans. Veh. Technol.*, 58(4):1776–1783, May 2009. ISSN 0018-9545.

[76] H. Inaltekin, S.B. Wicker, Mung Chiang, and H.V. Poor. On unbounded path-loss models: effects of singularity on wireless network performance. *IEEE J. Sel. Areas Commun.*, 27(7):1078 –1092, Sept. 2009. ISSN 0733-8716.

[77] Douglas H. Ring. Mobile telephony - wide area coverage. Bell Labs Technical Memoranda, Dec. 1947.

[78] Mobile communication system, May 1972. US Patent 3,663,762.

[79] D. Roessner, R. Carr, I. Feller, M. McGeary, and N. Newman. The Role of NSF's Support of Engineering in Enabling Technological Innovation: Phase II Final Report to the National Science Foundation. Technical report, Center for Science, Technology, and Economic Development (CSTED), May 1998. URL http://www.sri.com/policy/csted/reports/sandt/techin2/contents.html. Published on SRI International.

[80] J. Korhonen. *Introduction to 3G mobile communications*. Artech House Publishers, 2nd edition, 2001.

[81] B. Walke, P. Seidenberg, and M.P. Althoff. *UMTS: The Fundamentals*. John Wiley & Sons Inc, 2003.

[82] ITU-T Recommendation Q.1701. Framework for IMT-2000 networks. Standard, ITU-T, Mar. 1999. URL http://www.itu.int/rec/T-REC-Q.1701-199903-I.

[83] ITU Radiocommunication Assembly approves new developments for its 3G standards. Presse Release, Oct 2007. URL http://www.itu.int/newsroom/press_releases/2007/30.html.

[84] ITU-R Recommendation M.1457. Detailed specifications of the terrestrial radio interfaces of International Mobile Telecommunications-2000 (IMT-2000). Spec., ITU-R, May 2010. URL http://www.itu.int/rec/R-REC-M.1457-9-201005-I/en.

[85] ITU-D Study Group 2. Guidelines on the smooth transition of existing mobile networks to IMT-2000 for developing countries (GST): Report on question 18/2. Technical report, ITU, 2006. URL http://www.itu.int/dms_pub/itu-d/opb/stg/D-STG-SG02.18-1-2006-PDF-E.pdf.

[86] ITU-R M.2134. Requirements related to technical performance for IMT-Advanced radio interface(s). Report, ITU, Nov. 2008. URL http://www.itu.int/publ/R-REP-M.2134-2008/en.

[87] IEEE 802.16. Air Interface for Broadband Wireless Access Systems. Standard Std 802.16-2009, IEEE, May 2009.

[88] V. M. Nguyen and L. Thomas. Efficient dynamic multi-step paging for cellular wireless networks. *Bell Labs Technical Journal, Special issue on Core and Wireless Networks*, 14(2):203–221, Aug. 2009. doi: 10.1002/bltj.20380. URL http://dx.doi.org/10.1002/bltj.20380.

[89] Harri Holma and Antti Toskala, editors. *LTE for UMTS - OFDMA and SC-FDMA Based Radio Access*. John Wiley & Sons, Apr. 2009.

[90] 3GPP TS 36.300. Evolved Universal Terrestrial Radio Access (E-UTRA) and Evolved Universal Terrestrial Radio Access Network (E-UTRAN) - Overall description: Stage 2. Tech. Spec. v9.1.0, Sep. 2009.

[91] 3GPP TS 23.401. General Packet Radio Service (GPRS) enhancements for Evolved Universal Terrestrial Radio Access Network (E-UTRAN) access (Release 8). Tech. Spec. v8.12.0, Dec. 2010.

[92] 3GPP TS 23.402. Architecture enhancements for non-3GPP accesses (Release 10). Tech. Spec. v10.2.1, Jan. 2011.

[93] 3GPP TS 36.331. Evolved Universal Terrestrial Radio Access (E-UTRA) Radio Resource Control (RRC): Protocol Specification. Tech. Spec. v8.8.0, Dec. 2009.

[94] 3GPP TS 36.331. Evolved Universal Terrestrial Radio Access (E-UTRA) Radio Resource Control (RRC): Protocol specification (Release 9). Tech. Spec. v9.0.0, Sep. 2009.

[95] 3GPP TR 36.902. Evolved Universal Terrestrial Radio Access Network (E-UTRAN): Self-configuring and self-optimizing network use cases and solutions (Release 9). Tech. Rep. v2.0.0, Aug. 2009.

[96] M. David et al. On the Way towards Fourth-Generation Mobile: 3GPP LTE and LTE-Advanced. *IEEE Commun. Mag.*, 2009, 2009. ISSN 1687-1472.

[97] 3GPP TR 36.913. Requirements for further advancements for Evolved Universal Terrestrial Radio Access (E-UTRA) (LTE-Advanced). Tech. Rep. v9.0.0, Dec. 2009.

[98] Jordi Pérez-Romero, Oriol Sallent, Ramon Agustí, and Miguel Angel Díaz-Guerra. *Radio Resource Management Strategies in UMTS*. John Wiley & Sons, Oct. 2005.

[99] WiMAX Forum. Mobile System Profile Specification - Common Part. Spec. Release 1.5, Aug. 2009.

[100] 3GPP TS 23.009. Handover procedures. Tech. Spec. v7.0.0, Mar. 2007.

[101] 3GPP TS 36.331. Evolved Universal Terrestrial Radio Access (E-UTRA) Radio Resource Control (RRC): Protocol specification (Release 9). Tech. Spec. v9.3.0, June 2010.

[102] 3GPP TS 25.215. Physical layer - measurements (fdd) (release 8). Tech. Spec. v8.2.0, Sept. 2008.

[103] 3GPP TS 36.214. Evolved Universal Terrestrial Radio Access (E-UTRA): Physical layer – Measurements. Tech. Spec. v9.2.0, June 2010.

[104] J. Bannister, P.M. Mather, and S. Coope. *Convergence technologies for 3G networks: IP, UMTS, EGPRS and ATM*. John Wiley & Sons Inc, 2004.

[105] 3GPP TS 25.133. Requirements for support of Radio Resource Management FDD. Tech. Spec. v9.4.0, June 2010.

[106] Harri Holma and Antti Toskala, editors. *WCDMA for UMTS: Radio Access for Third Generation Mobile Communications*. John Wiley & Sons, 3rd edition, June 2004.

[107] J. Laiho, A. Wacker, and T. Novosad, editors. *Radio network planning and optimisation for UMTS*. John Wiley & Sons Inc, 2nd edition, 2006.

[108] 3GPP TS 25.331. Radio Resource Control (RRC): Protocol Specification (Release 8). Tech. Spec. v8.6.0, Mar. 2009.

[109] WiMAX Forum. Mobile System Profile. Approved Spec. Release 1.0, Revision 1.4.0, May 2007.

[110] NGMN Alliance. Next Generation Mobile Networks Use cases related to self-organising network, Overall description. Tech. Rep. v2.02, Dec. 2008.

[111] IEEE 802.21. Media Independent Handover Services. Standard Std 802.21-2008, IEEE, Jan. 2009.

[112] 3GPP TS 24.312. Access Network Discovery and Selection Function (ANDSF) Management Object (MO). Tech. Spec. v9.1.0, Mar. 2010.

[113] R. Rezaiifar, A.M. Makowski, and S.P. Kumar. Stochastic control of handoffs in cellular networks. *IEEE J. Sel. Areas Commun.*, 13(7):1348–1362, Sept. 1995. ISSN 0733-8716.

[114] N. Zhang and JM Holtzman. Analysis of handoff algorithms using both absolute and relative measurements. *IEEE Trans. Veh. Technol.*, 45(1):174–179, 1996.

[115] V.V. Veeravalli and O.E. Kelly. A locally optimal handoff algorithm for cellular communications. *IEEE Trans. Veh. Technol.*, 46(3):603–609, Aug 1997. ISSN 0018-9545.

[116] R. Prakash and V.V. Veeravalli. Adaptive hard handoff algorithms. *IEEE J. Sel. Areas Commun.*, 18(11):2456–2464, Nov 2000. ISSN 0733-8716.

[117] M. Akar and U. Mitra. Variations on optimal and suboptimal handoff control for wireless communication systems. *IEEE J. Sel. Areas Commun.*, 19(6):1173–1185, Jun 2001. ISSN 0733-8716.

[118] K.-I. Itoh, S. Watanabe, J.-S. Shih, and T. Sato. Performance of handoff algorithm based on distance and rssi measurements. *IEEE Trans. Veh. Technol.*, 51(6):1460–1468, Nov 2002. ISSN 0018-9545.

[119] Hyungkeuk Lee, Hyukmin Son, and Sanghoon Lee. Semisoft handover gain analysis over OFDM-based broadband systems. *IEEE Trans. Veh. Technol.*, 58(3):1443–1453, Mar. 2009. ISSN 0018-9545.

[120] R. Vijayan and J.M. Holtzman. A model for analyzing handoff algorithms [cellular radio]. *IEEE Trans. Veh. Technol.*, 42(3):351–356, Aug. 1993. ISSN 0018-9545.

[121] R. Vijayan and J.M. Holtzman. Foundations for level crossing analysis of handoff algorithms. In *IEEE International Conference on Communications, ICC '93*, volume 2, pages 935–939 vol.2, May 1993.

[122] A.E. Leu and B.L. Mark. A discrete-time approach to analyze hard handoff performance in cellular networks. *IEEE Trans. Wireless Commun.*, 3(5):1721–1733, Sept. 2004. ISSN 1536-1276.

[123] V. Vanghi and C. Chevallier. Wcdma handover parameters optimization. volume 7, pages 4133–4137 Vol.7, June 2004.

[124] C. Werner, J. Voigt, S. Khattak, and G. Fettweis. Handover parameter optimization in wcdma using fuzzy controlling. pages 1–5, Sept. 2007.

[125] A. Schröder, H. Lundqvist, and G. Nunzi. Distributed self-optimization of handover for the Long Term Evolution. In *Proceedings of the 3rd International Workshop on Self-Organizing Systems*, pages 281–286. Springer-Verlag Berlin, Heidelberg, 2008.

[126] R. Rouil and N. Golmie. Adaptive channel scanning for IEEE 802.16e. In *Military Communications Conference, MILCOM '06*, pages 1–6, 2006.

[127] A. Ulvan and R. Bestak. The Efficiency Performance on Handover's Scanning Process of IEEE802. 16m. In *Wireless and Mobile Networking: Second IFIP WG 6. 8 Joint Conference, WMNC '09*, page 321. Springer, 2009.

[128] K. Hiltunen, N. Binucci, and J. Bergstrom. Comparison between the periodic and event-triggered intra-frequency handover measurement reporting in WCDMA. In *IEEE Wireless Communications and Networking Conference, WCNC '00*, volume 2, pages 471 –475, 2000.

[129] D. Kim and J. Kim. The optimum parameter design for WCDMA intra-frequency handover initiation. *Lecture Notes in Computer Science, Springer Berlin / Heidelberg*, 3619/2005:239–248, Sept. 2005.

[130] A. Racz, A. Temesvary, and N. Reider. Handover performance in 3GPP Long Term Evolution (LTE) systems. In *16th IST Mobile and Wireless Communications Summit*, pages 1–5, July 2007.

[131] M. Anas, F.D. Calabrese, P.E. Mogensen, C. Rosa, and K.I. Pedersen. Performance evaluation of received signal strength based hard handover for UTRAN LTE. In *IEEE 65th Vehicular Technology Conference, VTC2007-Spring*, pages 1046–1050, Apr. 2007.

[132] M. Anas, F.D. Calabrese, P.-E. Ostling, K.I. Pedersen, and P.E. Mogensen. Performance analysis of handover measurements and layer 3 filtering for UTRAN LTE. In *IEEE 18th International Symposium on Personal, Indoor and Mobile Radio Communications, PIMRC '07*, pages 1–5, Sept. 2007.

[133] J. Kurjenniemi and T. Henttonen. Effect of measurement bandwidth to the accuracy of inter-frequency RSRP measurements in LTE. In *IEEE 19th International Symposium on Personal, Indoor and Mobile Radio Communications, 2008, PIMRC '08*, pages 1 –5, Sept. 2008.

[134] H. Olofsson, S. Magnusson, and M. Almgren. A concept for dynamic neighbor cell list planning in a cellular system. In *Seventh IEEE International Symposium on Personal, Indoor and Mobile Radio Communications, PIMRC '96*, volume 1, pages 138–142 vol.1, 1996.

[135] S. Magnusson and H. Olofsson. Dynamic neighbor cell list planning in a microcellular network. In *IEEE 6th International Conference on Universal Personal Communications*, pages 223–227, Oct. 1997.

[136] R. Guerzoni, I. Ore, K. Valkealahti, and D. Soldani. Automatic Neighbor Cell List Optimization for UTRA FDD Networks: Theoretical Approach and Experimental Validation. In *IWS/WPMC*, Denmark, 2005.

[137] D. Soldani and I. Ore. Self-optimizing neighbor cell list for UTRA FDD networks using detected set reporting. In *IEEE 65th Vehicular Technology Conference, VTC2007-Spring*, pages 694–698, 2007. ISBN 1550-2252.

[138] Flavio Parodi, Mikko Kylvaja, Gordon Alford, Juan Li, and Jose Pradas. An automatic procedure for neighbor cell list definition in cellular networks. In *IEEE International Symposium on a World of Wireless, Mobile and Multimedia Networks, WoWMoM '07*, pages 1–6, June 2007.

[139] Juan Li and R. Jantti. On the study of self-configuration neighbour cell list for mobile WiMAX. In *The 2007 International Conference on Next Generation Mobile Applications, Services and Technologies, NGMAST '07*, pages 199–204, Sept. 2007.

[140] M. Amirijoo, P. Frenger, F. Gunnarsson, H. Kallin, J. Moe, and K. Zetterberg. Neighbor cell relation list and physical cell identity self-organization in LTE. In *IEEE International Conference on Communications Workshops, ICC Workshops*, pages 37–41, May 2008.

[141] M. Amirijoo, P. Frenger, F. Gunnarsson, H. Kallin, J. Moe, and K. Zetterberg. Neighbor cell relation list and measured cell identity management in LTE. In *IEEE Network Operations and Management Symposium, NOMS '08*, pages 152–159, Apr. 2008.

[142] S. Foss, D. Korshunov, and S. Zachary. An introduction to heavy-tailed and subexponential distributions. Apr 2009. URL http://www.mfo.de/publications/owp/2009/OWP2009_13.pdf.

[143] P. Embrechts, C. Kluppelberg, and T. Mikosch. *Modelling Extremal Events for Insurance and Finance*. Springer, Feb. 1997.

[144] M. Fréchet. Sur la loi de probabilité de l'écart maximum. *Ann. de la Soc. polonaise de Math*, 6: 93–116, 1927.

[145] R.A. Fisher and L.H.C. Tippett. Limiting forms of the frequency distribution of the largest or smallest member of a sample. 24(2):180–190, 1928.

[146] EJ Gumbel. Les valeurs extrêmes des distributions statistiques. *Annales de l´IH Poincaré*, 308 (2):115–158, 1934.

[147] R. von Mises. La distribution de la plus grande de n valeurs. *Rev. Math. Union Interbalcanique*, 1(1), 1936.

[148] B.V. Gnedenko. Sur la distribution limite du terme maximum d´une serie aleatoire. *Ann. Math*, 44(3):423–453, 1943.

[149] M. R. Leadbetter, G. Lindgren, and H. Rootzén. *Extremes and Related Properties of Random Sequences and Processes*. Springer Verlag, 1983.

[150] S.I. Resnick. *Extreme values, regular variation, and point processes*. Springer Verlag, 1987. ISBN 0387964819.

[151] J. Galambos. *The asymptotic theory of extreme order statistics*. Krieger Pub Co, 1987. ISBN 0898749573.

[152] Laurens Haan. A form of regular variation and its application to the domain of attraction of the double exponential distribution. *Probability Theory and Related Fields*, 17:241–258, 1971. ISSN 0178-8051. 10.1007/BF00536760.

[153] Sidney I. Resnick. Tail equivalence and its applications. *Journal of Applied Probability*, 8(1): 136–156, 1971. ISSN 00219002.

[154] A.A. Balkema and L. De Haan. On R. Von Mises´ Condition for the Domain of Attraction of $\exp(-e^{-x})$. *The Annals of Mathematical Statistics*, 43(4):1352–1354, 1972.

[155] Rinya Takahashi. Normalizing constants of a distribution which belongs to the domain of attraction of the gumbel distribution. *Statistics & Probability Letters*, 5(3):197 – 200, 1987. ISSN 0167-7152.

[156] D. A. Darling. The influence of the maximum term in the addition of independent random variables. *Transactions of the American Mathematical Society*, 73(1):95–107, 1952. ISSN 00029947.

[157] RA Maller and SI Resnick. Limiting behaviour of sums and the term of maximum modulus. *Proceedings of the London Mathematical Society*, 3(3):385, 1984. ISSN 0024-6115.

[158] NH Bingham and JL Teugels. Conditions implying domains of attraction. In *Proceedings of the Sixth Conference on Probability Theory*, pages 10–15, 1981.

[159] P.J. Downey and P.E. Wright. The ratio of the extreme to the sum in a random sequence. *Extremes*, 10(4):249–266, 1994.

[160] T. Chow and J.L. Teugels. The sum and the maximum of iid random variables. *Asymptotic Statistics*, pages 81–92, 1978.

[161] C. W. Anderson and K. F. Turkman. The joint limiting distribution of sums and maxima of stationary sequences. *Journal of Applied Probability*, 28(1):33–44, 1991. ISSN 00219002.

[162] C. W. Anderson and K. F. Turkman. Sums and maxima of stationary sequences with heavy tailed distributions. *Sankhya: The Indian Journal of Statistics, Series A*, 57(1):pp. 1–10, 1995. ISSN 0581572X.

[163] H. Cramèr and M. R. Leadbetter. *Stationary and related stochastic processes: Sample function properties and their applications*, volume 7. John Wiley and Sons, Inc, 1967.

[164] VA Ivanov. On the average number of crossings of a level by the sample functions of a stochastic process. *Theory of Probability and its Applications*, 5:319, 1960.

[165] N.D. Ylvisaker. The expected number of zeros of a stationary gaussian process. *The Annals of Mathematical Statistics*, 36(3):1043–1046, 1965. ISSN 0003-4851.

[166] F. Graziosi and F. Santucci. Distribution of outage intervals in macrodiversity cellular systems. *IEEE J. Sel. Areas Commun.*, 17(11):2011–2021, 1999.

[167] Jie Lai and N.B. Mandayam. Fade margins for minimum duration outages in lognormal shadow fading and rayleigh fading. In *31st Asilomar Conference on Signals, Systems & Computers*, volume 1, pages 609–613, Nov 1997.

[168] Jie Lai and N.B. Mandayam. Minimum duration outages in rayleigh fading channels. *IEEE Trans. Commun.*, 49(10):1755–1761, Oct 2001. ISSN 0090-6778.

[169] Hai Jiang and C.H. Davis. Cell-coverage estimation based on duration outage criterion for cdma cellular systems. *IEEE Trans. Veh. Technol.*, 52(4):814 – 822, july 2003. ISSN 0018-9545.

[170] P.C. Pinto and M.Z.Salbaroli Win. Communication in a poisson field of interferers. In *40th Annual Conference on Information Sciences and Systems*, pages 432–437, Mar. 2006.

[171] J. Orriss and S.K. Barton. Probability distributions for the number of radio transceivers which can communicate with one another. *IEEE Trans. Commun.*, 51(4):676 – 681, april 2003. ISSN 0090-6778.

[172] A. Conti, D. Dardari, and R. Verdone. Collaborative signal processing for energy-efficient self-organizing wireless sensor network. In *International Workshop on Wireless Ad-Hoc Networks 2004*, pages 99 – 104, 2004.

[173] C. Bettstetter and C. Hartmann. Connectivity of Wireless Multihop Networks in a Shadow Fading Environment. *Wireless Networks*, 11(5):571–579, 2005.

[174] E. Salbaroli and A. Zanella. A connectivity model for the analysis of a wireless ad hoc network in a circular area. In *IEEE International Conference on Communications, 2007. ICC '07*, pages 4937 –4942, 2007.

[175] Tony Q.S. Quek, Davide Dardari, and Moe Z. Win. Energy efficiency of dense wireless sensor networks: to cooperate or not to cooperate. *IEEE J. Sel. Areas Commun.*, 25(2):459 –470, Feb. 2007. ISSN 0733-8716.

[176] H. Takagi and L. Kleinrock. Optimal transmission ranges for randomly distributed packet radio terminals. *IEEE Trans. Commun.*, 32(3):246 – 257, Mar. 1984. ISSN 0090-6778.

[177] T.C. Hou and V. Li. Transmission range control in multihop packet radio networks. *IEEE Trans. Commun.*, 34(1):38–44, 1986.

[178] ES Sousa and J. Silvester. Optimum transmission ranges in a direct-sequence spread-spectrum multihop packet radio network. *IEEE J. Sel. Areas Commun.*, 8(5):762–771, 1990.

[179] F. Baccelli, B. Blaszczyszyn, and P. Muhlethaler. A spatial reuse Aloha MAC protocol for multihop wireless mobile networks. *INRIA Research Report*, pages 1655–1664, 2003.

[180] M. Haenggi. Outage and throughput bounds for stochastic wireless networks. In *In proceedings of the International Symposium on Information Theory, 2005. ISIT 2005.*, pages 2070 –2074, 2005.

[181] E.S. Sousa. Performance of a spread spectrum packet radio network link in a poisson field of interferers. *IEEE Inf. Theory*, 38(6):1743–1754, Nov. 1992. ISSN 0018-9448.

[182] S. Ambike, J. Ilow, and D. Hatzinakos. Detection for binary transmission in a mixture of gaussian noise and impulsive noise modeled as an alpha-stable process. *IEEE Signal Process. Lett.*, 1(3):55 –57, Mar. 1994. ISSN 1070-9908.

[183] G.A. Tsihrintzis and C.L. Nikias. Performance of optimum and suboptimum receivers in the presence of impulsive noise modeled as an alpha-stable process. *IEEE Trans. Commun.*, 43(234): 904 –914, feb/mar/apr 1995. ISSN 0090-6778.

[184] S. Govindasamy, F. Antic, D.W. Bliss, and D.H. Staelin. The performance of linear multiple-antenna receivers with interferers distributed on a plane. In *IEEE 6th Workshop on Signal Processing Advances in Wireless CommunicationsBalkema*, pages 880 – 884, 2005.

[185] J. A. McFadden. The entropy of a point process. *SIAM Journal on Applied Mathematics*, 13(4): 988–994, 1965.

[186] William Feller. *An Introduction to Probability Theory and Its Applications*, volume 2. John Wiley & Sons, 2nd edition, 1971.

[187] E. Fox. North American ARPU growth outpaces the world: A look at wireless forecast drivers. *Yankee Group, Mar*, 2006.

[188] H. Claussen, L.T.W. Ho, and L.G. Samuel. Financial analysis of a pico-cellular home network deployment. In *IEEE International Conference on Communications, ICC '07*, pages 5604–5609, June 2007.

[189] W.C.Y. Lee. Smaller cells for greater performance. *IEEE Commun. Mag.*, 29(11):19–23, Nov. 1991. ISSN 0163-6804.

[190] A. Kajiwara. Effects of cell size, directional antenna, diversity, and shadowing on indoor radio cdma capacity. *IEEE Trans. Veh. Technol.*, 46(1):242–247, Feb. 1997. ISSN 0018-9545.

[191] T. Nihtila. Capacity improvement by employing femto cells in a macro cell hsdpa network. In *IEEE Symposium on Computers and Communications, ISCC '08*, pages 838–843, July 2008.

[192] V. Chandrasekhar, J. Andrews, and A. Gatherer. Femtocell networks: a survey. *IEEE Commun. Mag.*, 46(9):59–67, Sept. 2008. ISSN 0163-6804.

[193] Simon Saunders, Stuart Carlaw, Andrea Giustina, Ravi Rai Bhat, V. Srinivasa Rao, and Rasa Siegberg. *Femtocells: Opportunities and Challenges for Business and Technology*. Wiley, Jun. 2009.

[194] Alistair Urie. Keynote: The future of mobile networking will be small cells. In *IEEE International Workshop on Indoor and Outdoor Femto Cells*, Sep. 2009.

[195] Yoshioki Chika. Keynote: True BWA - eXtended Global Platform. In *IEEE International Workshop on Indoor and Outdoor Femto Cells*, Sep. 2009.

[196] Peter Judge. Vodafone launches Home 3G Femtocell in the UK. Eweekeurope, June 2009. URL http://www.eweekeurope.co.uk/news/vodafone-launches-home-3g-femtocell-in-the-uk-1203.

[197] D. Knisely, T. Yoshizawa, and F. Favichia. Standardization of femtocells in 3GPP. *IEEE Commun. Mag.*, 47(9):68–75, 2009.

[198] 3GPP TR 32.821. Telecommunication management: Study of Self-Organizing Networks (SON) related Operations, Administration and Maintenance (OAM) for Home Node B (HNB). Tech. Rep. v9.0.0, June 2009.

[199] 3GPP TS 25.467. UTRAN architecture for 3G Home Node B (HNB): Stage 2. Tech. Spec. v9.3.0, June 2010.

[200] 3GPP TS 22.220. Service requirements for Home Node B (HNB) and Home eNode B (HeNB). Tech. Spec. v10.3.0, June 2010.

[201] H. Claussen, L.T.W. Ho, and L.G. Samuel. An overview of the femtocell concept. *Bell Labs Technical Journal*, 13(1), 2008.

[202] ETSI TR 101.112. Universal Mobile Telecommunications System (UMTS); Selection procedures for the choice of radio transmission technologies of the UMTS. Tech. Rep. v3.2.0, Apr. 1998.

[203] NGMN Alliance. Next Generation Mobile Networks Recommendation on SON and O&M requirements. Req. Spec. v1.23, Dec. 2008.

[204] 3GPP TR 25.913. Requirements for Evolved UTRA and Evolved UTRAN (Release 8). Tech. Rep. v8.0.0, Dec. 2008.

[205] M.M. Zonoozi and P. Dassanayake. User mobility modeling and characterization of mobility patterns. *IEEE J. Sel. Areas Commun.*, 15(7):1239–1252, Sep 1997. ISSN 0733-8716.

[206] Wenye Wang and Ming Zhao. Joint effects of radio channels and node mobility on link dynamics in wireless networks. In *IEEE INFOCOM '08*, pages 933–941, Apr. 2008.

[207] S. Kullback and R.A. Leibler. On information and sufficiency. *Annals of Mathematical Statistics*, 22(1):79–86, 1951.

[208] S. Kullback. The kullback-leibler distance. *The American Statistician*, 41:340–341, 1987.

[209] B. Fuglede and F. Topsoe. Jensen-Shannon divergence and Hilbert space embedding. *International Symposium on Information Theory, ISIT '04*, pages 31–, July 2004.

Wireless Link Quality Modelling and Mobility Management Optimisation for Cellular Networks

Dissertation of Doctor of Philosophy by Van Minh Nguyen

The quality of communication in a wireless network is primarily determined by the wireless link signal quality expressed in term of signal-to-interference-plus-noise ratio. The fact that better signal quality enhances the communication quality incites to look for states where each receiver connects to a transmitter providing it with the best signal quality. Using stochastic geometry and then extreme value theory, we obtain the distribution of the best signal quality, of the interference, and of the maximum signal strength in both bounded and unbounded path loss conditions. We then investigate temporal variations of wireless links, which are also essential to wireless networking, in terms of level crossings of a stationary process $X(t)$. We prove that the length of an excursion of $X(t)$ above a level $\gamma \to -\infty$ has an exponential distribution, and obtain results associated with the crossings of several levels. These results are then applied to mobility management in cellular networks. We focus on the handover measurement function, which differs from the handover decision-execution by identifying the best neighbouring cell to which a connection switching is to be decided and executed. This function has an important influence on the user's experience, though its operation has been questionable due to the complexity of combining control mechanisms. We firstly address this topic with an analytical approach for emerging macro cell and small cell networks, and then with a self-optimisation approach for neighbour cell lists used in today's cellular networks.

La qualité de communication dans un réseau sans fil est déterminée par la qualité du signal, et plus précisément par le rapport signal à interférence et bruit. Cela pousse chaque récepteur à se connecter à l'émetteur qui lui donne la meilleure qualité du signal. Nous utilisons la géométrie stochastique et la théorie des extrêmes pour obtenir la distribution de la meilleure qualité du signal, ainsi que celles de l'interférence et du maximum des puissances reçues. Nous mettons en évidence comment la singularité de la fonction d'affaiblissement modifie leurs comportements. Nous nous intéressons ensuite au comportement temporel des signaux radios en étudiant le franchissement de seuils par un processus stationnaire $X(t)$. Nous démontrons que l'intervalle de temps que $X(t)$ passe au-dessus d'un seuil $\gamma \to -\infty$ suit une distribution exponentielle, et obtenons également des résultats caractérisant des franchissements par $X(t)$ de plusieurs seuils adjacents. Ces résultats sont ensuite appliqués à la gestion de mobilité dans les réseaux cellulaires. Notre travail se concentre sur la fonction de 'handover measurement'. Nous identifions la meilleure cellule voisine lors d'un handover. Cette fonction joue un rôle central sur l'expérience perçue par l'utilisateur. Mais elle demande une coopération entre divers mécanismes de contrôle et reste une question difficile. Nous traitons ce problème en proposant des approches analytiques pour les réseaux émergents de types macro et pico cellulaires, ainsi qu'une approche d'auto-optimisation pour les listes de voisinage utilisées dans les réseaux cellulaires actuels.

Keywords: max sinr, interference, max signal, shot noise, extreme values, level crossing, self-optimisation, mobility management, handover measurement, neighbour cell list